UNIVERSIDAD POLITÉCNICA DE MADRID

ESCUELA TÉCNICA SUPERIOR DE INGENIEROS INDUSTRIALES

TIME DOMAIN PASSIVITY CONTROL FOR DELAYED TELEOPERATION

DOCTOR OF PHILOSOPHY

AUTOMATION AND ROBOTICS

Jordi Artigas Esclusa

May 14, 2014

UNIVERSIDAD POLITÉCNICA DE MADRID

ESCUELA TÉCNICA SUPERIOR DE INGENIEROS INDUSTRIALES

DLR - GERMAN AEROSPACE CENTER

ROBOTICS AND MECHATRONICS CENTER

TIME DOMAIN PASSIVITY CONTROL FOR DELAYED TELEOPERATION

DOCTOR OF PHILOSOPHY

AUTOMATION AND ROBOTICS

Author: Jordi Artigas Esclusa
Electrical Engineer

Advisors: D. Rafael Aracil Santonja
Universidad Politécnica de Madrid

D. Gerd Hirzinger
Technische Universität München -
DLR - German Aerospace Center

May 14, 2014

TIME DOMAIN PASSIVITY CONTROL FOR DELAYED TELEOPERATION

Autor: Jordi Artigas Esclusa

Tribunal:

Presidente	D. Manuel Ángel Armada Rodríguez
Secretario:	D. Manuel Ferre Pérez
Vocal A:	D. Luis Basañez Villaluenga
Vocal B:	D. Alin Albu-Schäffer
Vocal C:	D. Jee-Hwan Ryu
Suplente A:	D. Luis Miguel Bergasa Pascual
Suplente B:	Dña. María Dolores Blanco Rojas

Acuerdan otorgar la calificación de:

Madrid, de 2014

Acknowledgments

First and foremost I would like to express my sincere appreciation to Prof. Gerd Hirzinger, Prof. Alin Albu-Schäffer and Prof. Rafael Aracil for making this work possible. I also would like to express a special gratitude to Prof. Manuel Ferre for really helpful discussions, his wise advices and for his guidance through a maze of bureaucracy induced by the recent implementation of the new European educational system. I also would like to specially thank Prof. Jee Hwan-Ryu for inspiring the research presented in this thesis, for the never-ending discussions we enjoyed together and for introducing me into the finest korean cuisine.

I would like to thank all the my colleagues from the DLR - Robotic and Mechatronics Center, with whom I had the honor to work alongside: Dr. Christian Ott, Ribin Balachandran, Marco De Stefano, Philipp Kremer, Carsten Preusche, Michael Panzirsch, Martin Stelzer, Albert Arquer, Simon Kielhoefer, Holger Urbanek, Alex Nothelfer and Werner Friedl. It has been a pleasure to work with you all! I would like to thank Dr. Enrico Stoll and Dr. Jan Harder for providing the communication infrastructures based on the ARTEMIS and the ASTRA satellites. I also would like to thank Dr. Gianni Borghesan and Prof. Cristian Secchi, with whom I had the pleasure to debate many vital aspects related to haptics and teleoperation.

Last but not least, I want to express my deepest gratitudes to Claudia García, for being an endless stream of happiness, love and patience; to my parents, Francesca Esclusa and Josep Artigas, for their unconditional love and support; and to my brother, Xavier Artigas, an unlimited source of inspiration in my life. To them I dedicate this thesis.

Jordi Artigas Esclusa.

Abstract

Telepresence combines different sensorial modalities, including vision and touch, to produce a feeling of being present in a remote location. The key element to successfully implement a telepresence system and thus to allow telemanipulation of a remote environment is force feedback. In a telemanipulation, mechanical energy is conveyed from the human operator to the manipulated object found in the remote environment. In general, energy is a property of all physical objects, fundamental to their mutual interactions in which the energy can be transferred among the objects and can change form but cannot be created or destroyed. In this thesis, we exploit this fundamental principle to derive a novel bilateral control mechanism that allows to design stable teleoperation systems with any conceivable communication architecture. The rationale starts from the fact that the mechanical energy injected by a human operator into the system must be conveyed to the remote environment and vice versa. As will be seen, setting energy as a control variable allows a more general treatment of the system than the more conventional setting of specific system variables, as can be position, velocity or force. Through the Time Delay Power Network (TDPN) concept, the issue of defining the energy flows involved in a teleoperation system is solved with independence of the communication architecture. In particular, communication time delays are found to be a source of virtual energy. This fact is observed with delays starting from 1 millisecond. Since this energy is intrinsically *added*, the resulting teleoperation system can be non-passive and thus become unstable. The Time Delay Power Networks are found to be carriers of the desired exchanged energy but also generators of virtual energy due to the time delay. Once these networks are identified, the Time Domain Passivity Control approach for TDPNs is proposed as a control mechanism to ensure system passivity and therefore, system stability. The proposed method is based on the simple fact that this intrinsically added energy due to the communication must be transformed into dissipation. Then the system becomes closer to the desired one, where only the energy injected from one side of the system is conveyed to the other one. The resulting system presents two qualities: On one hand, system stability is guaranteed through passivity, independently from the chosen control architecture and communication channel; on the other, performance is maximized in terms of energy transfer fidelity. The proposed methods are sustained with a set of experimental implementations using different control architectures and communication delays ranging from 2 to 900 milliseconds. An experiment that includes a communication Space link based on the geostationary satellite ASTRA concludes this thesis.

Resumen

La telepresencia combina diferentes modalidades sensoriales, incluyendo, entre otras, la visual y la del tacto, para producir una sensación de presencia remota en el operador. Un elemento clave en la implementación de sistemas de telepresencia para permitir una telemanipulación del entorno remoto es el retorno de fuerza. Durante una telemanipulación, la energía mecánica es transferida entre el operador humano y el entorno remoto. En general, la energía es una propiedad de los objetos físicos, fundamental en su mutua interacción. En esta interacción, la energía se puede transmitir entre los objetos, puede cambiar de forma pero no puede crearse ni destruirse. En esta tesis, se aplica este principio fundamental para derivar un nuevo método de control bilateral que permite el diseño de sistemas de teleoperación estables para cualquier arquitectura concebible. El razonamiento parte del hecho de que la energía mecánica insertada por el operador humano en el sistema debe transferirse hacia el entorno remoto y viceversa. Tal como se verá, el uso de la energía como variable de control permite un tratamiento más general del sistema que el uso de variables especificas del sistema, más común en este tipo de controladores. Mediante el concepto de Red de Potencia de Retardo Temporal (RPRT), el problema de definir los flujos de energía en un sistema de teleoperación es solucionado con independencia de la arquitectura de comunicación. Como se verá, los retardos temporales son la principal causa de generación de energía virtual. Este hecho se observa con retardos a partir de 1 milisegundo. Esta energía virtual es añadida al sistema de forma intrínseca y representa la causa principal de inestabilidad. Se demuestra que las RPRTs son transportadoras de la energía deseada intercambiada entre maestro y esclavo pero a la vez generadoras de energía virtual debido al retardo temporal. Una vez estas redes son identificadas, el método de Control de Pasividad en el Dominio Temporal para RPRTs se propone como mecanismo de control para asegurar la pasividad del sistema, y así la estabilidad. El método se basa en el simple hecho de que esta energía virtual debido al retardo debe transformarse en disipación. Así el sistema se aproxima al sistema deseado, donde sólo la energía insertada desde un extremo es transferida hacia el otro. El sistema resultante presenta dos cualidades: por un lado la estabilidad del sistema queda garantizada con independencia de la arquitectura del sistema y del canal de comunicación; por el otro, el rendimiento es maximizado en términos de fidelidad de transmisión energética. Los métodos propuestos se sustentan con sistemas experimentales con diferentes arquitecturas de control y retardos entre 2 y 900 ms. La tesis concluye con un experimento que incluye una comunicación espacial basada en el satélite geoestacionario ASTRA.

Contents

Chapter 1

Introduction

1.1 Energy Transfer from Intention to Goal

The possibility of manipulating unaccessible or remote environments has many potential applications, some of them being already visible in the medicine field and in the nuclear industry. The manipulation ability is closely related to the haptic perception. Humans recognize and manipulate objects by touching. The manipulation of an object involves tactile perception and proprioception and require muscular physical efforts that result in pressure, skin stretch, and forces that are distributed along the body's mechanical structure. Teleoperation extends this ability to far, unaccessible or harsh environments. Telepresence combines different sensorial modalities, including vision and touch, to produce a feeling of being present in a remote location. The key element to successfully implement a telepresence system and thus to allow the telemanipulation of a remote environment is the force feedback. This thesis deals with the control mechanisms that allow the transmission of proprioception information between a human operator and an object located in a remote location. A non-verbal long distance communication is therefore established between a human and a remote environment to be manipulated.

Teleoperation is an extremely interesting field, not only for its wide field of applications, but also because it represents a technological simile for understanding and modeling other types of interaction with environments. In teleoperation, the operator is an energy source governed by its intention to manipulate a remote environment. Here, *remote* has the meaning of distance but also that of a *barrier*. A barrier is what separates intention from goal and, in the field of teleoperation, can represent a scaling factor (i.e. micro tele-assembly for instance), an unaccessible environment (such as a human body or a nuclear plant), or time delay (i.g., in space applications or internet based teleoperation). What is common in all these applications fields is that a human injects energy into the system based on an intention; this energy is transferred through a set of mechanically linked elements; and this energy is finally dissipated in the interaction with the environment.

When a human decides to manipulate the environment, an intention is what first motivates the activation the necessary muscles to approach the target and interact with it. Humans strongly rely on experiences and patterns and so most objects are well known prior to be manipulated. Take for instance the action of grasping a cup of coffe. The

energy that the human has to invest in this action is optimized in many aspects. As humans, we know many parameters of the cup of coffe a priori. This allows us spending just the necessary amount of energy for approaching and grasping the cup. The fact that the human brain own a model of the cup based on its shape, its materials and, in general, the gathered infant experiences, allows us to execute perfect grasps. Understanding the mechanisms involved in human physical interaction belongs to neurologist and physiologist's fundamental research and is still far to be answered. There is, however, consensus on how biological mechanical structures are modulated in order to *adapt* the impedances of end-effector limbs to the impedances of the manipulated object. Impedance is the result of dividing force and displacement and this relationship can be given by any combination of the three fundamental mechanical parameters of mass, stiffness and damping. Thus, muscles and tendons are precisely contracted and co-contracted to provide the arm, hand and fingers with specific static and dynamic stiffness and damping properties to achieve goals, which can be very well defined in terms of energy. For instance, energy is maximally transferred when the impedances of transmitter and the receiver are matched; another example is the natural low stiffness setting of the human limbs when the environment is unknown (e.g. the game of recognizing someone's face with a subject with covered eyes.

when humans interact with the environment this is accomplished is one of the main research

The model and in particular the acquired impedance of the cup allows to optimally is thus optimally transferred,

Our mechanical structures in the sense that the impedance created by the biological structures necessary to accomplish the task will be matched to that of the environment. Thus, there is some sort of impedance adaptation between the human actuator and the environment.

Teleoperation can be seen as placing a strangely shaped tool between the human hand and the object being manipulated. This tool is usually not directly recognized by the human, as there is no previous acquired experience about it. As a such, it is hard for the human to adjust the necessary parameters to allow the impedance matching required for precise manipulability. One of the keys in teleoperation is precisely to make this tool transparent; if possible, such that the resulting impedance created by the system tool and environment does not differ from the impedance of the environment. If this is achieved, we will then talk of a fully transparent system.

A teleoperation system can be roughly described in terms of an energy source, an energy transfer and an energy dissipation. As will be seen throughout this theis, this is a useful description that will allow to design teleoperation systems for any given scenarios.

1.2 Physical Modeling

A representation framework which allows this type of energy description is thus necessary. In particular, the framework must allow input/output energy description and must allow energy transfer between the different elements involved in the system. The human operator is seen as an element capable of generating and dissipating energy. The haptic device is seen as an element capable of transforming energy, from human work to electrical and mechanical energy. The communication is seen as an element capable of

transferring energy. And the slave device is seen as an element capable of transforming electrical energy into mechanical energy.

In the field of electrical engineering, a system model is a set of mathematical equations that completely describe the dynamical behavior of the system in terms of some physically relevant variables. The model and its representation are fundamental tools in developing systems and control algorithms. The nature of the system determines the system variables. Thus, a mechanical system can be described in terms of force and velocity, an electrical system through voltage and current or a fluid system in terms of pressure and volumetric flow rate. Despite the differences in the various disciplines, these variables share some fundamental properties since they all describe oscillating systems in the different domains. Advanced methods for modeling, such as bond graph or network based, exploit these similarities and allow some sort of *deattachment* from the physical system and the model itself. For example, a mechanical system can be represented through electrical networks, or a thermodynamical system trough a bond graph. *Analogies*, later described in Sec. 2.3, are a powerful tool since they allow analysis in less explored fields. An unfamiliar system may be compared with one that is better known, where the relations and actions are more easily visualized, the mathematics more rapidly applied and thus the analytical solutions may be more easily obtained.

The main modeling tool in this work is the network representation. A *top-down-top* analysis methodology is used (see Fig. 1.2.1). The analysis starts from the highest possible level of abstraction using electrical networks. Those networks are chosen such that each of them encompass as many elements as possible while preserving a logical division that is in consonance with the main components of the system. Usually high level representations will allow different concretizations. The system is then concretized by means of a flow diagram [1], with high level of detail. The analysis follows by extracting the equivalent electrical circuit by using one of the mechanical-electrical analogies. The electrical domain offers powerful analysis and design tools which will be here exploited. Finally, one of the main benefits of the electrical representation is the straightforward abstraction of the specific electrical networks of the system. The main benefit of the network representation is that it provides a description of how the components of the system are energetically interrelated. It is this network domain where the system analysis and design will take place.

The first high level network representation can be normally easily extracted. The interconnection points between the main networks must be identified and the only condition is that the signals that connect the networks must be power correlated. The definitions of a network port and the concept of power correlation are reviewed in the next chapter. The flow diagram is a visual representation of a system which uses lines to connect boxes. Boxes in turn contain gains or transfer functions which transform an input into and output variable. The flow diagram is a detailed description widely used in control engineering. The electrical circuit is a graph of connected lines and edges from which Kirchoffs Laws can be stated in concise algebraic form and from which electrical networks can be identified. The network modeling offers as well proficient design and analysis tools. One of the most important characteristics is the intrinsic energy coherence. That is, the network representation of a system shows in a clear manner

[1] Alternatively block diagram. In this work both terms, flow and block diagram, will be used indistinctly

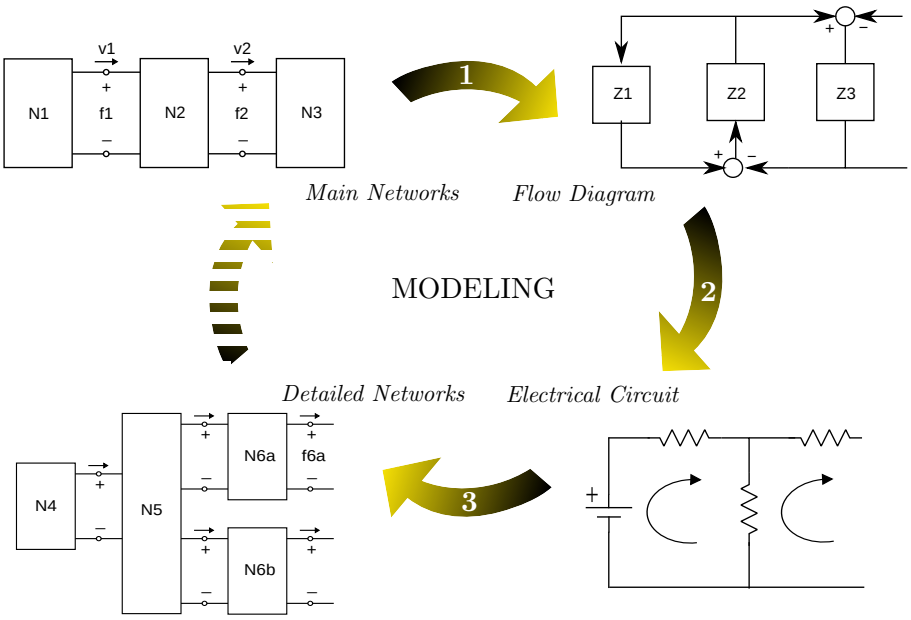

Figure 1.2.1: Top-Down-Top Modeling Methodology.

how energy is transferred between the components of the system. This allows an energy based analysis of the system which other representation domains can not offer.

Teleoperation Tools

The Position-Force computed architecture is energy consistent in that the operator interacts with the environment through a *tool*. The tool is an abstraction of the system composed of a haptic device, a communication channel and a slave robot. Energy is thus transferred to the environment by virtue of the tool. The tool can be given the physical meaning of a long and flexible beam in the mechanical domain, or a transmission line connected to a pair of impedances in the electrical / wave domain using the wave variables formulation. The tool is in essence an energy carrier. For instance, the transmission line model is in this context of great benefit since it is a delay-based model which can very well embed the tool.

A fundamental question is whether or not the concept of tool can be generalized to any teleoperation system. For instance, in the Position-Force measured architecture there is no such tool, in the above-described sense, but rather a direct connection between the master device and the environment; the master receives the interaction force that is sensed by the sensor, ignoring the fact that there is a slave robot interacting with the environment. The lack of a tool does not allow a transfer of energy since there is no medium or carrier through which energy can travel. The interpretation of the Position-Force measured is a master device in direct contact with the environment. Instead of a tool we speak of a *connection*. This connection is described by the commanded velocity to the slave, $\boldsymbol{v}_m$, and the measured force in the environment, $\boldsymbol{F}_{\text{msr}}$.

In the following we develop on the two exposed concepts of *tool* and *connection*. Fig. 1.2.2 shows a teleoperation scheme based on a tool. This representation is valid for architectures such as Position-Force computed or a Position-Position. This type

teleoperation can be represented as a cascade of three networks: the operator, the tool and the environment. The tool is such that allows energy to be transferred between operator and environment. Fig. 1.2.3 shows the network representation of a tool based system.

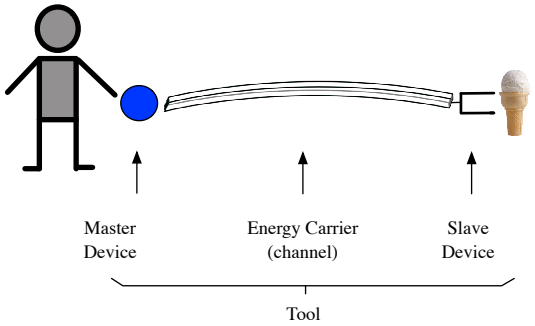

Figure 1.2.2: Teleoperation based on a Tool

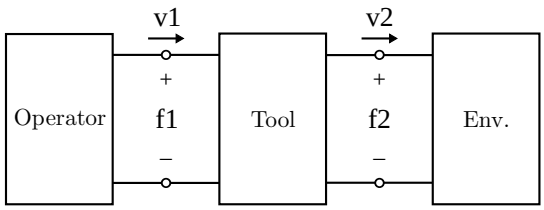

Figure 1.2.3: Network representation of a teleoperation system based on a Tool

On the other hand, Fig. 1.2.4 shows a teleoperation scheme without a tool but with a connection. Teleoperation without tool is given by the commonly used Position-Force measured architecture. The master device is directly attached to the environment through a connection instead of a tool. The connection is provided by the commanded master position and the measured force from the environment. The assumption is thus that the master *is* in the environment. In this type of schemes there is no intermediate medium which allows the energy to be transferred from on side to the other. The only possible transfer is the instant mechanical energy transfer, the same way humans interact with the environments without any tool. Fig. 1.2.5 shows the network representation of a connection based system.

The treatment of the communication channel has been matter of discussion in many publications. Indeed, a data channel linking two physical systems, as is the case of teleoperation (tool or connection based), has been proved to be a source of virtual energy and thus a cause of system instability [11]. The reasons lay into the fact that such channels are used to link physical systems but they miss physical meaning themselves. By way of illustration, a very long flexible beam connecting one mass to another could not ever become unstable (unless both masses would actively be moved in order to excite resonance frequencies). Instead, typical data channels, exchanging positions and forces for instance, implicitly reproduce the behavior of an ideal weightless infinitely rigid bar, but with delay. This is an element which cannot be physically modeled and misses

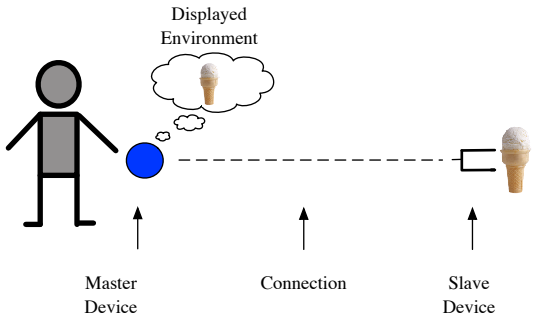

Figure 1.2.4: Teleoperation based on a direct connection to the environment

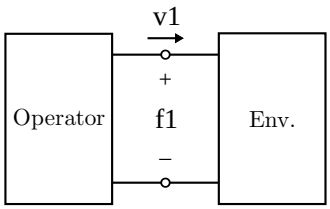

Figure 1.2.5: Network representation of a teleoperation system based on a Connection

therefore coherence with the rest of the system, i.e. master, slave, etc. The secular work based on the scattering parameters [11], or the wave variables formulation [73], uses a transmission line model for representing the communication channel. The data channel is thus given a physical meaning, i.e. a transmission line, and benefits from its physical characteristics, as is the passive nature of such elements, even in presence of time delay.

In general, the *tool* based system has the benefit that the tool can be shaped in many different manners. For instance through a spring, a spring with a damper, a long flexible beam, a transmission line, etc. In other words, the tool accepts many different shapes and all of them share the capability of transferring energy. Some of these tools can even incorporate time delays, as is the case of the transmission line, mentioned above. Instead, the *connection* based systems are in general harder to handle since a priori they do not allow to shape the connection in any possible form, that is, a connection can not benefit from physical properties the same way the tool intrinsically can. Thus the transfer of energy between operator and environment can only be immediate and direct. For instance, a wave variables representation of a position - force measured is in principle not possible [2].

One of the main contributions of this thesis is the definition of an energy carrier for those architectures lacking of a tool or for those where the tool is not obvious. Once the energy carrier is defined it is possible to modulate it such that the energy is transferred through a communication channel, coping thus with any communication channel characteristics.

[2] Wave variables schemes are in principle only possible in Position-Force computed architectures.

1.3 Haptic Telepresence

Telepresence is the feeling of existing in a location other than where the individual actually is, and the capacity of interacting in it. Feelings of being present somewhere else can be artificially produced to individuals by using a set of technologies which capture sensorial data from the distant reality, such as vision, audio or haptic information, and reproduce it locally by means of a Human-Machine-Interface (HMI). Interaction between individual and distant environment takes place by conveying individual's actions and reactions, such as spoken commands or manipulation actions, to the distant location. A tele-robotic system reproduces such individual's commands. In particular, the haptic channel is appealing because it allows to locally reproduce remote kinesthesia and tactile sense, two fundamental perceptions for environment manipulation. Telepresence extends thus human sensorial and manipulative capabilities to far / unreachable locations. Transparency describes the discrepancy between remote and local presence; ideal transparency means that the user is not able to distinguish remote presence to local presence. A good starting point in the haptics field is [7], [8], [6], [30], [90].

The term *Telemanipulation* suggests the act of handling an object which exists in a remote or inaccessible location and is commanded by human will, from the local site. In these situations, the perception of the interaction between the robot manipulator and the manipulated object by the user is essential in order to successfully complete the required task. This perception can be mediated through the different sensorial modalities. Transferring the kinesthesia from the distant manipulated environment, that is, interaction forces and torques, induces new dynamics to the human movements. Thus, the commands are not uni-directional but rather bidirectional since slave plus environment and master system plus human operator interact dynamically. This type of tele-action is called bilateral teleoperation. Bilateral Control is the discipline which investigates the closed-loop circuit created between the human operator and the remote environment. Special control methods are hereby applied in order to stabilize a closed loop system that often includes time delay, package loss, unavoidable non-linearities and subsystems that cannot be completely modeled, as the human operator and the remote environment. The fundamentals of bilateral control and teleoperation are well reviewed in [114], [73], [60] and [25].

Telepresence systems are of great interest for a wide range of applications. In the context of the SFB-453 Collaborative Research Centre, *High-Fidelity Telepresence and Teleaction* [4] several application fields have been targeted, such as space telepresence, telemedicine or multi-user assembly scenarios. While they all present different requirements and targets, the control problematic is rather similar and thus common methods and technologies can be applied. In [58] the two-armed DLR Justin robot is control through by means of telepresence using a human scaled haptic interface [54].

In the field of space robotics, the following experiments are highlighted: The first robot in space, which has been remotely controlled from ground, is the Robot Technology Experiment (ROTEX), aboard the space shuttle Columbia in 1993, [53], [51]. The operational modes were tele-sensor-programming (learning by showing), automatic (preprogrammed on ground), and teleoperation on-board (an astronaut controlled the robot using a stereo monitor). Further, a teleoperation by a human operator from ground, using predictive computer graphics, was performed, [49], [52]. ETS VII is a Japanese

Engineering Test Satellite (ETS) capable of demonstrating bilateral teleoperation in space [55], [117], [118]. The spacecraft, consisting of a pair of satellites, was launched in 1997. Autonomous capturing of the smaller target satellite, inspection procedures and a series of manipulation operations was demonstrated. See [102] for a review of delayed teleoperation from the early days, covering the first robot technologies from the 1960's to the 1990's.

The ROKVISS experiment (Robotic Component Verification on the ISS), [9] , [84], [17], launched in 2005, was composed by a 2 DoF robot equipped with video cameras and torque sensors. The robot was installed on the outer part of the russian module of the ISS. A force reflecting joystick along with the video streaming data was used to telemanipulate the robot.

Recently, experiments to prove feasibility of telepresence as a mean for on-orbit satellite servicing missions have been performed, [105]. In the ARTEMIS experiment [104], [106], [67], the european geostationary satellite Artemis was used as space mirror to communicate the HMI and an emulated malfunctioning satellite. The space link provided a mean delay of 650ms and a contact window of one to three hours. In [37] and [36] a discussion on the applicability of telepresence technologies for space missions compared to manned missions is given.

The Deutsche Orbitale Servicing Mission (DEOS) [1] will demonstrate diverse Satellite On-Orbit Servicing scenarios such as rendezvous, docking, inspection, capture, stabilization and servicing, and controlled de-orbiting of the target and servicer compound. In this connection two modes for commanding the servicer are foreseen. On the one hand, there will be active ground control via telepresence, i.e. a control with instantaneous feedback to the human operator. On the other hand, it will also be possible to passively monitor autonomous operations from ground.

One of the most relevant terrestrial application of teleoperation is the minimally invasive robotic surgery (MIRS), [68], [77], [78]. In the MIRS, the instruments are not directly manipulated by the surgeon anymore but rather held by specialized robot arms which are remotely commanded by the surgeon, who comfortably operates from an input console. The surgeon virtually regains direct access to the operating field inside the patient by having 3D endoscopic sight, force feedback, and restored hand-eye-coordination. Shared autonomy and human-robot cooperation is in general a promising approach in the medical field [29], [46].
The DLR telesurgery system, MIROSURGE [57], [38], consists of a bi-manual HMI (the master) and a 3 surgical MIRO robots (the slave), designed to be a flexible configurable platform. Two robots carry surgical instruments and one carries a stereo video laparoscope resulting in a complex system with 41 degrees of freedom, [110].

The bilateral control of telepresence system is not different from other control fields in the sense that the pursuit of stability often compromises performance, or transparency in the context of telepresence, once the system constraints are established. This trade-off is a common denominator in every single approach dealing with bilateral control [60], [116]. One of the most accounted issues in haptic telemanipulation scenarios is the time delay that affects the communication channel. The time delay is inherent on any telepresence system (i.e.*tele* is a Greek prefix which means "distant"). The handling of the time delay has gathered a great deal of attention in the field of teleoperation. The

communication delay of the transmissions between human operator and environment is a function of the length of the closed loop. Special methods must be applied to control loops such as the one in the afore mentioned ARTEMIS experiment, whose length was in the order of 70,000 Km.

One of the most remarkable approaches in dealing with time-delayed telepresence is the passivity criteria. Passivity is a sufficient condition for stability and provides the nice feature that system passivity is granted by passivity of all its subsystems. Moreover, passivity of a system can be analyzed without an exact knowledge of its contents. It is therefore a useful tool which can be used as design rule in those systems which incorporate communication elements, since, as it has been shown, delay is source of activity. A good example are the Scattering transformation [11] and its Wave Variables formulation [73], [75], which has become a classical approach in delayed teleoperation.

Most approaches that deal with delayed teleoperation end up using conservative techniques to detriment of the transparency and usability of the teleoperation system. In order to ensure passivity of the system, the bilateral control often introduces elements, which dissipate more energy than the strictly needed to compensate the energy introduced by the delayed communications. Wave variables -based methods, for instance, do present a non-lossy characteristic after applying the wave transformation; however, damping elements are then needed to minimize wave reflections and to achieve impedance matching [73] between master and slave.

1.4 Motivation

The work presented in this thesis builds from the idea of using the Time Domain Passivity Control approach (TDPA) [93], [92], in the context of time delayed teleoperation. The adaptive nature of the TDPA makes it a powerful tool in delayed scenarios. Besides time delay, communication channels often include package loss and variation of the delay. In general, these channel characteristics can not be modeled. This represents a big challenge in the field of control theory since most classical control tools cannot deal with such channel characteristics, which, besides creating a very long closed loop system, they are highly non-linear and cannot be circumvented.

A second motivation has been the search of a general solution for any possibile teleoperation scheme. A solution that applies to any possible architecture, be a Position-Force, be a Position-Position or any three or four channel architectures. Furthermore, a the methods should allows to design teleoperation systems for any real teleoperation scenario, targeting real field applications with real communication channels. In a fast changing world with innumerable high technological achievements, the demand on telepresence technologies increases every day. The hope is that this work will contribute into serving those demands.

1.5 Contributions

The main contributions of this work involve the following designs and experimental setups:

- Modeling: An augmented representation has been developed, which allows an accurate description of teleoperation system in terms of energy flows. This representation is valid for any known control architecture, that is, it copes with any input/output channel relationship. The concept of Time Delay Power Network (TDPN) has been developed and represents the fundament of these augmented representations. This is shown in Chapters 1 and 3.

- Stability: On the base of the Time Delay Power Network (TDPN), a distributed controller structure based on the Time Domain Passivity Control Approach (TDPA) is presented in Chapter 4. Attaching a pair of Passivity Observers / Passivity Controllers (PO/PC) at each side of the TDPN ensures passivity for any given communication channel characteristics.

- Design: Several architectures ranging from the classical Position-Force computed scheme to the four-channels architecture, are developed on the basis of TDPNs and distributed PO/PCs. In fact, the presented design methods are independent from the communication causality and can be thus applied to any conceivable architecture. This is shown in Chapter 5.

- Internet and Space communication links: The above tools and methods have been tested in different master - slave systems and different communication channel. Chapter 6 presents results of a coupled master and slave system via the Internet and through geostationary satellite ASTRA.

1.6 Outline

- Chapter 1 introduces the instruments used throughout this thesis. The mathematical modeling of lumped electromagnetic phenomena and its analysis constitutes a backbone for the methods explored in this work. It will be seen how teleoperation systems can be modeled in the electrical domain by virtue of the electro-mechanical analogy. Further, some basic concepts related to time delayed teleoperation will be given.

- Chapter 2 presents an essential component that will be necessary in the development of the methods later introduced in this work: The Time Delay Power Network (TDPN). The TDPN is defined as a two-port network that masks a fundamental communication element and allows the interconnection of electromechanical devices that exchange mechanical energy, be them robots connected to other robots, haptic devices connected to virtual environments or haptic devices connected to robots. As will be seen, the analysis based on the energy observation of the TDPN ports allows model free controller designs. The TDPN forms the basis of a general stability treatment valid for any teleoperation architecture.

- Chapter 3 presents the stability analysis of a delayed force reflecting teleoperation system using the Time Domain Passivity Control approach. An energy analysis of the communication channel is presented on the basis the TDPNs, the network representation of a fundamental communication element. The TDPN is a network which describes the energetic coupling between both sides of any teleoperation

system. The aim of this chapter is to show a systematic approach for treating passivity of the TDPN while maximizing performance using energy considerations. This treatment forms the basis of a general stability treatment valid for any teleoperation architecture, presented in the next Chapter.

- Chapter 4 combines the results of the previous two. Passivity is thus applied to a variety of control architectures that have been augmented on the base of TDPNs. The combination of TDPN and PO/PC elements provides a complete framework to design teleoperation architectures in any conceivable configuration and operating conditions. Next to the formal descriptions a set of experimental results are presented.

- Chapter 5 describes an experiment to show the performance of the presented methods in a real distributed master and slave setup using a combined Internet and Space communication link. The space link is based on the geostationary communications satellite ASTRA, which has been used as a data package mirror server. Furthermore, this chapter presents the mathematical formulation to adapt the presented control methods to the multi DoF cases.

- Chapter 6 concludes this thesis.

Chapter 2

Background on Bilateral Control

This chapter formally introduces some fundamental instruments used throughout this work. The mathematical modeling of electromagnetic phenomena with lumped elements and its analysis constitutes a backbone for the methods explored in this work. It will be seen how teleoperation systems can be modeled in the electrical domain by virtue of the electro-mechanical analogy. A literature review is given, which will be used as staring point for the later development of the proposed methods.

2.1 Introduction

The energetic relationships established between a human operator using a haptic device to telemanipulate a physical environment through a slave robot are complex and pose a challenging control aspect in the fields of haptics and teleoperation. Mechanical energy is exchanged between these actors through the closed loop system created between them. Stability can become an issue in these kind of systems since it is hard to obtain precise analytical models of the operator, the haptic device, the slave robot and the environment. Often, assumptions related to the human and the environment must be taken, which can lead to conservative designs.

In this chapter, some fundamental elements of the network theory are reviewed with a special focus on their application to delayed teleoperation. As it will be seen, the block diagram representation (often referred as flow diagram) lacks some features that will be needed for the treatment based on energy tackled in this work and, in particular, for the passivity analysis. The benefits of the network modeling are thus highlighted though some examples that illustrate the derivation of network models for teleoperation

schemes. Stability of delayed systems is furthermore introduced along with a review of some well established methods that cope with delayed and un-delayed system.

2.2 Network Theory

The network theory comes from the studies and synthesis of electrical circuits. It allows to describe vibrating systems of different natures (electrical, mechanical, thermodynamical, etc.) in terms of networks. The network is an element which masks a set of elements interconnected and is represented by one or more ports. A port is the interconnection medium to other networks. One of the most interesting aspects of representing a system as a port interconnection is that their networks can explicitly reveal how the energy flows within the system, since the port is by definition an energy transfer medium.

On the other hand, the bond representation is not associated to any physical phenomena, as is the case of the network based representation. The bond representation allows an abstract energy description of the interconnected elements of systems of different natures. In this sense, the bond representation would fit in this work as well. The network representation is chosen because of two reasons. The first is that of historical reasons; many fundamental state-of-the works in the field of teleoperation are developed in the electrical domain or network representation. The second reason, which also explains the first, is that, in general, the electrical domain and the network representation are proficient frameworks with powerful analysis and design tools. The fact that they are associated to a physical phenomena is here seen as a benefit since they provide a higher degree of intuitiveness without loosing generality. As will be seen, intuitiveness and generality are key qualities in the process of mapping the mechanical system into the electrical domain.

Electric Lumped Networks

As the name indicates, network methods for modeling have their historical roots in electrical circuit studies. Generally speaking, a network is a group or system of interconnected elements. In the electrical domain, a network masks an electrical circuit, i.e. a collection of electrical components which accomplish a specific task. Sometimes it is convenient to speak of an electrical circuit as a network, de-emphasizing the internals of the circuit while stressing the interconnectivity medium, i.e. the port (see Fig. 2.2.1). Indeed, the port, or *power port* to be accurate, is a two-terminal interface which allows connectivity between networks and thus a transfer of energy. A power port is entirely represented by the pair of dual variables, current and voltage, whose product is power. These variables are often categorized as being a physical instance of a more generic type of variables, *flow* and *effort*, which live in dual vector spaces. In order to formally define a *power port*, the concept of space duality between variables is first introduced.

Definition 1 ***Dual Space***
Let $\mathcal{V}$ be a vector space, its dual space $\mathcal{V}^*$ is the set of linear maps from $\mathcal{V}$ to $\mathbb{R}$:

$$\mathcal{V}^* = \left\{ f : \mathcal{V} \to \mathbb{R} | \forall v_1, v_2 \in \mathcal{V} \alpha_1, \alpha_2 \in \mathbb{R} f(\alpha_1 v_1 + \alpha_1 v_2) = \alpha_1 f(v_1) + \alpha_2 f(v_2) \right\}$$

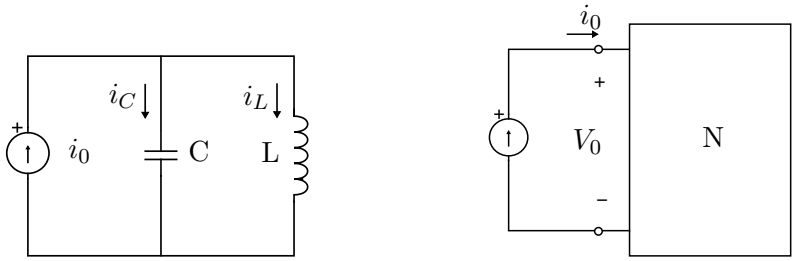

(a) L-C circuit (b) 1-port Network

Figure 2.2.1: L - C circuit and its network representation.

$\mathcal{V}^*$ is a vector space with the same dimension of $\mathcal{V}$, and the elements belonging $\mathcal{V}^*$ and $\mathcal{V}$ are said to be dual respect each other.

Definition 2 ***Duality Product***
Given $v \in \mathcal{V}$ and $v^* \in \mathcal{V}^*$, the duality product is defined as:

$$\langle , \rangle : \mathcal{V} \times \mathcal{V}^* \to \mathbb{R} \langle v, v^* \rangle = v^*(v)$$

In each physical domain there is a pair of dual variables, called *power conjugate* variables, whose duality product is power. These variables are abstractly defined as *flow*, f, and *effort*, e, without physical phenomena association, so that:

- $f \in \mathcal{F}, e \in \mathcal{E} \quad s.t. \quad \mathcal{F} = \mathcal{E}^*$
- $\langle f, e \rangle = P$, i.e. the duality product represents power.

An alternative nomenclature for power conjugate variables derived from [33], coming from the electrical studies, is defined as *through* and *across* variables.

Physical Domain	Flow / Across	Effort / Trough
Electrical	Current	Voltage
Translational Mechanics	Velocity	Force
Rotational Mechanics	Angular Velocity	Torque
Thermodynamical	Temperature	Entropy Flow
Hydraulic	Pressure	Volume Flow

Table 2.1: Flow and Effort correspondences in the various physical domains.

Table 2.1 shows the map of efforts and flows to the various physical domains. Definitions 1 and 2 allow to introduce the concept of power ports.

Definition 3 ***Power port***
Let $\mathcal{F}$, $\mathcal{E} = \mathcal{F}^*$ be the flow and effort vector spaces; a power port is defined as $P = \mathcal{E} \times \mathcal{F}$. Given $f \in \mathcal{F}$ and $e \in \mathcal{E}$, the product $\langle e, f \rangle$ is the power traversing the power port.

Power ports are the medium through which a physical system exchange power with the external world, and, in particular with other physical systems. The interconnection through a port between two systems is an energy preserving structure.

In the electrical domain only *lumped circuits* will be considered. A *lumped circuit* is composed of *lumped elements*. Furthermore, a terminal pair is said to be a network port when the current into one is identical to the current out of the other.

Definition 4 ***Lumped element***
An element is said to be lumped if its physical dimensions are small compared to the wavelength corresponding to the highest frequency of operation of that element, that is, $L_c \ll \lambda$, being L_c the length of the circuit and λ the operating wavelength.

Further, the lumped element model makes the simplifying assumption that each element is a finite point in space and that the wires connecting elements are perfect conductors.

Otherwise, more general models must be considered, such as the distributed element model, whose dynamic behaviour is described by the Maxwell equations.

Definition 5 ***Network Function***
It describes the response of a network to an excitation signal. In LTI systems the response has the same frequency as the excitation. If the excitation is a complex sinusoidal signal, the response is also a complex sinusoid. In that case the function can be represented by a rational function of polynomials that are function of the complex frequency $s = \sigma + jw$. Formally, the network function $\mathcal{N}(s)$ is defined as:

$$\mathcal{N}(s) = \frac{\sum_{j=0}^{m+1} a_j s^j}{\sum_{k=0}^{n+1} b_k s^k} = \frac{\prod_{j=0}^{m+1} (s - z_j)}{\prod_{k=0}^{n+1} (s - p_i)}. \tag{2.1}$$

Where z_j are the zeros of the transfer function, i.e. $z_j \mid N(s) = 0$, and p_i its poles, i.e. $p_i \mid N(s) = \infty$.

A network function can take the form of an impedance or an admittance depending on the causality (input / output relationship). If the input is a voltage and the measured signal (output) is a current the network behaves as an impedance. In the dual case the network behaves as an admittance.

Network Properties

The port of a network describes the overall behavior of the network, which masks a system. Indeed, the dual power of the conjugated pair voltage V across, and current I through, define electric power, which, if integrated, defines electric energy. This behavior leads to the classification linear, non-linear; time-variant, time-invariant; passive and active.

Definition 6 ***Linear and Nonlinear Networks***

In a linear network, the relationship between voltage and current is described by a linear equation. Let a network be characterized by

$$F(x_i) = y_i,$$

where x_i is the input and y_i is the output, and $F(.)$ denotes some function. The network is linear if, and only if, it satisfies the principle of superposition and homogeneity. This is,

$$F(\alpha_1 x_1 + \alpha_2 x_2) = \alpha_1 F(x_1) + \alpha_2 F(x_2) = \alpha_1 y_1 + \alpha_2 y_2,$$

where α_1 and α_2 are arbitrary constants, and x_1 and x_2 are any two allowable inputs.

Definition 7 ***Time invariant Networks***

A network characterized by $F[x(t)] = y(t)$ is said to be time invariant if

$$F[(x(t - t_0)] = y(t - t_0),$$

i.e. the output depends solely on the shape of the input, but not on the time of application.

A network composed of time-invariant elements is necessarily time-invariant. Nevertheless, a network composed of time-variant elements may still exhibit time invariant terminal behavior.

Definition 8 ***Passive, active and lossless networks***

Let $v(t)$ and $i(t)$ be the conjugate pair, voltage and current, at the port of a one-port network. Then the energy delivered to the network is the integral of the dual product of the conjugate pair. This is

$$W(t_o, t) = \int_{t_0}^{t} v(\tau) i(\tau) d\tau.$$

A network is said to be passive if, and only if

$$W(t_o, t) + E(t_o) \geq 0 \qquad \forall t \geq 0, \tag{2.2}$$

where $E(t_o)$ is the energy in the network at $t = t_0$. Otherwise the network is said to be active.

A lossless network is one which satisfies:

$$W(t_o, t) + E(t_o) = 0 \qquad \forall t \geq 0, \tag{2.3}$$

In other words, a network is passive if it dissipates more energy than it generates.

Definition 9 ***Current, voltage and energy sign conventions***

If the integrated dual product of a current entering the network and a positive voltage defined at the first terminal of the port with respect to the second one, is positive, the network is passive. Else, if it is negative, it is active. See Fig. 2.2.2. That means that energy flowing into the network results in positive energy. It is equivalent to speak of energy being injected from the outside of the network or energy being dissipated inside the network. Both result in a passive behavior.

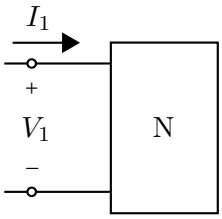

Figure 2.2.2: Current, Voltage and Energy sign conventions.

Two-port Networks

In order to begin with the network based analysis, the concept of two-port networks is first introduced. Two-port networks are a special case of four terminal networks where the port condition is met in both pair of terminals. Fig. 2.2.3 illustrates a four terminal network and a two-port network.

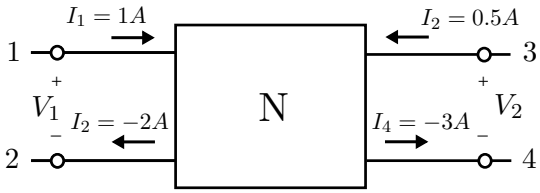

(a) Four terminal network

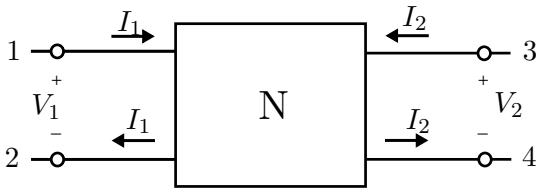

(b) Two-port network

Figure 2.2.3: The second network has equal and opposite currents in each terminal pair. The first one does not meet the port requirement.

Two-port networks are used to describe input / output relationships between a two-terminal pair. (or ports). This type of networks are also called four-terminal networks. The network analysis requires the following conditions to be met:

- Linearity, as described in Def. 6.
- No initial stored energy inside the network.
- Absence of independent current or voltage sources.
- Port condition as described in Def. 3 must be satisfied on both network ports.
- The port is the only permissible interconnection interface to other networks or elements.

Depending on the chosen input / output causalities, different relationships based on port voltage and currents are possible. For instance, relating output port voltages to

input port currents leads to the well known impedance parameters (Z) representations. The network is entirely represented by a group of four impedance parameters:

$$\begin{pmatrix} V_1 \\ V_2 \end{pmatrix} = \begin{pmatrix} Z_{11} & Z_{12} \\ Z_{21} & Z_{22} \end{pmatrix} \begin{pmatrix} i_1 \\ i_2 \end{pmatrix} \tag{2.4}$$

$$Z_{ij} = \frac{V_i}{I_j}\Big|_{I_n=0} \qquad n = \begin{cases} 1 & \text{if } j = 2, \\ 2 & \text{if } j = 1. \end{cases}$$

Other parameter combinations, i.e. input / output relationships, are possible, as the admittance (Y), the transmission (T) or the scattering (S). The choice depends on the system to be analyzed. In the fields of haptics and teleoperation, the Z-parameters are often used to describe input / output relations between master and slave, e.g. [89], [39].

One important characteristic of two-port networks has to do with its energetic behavior and its stability. The definition follows:

Stability

We consider a two-port attached to a voltage source with magnitude V_s and internal impedance Z_s at one side and a load, Z_L, at the other. The circuit is shown in Fig. 2.2.4.

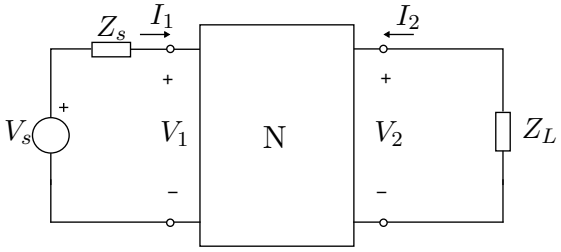

Figure 2.2.4: Two-port network terminated with a voltage source and a load.

The system can be described by using the impedance parameters as:

$$\begin{bmatrix} V_s \\ V_2 \end{bmatrix} = \begin{bmatrix} Z_{11} + Z_s & Z_{12} \\ Z_{21} & Z_{22} + Z_L \end{bmatrix} \begin{bmatrix} I_1 \\ I_2 \end{bmatrix}. \tag{2.5}$$

Stability means that the transfer function is zero for any passive terminations. Therefore we have that:

$$\begin{bmatrix} V_s \\ V_2 \end{bmatrix} = \begin{bmatrix} Z_{11} + Z_s & Z_{12} \\ Z_{21} & Z_{22} + Z_L \end{bmatrix} \begin{bmatrix} I_1 \\ I_2 \end{bmatrix} = 0. \tag{2.6}$$

The non-trivial solution to that condition can be obtained by equating the determinant of the matrix to 0 as:

$$(Z_{11} + Z_s)(Z_{22} + Z_L) - (Z_{21} Z_{12}) = 0. \tag{2.7}$$

Note that this equation can be rewritten as:

$$1 - \frac{(Z_{21} Z_{12})}{(Z_{11} + Z_s)(Z_{22} + Z_L)} = 0. \tag{2.8}$$

which is the classical form of the stability condition obtained by feedback system analysis.

The transfer function and the corresponding characteristic equation can be as well expressed using the admittance or hybrid parameters, yielding to the same results. Choosing one or the other parameters is a matter of convenience which depends on the circuit to be analyzed.

Absolute Stability

Absolute stability for a two-port network is given when stability only depends on the network parameters for any passive terminations (i.e., loads at each port). Thus, if the system represented in Fig. 2.2.4 is designed to be absolute stable, it is susceptible to be unstable for a group of non-passive Z_L and Z_s values, which produce poles on the transfer function of (2.6) on the right half of the complex-frequency plane.

Definition 10 ***Absolute (or unconditional) Stability*** *A two-port network is said to be absolutely stable under all possible passive port terminations if its input and output impedances are positive real. This is equivalent to require the following conditions:*

1. *The impedances have no poles in the right half of the complex-frequency plane.*
2. *Any poles of the impedances on the imaginary axis are simple with real and positive residues.*
3. Re $[Z(jw) \geq 0]$, *for all* w.

A convenient formulation for the above definition of *absolute stability* is given by the *Llewellyn's criterion for absolute stability* [66]:

1. $Z_{11}(s)$ and $Z_{22}(s)$ have no poles in the right half plane.
2. Any poles of the $Z_{11}(s)$ and $Z_{22}(s)$ on the imaginary axis are simple with real and positive residues;
3. For all real values of w:

$$\text{Re } Z_{11} \geq 0, \text{Re } Z_{22} \geq 0, 2\text{Re } Z_{11}\text{Re } Z_{22} - \text{Re } (Z_{12}Z_{21}) - |Z_{12}Z_{21}| \geq 0. \quad (2.9)$$

The most important restriction of the absolute stability criterion is that the loads attached at each port of network must be passive. In the field of haptics and teleoperation it is often conveniently assumed that the terminations of the network describing the teleoperator are passive. However, these terminations are a human operator controlling a haptic device on one side, and an arbitrary environment on the other. Both terminations can indeed be active [1]. Often it is assumed that the operator will behave in a *passive* manner, that is, even though the operator actively injects energy into the system, the operation is soft enough so that those frequencies that could lead the system to instability will not be excited.

The *Llewellyn's criterion* has been successfully applied in the field of teleoperation as a tool for designing stable controllers without time delay [39], [7], [5], with the mentioned assumptions, that both, environment and the operator are passive.

[1] The operator together with the haptic device is the primary energy source for the system, responsible thus for the movement of the system. An example of active environment is a tele-handshaking.

Passivity of Two-port Networks

Definition 11 ***Passivity of a two-port network*** *Let $V_1(t)$, $I_1(t)$, $V_2(t)$ and $I_2(t)$ be voltages and currents of the conjugate pairs at each port of the network. Using the sign convention as defined in Fig. 2.2.5 , the energy delivered to the network is the sum of the energy contribution at each port:*

$$E^N(t) = E^1(t) + E^2(t) \quad \forall t \geq 0. \tag{2.10}$$

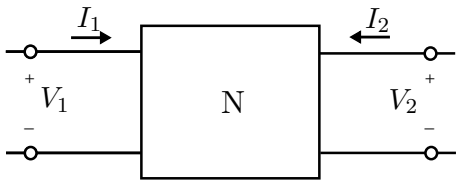

Figure 2.2.5: Two-port network.

Where each energy value at left and right ports of the two-port network, $E^1(t)$ and $E^2(t)$ is the integral of the dual product of the respective conjugate pair. This is

$$\begin{aligned} E^1(t) &= \int_0^t P^1(\tau)d\tau = \int_0^t V_1(\tau)I_1(\tau)d\tau, \quad \forall t \geq 0, \\ E^2(t) &= \int_0^t P^2(\tau)d\tau = \int_0^t V_2(t)I_2(t)d\tau, \quad \forall t \geq 0, \end{aligned} \tag{2.11}$$

being P^1 and P^2 left and right port powers. The two-port network will be passive as long

$$E^N(t) \geq 0, \quad \forall t \geq 0. \tag{2.12}$$

Passivity Using the Immitance and the Hybrid Parameters

The above definition is equivalent to require that

$$\mathrm{Re}[V_1(s)I_1^*(s) + V_2(s)I_2^*(s)] \geq 0 \quad \text{for } \mathrm{Re}\ s \geq 0, \tag{2.13}$$

where $I^*(s)$ is the complex conjugate of $I(s)$. From (2.4), the previous condition becomes:

$$\mathrm{Re}[Z_{11}(s)I_1(s)I_1^*(s) + Z_{12}(s)I_1^*(s)I_2(s) + Z_{21}(s)I_1(s)I_2^*(s) + Z_{22}(s)I_2(s)I_2^*(s) \quad \text{for } \mathrm{Re}s \geq 0. \tag{2.14}$$

Therefore, a linear two-port network is passive if and only if (2.14) is positive real. This implies that none of the Z-parameters can have any poles in the right half plane. In addition, if any of the Z-parameters have simple poles on the imaginary axis, positiv realness of (2.14) implies that the residues of the Z-parameters satisfy so-called *residues conditions* [64], [72], [111], [31]. These conditions and the above are known as the *Raisbeck* passivity criteria [88]:

Theorem 2.2.1 *A two-port network is passive if the following three conditions are satisfied (Z or Y matrix description) (Raisbeck Passivity Criteria):*

1. *The Z-parameters have no poles in the right-half-plane.*
2. *Any pole of the Z-parameters on the imaginary axis, jw, are simple, and the residues of the Z-parameters at these poles satisfy the following conditions:*

$$\begin{aligned} &k_{11} \geq 0 \\ &k_{22} \geq 0 \\ &k_{11}k_{22} - k_{12}k_{21} \geq 0, \quad \textit{with } k_{12} = k_{21}^* \end{aligned} \tag{2.15}$$

3. *Real and imaginary parts of the Z-parameters satisfy the following condition for $0 \leq w \leq \infty$:*

$$\text{Re } Z_{11}(jw) \text{ Re } Z_{22}(jw) - \text{Re } Z_{12}(jw) \text{Re } Z_{21}(jw) \geq \frac{|Z_{21}(jw)Z_{12}(jw)|^2}{4}$$

These conditions can be similarly expressed using any of the other Y-, H- or G-parameters. In the fields of haptics and teleoperation the hybrid parameters are often used to represent the system between operator and environment [44], [6]. Requiring passivity of a two-port network expressed with the H-parameters implies that the third condition becomes:

$$4 \text{ Re } H_{11} \text{Re } H_{22} - [\text{Re } H_{12} + \text{Re } H_{21}]^2 - [\text{Im } H_{12} - \text{Im } H_{21}]^2 \geq 0. \tag{2.16}$$

When both H_{11} and H_{22} are zero the system is regarded as ideal transformer or ideal communication channel. In that case the above condition can only be satisfied if:

$$\begin{aligned} \text{Re } H_{12} &= \text{Re } H_{21} \\ \text{Im } H_{12} &= \text{Im } H_{21}. \end{aligned} \tag{2.17}$$

Example 1 *Check passivity for the following two-port network represented through the Z matrix [72]:*

$$Z = \begin{bmatrix} \dfrac{5s}{s^2+9} & \dfrac{s-9}{s^2+9} \\ \dfrac{s+9}{s^2+9} & \dfrac{2s}{s^2+9} \end{bmatrix} \tag{2.18}$$

We first find the residues of Z_{ij} at the jw-axis pole at $s = j3$ as:

$$k_{ij} = (s-3)Z_{ij}|_{s=j3}$$

$$K = \begin{bmatrix} \frac{5}{2} & \frac{1}{2} + \frac{3}{2}j \\ \frac{1}{2} - \frac{3}{2}j & 1 \end{bmatrix}$$

As can be seen the condition (2.15) of Theorem 2.2.1 is satisfied. We need also to check the third condition of Theorem 2.2.1:

$$\begin{aligned} \text{Re } Y_{11}(jw) &= \text{Re } Y_{22}(jw) = 0 \\ \text{Re } Y_{12}(jw) &= \frac{-9}{9-w^2} \\ \text{Re } Y_{21}(jw) &= \frac{9}{9-w^2} \end{aligned} \tag{2.19}$$

Passivity Using the Scattering Matrix

Passivity can analogously be expressed through the scattering parameters. The scattering parameters are specially useful in the context of delayed teleoperation [11], [73] since they form a transformation matrix relating transmitted and reflected wave amplitudes at the network. The application of the scattering parameters in delayed teleoperation unfolds from the studies of the transmission lines field. A transmission line is characterized by having a characteristic length of similar order of magnitude as the operating wavelength, that is, it cannot be considered a lumped element (see Def. 4).

The scattering parameters are formed as linear combination of voltages and currents displayed at the network ports in such a way that they directly represent power. For an n-Port the scattering matrix $\boldsymbol{S}$ is defined as:

$$\boldsymbol{a} = \boldsymbol{S}(s)\boldsymbol{b}(s), \tag{2.20}$$

where $\boldsymbol{a}$ and $\boldsymbol{b}$ are input and output port wave amplitudes and are defined as:

$$\boldsymbol{a} = \frac{1}{2\sqrt{\boldsymbol{R}_o}}(\boldsymbol{V} + \boldsymbol{R}_o\boldsymbol{I}), \qquad \boldsymbol{b} = \frac{1}{2\sqrt{\boldsymbol{R}_o}}(\boldsymbol{V} - \boldsymbol{R}_o\boldsymbol{I}), \tag{2.21}$$

being $\boldsymbol{R}_o$ the $n \times n$ diagonal matrix created by the internal impedances of the sources attached to the network port. $\boldsymbol{R}_o$ is assumed to be positive definite.

For a two-port, we have:

$$\begin{bmatrix} a_1 \\ a_2 \end{bmatrix} = \begin{bmatrix} S_{11} & S_{12} \\ S_{21} & S_{22} \end{bmatrix} \begin{bmatrix} b_1 \\ b_2 \end{bmatrix} \tag{2.22}$$

Taking the network represented in Fig. 2.2.5, the average power absorbed by the network is given by:

$$P = |a_1|^2 - |b_1|^2 + |a_2|^2 - |b_2|^2 = a_1^T a_1 - b_1^T b_1 + a_2^T a_2 - b_2^T b_2. \tag{2.23}$$

Substituting (2.20) in (2.23) yields to the passivity condition:

$$\mathbf{1} - \boldsymbol{S}^T\boldsymbol{S} \geq \mathbf{0}, \tag{2.24}$$

where $\mathbf{1}$ is a 2×2 unitary matrix and $\mathbf{0}$ is the 2×2 null matrix. The condition in (2.24) is also often referred in terms of the norm of the scattering matrix as $\| \boldsymbol{S} \| \geq 1$.

The scattering matrix can be expressed in terms of the hybrid parameters as:

$$\boldsymbol{S} = \begin{bmatrix} 1 & 0 \\ 0 & -1 \end{bmatrix} (\boldsymbol{H}(s) - \boldsymbol{I})(\boldsymbol{H}(s) + \boldsymbol{I}))^{-1} \tag{2.25}$$

[11] showed that the scattering parameters can be used for representing the communication channel of a teleoperation system.

Passivity of network Interconnections

Complex system can be represented as a group of networks connected together allowing network analysis for through all the system. In this sense, a complex system can be understood as a group of subsystem and as an interconnection of networks, each of them fulfilling a specific task and allowing individual analysis.

When networks are connected together it is possible to synthesize two or more networks into an equivalent network. There are three types of connections: Series, parallel and cascade. The equivalent port parameters of the combined network can be found by performing matrix algebra on the matrices of parameters for the component ports. By choosing appropriate parameters, e.g. Z, Y, T, etc., the equivalent one-port or two-port parameter matrix can be extracted.

However, the rules for combining networks and extracting equivalent parameters must be carefully applied since some connections do invalidate the port condition as stated in Def. 3. For instance, a serial connection can result in different currents in the two terminals of a port (e.g. due to ground loop). A convenient validation test to ensure that the individual port parameters hold after the interconnection is the *Brune test* [28].

Definition 12 ***Parallel Connection***

If each terminal of two-port network N_a is connected to the homologous terminal of another two-port network N_b, the overall connection is called two-port parallel connection. (Fig. 2.2.6)

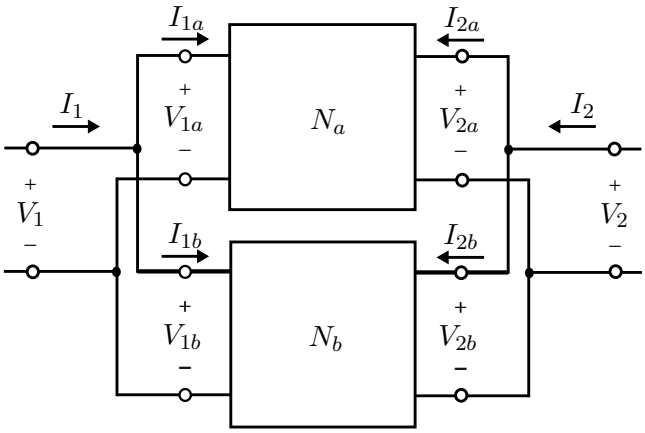

Figure 2.2.6: Two-port parallel connection.

The constraints imposed by this interconnection are:

$$\begin{aligned} V_1 &= V_{1a} = V_{1b}, & I_1 &= I_{1a} + I_{1b} \\ V_2 &= V_{2a} = V_{2b}, & I_2 &= I_{2a} + I_{2b} \end{aligned} \tag{2.26}$$

The combined admittance matrix (Y) of the interconnection is the sum of each admittance matrices, Y_a and Y_b of N_a and N_b respectively, i.e. $Y = Y_a + Y_b$.

Definition 13 ***Series Connection***

If the second terminals of both port of a two-port network are connected to the first terminals of both ports of another two-port network, the connection is called two-port series connection.

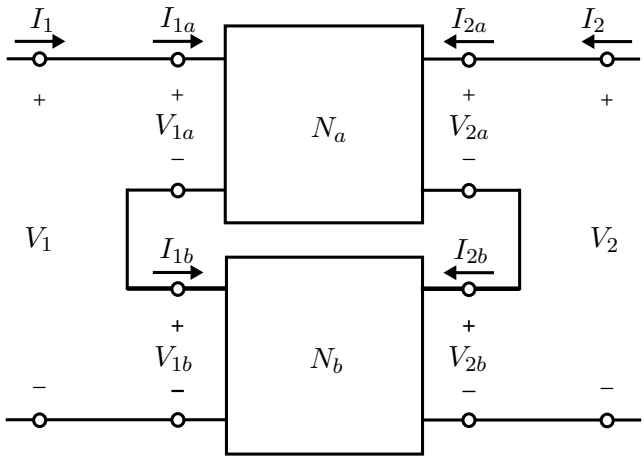

Figure 2.2.7: Two-port series connection.

The constraints imposed by this interconnection are:

$$\begin{aligned} I_1 &= I_{1a} = I_{1b}, & V_1 &= V_{1a} + V_{1b} \\ I_2 &= I_{2a} = I_{2b}, & V_2 &= V_{2a} + V_{2b} \end{aligned} \tag{2.27}$$

The combined impedance matrix (Z) of the interconnection is the sum of each impedance matrices, Z_a and Z_b of N_a and N_b respectively, i.e. $Z = Z_a + Z_b$.

In the series connection there are some networks which do not yield directly to this analysis, i.e. the connection does not preserve power ports. This is illustrated in the following example:

Example 2 *Consider the classical series connection of a two-port network consisting of two resistors, R1 and R2, as shown in Fig. 2.2.8.*

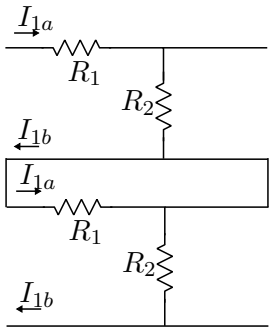

Figure 2.2.8: Two-port wrong series connection.

As can be seen R1 of the lower network has been short-circuited by the connection between two terminals of the right ports. This results in zero current flowing through one terminal in each of the left ports of the two networks. Consequently, the port condition is broken for both left ports of the original networks since current is still able to flow into the other terminal.

Definition 14 ***Cascade Connection***

If the output port of a two-port network is the input port of another network, then the connection is known as cascade connection (Fig. 2.2.9).

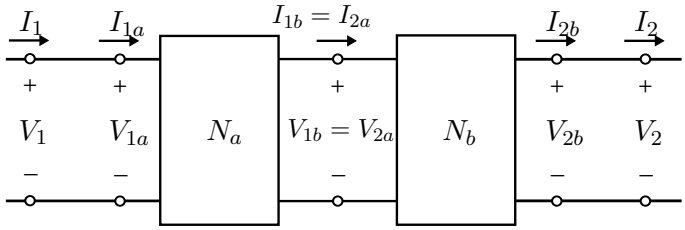

Figure 2.2.9: Cascade connection.

The constraints imposed by this interconnection are:

$$\begin{aligned} I_1 &= I_{1a}, & I_2 &= I_{2a} \\ V_1 &= V_{1a}, & V_2 &= V_{2a} \\ & & I_{1b} &= -I_{2a} \end{aligned} \tag{2.28}$$

The combined transfer matrix (T) of the interconnection is the product of each transfer parameters matrices, T_a and T_b of N_a and N_b respectively, i.e. $T = T_a T_b$.

2.3 Review of the Mechanical - Electrical Analogy

The electrical circuit is one of the most studied oscillating systems. While equations governing oscillating systems as sound or mechanical where developed long time before an electrical circuit was conceived, the electrical circuit theory enjoys a higher status due to higher popularity among the scientific community. The palette of analysis laws and tools is wider than in other disciplines, as the mechanical field for instance. The electrical circuit is graphed as a set of elements, such as resistances, inductances or capacitances, connected through lines and edges from which, concise algebraic forms can be derived by using Kirchoffs Laws.

We begin reviewing the concept of analogy. In general, an analogy is useful because it allows to analyze an unexplored domain by means of elements and laws which belong to another, more proficient one. Formally,

Definition 15 ***Analogy***

If a group of physical concepts or quantities are related to each other in a certain manner, as by equations of a certain form, and another group of concepts or quantities

are interrelated in a similar manner, then an analogy may be said to exist between the concepts of the one group and those of the other group. Structural consistency is maximal when the analogy is an isomorphism.

Definition 16 ***Analogous System***

A system which exhibits identical mathematical behavior to that of another, but physically different, is called an analogous system.

Definition 17 ***Elements***

An element or parameter in an electrical system defines a distinct activity in its part of the circuit. In the same way, in the translational mechanical domain, the rotational mechanical or the acoustical, an element defines a distinct activity in its part of the system. The elements in an electrical circuit are electrical resistance, inductance and electrical capacitance. The elements in a translational mechanics system are mechanical translational resistance, mass and compliance. The elements in a mechanical rotational system are mechanical rotational resistance, moment of inertia, and rotational compliance. The elements in an acoustical system are acoustical resistance, inertance and acoustical capacitance.

There are two possible analogies between the mechanical and electrical fields. The *velocity - current*, regarded as conventional analogy, and the *velocity - force*. In this work, the conventional analogy will be used. In general, the first, introduced in [76], allows better serial / parallel graphical correspondence. By way of illustration, in the conventional electrical - mechanical analogy, the inductance plays a similar role in an electric system to that of a mass in a mechanical system. The stored electromagnetic energy of the inductance $\frac{1}{2}LI^2$ recalls that of the potential energy of a mass $\frac{1}{2}mv^2$. The inductance tends to prevent change of current by generating an electromotive force (emf) of magnitude $L\frac{dI}{dt}$ the same way a mass prevents sudden changes in velocity by generating a reaction force of magnitude $m\frac{dv}{dt}$.

The conventional mechanical-electrical analogy is derived from the fact that for most mechanical systems, an electrical system can be derived such that the differential equations of motion in the two systems expressed in terms of displacement and charge, respectively, will be of the same form. Table 2.2 reports the analog elements and signals in the velocity - current analogy.

Mechanical	Electrical
Force (N)	Voltage (V)
Velocity (m/s)	Current (A)
Displacement (m)	Charge (C)
Impedance (ohms)	Impedance (ohms)
Mass (gr)	Inductance (H)
Stiffness coefficient (N/m)	Inverse of capacitance ($\frac{1}{farads}$)
Friction coefficient (Nm)	Resistor (ohms)
Power (W)	Power (W)

Table 2.2: Analogs in the velocity - current analogy

Example 3 *Mass - Spring - Wall (Serie)*

Consider a mass - spring system, where force is applied to the mass and the other end is attached to a rigid wall, as depicted in Fig. 2.3.1(a). Let m be the mass and k the spring stiffness constant. The system is subject to an oscillation of

$$m\frac{d^2x(t)}{dt^2} + kx(t) = 0$$

Consider now the circuit L - C depicted in Fig. 2.3.1(b). Applying Kirchoff's law the well know equations for this circuit are derived:

$$L\frac{di(t)}{dt} + \frac{1}{C}\int_0^t i(t) = 0$$

Both systems fulfill the following second order linear differential equation:

$$\frac{d^2z(t)}{dt^2} + wz(t) = 0$$

The analogy is here obvious. The following analogs can be extracted:

m (Mass) $\longleftrightarrow$ *L (Inductance),*
k (Spring) $\longleftrightarrow$ $\frac{1}{C}$ *(Inverse of capacitance)*

Furthermore, the same relationship can be found by comparing potential energy of the mass, $E_m = \frac{mv^2}{2}$*, and energy stored in the inductor,* $E_L = \frac{LI^2}{2}$*, being v the derivative of the position, that is, velocity as* $v(t) = \frac{dx}{dt}$*, and i, the derivative of the electric charge, that is, the current of the circuit* $i(t) = \frac{dq}{dt}$*.*

In the situation described in example 3, the two elements are connected in such a way that they share a common velocity. Such a connection results in a series relation. The opposite relation, that is, the parallel connection, results from elements connected in such a way that they are driven by a common force yet having independent velocities.

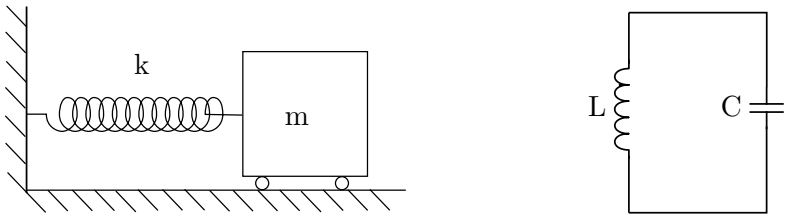

(a) Mechanical System (b) Electrical circuit

Figure 2.3.1: Analogous mechanical and electrical systems: Serial connection.

Example 4 *Spring - Damper (Parallel) Consider a spring - damper system as depicted in Fig. 2.3.2(a). Let K be the stiffness constant and b the damper coefficient. The force applied to the system can be split so that:*

$$F_{ext} = F_b + F_K = b\dot{x} + K\int_0^t \dot{x}$$

Consider now the circuit R - C depicted in Fig. 2.3.2(b). Applying Krichoff's law the equations for this circuit are derived as:

$$V = RI + \frac{1}{C}\int_0^t I d\tau. \tag{2.29}$$

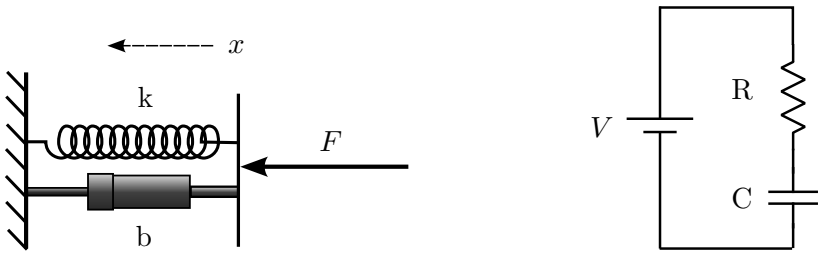

(a) Mechanical System (b) Electrical circuit

Figure 2.3.2: Analog mechanical and electrical systems. Parallel mechanical connection and analogous serial electrical circuit.

2.4 Time Domain Passivity Control

The tool used for stability in this work is the Time Domain Passivity Control Approach (TDPA) [40]. While other stabilization methods could be here considered, the TDPA presents two main advantages which make it distinctly convenient: Simplicity and flexibility. Moreover, the TDPA approach emerges from an ideal-case design, which is one of the main features of the framework. Briefly, the TDPA has two main elements: The Passivity Observer (PO), which monitors the energy flow of a network in the time domain; and the Passivity Controller (PC), which acts as a variable damper to dissipate the energy introduced by the network.

Passivity Observer and Controller for one-port Networks

Recalling Def. 8, the following widely known definition of passivity is used for a one-port network is used.

Definition 18 *The one-port network (Fig. 2.4.1), N, with initial energy storage $E(0) = 0$ is passive if and only if,*

$$\int_0^t f(\tau)v(\tau)d\tau + E(0) \geq 0 \tag{2.30}$$

holds for any admissible forces (f) and velocities (v). Power is defined positive when entering the network. Power is defined as negative when exiting the network. (2.30) states that the energy supplied to a passive network must be always positive.

The conjugate variables that define power, as defined in Def. 3, in such a network system are discrete-time values and the analysis is restricted to systems that have a

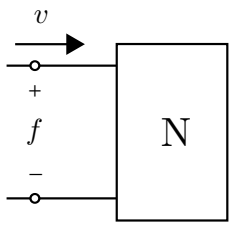

Figure 2.4.1: One-port network system representing components

sampling rate substantially faster than the system dynamics. This assumption allows to introduce the following Passivity Observer, (PO), for a one-port network (Fig. 2.4.1) in order to check the passivity.

$$E_{obsv}(n) = T_s \sum_{k=0}^{n} f(k)v(k), \tag{2.31}$$

where $E_{obsv}(n)$ is the observed energy and T_s is the sample time of the system. For and M-port network with $E(0) = 0$, the PO is the sum of each port contribution, this is:

$$E_{obsv}(n) = T_s \sum_{k=0}^{n} (f_1(k)v_1(k) + ... + f_M(k)v_M(k)). \tag{2.32}$$

If $E_{obs}(n) \geq 0$ for every $n \geq 0$, the system does not generate energy. If there is an instance when $E_{obs}(n) < 0$, the system generates energy and the amount of generated energy is $E_{obs}(n)$.

Once the energy flow can be observed, the remaining question is how to act when activity is reported. Since the exact amount of the generated energy is known, a time-varying damping element can be designed to dissipate only the required amount of energy. This element will be regarded as Passivity Controller (PC). The PC is a dissipative element which takes the form of a variable damper. Depending on the port causality of the network the PC can take the form of an impedance or admittance type of network. Fig. 2.4.2(a) and 2.4.2(b) show impedance and admittance configurations of the PO/PC for a one-port network system respectively. The coefficients α and β are the variable dampers attached to the port, which dissipate energy generated by the active network. The configuration choice depends on the causality of model underlying the port. In the impedance configuration, the PC obeys the following equation:

$$f_2 = f_1 + \alpha v. \tag{2.33}$$

And in the admittance configuration:

$$v_2 = v_1 - \beta f. \tag{2.34}$$

Note that Fig. 2.4.2(a) and 2.4.2(b) are represented using flow diagram representation. This representation is here useful since it allows to see the operation of the PC. In network terms, the PC represents a 2-port dissipative network connected in cascade to the port of a network. Fig. 2.4.3 shows the equivalent network representations.

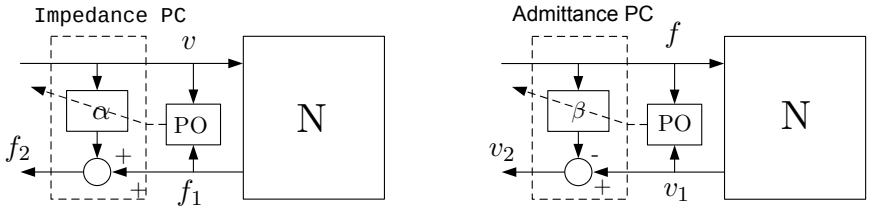

(a) Impedance type configuration of the PC/PC

(b) Admittance type configuration of the PO/PC

Figure 2.4.2: Impedance and admittance PC configuration for one-port networks

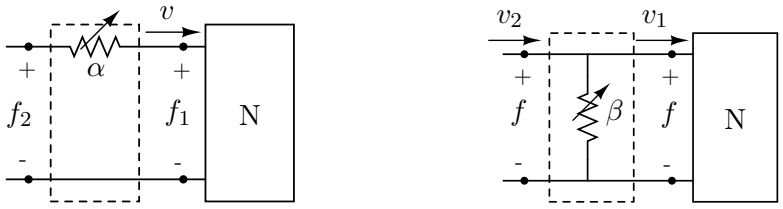

(a) PC in Impedance configuration

(b) PC in Admittance configuration

Figure 2.4.3: Network representation of the cascade N and the PC. The resulting network becomes passive

Impedance PC configuration

In the impedance configuration, velocity through the port is conserved and the force across is modified in order to produce the dissipation (see Fig. 2.4.3(a)). Therefore, the α coefficient must be such, that it dissipates the active energy observed by the PO. The power dissipated by the damping coefficient can be written as:

$$P_{PC}(n) = v(n)^2 \alpha(n). \tag{2.35}$$

Where v is the velocity to the 1-port and through the damper. Isolating α:

$$\alpha(n) = \frac{P_{PC}(n)}{v(n)^2} \tag{2.36}$$

And the dissipation coefficient α must be such, that it dissipates active energy observed by the PO. This is:

$$\alpha(n) = \begin{cases} \dfrac{-W(n)}{T_s v(n)^2} & \text{if } W(n) < 0 \\ \\ 0 & else \end{cases} \tag{2.37}$$

Where W is the observed energy updated with the action of the PC, that is, including with the energy dissipated in the previous time step. W is thus the observed energy of the cascade created by the 1-port network and the PC:

$$W(n) = W(n-1) + T_s(v(n) f_1(n)) + T_s(\alpha(n-1) v(n-1)^2). \tag{2.38}$$

And the output force of the network f_1 is modified according to:

$$f_2(n) = f_1(n) + \alpha(n)v(n). \tag{2.39}$$

Using (2.39) passivity can be proved by checking the resulting energy flow of the one-port defined by $\langle f_2, v\rangle$ as:

$$\begin{aligned} T_s\sum_{k=0}^{n} f_2(k)v(k) &= T_s\sum_{k=0}^{n} f_1(k)v(k) + T_s\sum_{k=0}^{n-1}\alpha(k)v(k)^2 + T_s\alpha(k)v(k)^2 \\ &= W(n) + T_s\alpha(n)v(n)^2. \end{aligned} \tag{2.40}$$

And using (2.37):

$$T_s\sum_{k=0}^{n} f_2(k)v(k) \geq 0, \quad \forall n \geq 0 \tag{2.41}$$

Admittance PC configuration

In the admittance configuration, force across the port is conserved and velocity through is modified in order to produce the dissipation (see Fig. 2.4.3(b). Consider the admittance configuration shown in Fig. 2.4.3(b). The β dissipation coefficient can be obtained as:

$$\beta(n) = \begin{cases} \dfrac{-W(n)}{T_s f(n)^2} & \text{if } W(n) < 0 \\ \\ 0 & else \end{cases} \tag{2.42}$$

The Passivity Observer is defined as:

$$W(n) = W(n-1) + T_s(v_1(n)f(n) + f(n-1)^2\beta(n-1)) \tag{2.43}$$

And the PC is as:

$$v_2(n) = v_1(n) - \beta(n)f(n), \tag{2.44}$$

The energy dissipated by the PC becomes:

$$E_{PC}(n) = T_s\sum_{k=1}^{k=n-1}\left(f^2(k)\beta(k)\right) + f^2\beta(n). \tag{2.45}$$

Similar to the impedance configuration, passivity is proved using (2.42), which gives:

$$T_s\sum_{k=0}^{n} f(k)v_2(k) \geq 0, \quad \forall n \geq 0 \tag{2.46}$$

Passivity Observer and Controller for n-port Networks

Recalling Def. 11 and Fig. 2.2.5 a two-port network is passive if:

$$\int_0^t f_1(\tau)v_1(\tau)d\tau + f_2(\tau)v_2(\tau)d\tau + E(0) \geq 0, \tag{2.47}$$

being v_1 and v_2 entering velocities at each port (analog to the currents signals i_1 and i_2 of Fig. 2.2.5) and f_1 and f_2 the conjugate forces across each port (analog to voltages v_1 and v_2 of Fig. 2.2.5).

Recalling (2.32), for a two-port network, the energy to be observed in the discrete time domain is written as:

$$E_{obs}(n) = T_s \sum_{k=0}^{n} (f_1(k)v_1(k) + f_2(k)v_2(k)). \tag{2.48}$$

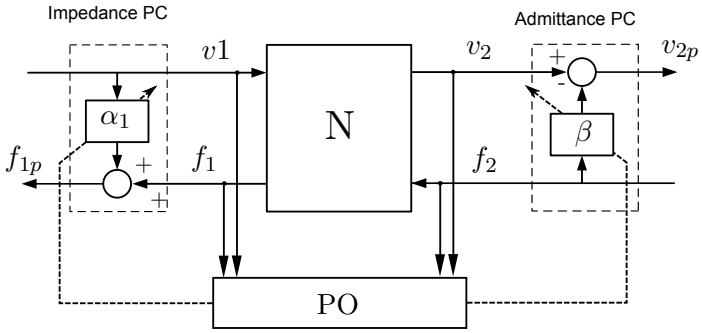

Figure 2.4.4: Passivation of a two-port network using a pair of PCs, one in impedance and the other in admittance, and a common PO.

Fig. 2.4.4 shows a two-port network with a PO element and a pair of PCs at each side. Since the velocity signal at the right port, v_2, is defined as exiting the two-port, the previous equation related to the observed energy must be modified according to the port sign convention, Def. 9. That is:

$$E_{obs}(n) = T_s \sum_{k=0}^{n} (f_1(k)v_1(k) - f_2(k)v_2(k)). \tag{2.49}$$

The PCs are triggered according to the PO. Nevertheless, in this situation, the PC must take into account the direction of the energy flow. Thus, if energy flows from left to right, the right PC will be triggered, while if energy travels toward the left port, the left PC will be triggered. This approach is extensively exposed in [93]. The resulting network, that is, the cascade of the impedance PC, N and the admittance PC, is a passive one.

Unfortunately, the energy flow through a two-port network cannot be observed if the network contains a time delay. The two-port PO/PC approach fails in satisfying the passivity condition since the PO cannot integrate the power flow at each port of the two-port network at the same sampling instant. This passivation method is therefore out of the scope of this work.

The above arguments for two-port networks can be extrapolated for a n-port network. Representing a system as a multi-port network and analyzing its passivity can be very useful in applications involving multiple degrees of freedom or multiple agents.

Example 5 *A manipulator with 6 joints can be represented as a 6-port network, each port being identified by a commanded torque, τ_i, and the joint angular velocity, $\dot{q}_i$ (see Fig. 2.4.5).*

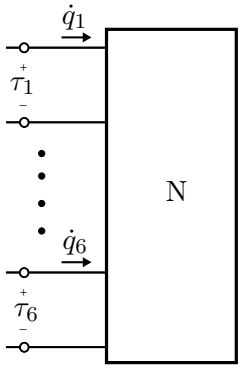

Figure 2.4.5: A 6-port network representing a 6 DoF manipulator.

Passivity of the manipulator can be then evaluated by summing each port energy contribution:

$$E_N(t) = T_s \sum_{k=0}^{n} \sum_{i=1}^{6} \tau_i(k)\dot{q}_i(k). \tag{2.50}$$

Thus, the PO can be built using (2.48). The PC must be built according to a criteria. Note that energy is a scalar quantity. How energy is to be dissipated, that is, distributed along the manipulator. Further discussion related to multi-port PCs will be given in Chapter 5.

2.5 Stability of time-delayed Systems

We first study the stability of delayed systems. In particular, it is interesting to see the evolution of the poles when a variable time delay is present in the transfer function. As it will be seen, some systems are able to *absorb* a certain amount of time delay without producing poles on the right-half-plane of the complex-frequency diagram. This will give us some insight on how to analyze and design what we here call the *bare configuration* for teleoperation systems. The bare configuration is the parametrization of the controllers of a given teleoperation system that ensures stability and a desired degree of transparency in a quasi ideal scenario. In the quasi ideal scenario, the integrating elements of the teleoperation system, i.e. environment, human, master, slave and communication, can be modeled; and the communication includes a short constant time delay.

The analysis continues with a network -based stability analysis. In the previous section, some properties of networks were reviewed. In this section some methods for

stability and passivity for delayed systems will be reviewed. By way of illustration, a Position-Position scheme will be analyzed in terms of stability regions. As will be seen, passivity is in general a more conservative rule than stability. In network theory, passivity and stability differ fundamentally in that the connection of two stable networks does not necessarily produce a stable system, while nearly[2] any multi-port connection of passive networks creates a passive system. Moreover, as will be seen, the passivity based analysis provides some other useful properties, specially in those systems including delays and elements that are difficult to model.

Stability of time-delayed systems

Typical stability methods for delay-free systems such as Nyquist, Bode, the root-locus or algebraic methods can also be applied in systems, which include a delay in the feedback loop. In the following we check the location of the poles of the transfer functions which include a time delay. The exposition begins with a simple arbitrary system with a know transfer function with time delay and evolves to two concrete examples of bilateral control schemes, a Position-Position architecture and a position-torque will be used as examples.

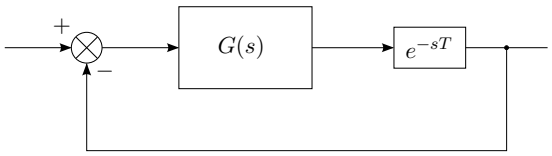

Figure 2.5.1: System with time delay

The difference in the study between delayed and non-delayed systems lies in the number of closed loop poles. While for the non-delayed case this number is equal to the number of open loop poles, for time-delayed systems, the number of closed poles become infinite [69]. Taking for instance the system represented in Fig. 2.5.1 with open loop transfer function

$$G(s) = \frac{100}{0.2s + 0.1s + 0.001}, \tag{2.51}$$

the characteristic equation of the denominator of the closed loop transfer function is given by:

$$p(s) = 1 + \frac{100}{0.2s + 0.1s + 0.001} e^{-sT} \tag{2.52}$$

The zeros and poles of the transfer function characterize the system natural response. The poles of the characteristic equation of the denominator of the transfer function determine the stability of the system. If all of them fall on the left-half-plane (LHP) of the complex diagram the system is stable since it implies that the natural frequencies will make the value of the transfer function decay to zero when an external source is disconnected. In order to see the effects of the time delay in the closed loop system,

[2] With exception of some serial interconnections, see Sec. 2.2.

consider first the system with $T = 0$, which makes the exponential term vanish in (2.52). The open loop transfer function presents two real poles located on the LHP. Now, if the delay is set as a variable, the location of those poles will vary according to the delay value. The evolution of the poles as the delay increases, that is, a root locus diagram with the delay swept between zero and infinity, can be seen in 2.5.2(a) and Fig. 2.5.2(b) at different zoom views.

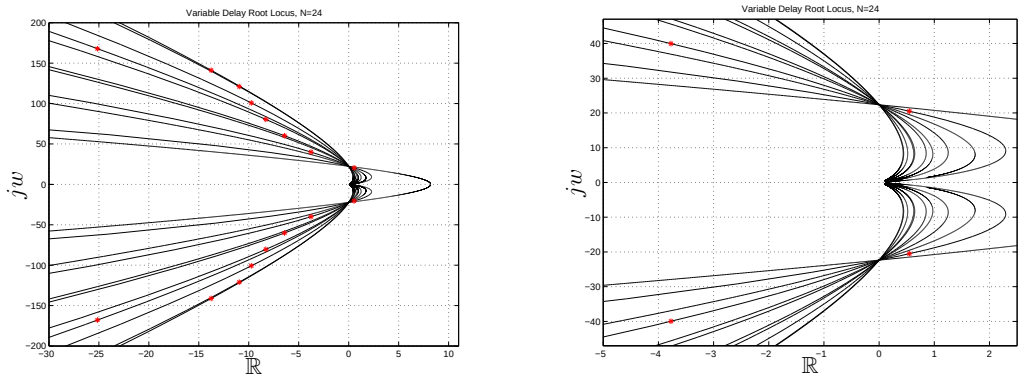

(a) Pole particularization at $T = 0.3s$. (b) Zoomed view.

Figure 2.5.2: Varying delay root locus.

As can be seen, for some delay values the poles fall into the right half plane. The diagram shows stability windows in some delay ranges, that is, a system which may be unstable for small delay values may attain stability for higher delay values. The figures particularize pole locations for a time delay $T = 0.3s$..

The stability boundaries can be analyzed by solving the characteristic equation for the case $s = jw$, that is, in the critical frequencies for critical stability. In this case, the characteristic equation must satisfy:

$$p(s)|_{s=jw} = p(jw) = h(w) + jg(w) = 0, \tag{2.53}$$

where h and g are real and imaginary parts of p. Equating both parts to zero:

$$h(jw) = 8 - w^2 + cos(wT + 2\pi k) + wsin(wt2\pi k) = 0 \tag{2.54}$$
$$g(jw) = 12w - 6w^2 - w^3 + wcos(wt2\pi k) - sin(wT2\pi k) = 0 \tag{2.55}$$

$$k = 0, 1, 2, 3, ...$$

Where k is the index representing the infinite periods of the *sin* and *cos* functions, which in turn come from the trigonometrical representation of Eurler's number e. From $h(jw)$ and $g(gw)$, which respectively correspond to real and imaginary parts of $p(jw)$, the frequency locations which bound stability and instability regions can be extracted, and their corresponding delays T for which these critical frequencies are reached. Note that $h(jw)$ and $g(jw)$ have an infinite number of solutions, representing the infinite number of poles due to the time delay. Each of these solutions is indexed by k.

In the following, the stability regions for the some of the reviewed architectures are examined.

Example: The Postion-Position Architecture

The system is represented in Fig. 2.7.11. We shall begin studying the system's transfer function without time delay. To simplify the analysis, both, Z_m and Z_s are assumed to be equal, as well as master and slave PD controllers:

$$\begin{aligned} Z_m = Z_s &= ms + b \\ Z_{cm} = Z_{cs} = Z_c &= \frac{Bs + K}{s} \end{aligned}$$

The open loop transfer function can be obtained as follows:

$$\begin{aligned} Zss &= \frac{Z_m^{-1} Z_c}{Z_m^{-1} Z_c + 1}, \\ G_O &= Z_m^{-1}[1 - Z_{ss}]Z_c \\ &= \frac{mBs^2 + (bB + mK)s + bK}{m^2 s^3 + (mB + 2bm)s^2 + (mk + b^2 + bB)s + bK} \end{aligned} \tag{2.56}$$

where m and b are mass and damping coefficient for both, master and slave devices; and K and B are proportional and derivative gains for both PD controllers. The system presents two zeros and three poles.

In order to study the stability for system with delay, the two delay elements in Fig. 2.7.11, that is, e^{-sT_f} and e^{-sT_b} can be substituted by one on either direction with argument $-sT$, i.e e^{-sT}. This simplification has no effects from the mathematical point of view. Thus, we can represent the delayed open loop transfer function as:

$$G_{ol} = G_O e^{-sT} \tag{2.57}$$

Applying the same condition as in (2.53), the stability boundaries for G_{ol} are given by $-m \leq B \leq \infty$ and $0 \leq K \leq \infty$. An analytical expression of the delay T as a function of b, m, K and B is difficult to obtain when the transfer function is of an order higher than two. In those cases numerical methods can be used to find the critical frequencies and phase margin swept on K and B ranges. Then the maximum possible values of T are given by:

$$T_i = \frac{\pi P_{m,i}}{360 W_{cp,i}} \tag{2.58}$$

Where P_m is the phase margin and w_{cp} is the critical frequency. The stability regions as a function of K and B and T are graphically shown in Fig. 2.5.3 and in Fig. 2.5.4.

In order to study individually the effect of the time delay on the location of the poles, we particularize the system with the following values:

$$m = 0.1Kg.; \quad b = 1n/m^2; \quad B = 1N/m^2; \quad K = 50N/m.$$

The variable root locus is shown in Fig. 2.5.5. As can be seen in the plot, the system presents multiple critical frequencies due to the higher order of the transfer function. This can result in multiple stability regions or stability windows [69] bounded by the critical frequencies. Fig. 2.5.5 also shows the poles particularized for a delay $T = 0.3s.$. As can be seen, such a delay results in an unstable system.

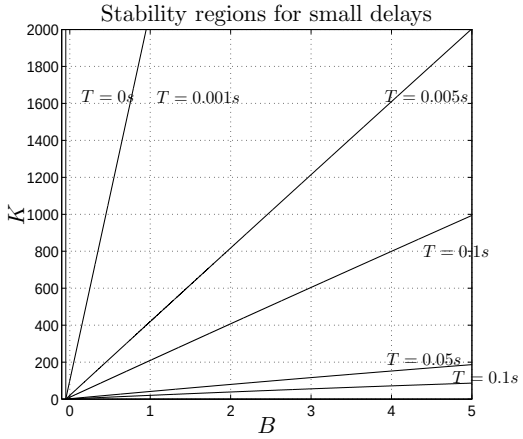

(a) The effects are significant as early as for small delays such $1ms$.

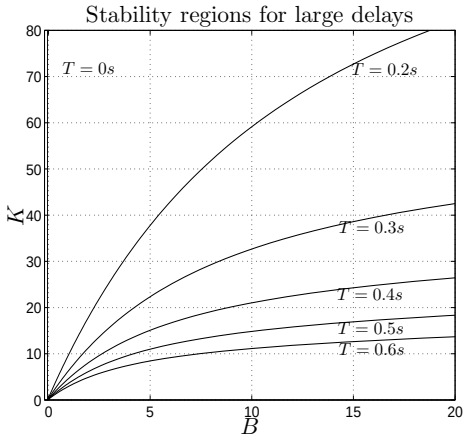

(b) Stability regions for large delays.

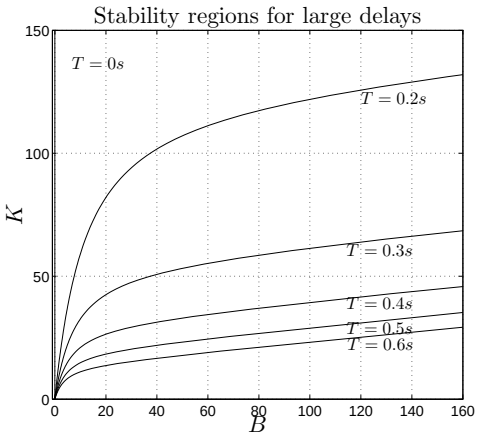

(c) The wide view shows a lineal dependency for larger values of K and B.

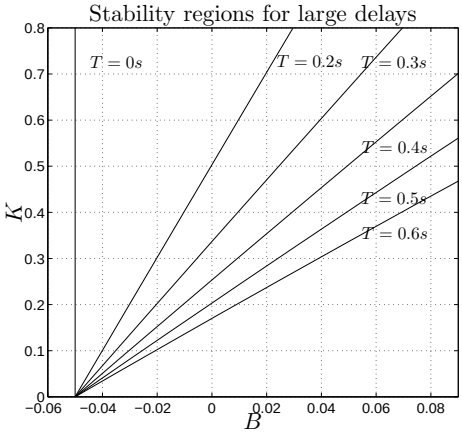

(d) The zoomed view shows a boundary on the negative values of B.

Figure 2.5.3: Stability regions of the PP architecture for small and large delays.

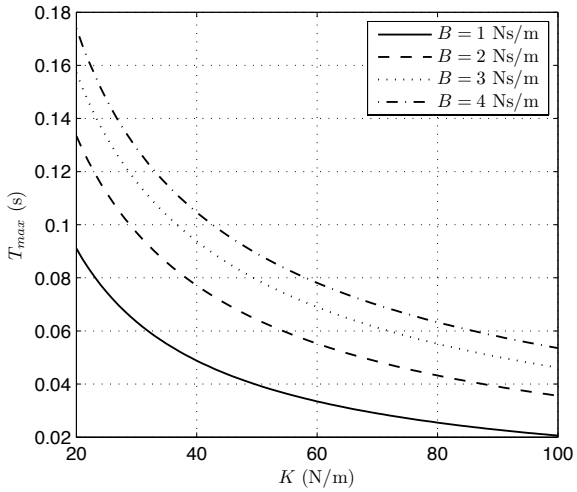

Figure 2.5.4: (m=0.1, b=0.1, B=2) As K increases the maximum allowed delay decreases. The four curves represent the time needed by the different poles to reach the critical frequencies. The smallest one is the more restrictive, therefore, the interesting one.

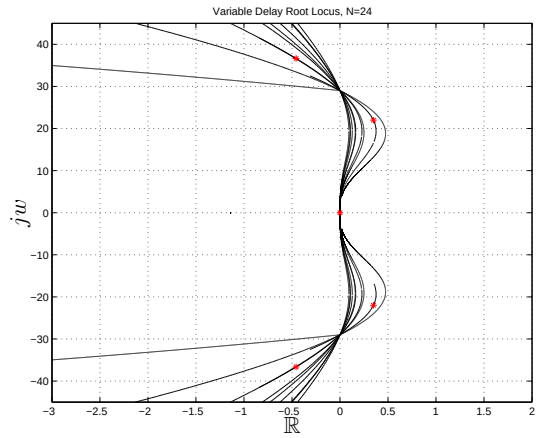

Figure 2.5.5: Variable delay root locus for a PP architecture

Example: The Postion-Force Architecture

The system is represented in Fig. 2.7.7. Its open loop transfer function including the delay is

$$G_{ol} = \frac{Bs + K}{ms^2 + (B + b)s + K} e^{-2sT}, \tag{2.59}$$

where m and b are mass and damping coefficient for both, master and slave devices; and K and B are proportional and derivative gains for both PD controllers. The system presents one zero and two poles. An analytical expression for the critical frequencies as well as for the maximum allowed delay can be found. Performing a similar analysis to previous one, the following critical frequencies are found.

$$w_1 = \frac{\sqrt{-b(b+2B)+2Km}}{m}, \qquad w_2 = -\frac{\sqrt{-b(b+2B)+2Km}}{m}, \tag{2.60}$$

Furthermore, the maximum tolerable delay such that the system remains stable is given by:

$$T = \frac{2m}{\sqrt{-b(b+2B)+2Km}} arctan((B+b)\sqrt{\frac{2}{mK}}). \tag{2.61}$$

2.6 Review of Bilateral Control Methods

We begin by reviewing the Master Slave 2-port Network (MSN), which provides the highest level of abstraction of a teleoperation system represented through network means. The MSN is a two-port network linking the human operator to the task. It includes master and slave manipulators as well as local and bilateral controllers, that is, all the networks between human and environment interaction ports from Fig. 2.7.1. Representing the teleoperation system as an MSN is useful since it allows to employ the passivity theory to design stable systems assuming that both, operator and environment, are passive [11], [89], [60]. A good starting point in the literature is [116], where the fundamentals of bilateral control are introduced.

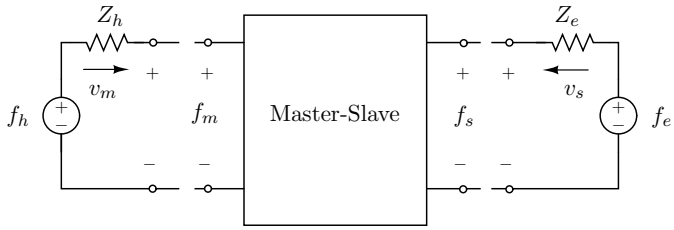

Figure 2.6.1: Network Model of a Master-Slave System

The MSN allows practically any architecture and controller configuration since the ports are specified at the outer part of the teleoperation system. In this sense it represents a high level of abstraction which masks the complete electro-mechanical system. This allows full two-port network treatment of the system benefitting thus from the network analysis tools. In order to review the MSN synthesis and the possibilities it offers to analyze stability and design bilateral controllers, we make use of the Lawrence's 4-Channel architecture representation [60], shown in Fig. 2.6.2. This representation is general in that it encompasses many teleoperation architectures. It allows many specific particularizations, such as a Position-Force or a Position-Position. [44] generalized the 4-Channel representation to all possible causalities displayed at the human and environment. This architecture can be embedded in a MSN or *Teleoperator Interface* as called in [60]. Fig. 2.6.2 shows four sections: Human, master, communication, slave and environment. Tab. 2.3 gives typical values for a Position-Force architecture:

The MSN is entirely described through any of the immittance or hybrid parameters. The hybrid equivalent MSN is shown Fig. 2.6.3 with h-parameters as:

Block	Function
Master impedance Z_m	$M_m s$
Master controller C_m	$B_m s$
Slave impedance Z_s	$M_s s$
Slave controller C_s	$\frac{B_s+K_s}{s}$
Velocity channel C_1	$\frac{B_s+K_s}{s}$
Force channel C_2	K_f
Force channel C_3	not used
Velocity channel C_4	not used

Table 2.3: Typical values of the elements represented in Fig. 2.6.2.

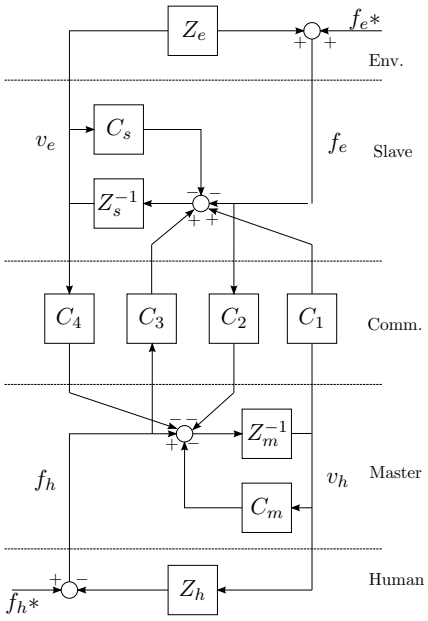

Figure 2.6.2: 4-Channel Architecture defined by Lawrence in [61]

$$\begin{bmatrix} f_h(s) \\ v_h(s) \end{bmatrix} = \begin{bmatrix} h_{11} & h_{12} \\ h_{21} & h_{22} \end{bmatrix} \begin{bmatrix} v_e \\ -f_e \end{bmatrix}. \tag{2.62}$$

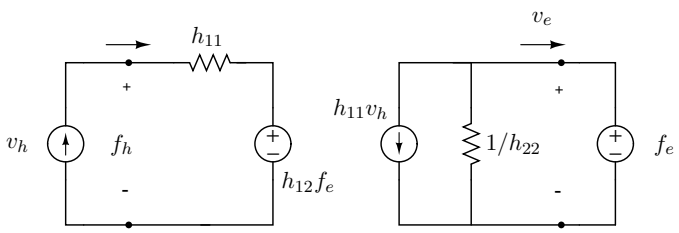

Figure 2.6.3: Hybrid equivalent MSN.

The MSN synthesis provides a full framework for analyzing the stability of teleop-

eration systems. Stability can be easily analyzed by applying Raisbeck's passivity or Lewellyn stability criterions. Some examples follow.

Passivity of the MSN

In the MSN representation, left and right ports of the network interact with the human operator and the environment respectively (see Fig. 2.6.1), where Z_h and Z_e are human and environment impedances as defined in (2.80), and Z_m and Z_s, master and slave impedances, (2.81). In [89] the impedance parameters are used to describe the network, and positive realness of the impedance matrix is applied to design an absolutely stable MSN. In [11] the system is modeled through the scattering parameters and a control rule is found which guarantees passivity of the MSN even in the presence of constant time delays. The system is represented as an MSN (*Teleoperator Interface* in [60]), and the passivity theorem based on the feedback theory [32] is applied to find the control parameters which ensures passivity of the system.

In [62] and [63] passivity is analyzed for bilateral teleoperation based on proportional-derivative control and delayed communication channels. The LyapunovKrasovskii criterion along with Parsevals identity the controller gains are adjusted to ensure a passive communication with a know worst-case time delay.

The following works are likewise highlighted:

- Passivity based on the network theory (Raisbeck's). [89], [112]
- Passivity based on feedback theory (Desoer). [60].
- Absolute Stability based on Lewellyn's criterion. [8], [44].
- Passivity based on the scattering parameters.[11], [73].

Example 6 *Passivity of a P-P architecture using the Raisbeck's passivity criterion*

The hybrid parameters for the Position-Position scheme shown in Fig. 2.7.11 are given by:

$$h_{11} = Z_m + \frac{Z_c}{\frac{Z_c}{Z_s}+1}, \qquad h_{12} = \frac{Z_c}{Z_s\left(\frac{Z_c}{Z_s}+1\right)}, \tag{2.63}$$

$$h_{21} = -\frac{Z_c}{Z_s\left(\frac{Z_c}{Z_s}+1\right)}, \qquad h_{22} = \frac{1}{Z_s\left(\frac{Z_c}{Z_s}+1\right)}. \tag{2.64}$$

Using the following, typical, impedance values

$$Z_m = Z_s = \frac{1}{b+m\,s}, \qquad Z_c = Z_{cm} = Z_{cs} = \frac{K+B\,s}{s}, \tag{2.65}$$

leads to:

$$h_{11} = \frac{1}{b+m\,s} + \frac{K+B\,s}{(b+m\,s)\;(K+B\,s)+s} \tag{2.66}$$

$$h_{12} = \frac{(b+m\,s)\;(K+B\,s)}{(b+m\,s)\;(K+B\,s)+s} \tag{2.67}$$

$$h_{21} = -\frac{(b+m\,s)\;(K+B\,s)}{(b+m\,s)\;(K+B\,s)+s} \tag{2.68}$$

$$h_{22} = \frac{s\,(b+m\,s)}{(b+m\,s)\;(K+B\,s)+s}. \tag{2.69}$$

From the first condition in Theorem 2.2.1, that is, all the poles of the parameters must be located in the left-half-plane, we see that $B \geq 0$. *Real and imaginary components of the h-parameters are given by:*

$$\text{Re } h_{11} = \frac{w^4\;\left(2\,b\,B^2\,m^2+B\,m^2\right)+w^2\;\left(2\,B^2\,b^3+3\,B\,b^2+\left(2\,K^2\,m^2+2\,K\,m+1\right)\;b\right)+2\,K^2\,b^3}{(b^2+m^2\,w^2)\;D(w)},$$

$$\text{Re } h_{12} = 1-\frac{w^2\;(B\,b+K\,m+1)}{D(w)},$$

$$\text{Re } h_{21} = -\left(1-\frac{w^2\;(B\,b+K\,m+1)}{D(w)}\right),$$

$$\text{Re } h_{22} = \frac{b\,w^2+B\,w^2\;\left(b^2+m^2\,w^2\right)}{D(w)},$$

$$\text{Im } h_{11} = -\frac{w^3\;\left(2\,K^2\,m^3+3\,K\,m^2+\left(2\,B^2\,b^2+2\,B\,b+1\right)\;m\right)+}{(b^2+m^2\,w^2)\;D(w)}$$

$$-\frac{+w\;\left(2\,m\,K^2\,b^2+K\,b^2\right)+2\,B^2\,m^3\,w^5}{(b^2+m^2\,w^2)\;D(w)}$$

$$\text{Im } h_{12} = -\frac{w\;\left(K\,b-B\,m\,w^2\right)}{D(w)},$$

$$\text{Im } h_{21} = \frac{w\;\left(K\,b-B\,m\,w^2\right)}{D(w)},$$

$$\text{Im } h_{22} = \frac{K\,b^2\,w+\left(K\,m^2+m\right)\;w^3}{D(w)},$$

where

$$D(w) = B^2\,b^2\,w^2+B^2\,m^2\,w^4+2\,B\,b\,w^2+K^2\,b^2+K^2\,m^2\,w^2+2\,K\,m\,w^2+w^2$$

Thus condition (2.16) can be checked, giving:

$$4\;\text{Re } h_{11}\text{Re } h_{22}-[\text{Re } h_{12}+\text{Re } h_{21}]^2-[\text{Im } h_{12}-\text{Im } h_{21}]^2 = \frac{4\,b\,w^2\;\left(2\,B\,b^2+b+2\,B\,m^2\,w^2\right)}{(b^2+m^2\,w^2)\;D(w)}. \tag{2.70}$$

From (2.70), the following two boundaries can be extracted:

$$K \geq \frac{2\,m\,w^2}{b^2 + m^2\,w^2}, \tag{2.71}$$

$$B \geq \frac{b}{2\,b^2 + 2\,m^2\,w^2} \tag{2.72}$$

The residues at the imaginary axis, $s = 0$, needed to fulfill the residues conditions in (2.15) are given by:

$$K = \begin{bmatrix} k_{11} & k_{12} \\ k_{21} & k_{22} \end{bmatrix}, \tag{2.73}$$

$$k_{11} = \frac{1}{b + m\,s} + \frac{K + B\,s}{s\left(\frac{(b+m\,s)\,(K+B\,s)}{s} + 1\right)}\bigg|_{s=0} = 0, \tag{2.74}$$

$$k_{12} = k_{21} = k_{22} = 0.$$

Therefore we have the conditions expressed in (2.71) which are dependent on the mass and damping parameters of master and slave devices, and on the system frequency. We can set a worst case by removing the dissipative term of master and slave devices, that is, $b = 0$. Conditions (2.71) reduce to

$$K \geq \frac{2}{m}, \qquad B \geq 0. \tag{2.75}$$

A less conservative approach can be achieved by considering b and a maximum w value at the price of making the controller more dependent on master and slave models and dependent on the system bandwidth. Limiting the system bandwidth implies reducing the maximum stiffness displayable by the teleoperation system.

Scattering Parameters and the Wave Variables

A network can be described in terms of immittance (*z and y*), hybrid (*h* and the inverse *g*) or chain-matrix parameters. These parameters are useful for circuits where the lumped model can be assumed, that is, where the size of the circuit and the wavelength are of different order of magnitude. However, at microwave frequencies scale or in transmission lines, the time of propagation of the signals becomes significant. As a such, the voltage and current signals become temporal and positional dependent. In those circuits it is useful to describe the networks in terms of scattering parameters (S) (see Sec. 2.2), which form a matrix of transformations between incident and reflected wave amplitudes carrying power. The scattering parameters or wave variables are linear combinations of port voltages and currents and are useful for handling problems related to power transfer between networks.

The scattering parameters were first applied to delayed teleoperation in [11]. In that work, the teleoperation system was modeled through the scattering parameters and a control rule was found which guarantees passivity of the MSN even in the presence of constant time delays. The notion of wave variables applied to teleoperation was

introduced in [73] and [75], and further developed in [108] and [109]. In the following, a review of wave variables is given.

The wave variables can be computed from the standard power or mechanical variables (f and v) by the transformation

$$\boldsymbol{\mu} = \frac{b\boldsymbol{v} + \boldsymbol{F}}{\sqrt{2b}}, \qquad \boldsymbol{\nu} = \frac{b\boldsymbol{v} - \boldsymbol{F}}{\sqrt{2b}}, \tag{2.76}$$

where b is the characteristic impedance and is a positive constant, and u and v are the wave variables which are arbitrary defined as outgoing (forward or right moving wave) and incoming (backward, or left moving wave) respectively. Moreover,

$$\boldsymbol{\mu}_s(t) = \boldsymbol{\mu}_m(t - T) \qquad \boldsymbol{\nu}_m(t) = \boldsymbol{\nu}_s(t - T). \tag{2.77}$$

Where T represents the time delay in the communication channel. u_s is the outgoing wave on the left side (slave) and u_m the outgoing wave right side (master). And the same is true for the incoming wave.

The transformation is bijective meaning that it is unique and invertible and may be thus used to determine any combination of power and wave variables. This means that any causality is possible (velocity as input and force as output, or force as input and velocity as output). Fig. 2.6.4 shows the wave transformer as a two port block for impedance causalitiy. Furthermore, no information is lost or gained by encoding the variables in this manner. The power variables can be computed from the wave variables as:

$$\boldsymbol{v} = \sqrt{\frac{1}{2b}}(\boldsymbol{\mu} + \boldsymbol{\nu}) \quad \boldsymbol{F} = \sqrt{\frac{b}{2}}(\boldsymbol{\mu} - \boldsymbol{\nu}) \tag{2.78}$$

Fig. 2.6.4 shows the a wave transformer for the master side.

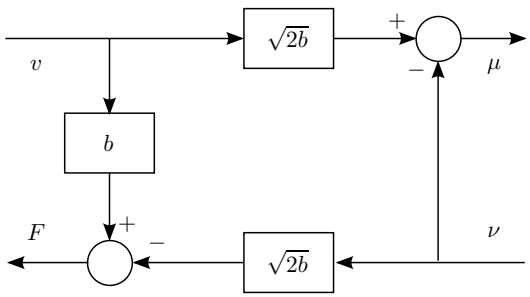

Figure 2.6.4: Impedance Wave Variables transformer. The right side belongs the wave domain. The left to the electric domain.

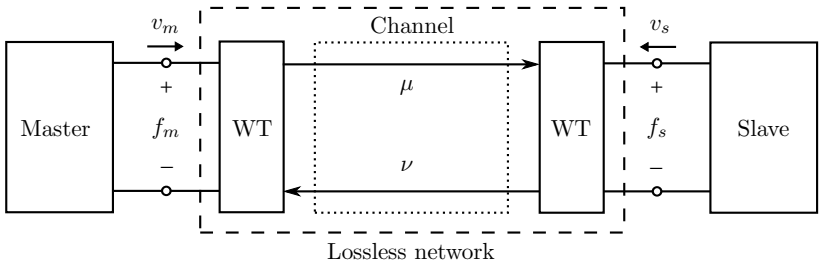

Figure 2.6.5: Wave Variables based generic teleoperator. Power magnitudes are transformed into waves.

By applying this transformation the delayed channel is not anymore an active element. This can be proofed by examining the power of the redefined communication element:

$$P = v^T f = \frac{1}{2}\boldsymbol{\mu}^T u - \frac{1}{2}\boldsymbol{\nu}^T \boldsymbol{\nu}. \tag{2.79}$$

The passivity condition is satisfied as shown in [74]:

$$\int_0^t \frac{1}{2}\boldsymbol{\nu}^T \boldsymbol{\nu} d\tau \leq \int_0^t \frac{1}{2}\boldsymbol{\mu}^T \boldsymbol{\mu} d\tau + E_{store}(0). \qquad \forall t \geq 0$$

From now on, the combination of a communication channel transmitting wave variables and the corresponding wave transformers at each side form a passive element (see Fig. 2.6.5).

One of the most quoted drawbacks of the wave variables formulation is that passivity can only be guaranteed for constant communication delays. In [114] and [115] and strategy to monitor the potential energy induced due to the varying delay and communication interruptions is proposed. The wave command is modified according to the energy modifications that are introduced by the varying delay incurred by the traveling waves. A similar method is presented in [48] and [47], where the strategies applied in case of a packet loss are analyzed. For instance, it is proved that a *holding last sample* action can generate virtual energy in the wave domain. The proposed solution is based on a passivity preserving modulation of the the wave command.

Wave variables are affected by energy reflection, just as any other *wavy* system. Power can bounce forth and back in the communication channel, unless dissipation elements are inserted and properly tuned on both sides of the channel. The discussion on whether wave reflections are more or less disturbing that the needed extra dissipation to damp them is still open. To fully damp the reflections, the transmission line impedance, that is, that of the wave -based communication channel, needs to be adapted or matched to the loads that it is attached to. This can result in high additional damping, which indeed, can notably impact on the performance [13], [87].

Wave variables can also be used for general distributed robotic systems, where, for instance, the plant and the controller coexist in different systems and are linked through

a communication. [65] and [81] show the effectiveness of the passive local controllers based on the scattering formulation for robotic distributed systems with inherent or acquired time delays.

Port-Hamiltonian-based Teleoperation

In [97], [99], the concept of intrinsically passive controllers (IPC) [107] is extended to intrinsically passive telemanipulation. The authors represent the teleoperation system using port hamiltonian systems linked with passive interconnections, which are developed on the basis of the *scatterization* of delayed communication channels (wave variables). The resulting system is a port-contact (due to the lack of a rigorous Dirac structure). Communication with variable time delay and package loss is studied. The proposed method preserves passivity, and so stability, with independence of the channel characteristics.
The work presented in [98] shows the potential that control methods based on energy considerations can offer. In particular, the concept of *energy tank* is presented. The tank is an energy reservoir that gets filled up and emptied according to the dissipated energy and the desired energy to achieve a performance goal. A limit in performance based on passivity is thus established that guarantees system stability with a well managed performance-stability trade-off. [98] is a good example of how a dissipated energy can be exploited to augment transparency; in particular, the issue of steady state position error found in wave variables based schemes is addressed. A virtual spring is proposed that computes the needed velocity from the dissipated power of an IPC to compensate the position error between master and slave devices. The potential energy required by the spring can be safely extracted from the tank without violating system passivity. Indeed, this represents a paradigm of how energy can be dissipated to prevent activity, but activity can be also be generated to prevent dissipative behaviors and, in turn, increase performance. The strategy presented can both, compensate the error during the contact and free-environment phases.

In a similar fashion, a two-layer control structure is presented in [35] and [34] that splits stability and performance related objectives using power variables [3] (rather than wave variables). The higher layer addresses a desired transparency level, and the lower layer guarantees stability based on passivity. Passivity is treated in the time domain using a similar strategy as that of the Time Domain Passivity Control. The tank can receive energy quanta on demand from the other side in order to achieve a performance goal but must provide at the same time the energy (power in fact, as described in the article) necessary to interact with the physical world. In case that the energy level of the tank does not suffice, a variable damper is defined, similar to a Passivity Controller, to increase the energy tank levels. An heuristic, system dependent, constant *desired* energy is needed for both, master and slave tanks that forces both tank levels to converge to that desired value. A potential issue of the presented approach is that there is an unavoidable time lag equal to the round trip communication delay between the energy requests and the actual received energy quanta. This can become an issue with large

[3] forces and velocities

enough communication delays.

State Variables Convergence

In state convergence bilateral control, the state of both, master and slaves are sent in both directions. In a sense, this approach exploits all the information that is available and can thus achieve high transparency levels. The state is defined by a position, a velocity and a force. [82] is a good starting point to state variables convergence based teleoperation.
In [113] a bilateral control design based on the state variables formulation is presented that follows master and slave state convergence criterion. The control algorithm is based on the implementation of an adaptive method that maximizes human operator perception of the environment while guaranteeing stable operation. Master and slave devices are modeled through linear differential equations that represent the state spaces. A state error between master and slave states is defined and its convergency is proved with dynamic parameters uncertainty. Through adaptive control techniques, robust stability can be guaranteed in the presence of dynamic identification errors.

The approach is extended in [23], [22] to tackle the case of delayed communications. By modeling the time delay as a Taylor expansion, tracking is achieved by state convergence. In the same context, a new methodology presented in [12] and [24] has been recently proposed that aims at reaching the highest transparency considering communication time delay. The method presents a modified scheme of the previous state convergence algorithm. A desired master - slave impedance reflection can be achieved while guaranteeing the stability of the system. The systems are modeled as second-order and feasibility is shown for the 3 DoF case.

Energy Bounding Algorithm (EBA)

The Energy Bounding Algorithm was presented in [56] for stable haptic interaction control. The bounding algorithm limits the amount of energy generated by the zero-order-hold according to the energy that can be dissipated by the physical damping of a haptic device. This principle is used to make the combination of a virtual environment and the haptic controller passive. The same concept has been applied to delayed teleoperation in [100] and [101] through a dual EBA controller structure: On one side, passivity of the network created by the human operator, the master controller and the communication channel, is tackled by means of an EBA controller located on the slave side; on the other, the network created by the environment, slave device, slave controller and communication channel is tackled by an EBA controller located on the master side. The combination of both controllers avoids instability due to delayed communications and discretization processes, however overall system passivity is not proved. One limitation of the EBA approach is the fact that the assumed passivity is dependent on a model parameters. In order to obtain the energy limitation to ensure passivity, a the physical damping coefficient of the haptic device must be estimated.

Bilateral Energy Transfer

The Bilateral Energy Transfer concept, presented in [15] and [16], is defined as the straightforward transfer of energy between the two opposite sides of a teleoperation network, the master and slave robots. The individual active energy leaks are isolated and independently addressed through energy -based control methods in the time domain. A discussion between an ideal telepresence paradigm and a real world scenario is given. In particular, the ideal case assumes master and slave robots to behave as rigid connected masses with a lossless power exchange between them; however, real scenarios include sources of energy leaks, i.e. elements that modify the power flows in the network. If the energy leak has an active nature, it become source of instability for system. In the bilateral energy transfer, two energy leaks are isolated: The time delay introduced by the communication channel that connects the master and slave systems; and the digital acquisition of master/slave robot position, followed by the velocity estimation. In order to correct these leaks, two independent controllers based on energetic consideration are designed in order to correct these two energy leaks and thus to allow the Bilateral Energy Transfer. Two separate and independent controllers are proposed: The Bilateral Passivity Controller (BiPC), split between Forward and Backward Passivity Controllers (FPC and BPC), which forces the delayed communication channel to passivity; and the Passive Continuous Discrete time Connector (PCDC), which operates on the velocity estimation in order to make the connection between the robots and the digital controller lossless. Fig. 2.6.6 shows the network cascade connection of a teleoperation system integrating the PCDC and the FPC and BPC.

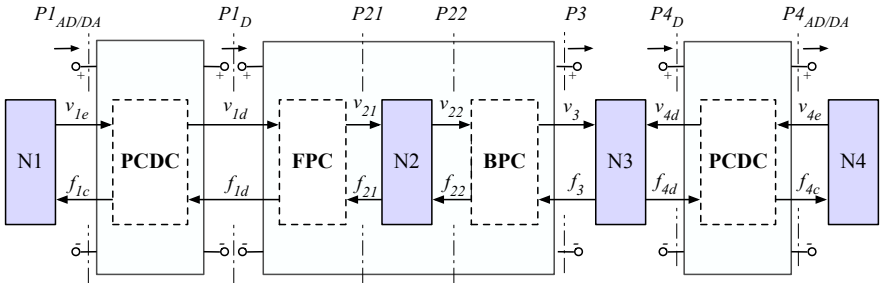

Figure 2.6.6: Network representation of a teleoperation system including PCDC and the FPC/BPC

The same rationale behind the solution proposed in [26] and [27] for passively interconnecting multi-rate systems is adopted for dealing with the problem of energy generation due to the discretization of position information. The result is an element, called PCDC (Passive Continuous Discrete time Connector), which connects the sampled data coming from the haptic interface to a discrete time systems. As the Passivity Observer / Passivity Controller, this element observes the power flows and modifies one of its output in order to minimize the power generation (or dissipation) due to time discretization and velocity estimation. Thus the output of the PCDC is a passive velocity estimation. In turn, the system can be designed to achieve greater performance goals since the energy leak due to discretization is not present throughout the rest of the system. As a con-

sequence, the passivity controllers on both sides of the communication network, FPC and BPC, can operate in a more relax fashion and therefore, performance is increased. Similar approaches have been presented in [71] and [70].

While the BiPC concept has shown stable interaction, the passivity of the overall system was not guaranteed.

2.7 Network Representation of Teleoperation Systems

As previously stated, one strong argument for using the network representation is because it allows to extract conclusions about system passivity by examining input and output energy flows of each subsystem. Another benefit is that it allows a generalized system analysis, that is, the passivity condition can be applied on every system as long it can be represented through network elements. The only requirement to that is to identify the conjugate pairs (force and velocity signals) for each subsystem in order to identify the ports. Fig. 2.7.1 depicts the general network representation of a teleoperation system. Each element is represented as a one-port or a two-port network. The data is exchanged through network ports. Tab. 2.4 gives a brief description of each network element. Fig. 2.7.1 encompasses every possible two-channel architecture. Fig. 2.7.2 adds another communication network which encompasses also four-channel architectures. The network masks one part of the system. The division of the system in networks is adjusted in a convenient manner such that it allows to isolate the analysis of specific elements or groups of elements. Usually the elements masked by the network in a teleoperation system can be modeled by LTI (linear-time-invariant) functions. Such models are necessary to study the system stability. In the following, the impedance models for the human, the environment, master and slave, the communication and the controllers are reviewed. The specific interconnection of the impedance model within the network is reviewed in the upcoming Sec. 2.7.

Although the human operator can behave as an active impedance (see Example 12), a common assumption is that the human behaves in a *passive* manner, that is, the energy which the operator brings into the system will not lead the system to instability. The same reasoning applies for the environment. Widely accepted, human and environment can be modeled as mass-damper-spring as:

$$Z_h(s) = \frac{M_h s^2 + B_h s + K_h}{s}, \qquad Z_e(s) = \frac{M_e s^2 + B_e s + K_e}{s}, \tag{2.80}$$

where M_h, B_h, K_h, M_e, B_e and K_e are mass, damper and spring components of the human and the environment, and Z_h and Z_e the human and environment impedances.

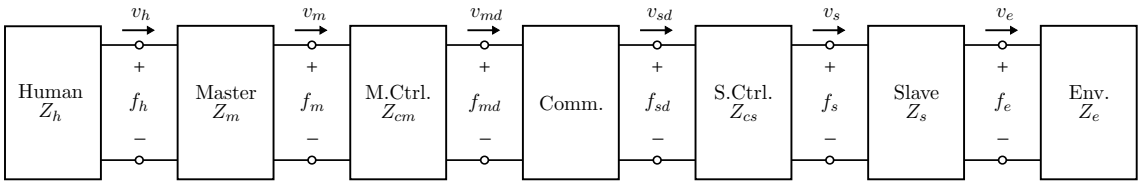

Figure 2.7.1: Network representation of a teleoperation system.

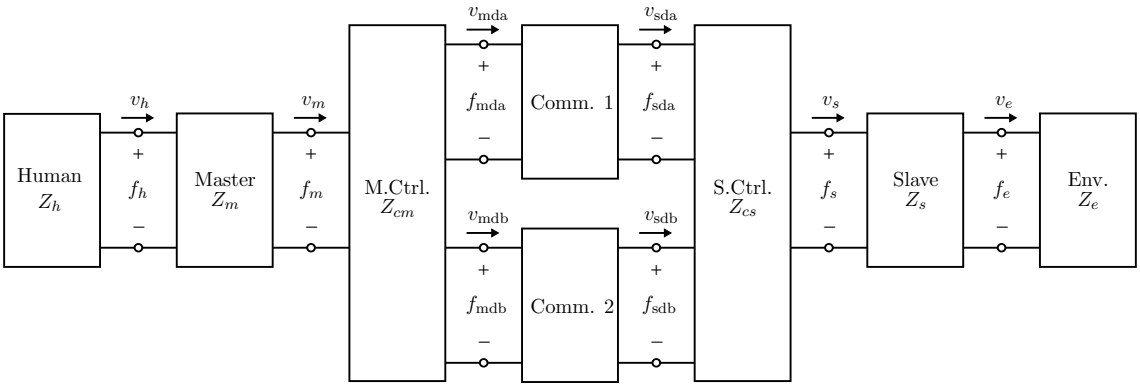

Figure 2.7.2: General four channel network scheme of a teleoperation system.

Master and slave devices can be modeled as simple electromechanical motors. Typically, the simplified model of a motor can be described by a mass-damper system or even a single mass. In this work the following models will be used:

$$Z_m(s) = M_m s + B_m, \qquad Z_s(s) = M_s s + B_s, \tag{2.81}$$

where M_m, B_m, M_s and B_s are mass and damping components of master and slave respectively, and Z_m and Z_s their impedances.

The models of the control networks, Z_{cm} and Z_{cs} depend on the chosen controller. For instance, for a PD controller (PI equivalent if the input is velocity), widely used in the field of teleoperation, the network function or equivalent impedance is given by:

$$Z_c(s) = \frac{Bs + K}{s}, \tag{2.82}$$

where B and K are virtual damping and stiffness values, that is, derivative and proportional gains.

As for the communication, in the case of an ideal transmission the, i.e., without delay nor package loss, the impedance is null. The transfer function of an ideal transmission can be expressed using the hybrid parameters as:

$$\begin{bmatrix} f_{md} \\ v_{sd} \end{bmatrix} = H_{cc} \begin{bmatrix} v_m \\ f_s \end{bmatrix} = \begin{bmatrix} 0 & 1 \\ 1 & 0 \end{bmatrix} \begin{bmatrix} v_m \\ f_s \end{bmatrix}, \tag{2.83}$$

The analysis of a delayed communication including package-loss is central aspect in this thesis and will be developed in the upcoming chapters.

Extracting the Network Model of Teleoperation Systems

Note that energetic behavior of the elements in Tab. 2.4 listed as passive is subject to the design, i.e. a *well designed* controller, master or slave device, should always be passive or behave as passive. In this work, these elements are assumed to be passive.

Element	Type	Energy behavior	Description	TF
Human Operator	1 p.	Active & passive	Responsible for system motion.	$\frac{M_h s^2+B_h s+K_h}{s}$
Master Device	2 p.	Passive	Haptic device. Transfers HO motion, displays force feedback.	$M_m s + B_m$
Master Controller	2 p.	Passive	Local control of haptic device. Master component of bilateral control.	$\frac{B_{cm} s+K_{cm}}{s}$
Comm. channel	2 p.	Active & passive	Transfers information from one side to the other. Active behavior if delay is present.	$\begin{bmatrix} 0 & 1 \\ 1 & 0 \end{bmatrix}$
Slave Controller	2 p.	Passive	Local control of slave robot. Slave component of bilateral control.	$\frac{B_{cs} s+K_{cs}}{s}$
Slave Device	2 p.	Passive	Robot which interacts with Environment.	$M_s s + B_s$
Environment	1 p.	Active & passive	Can be an active environment.	$\frac{M_e s^2+B_e s+K_e}{s}$

Table 2.4: Network elements of a teleoperation system.

One simple method to obtain the network model from the block diagram representation is to derive equivalent Kirchhoff's equations. The Kirchhoff' equations, described by Gustav Kirchhoff in 1845, deal with the conservation of charge and energy in electrical circuits.

Definition 19 *Kirchhoff's Current Law*
The algebraic sum of currents in a network of conductors meeting at a point is zero. (Assuming that current entering the junction is taken as positive and current leaving the junction is taken as negative).

Definition 20 *Kirchhoff's Voltage Law*
The directed sum of the electrical potential differences (voltage) around any closed circuit is zero.

The input / output (IO) function can be grouped in equivalent electrical potentials by using the mechanical-electrical analogy. Taking for instance the block diagram sketched in Fig. 2.7.3 (a), the IO function is given by $f_1 = Z_1 v_1$, which can be directly mapped to a circuit composed of an impedance, Z_1 with a current thorough of v_1 and a voltage across of magnitude f_1 as shown in Fig. 2.7.3 (b). See Sec. 2.3 for a review on the mechanical-electrical analogy.

As a rule of thumb, one can apply the following: A sum of forces in the block diagram representation maps into serially placed electrical potentials, that is, in the same branch of the circuit. A sum of velocities in the block diagram maps into electrical potentials placed in parallel, that is, in parallel branches of the circuit.

Figure 2.7.3: Block diagram of $f_1 = Z_1 v_1$ and its electrical analog.

Example 7 *Sum of forces*

Take the diagram in Fig. 2.7.4 (a). The function governing this system is given by $v_1 = (v_1 Z_1 - f_2) Z_2^{-1}$. *This equation can be rewritten as* $-v_1 Z_1 + v_1 Z_2 + f_2 = 0$, *which is equivalent to a circuit with an hypothetical voltage source of magnitude* f_2 *closing the loop. The circuit is thus constructed as in Fig. 2.7.4 (b).*

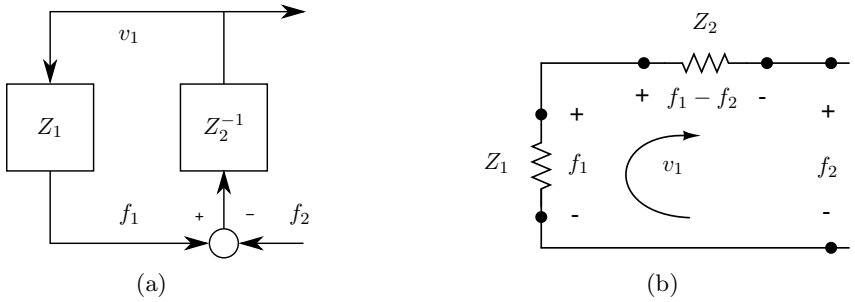

Figure 2.7.4: Block diagram and its electrical analog.

Example 8 *Sum of forces and velocities*

Take the diagram in Fig. 2.7.5 (a). The function governing this system is given by $v_1 = (v_1 Z_1 - (v_1 - v_2) Z_3) Z_2^{-1}$. *This equation can be rewritten as* $-v_1 Z_1 + v_1 Z_2 + (v_1 - v_2) Z_3 = 0$, *which is equivalent to a circuit with an hypothetical current source of magnitude* x_2 *closing the loop. The circuit is thus constructed as in Fig. 2.7.5 (b).*

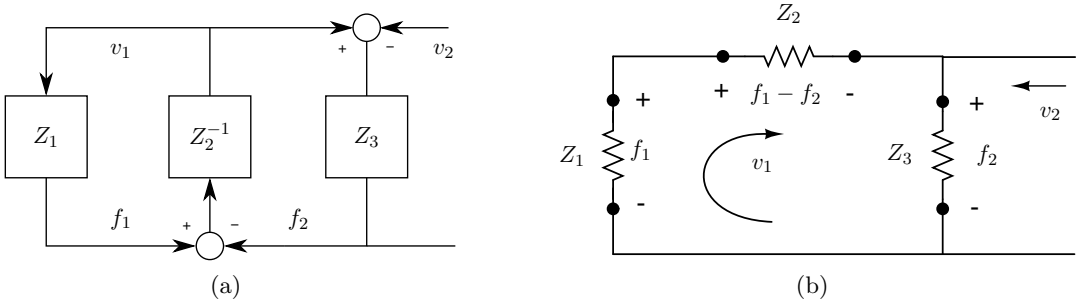

Figure 2.7.5: Block diagram and its electrical analog.

Remark 1 *The propagation direction of a signal in the flow diagram must not coincide with the sign of that signal in the electrical scheme. This is, by way of illustration, obvious in Fig. 2.7.4 by looking at the signal* v_1.

Network model of the Communication Channel

The communication block for a two channel architecture teleoperation system may have the following causalities:

- Position-Force: Position or equivalently velocity is transmitted forward, that is, from master to slave, and the computed force fed to the slave is also fed back to the master.
- Force-Position: Is the opposite of the previous.
- Position-Position: Master position or equivalently velocity is transmitted forward, and Slave position or velocity is fed back to the master.
- Force-Force: Master force is transmitted forward, and slave force is fed back to the master.

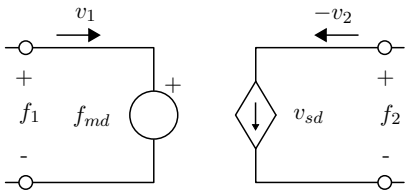

(a) Equivalent 2-port network of a Position-Force communication

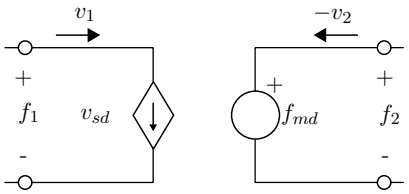

(b) Equivalent 2-port network of a Force - Position si communication

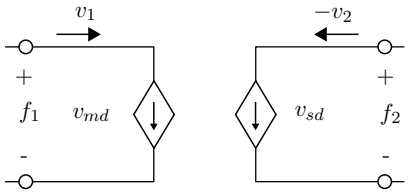

(c) Equivalent 2-port network of a Position-Position communication

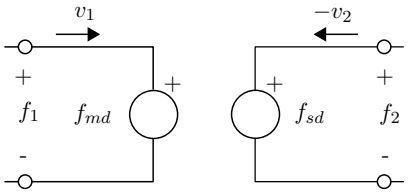

(d) Equivalent 2-port network of a Force - Force communication

Figure 2.7.6: Network representations of the different 2-channel communication architectures.

The network model of these communication configurations can be extracted by using *dependent power supplies*. Dependent power supplies are voltage or current sources whose voltage across or current through values depend on some other voltage or current value found in the circuit. These active elements are specially useful for representing delayed communication channels. The four communication configurations are respectively represented in Fig. 2.7.6(a), Fig. 2.7.6(b), Fig. 2.7.6(c) and Fig. 2.7.6(d). The repercussions of having dependent power supplies in the communication channel, specially in the

case of delayed communications, will be analyzed in Chapter 4.

Note that in the ideal, non-delayed case, the representations in Fig. 2.7.6 are equivalent to a pair of parallel wires (transparent network), that is, forces and velocities are identical on both ports: $f_1 = f_2$ and $v_1 = v_2$.

The Position-Force computed Architecture

This is one of the most reported teleoperation schemes in the literature. In the Position-Force computed (P-Fc) architecture, current master velocity is sent toward the slave side, where it becomes the reference input for a PD [4] controller which computes the force or torque to move the slave robot. This force is as well fed back to the master, where, in its bare configuration, it becomes the force input to the master haptic device. For this reason and in order to distinguished it from architectures that use measured signals from a sensor, this architecture is referred throughout this work as Position-Force computed (P-Fc). In this example we start with block diagram of the system and its equations of motion to extract mechanical and electrical schemes.

1. Block diagram

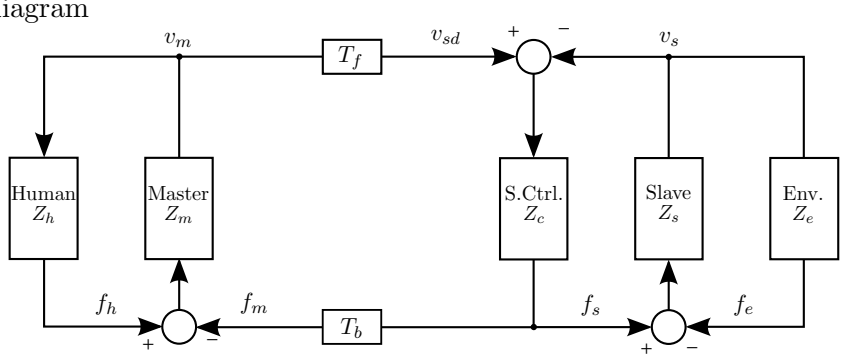

Figure 2.7.7: Block diagram of the P-Fc teleoperation architecture.

The equations governing the system are:

$$\begin{aligned} v_{sd}(t) &= v_m(t - T_f), \\ f_m(t) &= f_s(t - T_b), \\ f_s(t) &= K_d(v_{sd}(t) - v_s(t)) + K_p(x_{sd}(t) - x_s(t)), \\ f_m(t) &= f_s(t - T_b). \end{aligned} \tag{2.84}$$

Where f_m, x_m and f_s, x_s are master and slave computed force and position respectively and T_b and T_f are forward and backward delays; K_d, K_p are master controller derivative and proportional gains. Master dynamics are as:

$$\begin{aligned} (f_h(s) - f_m(s))\frac{1}{m_m s^2 + b_m s} &= x_m(s), \\ f_h(s) &= v_m(s)Z_h(s). \end{aligned} \tag{2.85}$$

[4] referred to position. PI referred to velocity

Where f_h is the human force; m_m and b_m are master mass and damping coefficients, and Z_h is the human impedance. Equations at the slave side can be obtained on a similar way.

2. Electrical scheme without time delay

For the sake of simplicity, we first extract the electrical scheme considering an ideal communication channel, this is, with no time delay. Fig. 2.7.8 depicts the scheme.

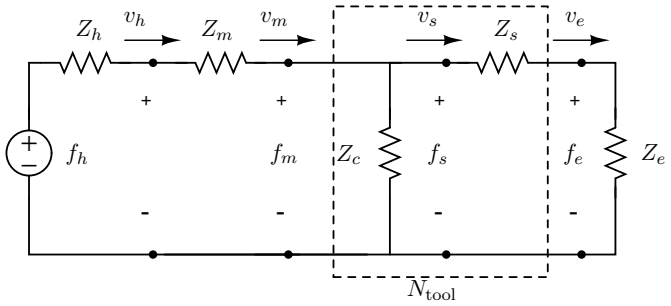

Figure 2.7.8: Electrical scheme of a P-Fc architecture without time delay.

Note the equations governing the system are identical to (2.84) setting both T_f and T_b to zero.

3. Electrical scheme with time delay

The communication time delay can be modeled by using dependent power sources as shown in Fig. 2.7.9.

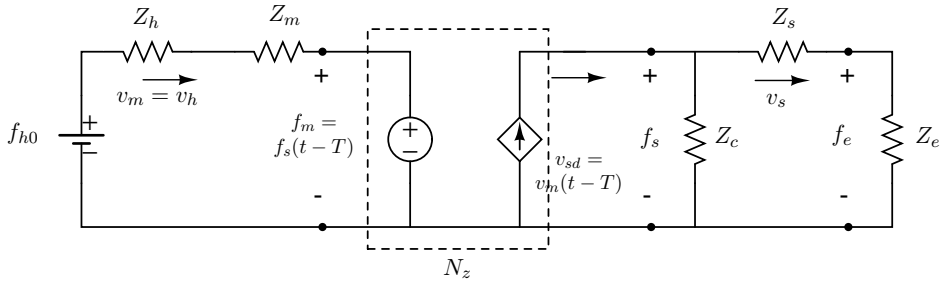

Figure 2.7.9: Electrical scheme of a P-Fc architecture with time delay.

4. Network scheme

Once the electrical scheme is defined, the network representation can be easily derived as can be seen in Fig. 2.7.10. Note the only difference between this graphic and Fig. 2.7.1 is the master controller, which is not present in the former one. Indeed, the Position-Force architecture is based on a unique controller at the slave side.

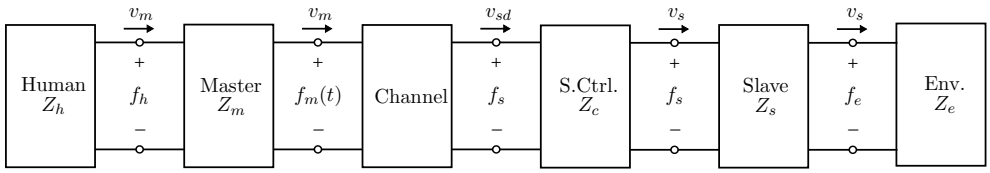

Figure 2.7.10: Network scheme of a P-Fc architecture with communication channel.

The Position-Position Architecture

In this architecture, both, master and slave controllers, are PI [5] linked with local and distant velocities. The desired command for the slave PI is the current master velocity delayed. The controller can thus immediately obey with a force response on the slave device. At the master side, the desired command is current master velocity, which in turn is the operator's motion intention, and the distant slave is the process to be controlled. This architecture usually presents higher degrees of resistance to the user as the delay increases compared to the P-Fc scheme.

We start with the blocks diagram of the system, shown in Fig. 2.7.11 and its equations of motion to extract mechanical and electrical schemes.

1. Block diagram

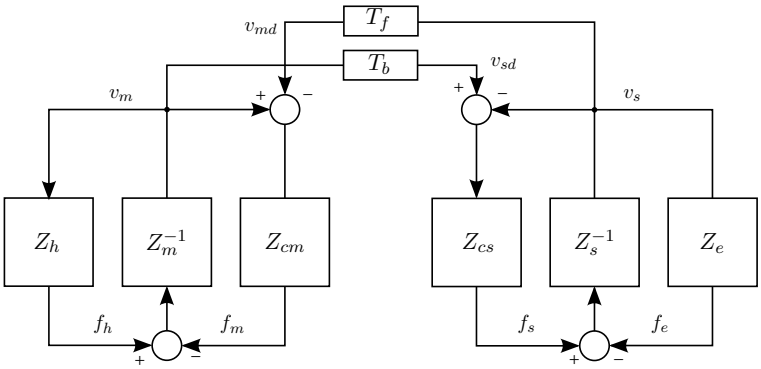

Figure 2.7.11: Block diagram of a P-P architecture.

Typical expressions for master, slave and the controllers are:

$$Z_m = \frac{1}{b + m\,s} \tag{2.86}$$

$$Z_s = \frac{1}{b + m\,s} \tag{2.87}$$

$$Z_c = Z_{cm} = Z_{cs} = \frac{K + B\,s}{s} \tag{2.88}$$

[5] PD equivalent referred to position

$$f_m(t) = B(v_m(t) - v_s(t - T_b)) + K(x_m(t) - x_s(t - T_b)),$$
$$f_s(t) = B(v_m(t - T_f) - v_s(t)) + K(x_m(t - T_f) - x_s(t)). \tag{2.89}$$

Where f_m, x_m and f_s, x_s are computed force and position from master and slave respectivelly, and T_b and T_f are forward and backward delays. Slave and master dynamics are as follows related:

$$(f_h(s) - f_m(s))\frac{1}{m_m s^2 + b_m s} = x_m(s),$$
$$f_h(s) = v_m(s)Z_h(s), \tag{2.90}$$

Where f_h, f_m and x_m are human force and master force and position; m_m and b_m are master device mass and damping coefficients; and Z_h is the human impedance. At the slave side the relations are as:

$$(f_s(s) - f_e(s))(\frac{1}{m_s s^2 + b_s s}) = x_s(s)$$
$$f_e(s) = v_s(s)Z_e(s), \tag{2.91}$$

where f_s, f_e and x_s are commanded force to the slave device, environment force and slave position; m_s and b_s are slave device mass and damping coefficients; and Z_e is the environment impedance.

2. Electrical scheme with time delay

Note the communication channel must be represented through ideal dependent current sources (with or without delay inclusion). Therefore no distinction is made between un-delayed and delayed communication as in the previous example.

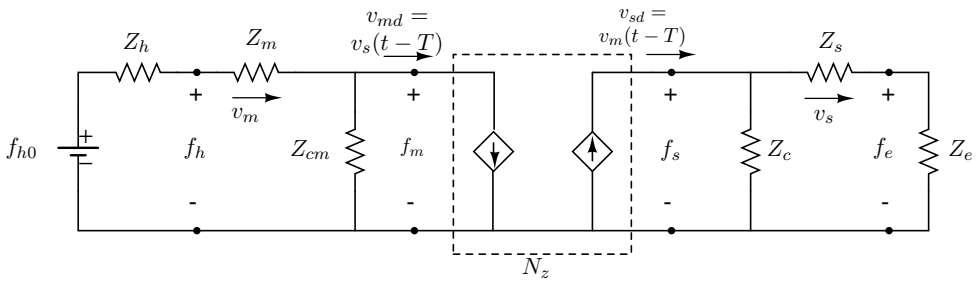

Figure 2.7.12: Electrical scheme of a P-P architecture.

3. Network scheme

The Position-Position can represented as Fig. 2.7.1 since it includes all the networks from the general teleoperation network representation.

Remark 2 *As it will be seen in Chapter 3, representing the P-P architecture through the networks cascade in Fig. 2.7.1 is ambiguous since the communication network contains not only the communication itself, but also a pair of delayed dependent current sources. These dependent sources are integral parts of the system which are masked due to the flow-effort ambiguity caused by a Position-Position, that is, flow - flow, -based communication. This is a fundamental result in this work which is further studied in detail in the afore mentioned section.*

The Position-Force measured Architecture

The scheme is shown in Fig. 2.7.13. The velocity (or position) command to the slave robot, v_{sd}, is the master velocity, v_m, delayed; the slave force sensor signal, f_e, is fed back to the master device.

1. Block diagram

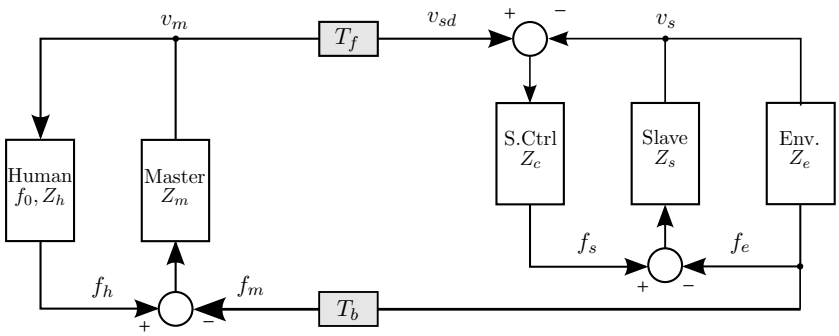

Figure 2.7.13: Block diagram of the P - measured F teleoperation architecture.

2. Electrical scheme with delay

The electrical analogue is shown in Fig. 2.7.14. In finding the network representation of the communication channel, a common mistake related to this kind of architectures is to consider the right port of the communication network by the variables f_e and v_{sd} since they are located in different parts of the scheme as can be seen in Fig. 2.7.14 but not in Fig. 2.7.13. Therefore they do not represent the communication medium. For instance, the use of that pair of signals for encoding wave variables leads to unstable systems since the modeled transmission line is carrying energy of non-power correlated signals. The electrical scheme indubitably unveils the signal pairs describing each port of the communication as:

$$Left: \begin{cases} f_m = f_e(t - t_b), \\ v_m(t). \end{cases} \qquad Right: \begin{cases} f_s(t), \\ v_{sd} = v_m(t - T_f). \end{cases}$$

By extracting the Kirchoff's equations of the circuit, it is possible to express f_e as a function of v_m and f_s, that is, the signals available at the two ports. This allows to model the communication as two-port network.

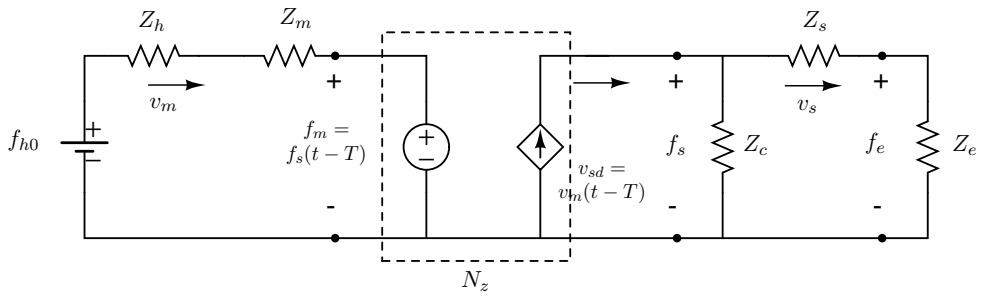

Figure 2.7.14: Electrical scheme of a P-Fmsr architecture.

3. Network representation

The system can be represented using the same network structure as for the P-Fc case, Fig. 2.7.10. However, note in this case the communication network contains an independent source, i.e. the voltage source is dependent on f_e which is not available at any of the communication ports. Thus, as such, the communication cannot be represented as a two-port network [72]. A workaround to that is to express the magnitude of the voltage source as a function of the signals available at the port:

$$\begin{aligned} f_e(t) &= f_s(t) - (v_s(t) - \frac{f_s(t)}{Z_{pd}(t)})Z_s) \\ Z_{pd}(t) &= K_{ds} + \frac{1}{K_{ps}} \int_o^t v_s(t) d\tau. \end{aligned}$$

Activity of a Delayed Communication Channel Network

The hybrid parameters of a communication channel with delay are as follows:

$$\begin{bmatrix} f_{md} \\ v_{sd} \end{bmatrix} = \begin{bmatrix} h_{11} & h_{12} \\ h_{21} & h_{22} \end{bmatrix} \begin{bmatrix} v_m \\ f_s \end{bmatrix} = \begin{bmatrix} 0 & e^{-sT} \\ e^{-sT} & 0 \end{bmatrix} \begin{bmatrix} v_m \\ f_s \end{bmatrix}, \tag{2.92}$$

where $f_{md}(t) = f_s(t - T_b)$ and $x_{sd}(t) = x_m(t)$, that is, master desired force is the slave current force delayed, and slave desired velocity is master current velocity (see Fig. 2.7.15).

Theorem 2.7.1 *A delayed communication channel (as represented through the hybrid matrix H) is always active.*

Proof In order to check the passivity of H, the 2-port network criterion for passivity (Def. 11) will be applied using the Hybrid parameters, that is, (2.16). In the particular case that h_{11} and h_{22} are zero, (2.16) reduces to:

$$-[\text{Re } h_{12} + \text{Re } h_{21}]^2 - [\text{Im } h_{12} - \text{Im } h_{21}]^2 \geq 0, \tag{2.93}$$

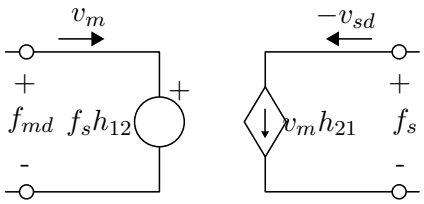

Figure 2.7.15: Hybrid parameters of a 2-port communication channel network with time delay.

which simplifies to the following conditions:

$$\begin{aligned} \text{Re } h_{12} &= -\text{Re } h_{21} \\ \text{Im } h_{12} &= \text{Im } h_{21}. \end{aligned} \tag{2.94}$$

Using the Euler transformation:

$$h_{12} = h_{21} = jsin(-wT) + cos(wT). \tag{2.95}$$

(2.94) shows that a two-port network whose h_{11} and h_{22} are both zero will be passive only if h_{12} is the negative of h_{21}. As can be seen from (2.95), H will never fulfill conditions (2.94) for any frequency value w. Therefore, it is concluded that a communication channel conveying force and velocity, both with delay, in opposite directions, as represented in Fig. 2.7.15, will always be active, no matter how small the delay. ∎

A similar analysis using the scattering parameters leading to the same result can be found in [11].

Remark 3 *The hybrid parameters are a more convenient two-port network for representing a teleoperation communication channel than the immittance parameters, since both, h_{11} and h_{22} turn to be zero. These type of networks produce non-finite equivalent impedance and admittance matrixes. Another example of this type of networks is the ideal transformer.*

Discussion

Stability for the quasi-ideal case is relevant in this work because it represents the mean the parametrize the bare configuration. The system in a real setup will deviate from that assumed one in the quasi-ideal parametrization. Deviation will occur because it is difficult to model master and slave parameters, specially in the multi DoF case, where the non-linearities must be taken into account. Besides the deviation in the parameters of the devices, the communication channel has been so far assumed to include null or small time delays. In a real teleoperation setup, time delayed shall be considered. There are different possibilities to address the afore mentioned deviations. The method proposed in this work is based on an online *modulation* of passivity, that is, passivity is treated in the time domain. The Time Domain Passivity approach (TDPA) allows to keep track of passivity by monitoring and controlling the energy flow of one and two-port networks. The main advantage in using the TDPA is precisely the fact that deviation can occur without compromising passivity since no models are required to monitor the

energy flows. The teleoperation systems analyzed in the next chapters are assumed to be *bare configured*, that is, they are parametrized for the quasi-ideal scenario. Delays greater than those assumed in the bare configuration, data losses in the communication channel and deviation in the parameters of master and slave devices will be handled by a bilateral structure based on the passivity controller.

Chapter 3

Time Delay Power Networks

The Time Delay Power Network (TDPN) is defined as a two-port network that masks a fundamental communication element and allows the interconnection of electromechanical devices that exchange mechanical energy, be them robots connected to other robots, haptic devices connected to virtual environments or haptic devices connected to robots. As will be seen, the analysis based on the energy observation of the TDPN ports allows model free controller designs. The TDPN forms the basis of a general stability treatment valid for any teleoperation architecture.

3.1 Introduction

This chapter presents a general network based analysis and representation for teleoperation systems. As previously mentioned, the electrical domain is appealing because it enjoys proficient analysis and design tools and allows a one step higher abstraction element, the network. Thus, in order to analyze the system by means of network elements, the mechanical system must be first modeled as an electric circuit. Only then power ports become apparent and networks can be defined. This kind of analysis has been previously performed in systems with well defined causalities in the communication channel. Indeed, a communication channel exchanging flow-like and effort-like signals, as for instance master velocity and force computed by a slave PD controller, has a well defined causality and can thus be directly mapped as a two-port electrical network. However, this is only one of the many possible system architectures. We investigate here other, more complex architectures, including those with ambiguous causalities.

A good example is the Position-Force measured (P-Fmsr) architecture, where the interaction forces and torques are sensed by a force-torque sensor and fed back to the haptic

device. If, as it may seem obvious, the transferred energy between master and slave is computed based on the power defined by the pair ⟨measured force , master velocity⟩ (see the figure in Table 3.3) the obtained energy transferred in the free environment operation turns to be nearly zero although energy is clearly transferred between the haptic device and the robot that is moving. In fact, as it will be seen, the block diagram representation is found to be misleading in the identification of the network ports involved in the communication. The causality of the communication channel, i.e. the input/output relationships between flow and effort, is therefore somewhat ambiguous. This ambiguity is even more obvious in other channel architectures such as a Position-Position or a Force-Force. In a Position-Position, the signals in the communication channel can be represented as flows (assuming position increments or velocity signals are sent instead of absolute positions). The paradox is that although energy is clearly transmitted through the outgoing and incoming velocity signals, the lack of an explicit effort signal does not allow to define power ports at each side of the communication. The main question is therefore how can energy be defined in those systems that are characterized by ambiguous causalities.

In this chapter it will be shown how these architectures can be modeled by means of a special type of networks, namely the Time Delay Power Networks (TDPN), even in the lack of flow or effort being transmitted. Later, in the next chapter, it will be shown and how they can be made passive for any communication channel characteristic (delay, package-loss and jitter).

3.2 TDPN for Bilateral Delayed Transmissions

The concept of Time Delay Power Network was first introduced by Artigas et al. in [19] and [20]. The TDPN assumes an ideal transmission of flow and effort signals. An ideal transmission is such that the signal on one side is received undistorted at the other with a time delay. This can be compared with a lossless finite transmission line properly terminated with an impedance equal to the line's characteristic impedance. In a TDPN however, this ideal transmission is imposed, independently from the load impedance. As such, a TDPN does not have a physical correspondency, as is the case of a transmission line. On the other hand, it is consistent with the definition of a two-port network and can thus be easily embedded in any electrical circuit. As will be seen, the TDPN is a source of virtual mechanical power and the main cause for system instability. Identifying the TDPNs of a system can be useful, since it allows to isolate the instability source in the form of an energy leak. Once the TDPN is identified (and so the energy leak), a passivity controller can be employed to dissipate the energy generated by the TDPN.

Based on the assumption that the interaction between the communication channel and the rest of the system depends only on the terminal behavior of the channel, the communication channel can be represented as a two-port network, irrespective of the characteristics that are imposed by the channel: Time delay, package loss, black outs and jitters.

Definition 21 *The Time Delay Power Network is an active two-port network, which masks a delayed transmission of one or both signals of a conjugated pair of flow and*

effort. Being ϕ_1 and e_1 the flow and effort signals at the left port and ϕ_2 and e_2 the corresponding signals at the right port, the signals are related to each other as:

$$\begin{aligned} e_2(t) &= e_1(t-T), \\ \phi_1(t) &= \phi_2(t-T). \end{aligned} \qquad \textit{or} \qquad \begin{aligned} e_1 &= e_2(t-T), \\ \phi_2 &= \phi_1(t-T). \end{aligned}$$

A communication channel that incurs a time delay in the forward and backward paths allows straightforward application of the TDPN. Fig. 3.2.1(a) shows an example of such a channel. Flow $e_{1,2}$, and effort $\phi_{1,2}$, variables could be any dual pair such as $\langle$current , velocity$\rangle$, $\langle$voltage , force$\rangle$, etc. The electrical representation of such a channel can be achieved by using ideal flow and effort dependent sources. These sources generate a delayed version of a signal found in another location of the circuit. Fig. 3.2.1(b) shows the electrical scheme that corresponds to the system represented in Fig. 3.2.1(a). The Time Delay Power Network is the two-port network given by the two ports defined by each dependent source, as seen in Fig. 3.2.2.
Note that the direction of ϕ_2 is chosen rightwards. This is done in order to be consistent with most teleoperation control schemes, where the desired velocity command at the slave points towards the controller. In accordance with the sign conventions of the network port definition, the flow through the right port of the TDPN needs be negative when computing the corresponding power.

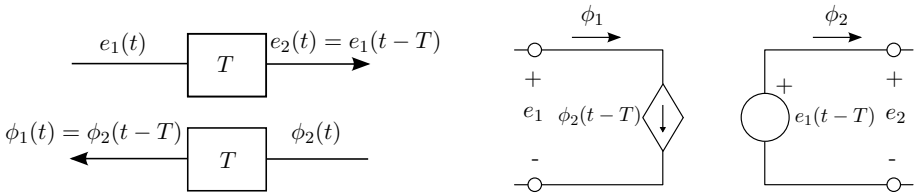

(a) Block diagram (b) Electrical circuit

Figure 3.2.1: Bilateral delayed transmission

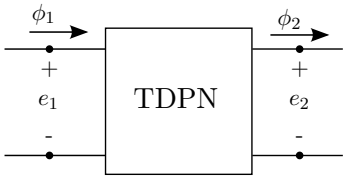

Figure 3.2.2: Equivalent Time Delay Power Network

3.3 Unfoldment of delayed dependent sources

Consider the circuit in Fig. 3.3.1(a). The dependent source generates a delayed version of the current through the resistor R_1. The circuit is divided within two sections, A and B. Section A can be regarded as the *near* section, since its variables are a function of the current time, that is, $t = t$. Section B, at the right side of the circuit, is fed by the dependent current source, and can be thus regarded as the *far* section.

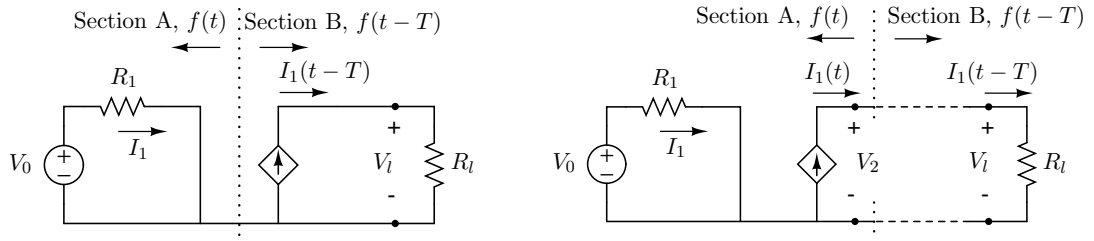

(a) Circuit containing a delayed dependent current source

(b) Replacement of the delayed dependent current source

Figure 3.3.1: Replacement of a delayed dependent current source to the non-delayed location

Proposition 1 *The circuits represented in Fig. 3.3.1(a) and Fig. 3.3.1(b) are equivalent.*

Proof Let R_l be the load in both circuits. Then the voltage across R_l is given by $V_l(t) = R_l I_1(t-T)$, in both cases. The load works under identical voltage and current relationships in both circuits. ∎

The only remaining variable in Fig. 3.3.1(b) to be determined is V_2. In fact, the port defined by $\langle I_1(t), V_2(t)\rangle$ does not exist, that is, it is not physically found in the original circuit. This port results from the model representation. Further, the choice of V_2 seems to be independent from the rest of circuit, as long the port variables at the load remain the same. Since the original circuit in Fig. 3.3.1(a) does not say anything about this voltage, a reasonable choice is $V_2(t) = V_l(t)$. Making use of the two-port network definition, an augmented representation based on the TDPN concept is proposed that implements a pure communication from the un-delayed current source to the delayed port. The augmented circuit is shown in Fig. 3.3.2. In a way, this representation unmasks a hidden two-port network, which is responsible for transporting the current signal to a location that is far enough that the transmission delay cannot be neglected. An equivalent diagram that illustrates the components of the TDPN *unfolded* is shown in Fig. 3.3.3.

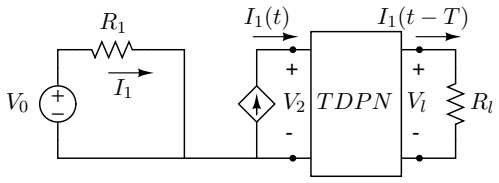

Figure 3.3.2: Augmented representation based on the unfoldment of a hidden communication network.

Remark 4 *While the scheme proposed in Fig. 3.3.2 assumes lumped elements on both sides of the TDPN, the TDPN itself cannot be regarded as lumped due to the fact that it contains a non-neglectable delay. In fact, the inclusion of the TDPN allows lumped treatment of the circuit since the delay is masked within an active network, the TDPN.*

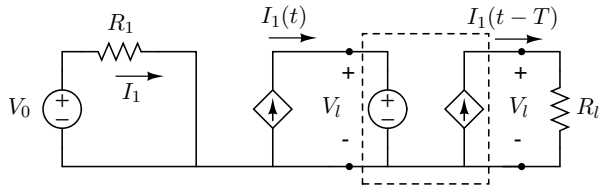

Figure 3.3.3: Equivalent representation showing the contents of the TDPN.

By using the Laplace transformation, the two-port network in Fig. 3.3.2 has the following H parameters as:

$$\begin{bmatrix} V_2 \\ I_l \end{bmatrix} = \begin{bmatrix} 0 & 1 \\ e^{-sT} & 0 \end{bmatrix} \begin{bmatrix} -I_1 \\ V_l \end{bmatrix} \tag{3.1}$$

Following Theorem 2.2.1, is clear that $TDPN$ is a non-passive network since it is not positive real as H_{12} may have poles on the right half plane depending on the T value. The non-passive property of this two-port is not surprising since it contains a pure time delay. We go one step further to seek the amount of energy introduced by such a network. As will be seen, the control strategy proposed in this work is based on dissipating this amount of energy.

Example 9 ***Delayed resistor*** *Consider an ideal current source connected to a resistor. The current generated by the source, i_0, is such that*

$$i_0(t) = \begin{cases} I_0, & \text{if } t \leq t_0, \quad \forall t \geq 0 \\ 0, & \text{if } t > t_0, \quad \forall t \geq 0, \end{cases} \tag{3.2}$$

Then, the energy dissipated by the resistor is given by:

$$E_R(t) = \int_0^t i_0(\tau)^2 R d\tau, \tag{3.3}$$

$$E_R(t \to \infty) = I_0^2 R t_0. \tag{3.4}$$

Following, a two-port network containing a pure delay in the forward path is placed between the source and the resistor. A discrepancy is found between the energy supplied by the source and the energy dissipated by the resistor. This is given by the energy of the two-ports:

$$E_N(t) = \int_0^t i_o(\tau) i_0(\tau - T) R d\tau - \int_0^t i_0(\tau - T)^2 R d\tau = E_{NL}(t) - E_{NR}(t),$$

where E_{NL} and E_{NR} are the energies at the left and right ports of the network. Rear-

ranging and substituting i_0 by its definition, we have that:

$$\begin{aligned} E_N(t\to\infty) &= \int_0^\infty i_o(\tau)i_0(\tau-T)Rd\tau - \int_0^\infty i_0(\tau-T)^2Rd\tau = \int_0^\infty \dots d\tau \\ &= \underbrace{\int_0^T \dots d\tau}_{\substack{=0 \ since \\ i_0(t-T)=0}} + \underbrace{\int_T^{t_0} \dots d\tau}_{\substack{=0 \ since \\ E_{NL}=E_{NR}}} + \int_{t_0}^{t_0+T} \dots d\tau + \underbrace{\int_{t_0+T}^\infty \dots d\tau}_{\substack{=0 \ since \\ i(t-T)=0}} = \\ &= \int_{t_0}^{t_0+T} i_o(\tau)i_0(\tau-T)Rd\tau - \int_{t_0}^{t_0+T} i_0(\tau-T)^2Rd\tau = -I_0^2RT. \end{aligned}$$

From these results, the following is concluded related to the two-port network:

1. *E_N is negative defined and so the two-port network is of active nature.*
2. *Its magnitude is proportional to the time delay value T and to the resistor, R.*

It follows with the energy of the source, given by:

$$\begin{aligned} E_s(t) &= \int_0^t i_o(\tau)i_0(\tau-T)Rd\tau, \\ E_s(t\to\infty) &= -I_0^2Rt_0 + I_0^2RT = -I_0^2Rt_0 - E_N. \end{aligned}$$

We see that by adding a pure delay in the current signal, the energy that will be dissipated over time by the resistor comes partly from the source and partly from the communication. While the reasoning behind this behavior is rather obvious, it may sound paradoxical in terms of generated and dissipated energies by the source and the load.

In the following sections, the effect of time delays will be studied in different system. In particular, it is interesting to see the behavior of a delayed spring-damper or a delayed mass-damper. A spring-damper system is analogous to a PD controller, widely extended in robotics. And a mass-damper captures well the dynamical behavior of a single DoF haptic device or a robot arm. Since the analysis is in the electrical domain, the electrical DC circuits analogous to those systems will be investigated:

- Delayed spring-damper $\Longleftrightarrow$ Delayed resistor-capacitor (R-C) circuit
- Delayed mass-damper $\Longleftrightarrow$ Delayed resistor-inductor (R-L) circuit

Delayed Resistor - Capacitor

Consider the R-C circuit in Fig. 3.3.4

The voltage source generates $v_0(t)$ such that

$$v_0(t) = \begin{cases} V_0, & \text{if } t \le t_0, \quad \forall t \ \ge 0 \\ 0, & \text{if } t > t_0, \quad \forall t \ \ge 0. \end{cases} \tag{3.5}$$

The voltage and current equations for a R-C circuit are as follow:

$$v_C(t) = V_0(1 - e^{-\frac{t}{RC}}), \qquad i_R(t) = \frac{V_0}{R}e^{-\frac{t}{RC}}.$$

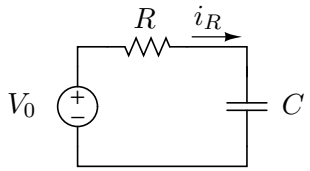

Figure 3.3.4: R-C circuit

Considering only the charging transient of the capacitor and assuming zero initial voltage, the energy stored by the capacitor is given by:

$$\begin{aligned} E_C(t=-0) &= 0, \\ E_C(t\to\infty) &= \frac{1}{2}CV_0^2. \end{aligned}$$

The energy dissipated by the resistor is then given by:

$$E_R(\to\infty) = \int_0^\infty i_R(\tau)v_R(\tau)d\tau = \frac{V_0^2}{R}\int_0^\infty e^{-\frac{2\tau}{RC}}d\tau = \frac{1}{2}CV_0^2,$$

where

$$v_R(t) = v_0(t) - v_c(t) = V_0 - V_0(1-e^{-\frac{t}{RC}}) = V_0 e^{-\frac{t}{RC}}.$$

The energy supplied by the voltage source is given by:

$$E_v(t\to\infty) = \int_0^\infty i_R(\tau)v_0(\tau)d\tau = \frac{V_0^2}{R}\int_0^\infty e^{\frac{t}{RC}}d\tau = CV_0^2.$$

Thus, the energy supplied by the voltage source is distributed between the resistor and the capacitor as:

$$E_v = E_R + E_C.$$

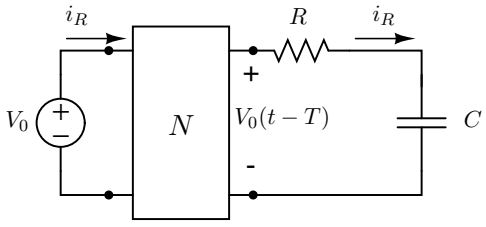

Figure 3.3.5: R-C circuit with a voltage delay network

Following, a two-port network containing a pure delay in the forward path is placed between the source and the resistor, as shown in Fig. 3.3.5. This delay affects only the voltage, such that the R-C is fed with a delayed version of the v_0. The current is consequently also affected by the delay but imposted to be the same on both sides of the two-ports.

We rewrite the system equations for the new configuration:

$$\begin{aligned} v_C(t) &= V_0(1-e^{-\frac{t-T}{RC}}), \\ i_R(t) &= \frac{V_0}{R}e^{-\frac{t-T}{RC}}, \\ v_R(t) &= V_0 - V_0(1-e^{-\frac{t-T}{RC}}) = V_0 e^{-\frac{t-T}{RC}}. \end{aligned}$$

Energy of the capacitor:

$$\begin{aligned} E_C(t\to\infty) &= \int_0^\infty i_R(\tau)v_C(\tau)d\tau \\ &= \int_0^T i_R(\tau)v_C(\tau)d\tau + \int_T^{t_0+T} i_R(\tau)v_C(\tau)d\tau + \int_{t_0+T}^\infty i_R(\tau)v_C(\tau)d\tau \\ &= 0 + \int_T^{t_0+T} i_R(\tau)v_C(\tau)d\tau + 0 = \int_T^{t_0+T} \frac{V_0^2}{R}\left[e^{-\frac{t-T}{RC}} - e^{-2\frac{t-T}{RC}}\right]d\tau \\ &= V_0^2 C e^{\frac{2T}{RC}}\left[-\frac{e^{-\frac{t_0+T}{RC}} - e^{\frac{-T}{RC}}}{e^{\frac{T}{RC}}} + (e^{-2\frac{t_0+T}{RC}} - e^{\frac{-2T}{RC}})\right]. \end{aligned}$$

Energy of the resistor:

$$\begin{aligned} E_R(t\to\infty) &= \int_0^\infty i_R(\tau)v_R(\tau)d\tau \\ &= \int_0^T i_R(\tau)v_R(\tau)d\tau + \int_T^{t_0+T} i_R(\tau)v_R(\tau)d\tau + \int_{t_0+T}^\infty i_R(\tau)v_R(\tau)d\tau \\ &= \int_T^{t_0+T} \frac{V_0^2}{R^2}e^{\frac{-2(\tau-T)}{RC}}Rd\tau = V_0^2\int_T^{t_0+T} e^{\frac{-2(\tau-T)}{RC}}d\tau \\ &= -V_0 C e^{\frac{2T}{RC}}\left[e^{-2\frac{(t_0+T)}{RC}} - e^{\frac{-2T}{RC}}\right]. \end{aligned}$$

So the total energy of the R-C is given by:

$$E_R + E_C = V_0^2 C e^{\frac{T}{RC}}\left[-e^{-\frac{t_0+T}{RC}} + e^{\frac{-T}{RC}}\right]$$

Energy supplied by the voltage source:

$$\begin{aligned} E_v(\to\infty) &= \int_0^\infty i_R(\tau)v_0(\tau)d\tau \\ &= \int_0^T i_R(\tau)v_0(\tau)d\tau + \int_T^{t_0} i_R(\tau)v_0(\tau)d\tau + \int_{t_0}^\infty i_R(\tau)v_0(\tau)d\tau \\ &= 0 + \int_T^{t_0} i_R(\tau)v_0(\tau)d\tau + 0 = \int_T^{t_0} \frac{V_0^2}{R}e^{-\frac{t-T}{RC}}d\tau \\ &= V_0^2 C e^{\frac{T}{RC}}\left[-e^{\frac{-t_0}{RC}} + e^{\frac{-T}{RC}}\right]. \end{aligned}$$

Finally, the difference between the energy supplied by the voltage source and the energy stored and dissipated by the R-C is given by:

$$E_N = E_v - (E_R + E_C) = V_0^2 C e^{\frac{T-t_0}{RC}} \left[-1 + e^{\frac{-T}{RC}}\right], \tag{3.6}$$

whose negative value due to the $(-1 + e^{-a})\ \forall a \geq 0$ term indicates a purely active behavior. So the delay network N is an active network and generates an amount of energy E_N.

Example 10 *Consider the circuit in Fig. 3.3.5 with the following values:*

$$R = 10\ \Omega, \quad C = 0.01\ F, \quad T = 0.1\ s, \quad V_0 = 1V \quad t_0 = 0.2\ s \tag{3.7}$$

The resulting plots from the above simulated circuit are shown in Fig. 3.3.6. As can be seen, the capacitor C starts charging as soon the delayed voltage reaches the left port of N. At $t = 0.2s$, $v_0(t_0) = 0$ and thus there is no further energy contribution at the left port of N. Instead, the right port of N keeps generating until $t = 0.3s$ and so its energy, $E_{RC} = E_R + E_C$, keeps increasing.

Note the difference between the energy supplied by the source, E_v, and that of the R-C, E_{RC}.

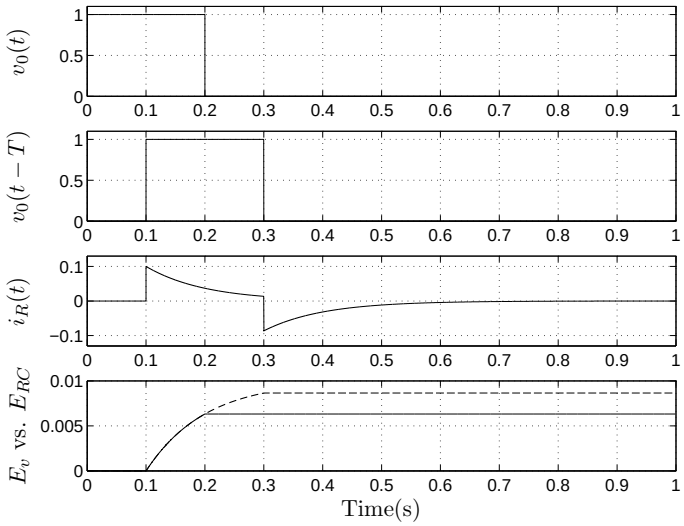

Figure 3.3.6: Signals of a delayed R-C. E_v (solid) , E_{RC} (dashed)

Delayed Resistor - Inductor

Consider the R-L circuit in Fig. 3.3.7

The voltage source generates $v_0(t)$

$$v_0(t) = \begin{cases} V_0, & \text{if } t \leq t_0, \quad \forall t \geq 0 \\ 0, & \text{if } t > t_0, \quad \forall t \geq 0, \end{cases} \tag{3.8}$$

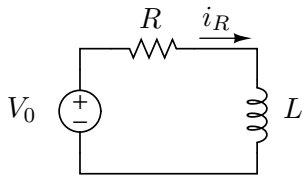

Figure 3.3.7: R-L circuit

The current and voltage equations for a L-C circuit are as follow:

$$v_L(t) = V_0 e^{-\frac{tR}{L}}, \quad v_R(t) = V_0(1 - e^{-\frac{tR}{L}}), \quad i_R(t) = \frac{V_0}{R}(1 - e^{-\frac{tR}{L}}).$$

The energy supplied by the voltage source equals the energy of the impedance given by the inductance and the resistance. This is:

$$E_{RL}(t \to \infty) = \int_0^\infty i_R(\tau) v_0(\tau) d\tau = \frac{V_0^2}{R} \int_0^{t_0} (1 - e^{-\frac{\tau R}{L}}) d\tau = \frac{V_0^2 t_0}{R} + \frac{V_0^2 L}{R^2} \left[-1 + e^{-\frac{t_0 R}{L}} \right].$$

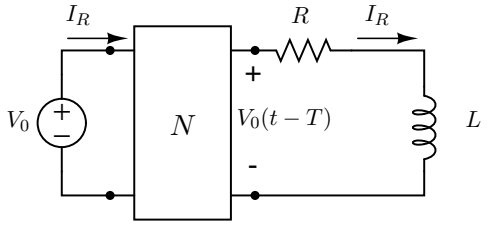

Figure 3.3.8: R-L circuit with a voltage delay network

Following, a two-port network containing a pure delay in the forward path is placed between the source and the resistor. As in the previous case, this delay affects only the voltage, such that the R-L is fed with a delayed version of the v_0. The current is consequently also affected by the delay but note that the same current value is imposted on both sides of the two-ports. The circuit is shown in Fig. 3.3.8. The system equations for the new configuration are given by:

$$v_L(t) = V_0 e^{-\frac{(t-T)R}{L}}, \quad v_R(t) = V_0(1 - e^{-\frac{(t-T)R}{L}}), \quad i_R(t) = \frac{V_0}{R}(1 - e^{-\frac{(t-T)R}{L}}).$$

The energy at the right port of the two-ports N remains the same as for the undelayed case, that is:

$$E_{RL}(t \to \infty) = \int_0^\infty i_R(\tau) v_0(\tau - T) d\tau = \frac{V_0^2}{R} \int_0^{t_0} (1 - e^{-\frac{\tau R}{L}}) d\tau = \frac{V_0^2 t_0}{R} + \frac{V_0^2 L}{R^2} \left[-1 + e^{-\frac{t_0 R}{L}} \right].$$

It follows with the energy at the left port of N:

$$\begin{aligned} E_v(t\to\infty) &= \int_0^{\infty} i_R(\tau)v_0(\tau)d\tau \\ &= \int_0^{T} i_R(\tau)v_0(\tau)d\tau + \int_T^{t_0} i_R(\tau)v_0(\tau)d\tau + \int_{t_0}^{\infty} i_R(\tau)v_0(\tau)d\tau \\ &= 0 + \int_T^{t_0} i_R(\tau)v_0(\tau)d\tau + 0 \\ &= \frac{V_0^2}{R}\int_T^{t_0}(1-e^{-\frac{(\tau-T)R}{L}})d\tau = \frac{V_0^2(t_0-T)}{R} + \frac{V_0^2 L}{R^2}\left[-e^{-(t_0-T)\frac{R}{L}}-1\right]. \end{aligned} \tag{3.9}$$

The energy of the two-port network N is given by:

$$E_N = E_v - E_{RL} = -V_0^2\frac{T}{R} + V_0^2\frac{L}{R^2}e^{-t_0\frac{R}{L}}\left[-1+e^{T\frac{R}{L}}\right].$$

And, as it can be seen, E_N is negative defined. So the delay network N is an active network and generates an amount of energy E_N.

Example 11 *Consider the circuit in Fig. 3.3.8 with the following values:*

$$R = 100\ \Omega, \quad L = 1\ H, \quad T = 0.01\ s, \quad V_0 = 1V \quad t_0 = 0.3\ s \tag{3.10}$$

Fig. 3.3.9 show the plots of the circuit variables. The inductor L starts charging as soon the delayed voltage reaches the left port of N. At $t = 0.3s$, $v_0(t_0) = 0$ and thus there is no more energy contribution at the left port of N. Instead, the right port of N keeps increasing until $t = 0.31s$.

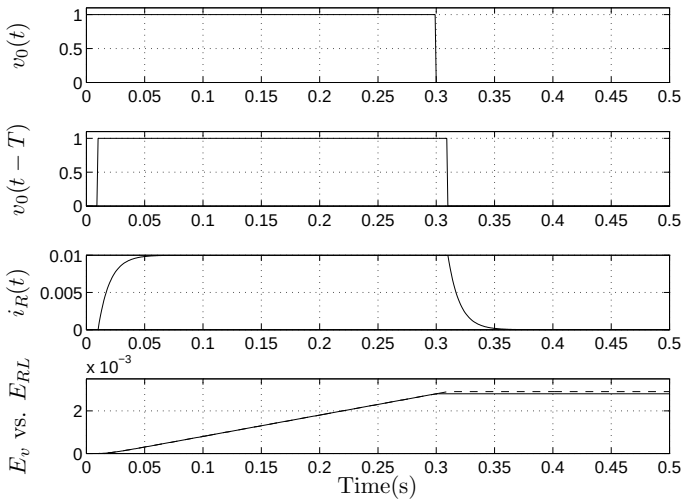

Figure 3.3.9: Signals of a delayed R-L. E_v (solid) , E_{RL} (dashed)

3.4 TDPN Properties

A TDPN must fulfill the following two conditions:

1. Each port of the TPDN must fulfill the port condition (Def. 3), i.e., the input and output current through the two-port terminals must be the same.

2. The signal traveling into one direction must be the power conjugates of the signal traveling in the opposite direction. In other words, if velocity is traveling forward, force must be traveling backward and vice versa. See Fig. 3.2.2.

A TDPN is a LTI network if both, forward and backward delays are constant, that is, a network having the linear input-output relationship $y(t) = ku(t)$ in both directions will be time invariant if $y(t-T) = ku(t-T)$.

A TDPN will be time variant if it is not time invariant. This will happen if at least one of the time delays is not constant or there is package loss. In this work we shall be concerned with both, time variant and time invariant TDPNs. Note that many tele-operation systems use packed switched networks for communicating both sides of the system, introducing varying time delays and package loss.

Finally, as it has been seen in the previous sections, the TDPN is as an active network because it includes a time delay. The proof has been shown in Sec. 2.7.

3.5 Energy Splitting: Left to Right and Right to Left Energy Flows

Consider the TDPN shown in Fig. 3.5.1.

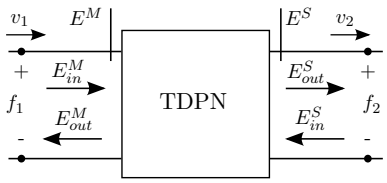

Figure 3.5.1: *in* and *out* energies of a TDPN

The energy flow of a TDPN can be split into left to right (L2R) and (R2L) energy flows. As will be seen, this segmentation is necessary for the stability analysis. The energy of the TDPN is given by:

$$E_N(t) \;=\; E^M(t) + E^S(t), \quad \forall t \;\geq 0, \tag{3.11}$$

where left and right port energy contributions, E^M and E^S respectively, are

$$\begin{aligned} E^M(t) &= \int_0^t P^M(\tau)d\tau = \int_0^t f_1(\tau)v_1(\tau)d\tau, \;\forall t \;\geq 0, \\ E^S(t) &= \int_0^t P^S(\tau)d\tau = \int_0^t -f_2(\tau)v_2(\tau)d\tau, \;\forall t \;\geq 0, \end{aligned} \tag{3.12}$$

being P^M and P^S left and right port powers. Further, the following proposition holds:

Proposition 2 *The energy flow observed at a port of a network, E, can be split into positive and negative components, each of which indicates the direction of propagation.*

Splitting positive and negative port powers as:

$$\begin{aligned} P_+(t) &= P(t) \quad \forall f(t), v(t) \quad s.t. \quad f(t)v(t) > 0, \\ P_-(t) &= -P(t) \quad \forall f(t), v(t) \quad s.t. \quad f(t)v(t) < 0. \end{aligned} \tag{3.13}$$

Positive and negative contributions of the energy flow are

$$\begin{aligned} E_+(t) &= \int_0^t P_+(\tau)d\tau, \quad \forall t \geq 0, \\ E_-(t) &= \int_0^t P_-(\tau)d\tau, \quad \forall t \geq 0, \end{aligned} \tag{3.14}$$

both being monotonic and positive defined.

Definition 22 *Input and output components of left and right port energies are related to positive and negative power as:*

$$\begin{aligned} E^M_{in}(t) &= E^M_+(t), \quad E^M_{out}(t) = E^M_-(t), \\ E^S_{in}(t) &= E^S_+(t), \quad E^S_{out}(t) = E^S_-(t), \quad \forall t \geq 0, \end{aligned} \tag{3.15}$$

where the subscript *in* refers to energy injected into the TDPN from either side and *out* to energy coming out from the TDPN. For instance, the signal E^M_{in} is the energy flowing into the TDPN from the left (master) side; the signal E^S_{out} is the energy flowing out from TDPN at the right (slave) side. See Fig. 3.5.1.

Proposition 2 and Def. 22 allow right and left port energy flows to be written as:

$$\begin{aligned} E^M(t) &= E^M_{in}(t) - E^M_{out}(t), \quad \forall t \geq 0, \\ E^S(t) &= E^S_{in}(t) - E^S_{out}(t), \quad \forall t \geq 0. \end{aligned} \tag{3.16}$$

Using (3.16), (3.11) can be rewritten as:

$$E_N = E^M_{in}(t) - E^M_{out}(t) + E^S_{in}(t) - E^S_{out}(t). \tag{3.17}$$

As will be seen in the next chapter, (3.16) and (3.17) are vital in the passivity analysis and passivity control of the TDPN type of networks.

3.6 The TDPN in Teleoperation Schemes

The interest in representing a communication as a TDPN lies in that (a) it is analogous to an electrical circuit, benefiting thus from the proficiency of the electrical domain, and (b) the interconnection medium, i.e. the ports, is emphasized rather than the internals of communication. The network masks a set of properties that result in energy generation or dissipation visible at the ports. In this sense, an analysis in the time domain based on the energy displayed at the port allows a description of the communication element by just looking at the network ports, irrespective of time delay, package loss, black outs and jitter. All these factors have an impact on the energy flow through the network. In this section we show the application of the TDPN in several teleoperation schemes.

As mentioned above, a communication channel that transfers velocity signals in both directions does not present the clear network representation due to the lack of an effort signal being transmitted. Taking the Position-Position example, the first step to analyze the system is to identify the communication channel in a comprehensive network representation to allow examination of the system in terms of energy flows. As will be seen, the Position-Position channel can in fact be represented by means of TDPNs. By extracting and expanding the analogous electrical scheme the system unveils a network arrangement which allows segmentation of active energy due to the delays. As it has been shown, *delayed* dependent current sources are the cause of *TDPN masking*. Once the TDPN networks of the Position-Position are identified, a Passivity Controller that encompasses the TDPN can be easily designed to dissipate the virtual energy generated by the TDPN. The control of TDPN passivity is subject of Chapter 4.

3.7 Position-Position and the ambiguity of the network causality

Consider the classical Position-Position architecture shown as a block diagram representation in Table 3.1. When using the passivity framework, system input and output variables must be power conjugated, i.e. each input must be related to an output and their product must be power. Hence, if only the mechanical domain is considered, inputs and outputs must be generalized velocities and torques [39], [97]. This presents a difficulty when representing a Position-Position system since a mapping to flow and effort representations is not obvious. The causality of the communication channel, i.e. the input/output relationships between flow and effort, is therefore ambiguous. In other words, the block diagram misleads the extraction of the network representation.

A solution to solve the ambiguity in the network causalities is presented here on the based of TDPNs. The employment of delayed dependent sources in the model unveils hidden, power-port conform, network structures, which allows electrical network treatment.

The augmented circuit is shown in Fig. 3.7.1[1]. The port variables for each TDPN are as follows:

[1]The connection between the two dependent sources through the lower terminals of the sources is omitted in this representation for the sake of clarity.

$$\text{TDPN A}: \begin{cases} \langle \quad f_m(t) \quad , \; v_s(t-T) \; \rangle & \text{at the master} \\ \langle \; f_m(t-T) \; , \quad v_s(t) \quad \rangle & \text{at the slave} \end{cases}$$

$$\text{TDPN B}: \begin{cases} \langle \; f_s(t-T) \; , \quad v_m(t) \quad \rangle & \text{at the master} \\ \langle \quad f_s(t) \quad , \; v_m(t-T) \; \rangle & \text{at the slave} \end{cases}$$

Proposition 3 *The representation in Fig. 3.7.1 is analogous to that of Table 3.1(2n row) and so to the block diagram representation in Table 3.1(1st row).*

Proof Consider the network $\hat{N}_z$ in Fig. 3.7.1. Its energy is given by:

$$E_{\hat{N}_z}(t) = E_{Na}(t) + E_{Nb}(t) + E^{Ca}(t) + E^{Cb}(t), \tag{3.18}$$

where E_{Na} and E_{Nb} are the energy contributions of TDPN A and TDPN B respectively, and E^{Ca} and E^{Cb} are the energy supplied by the non-delayed dependent sources. Their values are given by:

$$\begin{aligned} E_{Na}(t) &= \int_0^t [f_m(\tau)v_s(\tau - T)] - [f_m(\tau - T)v_s(\tau)]\, d\tau \\ E_{Nb}(t) &= \int_0^t [f_s(\tau - T)v_m(\tau)] - [f_s(\tau)v_m(\tau - T)]\, d\tau \\ E^{Ca}(t) &= \int_0^t f_m(\tau - T)v_s(\tau) d\tau \\ E^{Cb}(t) &= -\int_0^t f_s(\tau - NT)v_m(\tau) d\tau \end{aligned}$$

Note the negative sign of E^{Cb} due to the outgoing direction of v_m w.r.t the source port. Consider now the network N_z in Table 3.1(2n row). Its energy is given by:

$$E_{Nz}(t) = \int_0^t [f_m(\tau)v_s(\tau - T)] - [f_s(\tau)v_m(\tau - T)]\, d\tau \tag{3.19}$$

Where it can be seen that, $E_{\hat{N}_z} = E_{Nz}$. ∎

Table 3.1: Block diagram and electrical scheme of the P-P architecture.

1. Block Diagram	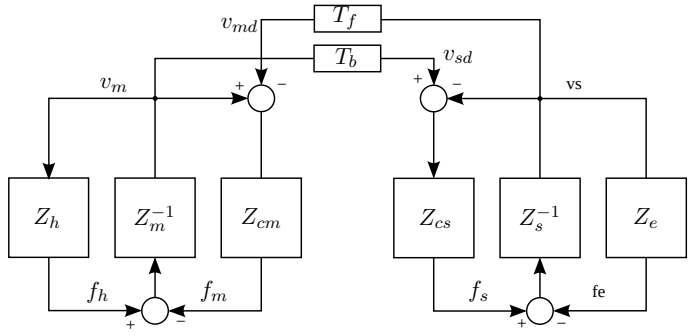
2. Electrical Scheme	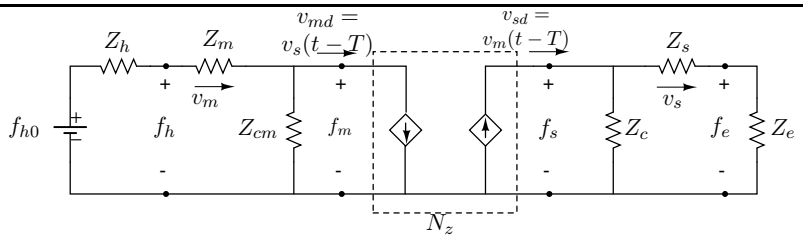

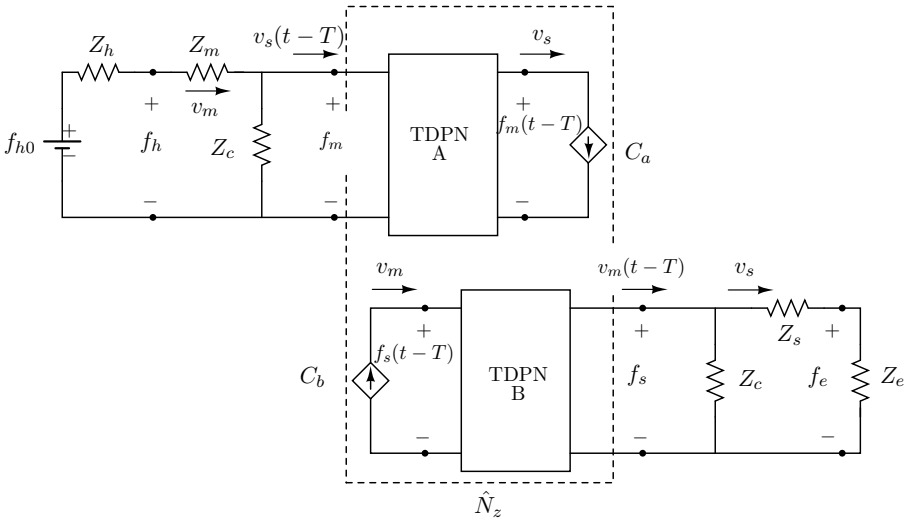

Figure 3.7.1: Position-Position architecture augmented with a pair of TDPNs

3.8 Position-Force computed Architecture

In this architecture, the application of the TDPN is rather straightforward. In fact, as will be seen, it adds unnecessary redundancy into the system. It is however a good example to understand how TDPNs enhance the network representation of a teleoperation scheme. The true potential of the TDPN augmentation is visible in those, less intuitive architectures, as are Position-Position, Position-Force measured, Force-Force and any three or four channels configurations.

Recall the block diagram and network representation schemes in Sec. 2.7, reproduced here for the reader's convenience within Table 3.2.

Table 3.2: Block diagram and electrical scheme of the P-Fc architecture.

1. Block Diagram	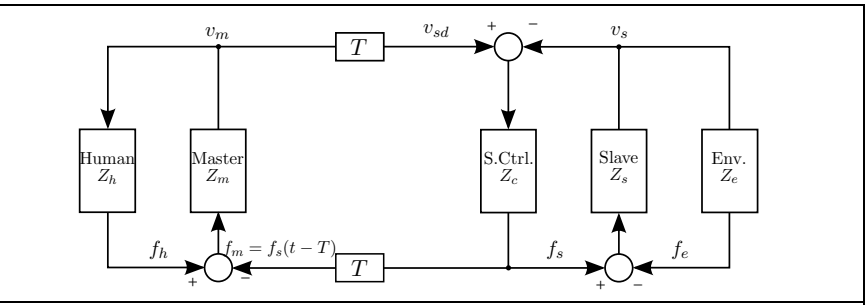
2. Electrical Scheme	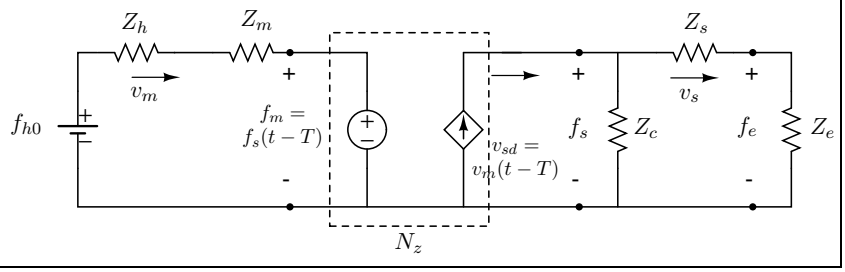

Following, the delayed dependent force and velocity sources are shifted to their respective non-delayed locations by virtue of two TDPNs. The augmented circuit is shown in Fig. 3.8.2. The representation in Fig. 3.8.1 is an alternative rearrangement of the previous one. The port variables for each TDPN are as follows:

$$\text{TDPN A}: \begin{cases} \langle\ f_s(t-T)\ ,\quad v_m(t)\ \rangle & \text{at the master} \\ \langle\ f_s(t)\ ,\ v_m(t-T)\ \rangle & \text{at the slave} \end{cases}$$

$$\text{TDPN B}: \begin{cases} \langle\ f_s(t-T)\ ,\ v_m(t)\ \rangle & \text{at the master} \\ \langle\ f_s(t)\ ,\quad v_m(t-T)\ \rangle & \text{at the slave} \end{cases}$$

Proposition 4 *The representation in Fig. 3.8.2 is analogous to that of Table 3.2(2nd row) and so to the block diagram representation in Table 3.2(1st row).*

Proof Consider the network $\hat{N}_z$ in Fig. 3.8.2 (or Fig. 3.8.1). Its energy is given by:

$$E_{\hat{N}_z}(t) = E_{Na}(t) + E_{Nb}(t) + E^{Ca}(t) + E^{Cb}(t), \tag{3.20}$$

where E_{Na} and E_{Nb} are the energy contributions of TDPN A and TDPN B respectively, and E^{Ca} and E^{Cb} are the energy supplied by the non-delayed dependent sources. Their values are given by:

$$
\begin{aligned}
E_{Na} &= \int_0^t [f_s(\tau - T)v_m(\tau)] - [f_s(\tau)v_m(\tau - T)]\, d\tau \\
E_{Nb} &= \int_0^t [f_s(\tau - T)v_m(\tau)] - [f_s(\tau)v_m(\tau - T)]\, d\tau \\
E^{Ca} &= \int_0^t f_s(\tau)v_m(\tau - T)d\tau, \qquad E^{Cb} = -\int_0^t f_s(\tau - T)v_m(\tau)d\tau
\end{aligned}
$$

Consider now the network N_z in Table 3.2(2n row). Its energy is given by:

$$
E_{Nz}(t) = \int_0^t [f_s(\tau - T)v_m(\tau)] - [f_s(\tau)v_m(\tau - T)]\, d\tau
$$

Where it can be seen that, $E_{\hat{N}z} = E_{Nz}$. ∎

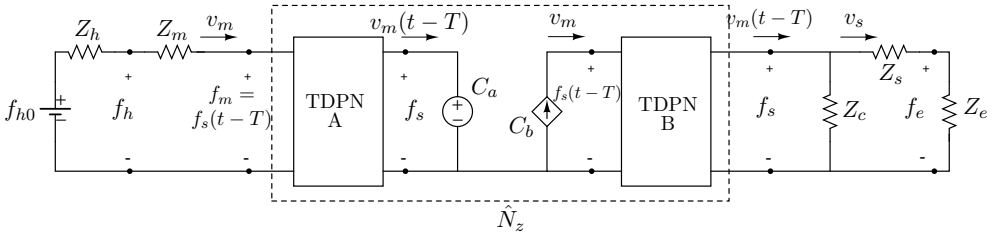

Figure 3.8.1: Position-Force architecture augmented with a pair of TDPNs

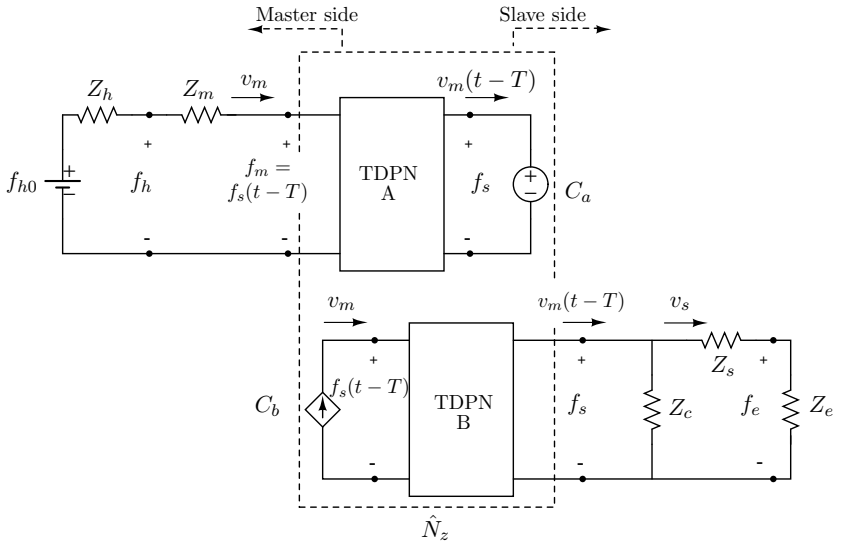

Figure 3.8.2: Position-Force computed architecture augmented with a pair of TDPNs

Table 3.3: Block diagram and electrical scheme of the P-Fmsr

1. Block Diagram	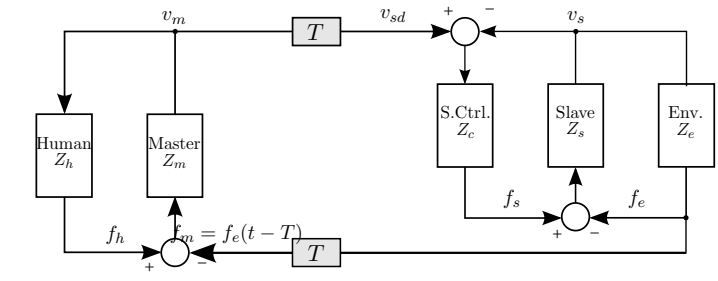
2. Electrical Scheme	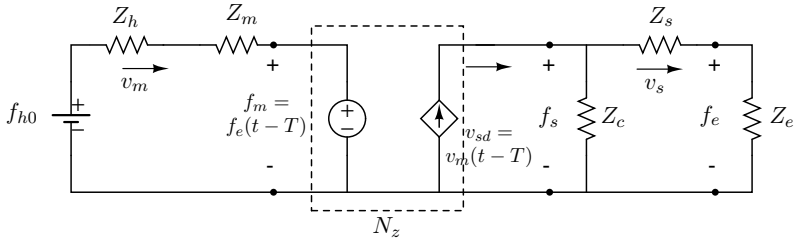

3.9 Position-Force measured Architecture

Following the same procedure as in the previous sections, the scheme of a Position-Force measured (PFmsr) architecture with the TDPNs augmentation can be extracted. Those are shown in Table 3.3 and in Fig. 3.9.1 The port variables for each TDPN are given by:

$$\text{TDPN A}: \begin{cases} \langle \quad f_e(t-T)\ ,\ v_m(t) \quad \rangle & \text{at the master} \\ \langle \quad f_e(t)\ ,\ v_m(t-T) \ \rangle & \text{at the slave} \end{cases}$$

$$\text{TDPN B}: \begin{cases} \langle \quad f_s(t-T)\ ,\ v_m(t) \ \rangle & \text{at the master} \\ \langle \ f_s(t)\ ,\ v_m(t-T) \quad \rangle & \text{at the slave} \end{cases}$$

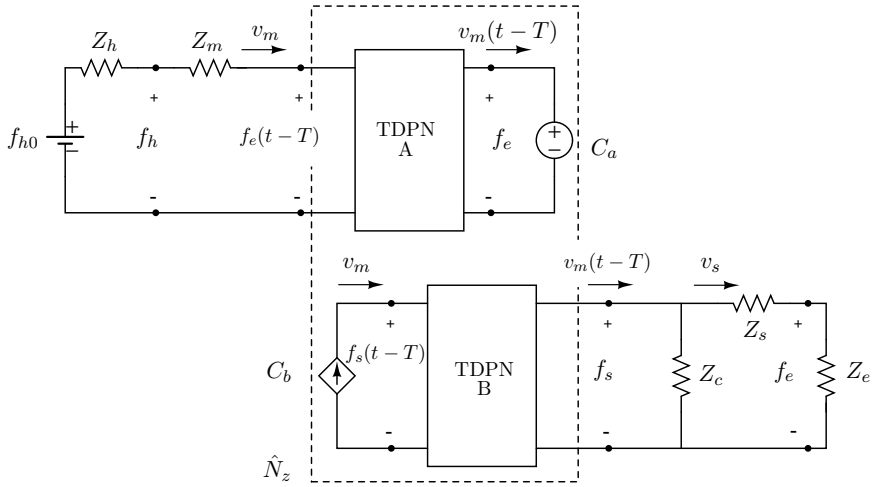

Figure 3.9.1: Position-Force measured architecture augmented with a pair of TDPNs

3.10 Four Channels Architecture

In the four channels architecture, both position and force signals are sent in both directions. Forces/ torques are captured by sensors located at the master device and the slave robot. It was first proposed by Lawrence in [61] and later extended by Hashtrudi-Zaad and Salcudean in [45]. This architecture is of special relevance since it can achieve theoretical ideal response, as defined by position and force errors between master and slave devices. An alternative representation is here presented in Fig. 3.10.1, where the main difference is the omission of local force feedback loops at master and slave since the main concern here is on the communication channel. G_m and G_s are master and slave gains for the force channels respectively and will be assumed unitary in the next steps. Note that human operator and master device are combined in a single block, named

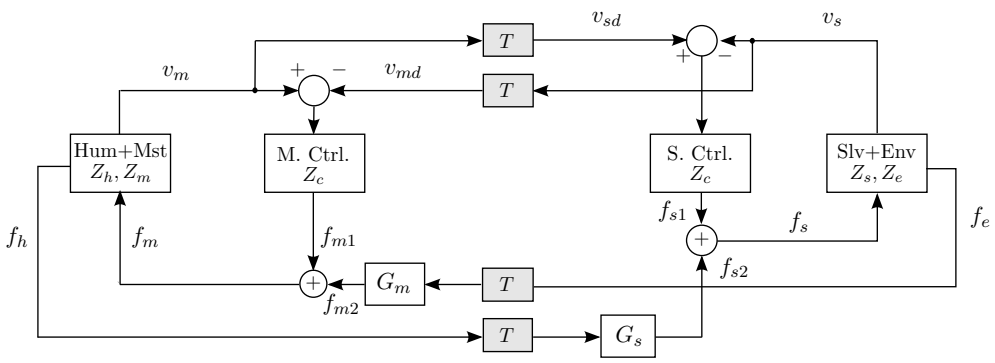

Figure 3.10.1: Block diagram of a four Channels architecture

according to their impedances Z_h, Z_m. The same simplification is applied at the slave side, with the environment impedance, Z_e and the slave robot, Z_s. Apart from that, the scheme is self-explanatory and can be seen as a combination of a Position-Position and a Position-Force measured.

The equivalent electrical scheme is shown in Fig. 3.10.2. Not surprisingly the electrical representation of the four channels contains four delayed dependent sources: Two for the force signals transmission, and two for the velocity signals transmission. Note the parallel interconnection at master and slave sides to produce the force commands, $f_m = f_{m1} + f_{m2}$ and $f_s = f_{s1} + f_{s2}$. Once again, the electrical scheme tells us the conjugate pairs at each network port. The same procedure as in the previous sections is followed in order to obtain the hidden networks that are responsible for the energy transmission, that is, the TDPNs. The TDPN based augmented scheme is presented in Fig. 3.10.3 and the port variables for the new networks are:

$$\text{TDPN A}: \begin{cases} \langle \quad f_e(t-T)\ ,\ v_m(t) \quad\quad \rangle & \text{at the master} \\ \langle \quad\quad f_e(t)\ ,\ v_m(t-T) \rangle & \text{at the slave} \end{cases}$$

$$\text{TDPN B}: \begin{cases} \langle \quad\quad f_{m2}(t)\ ,\ v_s(t-T)\ \rangle & \text{at the master} \\ \langle\ f_{m2}(t-T)\ ,\ v_s(t) \quad\quad \rangle & \text{at the slave} \end{cases}$$

$$\text{TDPN C}: \begin{cases} \langle \quad\quad f_h(t)\ ,\ v_s(t-T)\ \rangle & \text{at the master} \\ \langle\ f_h(t-T)\ ,\ v_s(t) \quad\quad \rangle & \text{at the slave} \end{cases}$$

$$\text{TDPN D}: \begin{cases} \langle \quad f_{s2}(t-T)\ ,\ v_m(t) \quad\quad \rangle & \text{at the master} \\ \langle \quad\quad f_{s2}(t)\ ,\ v_m(t-T) \rangle & \text{at the slave} \end{cases}$$

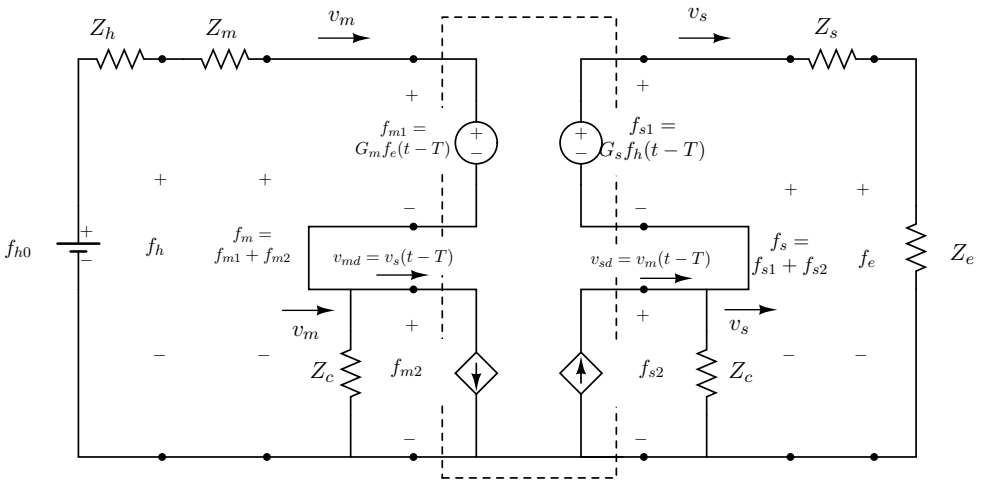

Figure 3.10.2: Electrical scheme of a 4 Channels architecture

3.11 Discussion

We have seen augmented representations of various teleoperation architectures based on the TDPN concept. The TDPN unveils a hidden two-port network that is responsible for the energy transportation. Its usefulness relies on the fact that the energy due to a delayed communication can be isolated from the rest of the scheme. As it has been seen, this energy results in non-passive systems. The next chapter deals with passivity of the TDPNs. This will be done on the basis of Time Domain Passivity controllers, designed such that they dissipate the amount of energy introduced by the TDPNs.

As it has been shown, it is in the electrical domain where TDPNs can be made visible. Roughly, the *modeling chain* starts from the block diagram, a representation that is not attached to any physical phenomena; by using the electro-mechanical analogy an analogous circuit representation can be easily extracted. It is in this domain, where the TDPN analysis is possible. Back mapping to block diagrams is straightforward. In the next chapters, a few examples are shown.

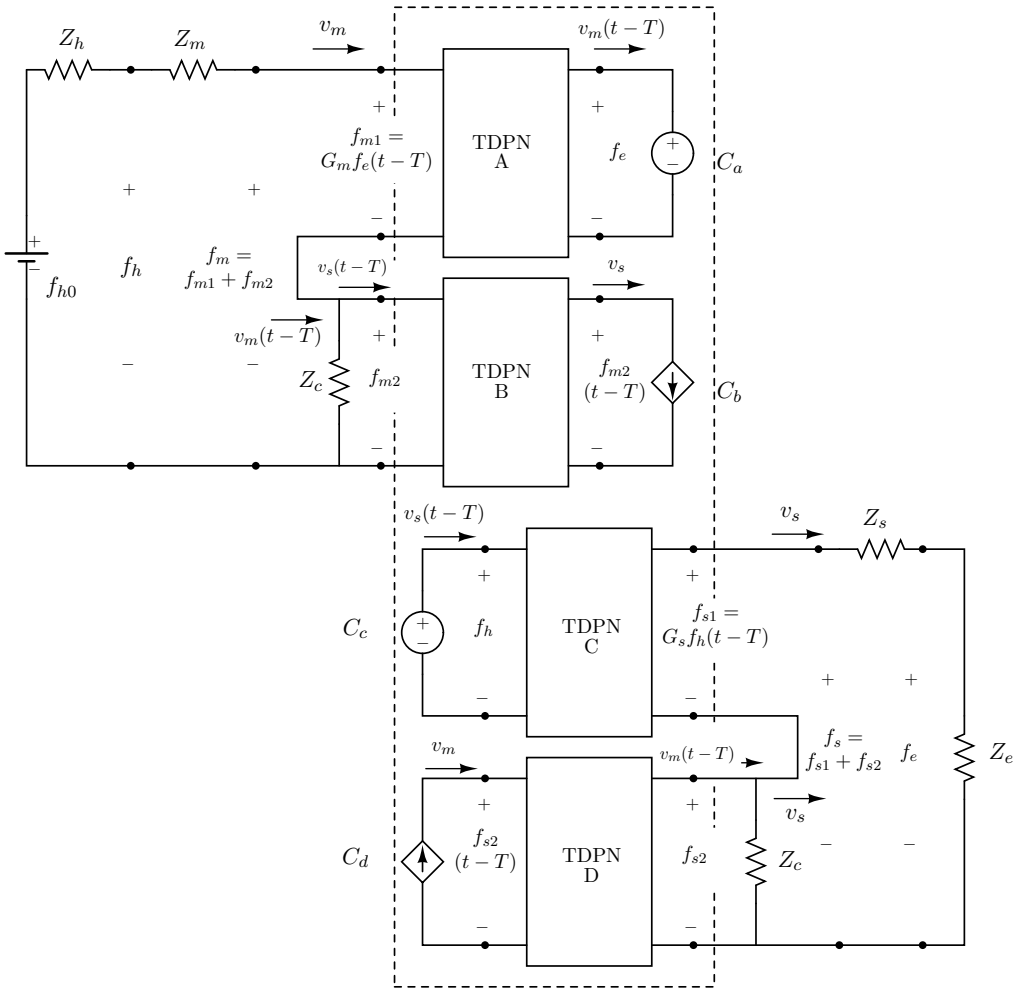

Figure 3.10.3: 4 Channels architecture augmented with a pair of TDPNs

The generality of the electrical representation suggests that TDPNs could be used in domains other than teleoperation or even robotics. Some applications in other robotics fields can be already found in the literature. For instance, rate control systems and multilateral control systems are tackled by using TDPNs in [86] and [85]. In [103], passivity of virtual free-floating masses is analyzed using the TDPN concept as well.

Chapter 4

Time Domain Passivity Control for Delayed Networks

This chapter presents the stability analysis of a delayed force reflecting teleoperation system using the Time Domain Passivity approach. An energy analysis of the communication channel is presented on the basis the Time Delay Power Network (TDPN), the network representation of a fundamental communication element. The TDPN is a network which describes the energetic coupling between both sides of any teleoperation system. The aim of this chapter is to show a systematic approach for treating passivity of the TDPN while maximizing performance using energy considerations. This treatment forms the basis of a general stability treatment valid for any teleoperation architecture, presented in the next chapter.

4.1 Motivation

The Time Domain Passivity Control Approach (TDPA) is an adaptive control method based on modulating a dissipative term in order to keep the passivity of a network. The dissipation is computed in the time domain as a function of an observed energy of the network. This approach has opened new perspectives in the control field since passivity is not considered in the design process but rather controlled during operation. Methods based on absolute stability or the convenient *Raisbeck's* passivity criterion (see Sec. 2.2) are based on some assumptions that can narrow the application field. These assumptions include the consideration of the system as linear and time invariant. Real teleoperation scenarios are of discrete nature, include numerous nonlinearities and are affected by

variable time delays and data loss in the communication channel. In those contexts the TDPA becomes a powerful tool since it does not assume anything and accepts any form of energy generation without requiring a model of the energy source. Indeed, all those characteristics of a teleoperation system result in some energy generation or dissipation. The TDPA has been already successfully applied as a control mechanism in the fields of haptics [41], [95], teleoperation [21], [104], [19], mechanical multi-body systems, [79], [83] and flexible manipulators [94].

As seen in the previous chapters, passivity can be used as a tool to guarantee stability. Passivity is clearly more conservative than stability, since a system may be stable without being passive. In other words, all passive networks fulfill the conditions for stability and absolute stability; but not all stable and absolutely stable networks are passive. That said, passivity offers the nice feature that the stability behavior of a network is unaffected by the systems that are connected to it. Moreover, cascade, parallel and most serial connections of passive networks create passive systems (see Sec. 2.2). In teleoperation there is always at least one active network which is responsable for the motion of the system (see Sec. 2.7). Still, general passivity can be guaranteed as long the activity produced by the active network is dissipated by some other network. Typically, the energy generated by the operator is distributed between master and slave devices.

It is therefore reasonable to consider a teleoperation system as connection of networks, most of them being passive. The approach pursued in this work distinguishes two stages in the design of a teleoperation system: One, which takes place in an ideal scenario and adopts the assumption that master and slave are two masses rigidly connected by a weightless bar (i.e., linear and with null time delay) [116]; and the second one, which *adapts* the ideal system to a realistic scenario, assuming discretization, nonlinearities, communication time delay and data losses.

Ideal Case Design

The ideal case scenario is an idealized teleoperation system which is used as a backbone system to perform the design. Its performance will be considered as ideal performance. The system in the real case scenario will aim at this performance under the influence of the deviations between ideal and the real case scenarios. The ideal case scenario is characterized by:

- Communication with zero transmission delay.
- Communication with zero data loss.
- Master and slave devices being modeled as pure masses.
- Human and environment being modeled as a passive impedances.
- Being a continuos LTI system.

There are different methods which can be used to design the system in the ideal scenario, some of them have been reviewed in Chapter 2. The particular choice is left open in this work, as it depends on the requirements and the aim of the teleoperation

system. Fig. 4.1.1 [1] shows a general (two channel based) teleoperation system as a cascade of one and two-port networks. The ideal case design is thus concerned with the master and slave controller networks and neglects the communication channel network, that is, it assumes to be a transparent network, where input and output are identical. The only requirement here is that these two networks must be at least absolutely stable, so that when connected across the input and output ports respectively, the system created is also stable.

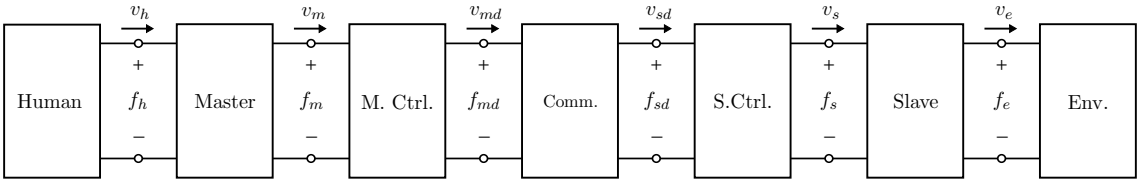

Figure 4.1.1: Network representation of a teleoperation system.

Real Case scenario

As it has been shown in Sec. 2.7, a delayed communication channel is an active network. The design of the real case scenario adds a Passivity Controller on each side of the communication channel in order to passivate the communication network, i.e. the two-port created by the cascade of the two PC's and the communication creates a passive network. Since this new network is passive, it should not affect the rest of the system since, as mentioned above, master and slave controllers must be, at least, absolutely stable.

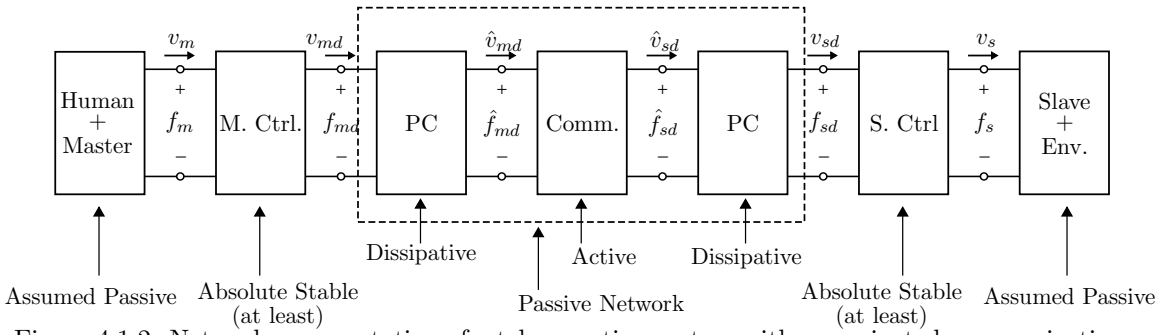

Figure 4.1.2: Network representation of a teleoperation system with a passivated communication channel.

The communication channel network considered in the scope of this work is characterized by containing a forward and a backward time delay, which can be constant or variable, and can be affected by data transmission losses. These characteristics result in a virtual energy generation which makes the communication network active.

The assumption that the networks created by the human operator and the master device on one side, and by the environment and the slave device on the other, are passive is necessary for the overall stability analysis of the teleoperation system. But in fact,

[1] For better readability, Fig. 2.7.1 is shown in this section again.

the first network at least, is intrinsically active since it is the energy source responsible for the motion of the system. The passivity assumption, found often in other works, can be made because the amount of energy injected to the system will be dissipated at the slave side through the slave system and the environment, assuming a lossless (or at least passive) transfer between both systems.

Example 12 ***Moving a coffee cup with a pen***

Consider a human operator grasping a pen tightly with a hand. Consider also a coffee cup on a table with a mass $m = 500g$*. Now, the operator applies a constant force* $F = 1N$ *orthogonal to the vertical surface of the cup, such that the cup moves at a constant speed* $v = 0.3m/s$*. The friction coefficient of the surface is* $\mu = 0.158$

The energy injected by the human through the pen to trace a $10cm$ *straight line displacement of the cup is associated to the mechanical work as:*

$$W_h = \Delta E(t = k_1) - \Delta E(t = k_2) = \int_C F dx = \int_0^{.10} 1 \; dx = 0.1J.$$

Part of this energy will be transformed into kinetic energy and part into heat due to the friction:

$$\begin{aligned} E_k &= \frac{1}{2} 0.5 \times 0.1^2 = 0.0225J. \\ E_f &= \mu \int_C -f_z dx = 0.158 \int_0^{.10} 0.5 \times 9.8 dx = 0.0775J. \end{aligned}$$

We can represent the system as cascade connection of three networks as shown in Fig. 4.1.4. The first network represents the human hand, which generates an energy of W_h*. The 2-port network representing the pen can be assumed to be lossless; therefore the following relations hold:*

$$\begin{aligned} v_1(t) &= v_2(t) \\ f_1(t) &= f_2(t) \end{aligned}$$

The one-port networking representing the coffee cup standing on the surface can be seen as a load which dissipates energy in form of kinetic energy, E_k *and heat,* E_f*.*

The three networks system is passive since:

$$W_h - E_k - E_f = 0. \tag{4.1}$$

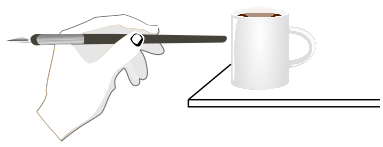

Figure 4.1.3: The Hand-Pen-Cup simile.

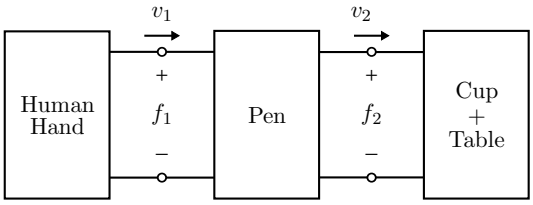

Figure 4.1.4: Network representation of the hand-pen-cup system.

4.2 Time Domain Passivity Control of the TDPN

Recall the TDPN shown in Fig. 3.5.1, replicated in Fig. 4.2.1 for the reader's convenience.

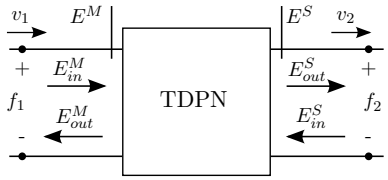

Figure 4.2.1: *in* and *out* energies of a TDPN

Recalling (3.17), the following theorem is stated:

Theorem 4.2.1 *A TDPN will be passive if*

$$E_N(t) = E^M(t) + E^S(t) = E^M_{in}(t) - E^M_{out}(t) + E^S_{in}(t) - E^S_{out}(t) \geq 0, \quad \forall t \geq 0, \quad (4.2)$$

which can be easily demonstrated by recalling (3.17) and the definition of passivity (Def. 8). ∎

The input and output components of the energy signal, (3.15), are monotonic functions which describe the energy exchange between both sides of the TDPN. Ideally *in* values at the one side match *out* values at the other side in both directions, i.e. they are identical. This would be the case of a lossless TDPN:

$$\begin{aligned} E^S_{out}(t) &= E^M_{in}(t) \\ E^M_{out}(t) &= E^S_{in}(t) \end{aligned}$$

Unfortunately, (4.2) cannot be directly used to check passivity because both port energy values of the communication channel network cannot be simultaneously observed on one site. To observe the energy flow of a TDPN, the direction of propagation must be taken into account.

The benefit of splitting the energy signal into flows toward right and left is that it allows a *decoupled port energy* analysis. By splitting the energy into its propagation paths, the active / passive characteristic of the network can be determined by checking each port individually rather than requiring both port energy values to be available at the same time and site (as required by (4.2)).

Fig. 4.2.2 shows responses of *in* and *out* values of a delayed communication channel. The network is active since more energy is received than was sent.

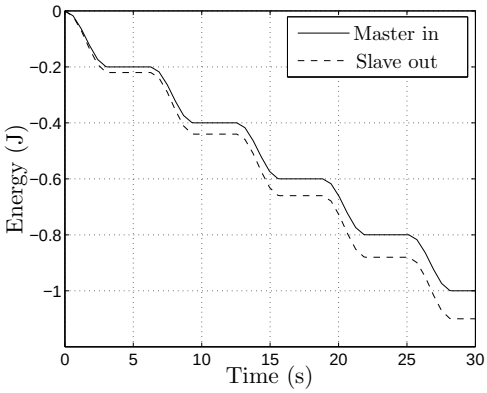

Figure 4.2.2: Master sent energy vs. slave received energy. Typical delayed channel active behavior.

Using *in* and *out* components, passivity of the channel can be checked using the decoupled energy flow expressions:

$$\begin{aligned} E_N(t) &= E^{L2R}(t) + E^{R2L}(t) \geq 0, \quad \forall t \geq 0, \\ E^{L2R}(t) &= E^M_{in}(t) - E^S_{out}(t), \quad \forall t \geq 0, \\ E^{R2L}(t) &= E^S_{in}(t) - E^M_{out}(t), \quad \forall t \geq 0, \end{aligned} \tag{4.3}$$

where E^{L2R} and E^{R2L} are the flows from left to right and from right to left respectively. A sufficient condition for (4.2) is:

$$\begin{aligned} E^{L2R}(t) &\geq 0, \quad \forall t \geq 0, \\ E^{R2L}(t) &\geq 0, \quad \forall t \geq 0. \end{aligned} \tag{4.4}$$

As mentioned above, E_N is an energy which is not observable in a real system. To that end, the following observable energies are used that represent the flow from left to right monitored at the right (slave) port and the flow from right to left monitored at the left (master) port:

$$\begin{aligned} E^{L2R}_{obs}(t) &= E^M_{in}(t - T_f) - E^S_{out}(t), \quad \forall t \geq 0 \quad \textit{(observed at the right)} \\ E^{R2L}_{obs}(t) &= E^S_{in}(t - T_b) - E^M_{out}(t), \quad \forall t \geq 0 \quad \textit{(observed at the left)} \end{aligned} \tag{4.5}$$

where T_f and T_b are forward and backward time delays. (4.5) will be valid flows as long (4.4) holds. This is statement is sustained through the following theorem.

Theorem 4.2.2 *If both observed energy flows of a TDPN are $E^{L2R}_{obs}(t) \geq 0$ and $E^{R2L}_{obs}(t) \geq 0$, then the system is passive.*

Proof To check passivity means to prove (4.2). Since both E^M_{in} and E^S_{in} are monotonic by definition ((3.15)) the following relationships hold:

$$\begin{aligned} E^M_{in}(t - T_f) &\leq E^M_{in}(t), \quad \forall t \geq 0, \\ E^S_{in}(t - T_b) &\leq E^S_{in}(t). \quad \forall t \geq 0. \end{aligned} \tag{4.6}$$

The observed decoupled energy expressions, E_{obs}^{L2R} and E_{obs}^{R2L} from (4.5), are thus lower bounded by the decoupled actual expressions, E^{L2R} and E^{R2L} from (4.3). This is:

$$\begin{aligned} E_{obs}^{L2R}(t) &\leq E^{L2R}(t), \quad \forall t \geq 0, \\ E_{obs}^{R2L}(t) &\leq E^{R2L}(t). \quad \forall t \geq 0. \end{aligned} \tag{4.7}$$

Therefore if both,

$$\begin{aligned} E_{obs}^{L2R}(t) &\geq 0 \text{ and} \\ E_{obs}^{R2L}(t) &\geq 0 \end{aligned} \tag{4.8}$$

are satisfied, so do (4.4) and thus (4.2). Conditions (4.8) are more naturally expressed as:

$$E_{out}^{S}(t) \leq E_{in}^{M}(t - T_f), \tag{4.9}$$

$$E_{out}^{M}(t) \leq E_{in}^{S}(t - T_b). \tag{4.10}$$

In other words, output energy flows must be bounded by their corresponding input energy flows.

It is clear from (4.7) that there exists an error between actual and observed energies. Conditions in (4.7) add, in fact, some conservatism in the sense that some extra energy must be dissipated than strictly needed. This can be seen as a *passive* energy leak and is actually the current energy accumulated in the communication. Clearly, due to the nature of the delayed system this leak can not be captured in the current time, $t = t$. An estimation would be possible by using a precise model of the time delay. In real scenarios however, time delay is difficult, if not impossible, to model (e.g. radio links, UDP Internet communications, etc.). Passivity is precisely a powerful tool is such contexts, that is, where things are difficult to model and predict. In Sec. 4.4 the effects of the passive energy leaks due to resulting estimation of the actual energy flows are analyzed.

Passivity Observer and Passivity Controller

Once the flows to check for passivity of the communication channel are identified, Passivity Observer (PO) and Passivity Controller (PC) can be defined. Recalling the concepts introduced in Sec. 2.4 for the Time Domain Passivity Control approach (TDPA), two fundamental elements were introduced: The Passivity Observer (PO), which monitors the energy flow of a network in the time domain; and the Passivity Controller (PC), which acts as a variable damper to dissipate active energy observed by the PO, i.e. introduced by the network. In Sec. 2.4, the rationale of controlling passivity in the time domain was given for 1-port networks and 2-port networks. In non-delayed systems, the previous two-port TDPA proved stable performance through passivity [93]. However, once time delay is introduced, the passivity condition in [93] cannot be satisfied anymore. The main reason is the fact that the PO in Sec. 2.4 cannot not integrate the power flow at each port of the bilateral controller at the same sampling time.

From (4.5) it is clear that passivity of the channel must be checked by monitoring the two flows. The observed energy on one port is thus sent to the other port and compared with the computed energy at the receiving port. This is done for both flows, left to right and right to left. Thus, the Passivity Observer must consist of a distributed structure involving two observers placed on each side of the communication network. The Passivity Observer is the algorithmic formulation of (4.5) plus the correction introduced by the Passivity Controller to satisfy passivity. The two Passivity Observers are thus defined as:

$$\begin{aligned} W_s(n) &= E^M_{in}(n-D_f) - E^S_{out}(n) + E^S_{PC}(n), \\ W_m(n) &= E^S_{in}(n-D_b) - E^M_{out}(n) + E^M_{PC}(n), \end{aligned} \tag{4.11}$$

where M and S accompanying the observed energies, W_x, stand for master and slave observers, corresponding to the right and left side of the communication respectively. D_f and D_b are forward and backward delays as sample time units so that $D_f = \frac{T_f}{T_s}$ and $D_b = \frac{T_b}{T_s}$, being T_f and T_b defined as multiples of the sampling time, T_s. Both E^M_{PC} and E^S_{PC} (later defined in (4.13)) are master and slave dissipated energies by both Forward Passivity Controller (FPC) and Backward Passivity Controller (BPC) respectively. Their specific expressions, are dependent on the causality of the local PC.

As in [40] the Passivity Controller comes in the form of a variable damping which adapts as a function of the observed flow: If the observer indicates active behaviour, the damping coefficient, β, must be such that it dissipates the active energy. Taking the right side of a TDPN whose output is velocity and input force, the PC is defined as:

$$v_{sd}(n) = \hat{v}_{sd}(n) - \beta(n) f_s(n), \tag{4.12}$$

where $\hat{v}_{sd}$ is the *untouched* velocity signal coming from the TDPN (and correspondingly from the master) and β is the dissipation coefficient, obtained as:

$$\beta(n) = \begin{cases} 0 & \text{if } W_s(n) > 0 \\ \dfrac{-W_s(n)}{T_s f_s^2(n)} & \text{else, if } |f_s| > 0 \end{cases}$$

And the dissipated energy:

$$E^S_{PC}(n) = T_s \sum_{k=1}^{k=n-1} f_s^2(k)\beta(n). \tag{4.13}$$

Applying (4.12) keeps $W_s \geq 0$, which in turn keeps $E^{L2R}_{obs} \geq 0$ and therefore $E^{L2R} \geq 0$ (4.4).

In a similar way the PC controller for the impedance case (velocity is conserved while force is modified to produce the dissipation) can be derived. The input energy from the right side (E^S_{in}) is observed and transmitted to the left side. A damping element with coefficient α is thus defined to satisfy (4.10), which bounds the output energy of the master ($E^M_{out}(n)$) below the delayed input energy from the slave ($E^S_{in}(n-D_b)$):

$$\alpha(n) = \begin{cases} 0 & \text{if } W_m(n) > 0 \\ \dfrac{-W_m(n)}{T_s v_m^2(n)} & \text{else, if } |f_s| > 0 \end{cases}$$

And the PC:

$$f_m(n) = f_{md}(n) + \alpha(n) v_m(n) \tag{4.14}$$

As a result, the force command to the master, f_{md}, is modified by virtue of the dissipation produced by the adaptive coefficient α.

The system created by the cascade of the Master PC (E^M_{PC}), the TDPN (E_N) and the Slave PC (E^S_{PC}), shown in Fig. 4.2.3, is thus a passive one:

$$E^M_{PC}(n) + E_N(n) + E^S_{PC}(n) \geq 0 \tag{4.15}$$

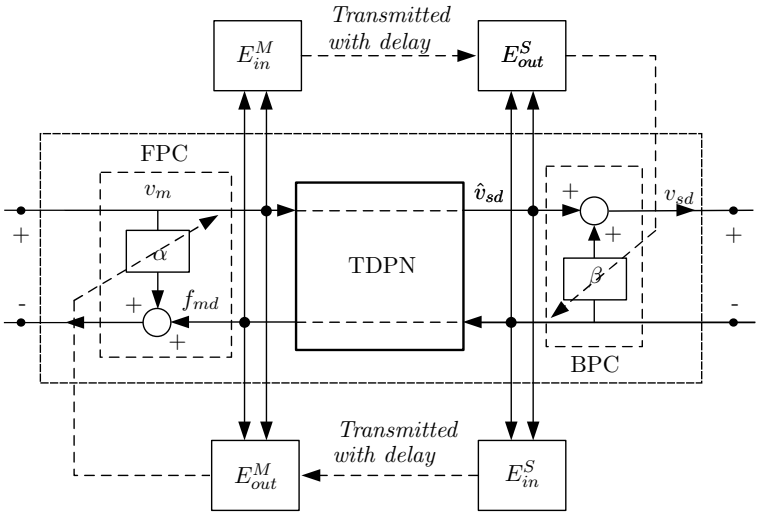

Figure 4.2.3: Passivated TDPN using master and slave PO / PC.

4.3 Basic Position Force Architecture

In the Position-Force computed (P-Fc) architecture, the PO/PC pairs shown in Sec. 4.2 are embedded into a teleoperation system, which sends position forth and feeds computed force back. The computed force is generated by a virtual spring and damper located at the slave side. The computed force is the command to the slave robot and the feedback to master device through the channel. This architecture was first presented in [91] and [18]. Recalling the system presented in Fig. 2.7.7, Fig. 4.3.1 shows the basic P-Fc architecture scheme in a combined representation, that is, the scheme combines elements from the network representation and the flow diagram. The network representation is used to show the system as a cascade one and two-port networks. Each network element is however detailed by an internal flow diagram. The system equations are as follow,

$$Z_m(s) = M_m s + B_m, \quad Z_s(s) = M_s s + B_s, \quad Z_{sc}(s) = \frac{B_{cs} s + K_{cs}}{s},$$

$$\hat{v}_{sd}(s) = v_m(s)e^{-sT_f}, \quad f_{md}(s) = f_s(s)e^{-sT_b},$$

where Z_m, Z_s are master and slave dynamics, Z_{sc} is a PI controller, that is, a virtual spring and damper; M_m, M_s, B_m and B_s are master and slave masses and viscous frictions, and K_{sc}, B_{sc} are integral and proportional gains; T_f and T_b are forward and backward delays. These equations are analogous to (2.84), (2.85).

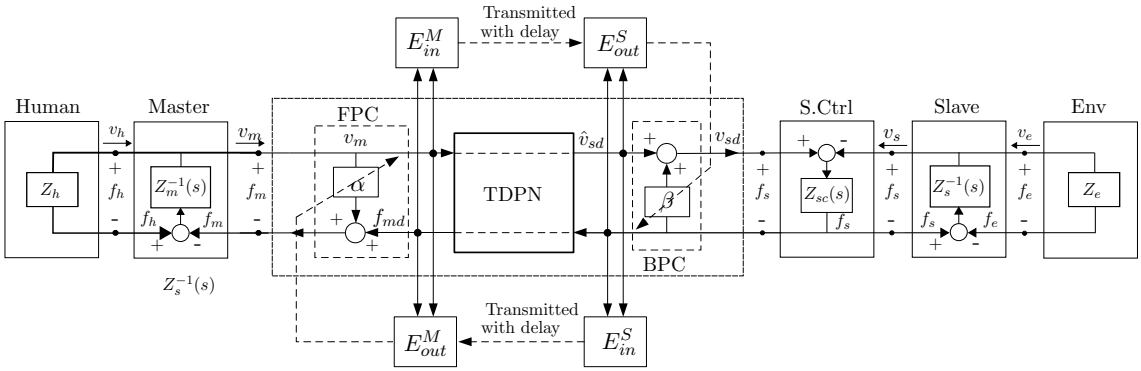

Figure 4.3.1: The basic P-Fc architecture.

In the basic P-Fc architecture, two POs are attached to each port of the network channel in order to monitor the input and output energies separately. Based on the causality of the communication network, the PC at the left side, placed between the master and the channel, is of impedance type; the PC at the right side of the communication is of admittance type. The input energy to the channel at the master side (E^M_{in}) is monitored and transmitted to the slave side. The damping element β is modulated such that it bounds the output energy of the slave (E^S_{out}) below the delayed input energy from the master ($E^M_{in}(n - D_f)$), thus satisfying (4.9). The same rationale applies for the energy flow from the slave to the master.

Experimental results

The setup for the experiments is described in Sec. B.2, based on two 3 DoF PHANToMs. The PI controller was parametrized for maximum performance assuming a nearly ideal case, i.e. high stiffness (P) and null damping (D). The sampling rate was set to 1000 Hz. Overall, the bare system configuration (without any PO / PC) presented very narrow stability regions, allowing a maximum round-trip delay of $T_{rt} = 10\ ms$.

Fig. 4.3.2(a) and Fig. 4.3.2(a) show the responses in free environment and hard contact situations.

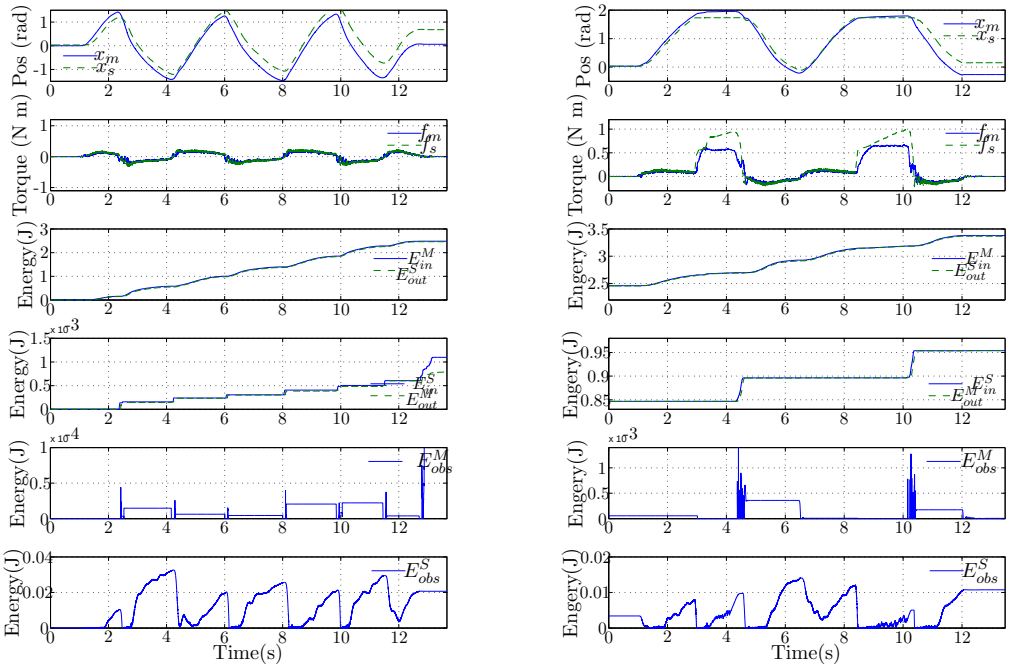

(a) Basic Position-Force Architecture in a free environment, $T_{rt} = 200\ ms$

(b) Basic Position-Force Architecture contacting a hard wall, $T_{rt} = 200\ ms$

Figure 4.3.2: Position-Force Architecture with 100 ms time delay

4.4 Over dissipation of the Passivity Controller and Position Tracking

A weakness of the TDPA is the impossibility of observing the exact amount of energy stored in the communication channel due to its delayed nature. In fact, the Passivity Observer in (4.11) or (4.5) can observe more active energy than the amount of virtual energy that is actually produced in the communication channel. While passivity is guaranteed by virtue of (4.6, 4.7), the proof shows that the observed energy gotten from the delayed energy values is lower bounded by the actual virtual energy, that is, the energy value computed using hypothetical current energy values. Thus, Theorem 4.2.2 is based on a passive estimation of the channel energy and the PC dissipates more energy than strictly needed, i.e., it over-dissipates. This in turn can have an effect on performance. In the P-Fc architecture, the effects can be apparent if delay is high and variable. Since the slave PC is configured in admittance, velocity is modified to dissipate energy, and over-dissipation can result in an over modification of velocity. Since the force command to the slave is obtained through the PI controller, a position drift may occur due to the accumulative nature of the integral term. This drift is visible in Fig. 4.3.2(a) and Fig. 4.3.2(a).

In order to analyze the over-dissipation and a potential position drift associated, the equations of Sec. 4.2 must be thoroughly examined. The channel energy observability comes at the price of adding conservatism to the passivity condition. In the following, the reasons to this statement are exposed.

Conservative Postulates: Decoupled and Observable Flows

1st Conservative Postulate: Decoupled Flows

The first step in making (3.11) useful, that is, observable to extract conclusions about channel passivity from it, is to split channel energy flow into flows from left to right, E^{L2R} and from right to left, E^{R2L}. Recalling (4.3):

$$\begin{aligned} E^{L2R}(n) &= E^{M}_{in}(n) - E^{S}_{out}(n), \\ E^{R2L}(n) &= E^{S}_{in}(n) - E^{M}_{out}(n). \end{aligned} \tag{4.16}$$

E.g., E^{L2R}, is the energy flow fed into the channel from the master side minus the energy coming out from the channel at the slave side. Condition (3.11) becomes:

$$E_N(n) = E^{L2R}(n) + E^{R2L}(n) \geq 0, \tag{4.17}$$

(4.17) allows to *analyze* passivity on a *decoupled* manner, since (4.4):

Proposition 5 *If both energy flows, $E^{L2R} \geq 0$ and $E^{R2L} \geq 0$, (4.17) is satisfied and therefore (3.11) as well.*

This is a conservative postulate since it forces both flows to be greater than zero in order to satisfy (3.11).

2nd Conservative Postulate: Observable Flows

The flows identified in (4.16) are not yet *observable*, i.e. usable by the POs, at either side because they are dependent on current values from opposite sides. The following observable versions are thus defined:

$$\begin{aligned} E^{L2R}_{obs}(n) &= E^{M}_{in}(t - D_f) - E^{S}_{out}(n), \\ E^{R2L}_{obs}(n) &= E^{S}_{in}(t - D_b) - E^{M}_{out}(n), \end{aligned} \tag{4.18}$$

where now, E^{L2R}_{obs} and E^{R2L}_{obs}, are visible at right and left sides of the channel respectively, since delayed signals (instead of current ones), $E^{M}_{in}(t - D_f)$ and $E^{S}_{in}(t - D_b)$, are taken from the opposite side where the observer is placed. Therefore, the right PO observes $E^{L2R}_{obs}(n)$ and the left PO $E^{R2L}_{obs}(n)$.

(4.18) allow to *check* for passivity on a *decoupled* manner, since:

Proposition 6 *If both observable energy flows, $E^{L2R}_{obs} \geq 0$ and $E^{R2L}_{obs} \geq 0$, (4.17) is satisfied and therefore (3.11) as well.*

Proof *If $E^{L2R}_{obs} \geq 0$ and $E^{R2L}_{obs} \geq 0$ then $E^{L2R} \geq 0$ and $E^{R2L} \geq 0$ since*

$$\begin{aligned} E^{L2R}_{obs}(n) &\leq E^{L2R}(n)\ \forall n\ \geq 0, \\ E^{R2L}_{obs}(n) &\leq E^{R2L}(n)\ \forall n\ \geq 0. \end{aligned} \tag{4.19}$$

See Theorem 4.2.2 for proof of (4.19).

Origin of the Position Drift

At the slave side, the Passivity Controller slows down slave motions according to energy behavior captured by the PO. The PC applies a variable damper aimed for dissipating active energy observed by the PO. Recalling (4.12) and assuming a continuous time, the commanded velocity to the slave is thus modified as:

$$v_{sd}(t) = \hat{v}_{sd}(t) + \beta(t) f_s(t), \tag{4.20}$$

where $\hat{v}_{sd}$ is the *untouched* velocity signal coming from the master and β is the variable damper. (4.12) is analogous to the *normal PC operation* mode in (4.29).

The desired velocity must be integrated in order to be commanded as desired position to the slave robot:

$$x_{sd}(t) = \int_0^t v_{sd}(\tau) d\tau. \tag{4.21}$$

The desired position, x_{sd}, is an input to the robot, to a PD controller or similar, as suggested in Fig. 2.7.7. Since x_{sd} is the integral of a modified velocity (as a function of passivity), it accumulates the history of passivity corrections. There is therefore a drift between the integral of the *untouched* velocity and the modified one:

$$\Delta x_{err}(t) = \int_0^t v_{sd}(\tau) d\tau - \int_0^t \hat{v}_{sd}(\tau) d\tau. \tag{4.22}$$

Δx_{err} is the drift between master and slave devices.

4.5 Enhanced Position-Force Architecture: quasi-lossless Bilateral TDPA

There are mainly two options to prevent the position drift:

a) Dissipate less energy, if possible the exact amount stored in the communication. By doing so, drift will not occur because the PC will only modify velocity in order to dissipate the exact amount of energy introduced by the channel.

b) Generate energy to actively prevent the drift as allowed by passivity of the communication.

The first one avoids over-dissipation from scratch. The second one accepts over-dissipation but avoids its potential effects. Clearly, avoiding over-dissipation from scratch would be the preferred approach. However, this seems to be unfeasible due to the impossibility of having both port flows available at the same time. Even if the conservative assumption of having previous knowledge of the delay is used, the energy observed on one of the sides will still need to travel to the other side.

The proposed approach in this work is based on the second option. The reasoning behind is the emulation of the behavior of an ideal communication channel, that is, a communication channel with a perfect and instantaneous data transmission. In particular, the lossless property is here exploited by forcing the channel to exhibit null energy rather than positive energy, i.e. classic passivity. Over-dissipation comes as a result of applying (4.17) and (4.18). Clearly, the passivity condition in (3.11) and in (4.18)

(using *decoupled observed* energy flows) differ in restrictionism, in that the second one is obviously more restrictive than the first one. In other words, by using (4.18), the controller dissipates energy more than strictly needed, i.e. (3.11).

Using the flow from left to right as an example, over-dissipation due to the *2nd Postulate* (Sec. 4.4) is given by:

$$\begin{aligned} E^{L2R}(n) - E^{L2R}_{obs}(n) &= \\ E^{M}_{in}(n) - E^{S}_{out}(n) - E^{M}_{in}(n - D_f) + E^{S}_{out}(n) &= \\ E^{M}_{in}(n - D_f, n). & \end{aligned} \tag{4.23}$$

Unfortunately, since it is the right-side PO (slave) which makes use of the flow left to right (4.18), (4.23) cannot be used on the right side since it would imply a non-casual system. It could be argued that the extra amount of energy on the left (master) can be compensated on the right (slave) side by using previous knowledge of the time delay. However, a) such an assumption adds considerable conservatism and hindrance to the field of application; and b) both possibilities, compensating the extra energy at the master side, or injecting energy from the master side to the channel, do not allow passivity proof. Due to obvious space limitation this proof is omitted.

Over-dissipation due to the *1st Postulate* (Sec. 4.4) seems more difficult, if not impossible, to compute due to the splitting of the passivity condition, (3.11), in the two sub-conditions, (4.18).

Resembling Ideal Communications

Looking at Fig. 2.7.7, the ideal communication channel is given by the following equations:

$$T_f = 0 \quad ; \quad T_b = 0, \tag{4.24}$$

$$v_m(t) = \hat{v}_{sd}(t), \tag{4.25}$$

$$\hat{f}_m(t) = f_s(t), \tag{4.26}$$

$$E_N(t) = 0. \tag{4.27}$$

(4.24) is obviously impossible to satisfy. Approaches based on prediction and estimation typically minimize the errors between both sides of (4.25), (4.26) or both. The approaches pursued in this work resemble (4.27) as faithful as allowed by the system, and as a consequence (4.25) is minimized.

The energy behavior of a communication channel network is rather stochastic. Unless the delay is constant and fixed parameters are used in the system, the energy behavior of a delay network is unpredictable. Often, telerobotic applications involve complex communication infrastructures characterized by highly variable time delays and package loss (e.g. if UDP protocol is used over the Internet or in space communications [104]).

From the energy point of view, the communication channel exhibits a similar behavior to that of a spring. Energy is continuously being accumulated and released during master and slave motions. Activity occurs when more energy is released than accumulated. This is exactly what the PC typically prevents, i.e. the variable damper is triggered in order to compel the energy's lower boundary to zero. However, the channel often exhibits

accumulation periods, *passivity gaps* from now on, which allow some margin for acting oppositely. By injecting energy (as opposed to dissipating) the energy null boundary can also be compeled during those passivity gaps.

Lossless Controller for Compensating the Position Drift

The main idea is to generate energy during passivity gaps in order to correct (and thus prevent) position drift. In other words, the PC is augmented in a way that energy is injected during the passivity gaps observed by the PO. Thus, the Passivity Observer and the augmented PC are defined as follows:

- Passivity Observer

$$E^S_{obs}(n) = E^M_{in}(n - D_f) - E^S_{out}(n) + E_{PC}(n). \tag{4.28}$$

  Where $E_{PC}(n)$ is the energy update corresponding to the PC previous operation.

- Passivity Controller with Energy Injection

$$\beta(n) = \begin{cases} -\dfrac{E^S_{obs}(n)}{T_s f_s(n)^2} & \text{if } E^S_{obs}(n) \leq 0 \quad \textit{(classic PC)} \\ \\ \dfrac{\varphi(n)}{f_s(n) T_s} min(|\Delta x_{err}(n)|, |\Delta x_{max}(n)|) & \text{else.} \end{cases} \tag{4.29}$$

$$\varphi(n) = sgn(T_s \sum_0^n \hat{v}_{sd}(n) - x_{sd}(n)), \tag{4.30}$$

$$v_{sd}(n) = \hat{v}_{sd}(n) + \beta(n) f_s(n), \tag{4.31}$$

$$E_{PC}(n) = T_s \beta(n) f_s(n)^2 + E_{PC}(n-1). \tag{4.32}$$

Where $\beta(n)$ is the dissipation coefficient, D_f forward time delay in sampling time units, and T_s the sampling time. φ determines the sign of the correction and E_{PC} is the energy dissipated or injected by the PC. Furthermore, the maximum allowed position drift compensation in order not to violate passivity of (4.28) is given by:

$$\Delta x_{max}(n) = \frac{E^S_{obs}(n)}{f_s(n)}. \tag{4.33}$$

The current drift, Δx_{err}, is given by (4.22). Therefore, in passivity gaps, i.e. $E^S_{obs}(n) \geq 0$, a complete drift compensation, Δx_{err}, will be possible as long the passivity gap gives enough margin, $E^S_{obs}(n)$. Otherwise, the maximum allowed compensation, Δx_{max}, will be commanded.

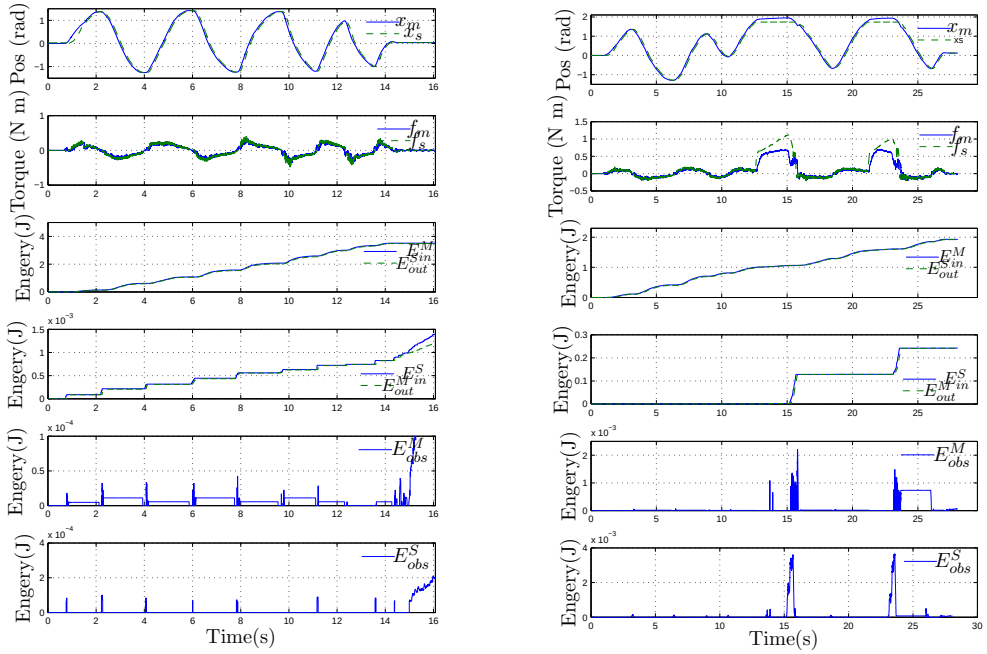

(a) $T_{rt} = 200\ ms$. Drift Compensator on. Free env.

(b) $T_{rt} = 400\ ms$. Drift Compensator on. Hard contact

Figure 4.5.1: Effect of the Drift Compensator

Experimental results

The system employed was the same as described in Sec. 4.3. Fig. 4.3.2(a) shows how the drift becomes significant after a few seconds in a free environment motion due to the dissipation of the slave PC. Note that the drift is related to the operation of the slave PC. The sixth plot, i.e. E^S_{obs}, shows (4.28) (removing the energy injection component). Positive intervals (passivity gaps) indicate passive behaviors, null intervals reveal the PC operation, i.e. the active tendency is regulated by the controller by dissipating energy. Fig. 4.3.2(b) shows the responses in hard contact situations. Note how the passivity conditions in *Proposition 2* are satisfied in both figures (plots 3 and 4).

Fig. 4.5.1(a) shows a similar test in free environment using the proposed drift compensator. Plot 6 shows the operation of the augmented PC: The passive gaps are exploited to compensate for the drift. As a result, the total observed energy becomes nearly null during whole operation since energy was injected, as allowed by the channel passiveness, in order to avoid accumulation of the dissipation error in the integral of v_{pc}. Fig. 4.5.1(b) shows the response is hard contact conditions $T_{rt} = 400\ ms$.

4.6 Removing Sudden Force Changes

One of the problems of the TDPA, especially in impedance type PC, is the sudden force changes due to the activation and deactivation of the PC. This can result in a noisy behavior, which in extreme cases [2] can be disturbing for the operator. In order to solve

[2]This depends on the quality of the communication channel, i.e., the amount of delay, package loss, etc.

this issue it is possible to place a passive virtual system, composed of a mass, m_c, and a spring, k_c, between the master and the impedance type [91].

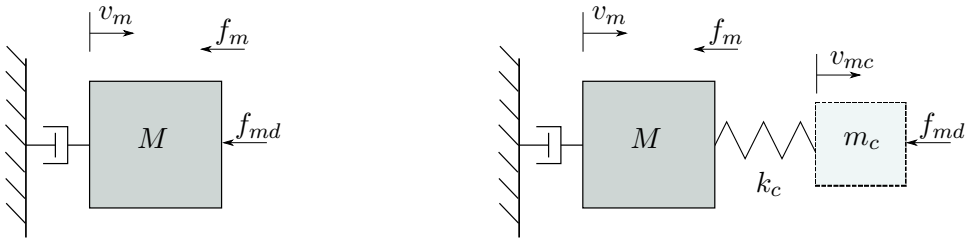

(a) Virtual mass and spring between the master and the feedback force.

(b) One DoF master with a feedback force.

Figure 4.6.1: Employing the virtual mass - spring system onto a master with force feedback

Fig. 4.6.1(a) shows a master device with force feedback (f_{md}). Since the feedback force is directly applied to the master, the operator may be able to feel a sudden force changes if the feedback force is suddenly modified. By placing the virtual mass and spring between the master and feedback force, the sudden force from the PC vanish thanks to the inertia effect (Fig. 4.6.1(b)). While this mechanism greatly reduces the noisy behavior, distortion in force and velocity may occur. The applied force to the master changes to f_m, and the velocity signal from the master to slave changes to v_{mc} (Fig. 4.6.2). The following two relationships are used to calculate f_m and v_{mc} in real-time.

$$f_m = k_c(x_m - x_{mc}), \tag{4.34}$$

$$m_c\dot{v}_{mc} = f_m - f_{md}. \tag{4.35}$$

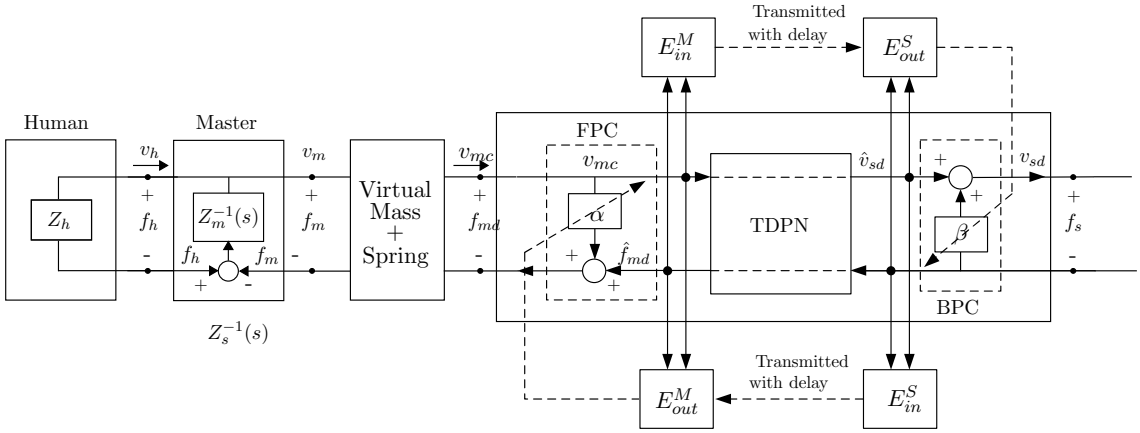

Figure 4.6.2: Detail of the P-Fc architecture with added virtual mass-spring to the remove noisy behavior.

Note that the virtual mass-spring behaves similar to a low pass filter on force and velocity in both directions. If a directional filter, such as a low pass filter for the force signal filter, or one for velocity, is added, it would make the system active. The bi-

directional filter keeps the system's passivity. Passivity of the inserted virtual system can be checked as follows:

$$\begin{aligned}
& \int_0^t (f_m(\tau)v_m(\tau) - f_{md}(\tau)v_{mc}(\tau))d\tau \\
= & \int_0^t (f_m(\tau)v_m(\tau) - f_{md}(\tau)v_{mc}(\tau) + f_m(\tau)v_{mc} - f_m(\tau)v_{mv}(\tau))d\tau \\
= & \int_0^t (f_m(\tau)v_m(\tau) - v_{mc}(\tau) + (f_m(\tau) - f_{md}(\tau))v_{mc}(\tau))d\tau \\
= & \int_0^t (k_c e\dot{e} + m_c v_{mc}\dot{v}_{mc})d\tau \\
= & \frac{1}{2}k_c e^2 + \frac{1}{2}m_c v_{mc}^2 \geq 0,
\end{aligned} \tag{4.36}$$

where $e = x_m - x_{mc}$

The equivalent transfer functions of the force and velocity low pass filters are given as:

$$\frac{f_m(s)}{f_{ms}(s)} = \frac{k_c}{m_c s^2 + k_c}, \tag{4.37}$$

$$\frac{v_{mc}(s)}{v_m(s)} = \frac{k_c}{m_c s^2 + k_c}. \tag{4.38}$$

If the cutoff frequency of the force filter is lower than the frequency of the PC noise from the sudden force change, the PC noise can be filtered out, and only low frequency force component would be transmitted to the operator. Please note that the distorted force can be ignorable, if the stiffness (k_c) is high enough, and the mass (m_c) is as low as possible until the cutoff frequency of the force filter is lower than the frequency of the PC noise.

4.7 Time Domain Passivity Control for multi-DoF Manipulators

So far the analysis in this work has been restricted to single DoF systems. In multi-DoF manipulators, a coupling in Cartesian space is necessary. To that end, a unique representation of forces and velocities of the robot end-effector poses is required. This chapter presents methods to apply the distributed PO/PC control structure surrounding a TDPN in multi-DoF.

Dynamics in Cartesian Space

The case analyzed for developing the rationale of the Time Domain Passivity Control in the task space is the Position-Force computed architecture. In this architecture, the position and orientation of the master device end-effector, that is, in the Cartesian space, is sent to the slave robot. The slave robot is set with a compliant behavior defined by a

spatial stiffness and a damping. A vector of generalized Cartesian forces is thus generated using the generalized position command from the master. The Cartesian forces are at both sides transformed to the joint space through the Jacobian relating both, Cartesian and joint spaces.

The joint space dynamic model of a robot manipulator with n joints can be written as:

$$\boldsymbol{M}(q)\ddot{\boldsymbol{q}} + \boldsymbol{C}(\boldsymbol{q}, \dot{\boldsymbol{q}})\dot{\boldsymbol{q}} + \boldsymbol{g}(\boldsymbol{q}) = \boldsymbol{\tau} + \boldsymbol{\tau}_{ext}, \tag{4.39}$$

being $q \in \mathbb{R}^{n\times n}$ the vector of generalized coordinates, $M(q) \in \mathbb{R}^{nxn}$ the symmetric and positive definite inertia matrix, $C(q, \dot{q}) \in \mathbb{R}^{nxn}$ representing the centrifugal and Coriolis terms and $g(q) \in \mathbb{R}^{nxn}$ the gravity torques. $\tau \in \mathbb{R}^{n\times n}$ represent the control input of generalized forces (torques, as rotational joints will be here considered) and $\tau_{ext} \in \mathbb{R}^{n\times n}$ denotes external generalized forces due to the interaction between the environment and the robot. A particular choice of $C(q, \dot{q})$ such that $\dot{M}(q) = C(q, \dot{q}) + C(q, \dot{q})^T$ can be made, which leads to the skew symmetric matrix $\dot{M}(q) - 2C(q, \dot{q})$ [96]. This property implies passivity of the system with respect to the input τ and the output $\dot{q}$.

Since the goal is to couple master and slave end-effector positions and forces, the control goal must also take place in the Cartesian space. The mapping from joint velocities to Cartesian velocities is given by the Jacobian matrix $J(q) \in \mathbb{R}^{n\times n}$:

$$\dot{\boldsymbol{x}} = \boldsymbol{J}(\boldsymbol{q})\dot{\boldsymbol{q}}, \qquad \boldsymbol{J}(\boldsymbol{q}) = \frac{\partial f(\boldsymbol{q})}{\partial \boldsymbol{q}}. \tag{4.40}$$

The equation of motion in the task space can be written as:

$$\boldsymbol{\Lambda}_x(q)\ddot{\boldsymbol{x}} + \boldsymbol{V}(q, \dot{q})\dot{\boldsymbol{x}} + \boldsymbol{G}(q) = \boldsymbol{F} + \boldsymbol{F}_{ext}, \tag{4.41}$$

being the Cartesian space force vector $F \in \mathbb{R}^{n\times n}$ related to the torque space as:

$$\tau = J(q)^T F, \tag{4.42}$$

and

$$\begin{aligned} \boldsymbol{\Lambda}_x(\boldsymbol{q}) &= \boldsymbol{J}(\boldsymbol{q})^T \boldsymbol{M}(\boldsymbol{q}) \boldsymbol{J}(\boldsymbol{q})^{-1} \\ \boldsymbol{V}(\boldsymbol{q}, \dot{\boldsymbol{q}}) &= -\boldsymbol{J}(\boldsymbol{q})^{-T} \boldsymbol{M}(\boldsymbol{q}) \dot{\boldsymbol{J}} \dot{\boldsymbol{q}} + \boldsymbol{J}^{-T} \boldsymbol{C}(\boldsymbol{q}, \dot{\boldsymbol{q}}) \\ \boldsymbol{G}(q) &= \boldsymbol{J}(q)^{-T} \boldsymbol{g}(q) \end{aligned}$$

In workspaces with Jacobian full row-rank, the desired compliance at the slave robot coming from the master can be implemented with the following controller:

$$\boldsymbol{F} = \boldsymbol{G}(\boldsymbol{q}) - (K(x - x_m) + D\dot{\boldsymbol{x}}),$$

where $K \in \mathbb{R}^{n\times n}$ is the symmetric and positive definite stiffness matrix, and $D \in \mathbb{R}^{n\times n}$ is the positive definite damping matrix. And thus:

$$\boldsymbol{\tau} = \boldsymbol{g}(\boldsymbol{q}) - \boldsymbol{J}^T(K(x - x_m) + D\dot{\boldsymbol{x}})). \tag{4.43}$$

For further reference, the following energy based norms on the different velocity coordinates are defined:

$$\begin{aligned} ||\dot{\boldsymbol{q}}||_M^2 &:= \dot{\boldsymbol{q}}^T \boldsymbol{M}(\boldsymbol{q})\dot{\boldsymbol{q}} = 2\Psi(\boldsymbol{q}, \dot{\boldsymbol{q}}) \ , \\ ||\dot{\boldsymbol{x}}||_x^2 &:= \dot{\boldsymbol{x}}^T \boldsymbol{\Lambda}_x(\boldsymbol{q})\dot{\boldsymbol{x}} = 2\Psi_x(\boldsymbol{q}, \dot{\boldsymbol{x}}) \ , \end{aligned} \tag{4.44}$$

Time Domain Passivity for Mechanical muti-body Systems

The general expression for a M-port PO can be written as:

$$\Psi_{obs}(k) = T_s \sum_{j=0}^{k} (f_1(j)v_1(j) + ... + f_M(j)v_M(j)). \tag{4.45}$$

The energy flow due to an environment interacting with a robot can be regarded as a multi-port network, where the number of ports is in general the dimensions of the external torques $\boldsymbol{\tau}_{\text{ext}}$:

$$\Psi_{obs}(k) = -T_s \sum_{j=0}^{k} \dot{\boldsymbol{q}}^T(j)\boldsymbol{\tau}_e(j), \tag{4.46}$$

The question arises on how to dissipate energy in case (4.46) ≤ 0 $\Psi_{obs}(k) \leq 0$, along the multiple joints of a robot manipulator. One could think of handling passivity for each degree of freedom independently. This would however result in a conservative approach since, as can be deduced from (4.46), an active dimension in the environment does not necessary imply that the whole environment is active. The PC must be built according to a criteria on how to distribute that energy.

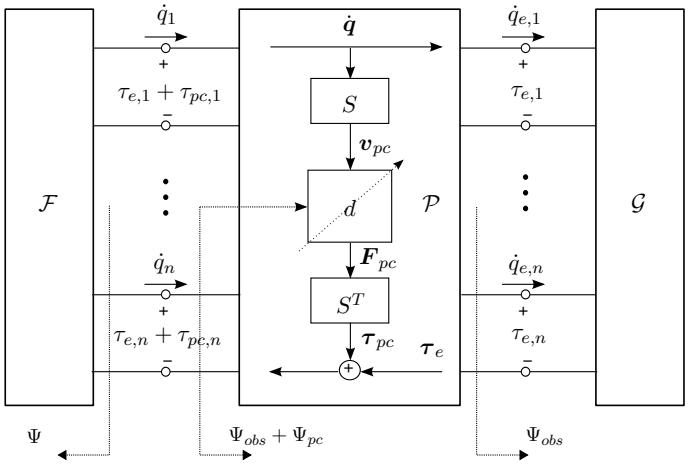

Figure 4.7.1: Cascade network connection of a multi-dimensional environment, $\mathcal{G}$, a multi-port PC in impedance, $\mathcal{P}$, and a multi-DoF robot plus controller, $\mathcal{F}$.

Fig. 4.7.2 shows the network representation of the general structure of a PO/PC connected to a multi-body system. The n port network $\mathcal{F}$ contains the robot and a generic controller whose specification depends on the application, e.g. a PD controller

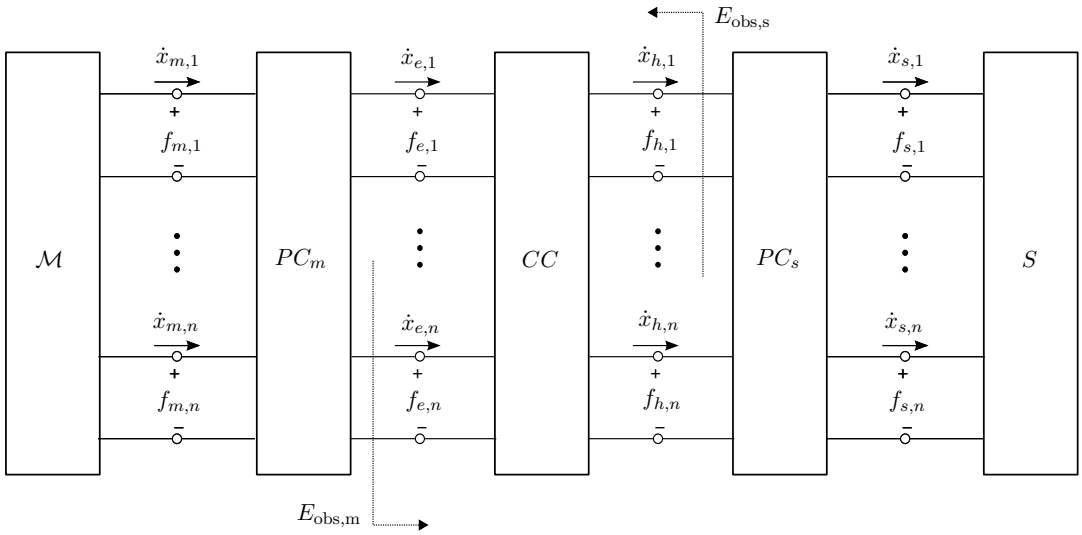

Figure 4.7.2: General structure of a PO/PC connected to a multi-body system

plus a trajectory generator or a Cartesian compliance. The network $\mathcal{G}$ is a generic environment which represents the source of energy to be dissipated, e.g. an environmental disturbance, a virtual reality (VR) or a teleoperator. The multi-port PC in impedance is represented by $\mathcal{P}$ and regulates the interaction between $\mathcal{G}$ and $\mathcal{F}$. S is a transformation from the joint space to the space where the PC is implemented and, as will be seen, depends on the specific PC approach. This representation is general and allows multiple solutions.

The presentation in this thesis is limited to an impedance configuration of the PC. In that case the the following relations are established:

$$\begin{aligned} \dot{\boldsymbol{q}} &= \dot{\boldsymbol{q}}_e, && \text{(velocity input)} \\ \boldsymbol{\tau} &= \boldsymbol{\tau}_c' + \boldsymbol{\tau}_e + \boldsymbol{\tau}_{pc}, && \text{(torque output)} \end{aligned} \tag{4.47}$$

where $\boldsymbol{\tau}_{pc}$ is the dissipation torque vector whose expression will be specified in the following subsections and represents the correction upon $\boldsymbol{\tau}_e$ such that the interaction with $\mathcal{G}$ becomes passive. Thus the control input to the robot becomes $\boldsymbol{\tau}_c = \boldsymbol{\tau}_c' + \boldsymbol{\tau}_{pc}$, where $\boldsymbol{\tau}_c'$ is the contribution of the general purpose controller.

Joint Level Approach

The first solution is sought entirely in the joint space. An active environment in the joint space can be for instance a disturbance on some joint. Thus the PC is computed also in the joint space and $\boldsymbol{S}$ contains just an identity transformation $I^{n\times n}$. The dissipation can be distributed at the joint level by using the inertia matrix of the manipulator. Thus

and analogous to (2.33), the PC for a multi-dimensional environment can be written as:

$$\begin{aligned} \boldsymbol{\tau}_{pc}(k) &= -d_q(k)\boldsymbol{M}(\boldsymbol{q}(k))\dot{\boldsymbol{q}}(k) \\ d_q(k) &= \begin{cases} -\frac{1}{T_s}\frac{\Psi_{obs}(k)+\Psi_{pc}(k-1)}{\left\|\dot{\boldsymbol{q}}(k)\right\|_M^2} & \text{if } \mathcal{X}_q \\ 0 & else \end{cases} \\ \mathcal{X}_q: &= \Psi_{obs}(k)+\Psi_{pc}(k-1)<0 \;\&\; ||\dot{\boldsymbol{q}}(k)||_M > 0. \end{aligned} \tag{4.48}$$

Where the $\Psi_{pc}(k-1)$ is the update of the dissipated energy by the PC, which can be computed as:

$$\Psi_{pc}(k) = T_s \sum_{j=0}^{k} d_q(j)\left\|\dot{\boldsymbol{q}}(j)\right\|_M^2$$

The additional torque $\boldsymbol{\tau}_{pc}$ from the PC is added to the control torque $\boldsymbol{\tau}_c'$ of a nominal control action, i.e. $\boldsymbol{\tau}_c = \boldsymbol{\tau}_c' + \boldsymbol{\tau}_{pc}$. The controller in (4.48) guarantees passivity for any active environment $\mathcal{G}$. However, it does not enforce any rule on how active energy must be dissipated beyond projecting it on the joint space mass matrix. Therefore, the distribution of the damping among the multiple degrees of freedom is handled implicitly, which can lead to undesired disturbances of a given control goal (e.g. a task space related control goal).

Cartesian Space Approach

Since the control goal is often established in the Cartesian space, it is reasonable to specify the dissipation criteria also in the Cartesian space. In [83] the energy to be dissipated was projected on the force vector resulting from the interaction with a VR. While this method allows intuitive interaction with the VR, the dissipation capacity is limited by the norm of the velocity along the force vector. Indeed, the dissipation capacity of a manipulator in a sampling lag depends on the joint configuration, the mass distribution, the velocity and the maximum torques that the robot can apply.

A reasonable way to distribute the energy along the joints is by using the mass distribution of the manipulator.

Thus and analogous to (2.33), the PC for a multi-dimensional environment can be written as:

$$\begin{aligned} \boldsymbol{F}_{pc}(k) &= -\boldsymbol{\Lambda}_x(\boldsymbol{q}(k))d_x(k)\dot{\boldsymbol{x}}(k) \\ d_x(k) &= \begin{cases} -\frac{1}{T_s}\frac{\Psi_{obs}(k)+\Psi_{pc}(k-1)}{\left\|\dot{\boldsymbol{x}}(k)\right\|_x^2} & \text{if } \mathcal{X}_x \\ 0 & else \end{cases} \\ \mathcal{X}_x: &= \Psi_{obs}(k)+\Psi_{pc}(k-1)<0 \;\&\; \left\|\dot{\boldsymbol{x}}(k)\right\|_x > 0. \end{aligned} \tag{4.49}$$

Where the $\Psi_{pc}(k-1) := T_s \sum_{j=0}^{k} d_x(j)||\dot{\boldsymbol{x}}(j)||_x^2$ is the update of the dissipated energy by the PC. The PC is computed in the Cartesian space which is given by the transformation $\boldsymbol{S} = \boldsymbol{J}(\dot{\boldsymbol{q}})$ from Fig. 4.7.2. Notice that this solution is equivalent to the joint level case for a non-redundant manipulator (apart from singular configurations). However, for a redundant robot the damping is only implemented in Cartesian space, while the dissipation capacity according to the nullspace motion is not exploited. This demerit will be removed in the detail in the following section.

4.8 Final Remarks

In this chapter, the fundamental elements of the Time Domain Passivity Approach have been reviewed. Furthermore, a general passivity treatment by energetic means of a fundamental communication element characterized by the delay has been given which, as will be seen in the proceeding chapters, it will allow to further develop the TDPA framework in less obvious contexts such as those with less intuitive flow - effort mapping (e.g. a Position-Position architecture) or those with noncollocated feedback signals (e.g. using force - torque sensors).

Chapter 5

Designing with Time Delay Power Networks

This chapter combines the results from the previous two. Passivity is thus applied to a variety of control architectures that have been augmented on the base of TDPNs. The combination of TDPN and PO/PC elements provides a complete framework to design teleoperation architectures in any conceivable configuration and operating conditions. Next to the formal descriptions a set of experimental results are presented.

5.1 Introduction

As it will be seen, bringing together the elements from the previous chapter will result in a framework that will allow to design teleoperation systems. The main aspects covered by the framework are:

a) The channel TDPN network unfoldment, a tool for extracting network-conform representations of the virtually any communication structure linking both sides of the teleoperation system.

a) The quasi-lossless PO/PC structure.

b) The mechanism to remove sudden force changes.

The application of the PO/PC control structure on TDPNs that are attached to depend flow/effort sources is here further explored. This is the only piece that is missing towards the design of teleoperation schemes. The following steps for the design process are proposed:

1. Design in the ideal case (no delay nor package loss) using the block diagram representation.
2. Extraction of the electrical system incorporating the time delay.
3. Augmentation of delayed dependent sources such that they become a combination of TDPNs and a non-delayed ideal sources, as described in Chapter 3.
4. TDPNs identification and passivity treatment by means of PO/PC blocks at the opposite side of the non-delayed source as described in Chapters 3 and 4.

These steps are followed to derive the designs for the following architectures:

- Position-Position with Time Delay.
- Position-Force measured with Time Delay.
- Four Channels with Time Delay.

A complete development is given for the Position-Position in order to show the application of the tools presented in the previous chapters to the specific architecture. Simulation and experimental results are as well exposed.

5.2 Passivity analysis with dependent delayed flow and effort sources

Consider a non-delayed dependent source, be it of velocity type or force type, attached to a TDPN. As has been seen in Chapter 3, the source is modeled as ideal and it represents the element that supplies energy to one part of the system. This section deals with the placement of the Passivity Controller(s) that will make the TDPNs passive. We first introduce a well known characteristic of ideal sources.

Proposition 7 *An ideal current source can supply and absorb unlimited power forever and so it represents an unlimited source of energy.*

Proof The current through an ideal current source is independent of the voltage across it. The internal resistance of an ideal current source is infinite [1] (setting the source with zero current is identical to an ideal open circuit). The voltage at the port of an ideal current source is thus completely determined by the circuit it is connected to. When connected to an external load, for instance, the voltage across the source approaches infinity as the load resistance approaches infinity (an open circuit). The power of an ideal current source is independent from the internal resistance (due to its infinity value) and is proportional to the voltage (positive or negative) across the source.

Given this property, it does not seem reasonable to place a PC on the left side of the TDPN as it will have no effect on the rest of the system. Note that the PC only dissipates on the output variables of the network to be treated. On the other hand, the left side of the TDPN is unproblematic, however, only the flow from left to right can be considered. See Fig. 5.2.1.

[1] The internal resistance of a current source is modeled in parallel with the source.

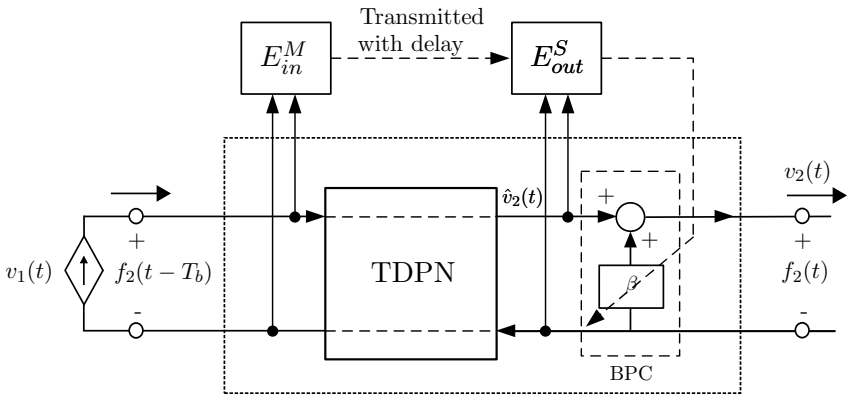

Figure 5.2.1: The left PC is not needed due to the ideal current source.

5.3 Position-Position Architecture with Time Delay

A complete design procedure based on passive TDPNs is presented in this section. A Position-Position architecture is used to extract the TDPNs related to the energy transfer through the channel and to derive the corresponding controllers to guarantee the system passivity.

Passivity of the Position-Position architecture has been previously studied in [63] where proportional derivative control and robust control techniques are used; and in [19], where the TDPA is employed. In a Position-Position architecture, both master and slave controllers, are PI [2] linked with local and distant velocities. The desired command for the slave PI is the delayed master velocity. The controller can thus immediately obey with a force response on the slave device. At the master side, the desired command is current master velocity, which in turn is the operator's motion intention, and the distant slave is the process to be controlled.

The operation is shown in the block diagram representation sketched in the upper figure of Table 3.1. which is the first step in the design. The ideal system, that is, without considering the communication channel, is first parametrized by fixing the PI constants using conventional control techniques [59], such that the system is stable and fulfills a desired degree of transparency.

This architecture presents higher viscosity levels in the free space operation than conventional P-Fc or P-Fmsr systems. As the delay increases, the dynamics of both, master and slave controllers become more apparent. On the other hand, since positions can be explicitly be tracked on both sides, position drift between master and slave can be avoided.

System Description

The equations describing the system are given by:

$$\begin{aligned} f_m(t) &= K_{dm}(v_m(t) - v_s(t-T_b)) + K_{pm}(x_m(t) - x_s(t-T_b)), \\ f_s(t) &= K_{ds}(v_m(t-T_f) - v_s(t)) + K_{ps}(x_m(t-T_f) - x_s(t)). \end{aligned} \tag{5.1}$$

[2] PD equivalent referred to position

Where f_m, x_m and f_s, x_s are master and slave computed forces and positions respectively and T_b and T_f are forward and backward delays; K_{dm}, K_{pm}, K_{ds} and K_{ps} are derivative and proportional gains for master and slave respectively. Master dynamics are as:

$$\begin{aligned}(f_h(s) - f_m(s))\frac{1}{m_m s^2 + b_m s} &= x_m(s), \\ f_h(s) &= v_m(s) Z_h(s). \end{aligned} \tag{5.2}$$

Where f_h is the human force; m_m and b_m are master mass and damping coefficient, and Z_h is the human impedance[3]. Equations at the slave side can be obtained on a similar way.

At the slave side the relations are as:

$$\begin{aligned}(f_s(s) - f_e(s))(\frac{1}{m_s s^2 + b_s s}) &= x_s(s) \\ f_e(s) &= v_s(s) Z_e(s), \end{aligned} \tag{5.3}$$

where f_s, f_e and x_s are commanded force to the slave device, environment force and slave position; m_s and b_s are slave device mass and damping coefficient; and Z_e is the environment impedance.

TDPN Identification through Network Representation

The system can be represented using analogous electrical components as shown in the lower figure of Table 3.1. The 2-port network named, N_z, contains the communication channel. As seen in Sec. 3.7 a wrong assumption would be to consider N_z as a network that contains *only* the communication channel. The network contains two networks: The left source, which is dependent on previous values of the slave velocity; and the right source, which is dependent on previous values of master velocity:

$$\begin{aligned}\hat{v}_{md}(t) &= v_s(t - T_b), \quad \forall t \geq 0, \\ \hat{v}_{sd}(t) &= v_m(t - T_f), \quad \forall t \geq 0. \end{aligned} \tag{5.4}$$

Looking at both N_z ports, its energy flows is given by:

$$E_{Nz}(t) = \int_0^t (f_m(\tau)\hat{v}_{md}(\tau) - f_s(\tau)\hat{v}_{sd}(\tau))d\tau, \quad \forall t \geq 0. \tag{5.5}$$

Following Proposition 3:

Axiom 1 *The network N_z, containing two delayed dependent current sources (Table 3.1), can be represented by the combination of two non-delayed dependent current sources and two TDPNs carrying the energy of each un-delayed dependent current source.*

This augmented representation is obtained by bringing the delayed dependent current sources to its non-delayed location through the networks N_a and N_b, being both of TDPN type. It is clear now, that N_z does not only carry the energy due to the delay, but also

[3]These equations are purely for understanding purposes. Note the methods exposed here are independent from master and slave dynamics.

the energy due to the current sources C_a and C_b. This can be seen by expanding (5.5) as follows:

$$\begin{aligned} E_{Nz}(t) &= \int_0^t (f_m(\tau)v_s(\tau - T_b) - f_s(\tau)v_m(t - T_f))d\tau \\ &= E_{Na}(t) + E^{Ca}(t) + E_{Nb}(t) + E^{Cb}(t), \end{aligned} \tag{5.6}$$

where E_{Na} and E_{Nb} are the energy flows of N_a and N_b; and E^{Ca} and E^{Cb} the energy flows of the current sources C_a and C_b. In the discrete domain:

$$\begin{aligned} E_{Na}(n) &= T_s \sum_{k=0}^{k=n} v_s(k - D_b)f_m(k) - v_s(k)f_m(k - D_b), \\ E_{Nb}(n) &= T_s \sum_{k=0}^{k=n} v_m(k)f_s(k - T_f) - v_m(k - D_f)f_s(k), \end{aligned} \tag{5.7}$$

Furthermore, the energy flow in the discrete domain of the current sources C_a and C_b are as follows:

$$\begin{aligned} E^{Ca}(n) &= T_s \sum_{k=0}^{k=n} f_m(k - D_b)v_s(k), \\ E^{Cb}(n) &= -T_s \sum_{k=0}^{k=n} f_s(k - D_f)v_m(k). \end{aligned} \tag{5.8}$$

The new representation allows to segment the energy flow introduced by the TDPNs, i.e. the flow produced by the delay, from the rest of the system. Clearly the only admissible energy sources in N_z are both E^{Ca} and E^{Cb}. The pursuit of channel passivity goes therefore through observation and passivation of $E_{Na}(n)$ and $E_{Nb}(n)$. Note in the ideal situation $D_f = 0$ and $D_b = 0$, both $E_{Na}(n)$ and $E_{Nb}(n)$ become null.

Theorem 5.3.1 *A P-P system with delay in the communication channel will be passive if both of its TDPNs, N_a and N_b, are kept passive (assuming human, master, slave and PD controllers passive)*

Proof Using Def. 22 and (4.3), both port energies of N_z in (5.5), E_{z1} and E_{z2}, can be written as:

$$\begin{aligned} E_{z1}(t) &= E_{Na}(t) + E^{Ca}(t) = E^{L2R}_{Na}(t) + E^{R2L}_{Na}(t) + E^{Ca}_{in}(t) + E^{Ca}_{out}(t), \\ E_{z2}(t) &= E_{Nb}(t) + E^{Cb}(t) = E^{L2R}_{Nb}(t) + E^{R2L}_{Nb}(t) + E^{Cb}_{in}(t) + E^{Cb}_{out}(t), \end{aligned}$$

where $E^{Ca/b}_{in}$ and $E^{Ca/b}_{out}$ are *in* and *out* components of $E^{Ca/b}$. And $E^{L2R}_{Na/b}$ and $E^{R2L}_{Na/b}$ are left-to-right and right-to-left components, i.e. decoupled as in (4.3).

Lemma 5.3.2 *In a system composed by the cascade of a TDPN and an ideal current source, effective energy can only travel from the current source to the TDPN. E^{L2R}_{Na} and E^{R2L}_{Nb} are cancelled out by E^{Ca}_{in} and E^{Cb}_{in} respectively.*

Recalling Proposition 7, E_{z1} and E_{z2} can be rewritten as:

$$\begin{aligned} E_{z1}(t) &= E_{Na}^{R2L}(t) + E_{out}^{Ca}(t), \\ E_{z2}(t) &= E_{Nb}^{L2R}(t) + E_{out}^{Cb}(t). \end{aligned} \tag{5.9}$$

Therefore making Na and N_b passive requires only the following two conditions:

$$E_{Na}^{R2L}(t) \geq 0 \quad , \quad E_{Nb}^{L2R}(t) \geq 0. \tag{5.10}$$

E_{out}^{Cb} represents the amount of energy from the master transferred to the slave. It is assumed that the system created by C_b, slave and environment is passive. Note this is not a severe constraint since it implies that the energy produced on one side is dissipated on the other without taking the delay into account. The same reasoning is applied for E_{out}^{Ca} (where the human is assumed to be a passive system as well). This is,

$$\begin{aligned} E_{out}^{Cb}(t) + E_S(t) + E_{env}(t) \geq 0, \\ E_{out}^{Ca}(t) + E_M(t) + E_H(t) \geq 0, \end{aligned} \tag{5.11}$$

where $E_{M/S}$ are master and slave energy flows, E_H the energy of the human operator, and E_{env} the energy of the environment. Using (5.9) and (5.11) and the conditions in (5.10) system passivity is proved as:

$$E_H(t) + E_M(t) + E_{z1}(t) + E_{z2}(t) + E_S(t) + E_{env}(t) \geq 0. \tag{5.12}$$

∎

The delayed sources are therefore *expanded* in order to unveil the networks transporting channel energy. In this representation it is clear that N_z contains not only the channel, but also the dependent current sources. Finally, once it is clear where the TDPN are, the PO / PC algorithms can be applied in order to passivate the channel. The final scheme is shown in Fig. 5.3.1.

Passivity Observer and Passivity Controller for P-P Architectures

As seen in (5.12) the energy flows to be observed and controlled are (5.10) since E_{Na}^{R2L} and E_{Nb}^{L2R} are the energies introduced by the delay. In order to determine both PO and PC expressions, the same procedure seen in Sec. 4.2 to observe the energy flow for the TDPN is here applied for both, N_a and N_b networks. Thus, E_{Na} and E_{Na} can be split into master and slave in and out energies:

$$E_{Na}(t) = E_{in}^{Ma}(t) - E_{out}^{Sa}(t) + E_{in}^{Sa}(t) - E_{out}^{Ma}(t) = E_{Na}^{L2R}(t) + E_{Na}^{R2L}(t). \tag{5.13}$$

$$E_{Nb}(t) = E_{in}^{Mb}(t) - E_{out}^{Sb}(t) + E_{in}^{Sb}(t) - E_{out}^{Mb}(t) = E_{Nb}^{L2R}(t) + E_{Nb}^{R2L}(t), \tag{5.14}$$

Where E_{in}^{Ma} for instance, stands for *in* energy to network N_a at master side (i.e. left port of N_a); E_{out}^{Sb} stands for the *out*going energy from N_b at the slave side. Using (3.13) and (3.14) expressions of $E_{in/out}^{Ma}$, $E_{in/out}^{Sa}$, $E_{in/out}^{Mb}$ and $E_{in/out}^{Sb}$ can be easily derived.

As shown in (5.9) only energies flowing from the ideal current source to the circuit are effective. Therefore a PC is placed at the left port of N_a controlling E_{Na}^{R2L}; and a PC

is placed at the right port of N_b controlling the energy flow E_{Nb}^{L2R}. The POs are defined as:

For the TDPN B *(from master to slave)*

$$\begin{aligned} W_s(n) &= E_{in}^{Mb}(n-D_f) - E_{out}^{Sb}(n) + E_{PC}^{S}(n) \\ E_{in}^{Mb}(n) &= f(f_s(n-D_f), v_m(n)) \\ E_{out}^{Sb}(n) &= g(f_s(n), v_m(n-D_f)) \end{aligned} \tag{5.15}$$

For TDPN A *(from slave to master)*

$$\begin{aligned} W_m(n) &= E_{in}^{Sa}(n-D_b) - E_{out}^{Ma}(n) + E_{PC}^{M}(n) \\ E_{in}^{Sa}(n) &= f(f_m(n-D_b), v_s(n)) \\ E_{out}^{Ma}(n) &= g(f_m(n), v_s(n-D_b)) \end{aligned} \tag{5.16}$$

Where W_s and W_m are the observed energies at slave and master side respectively, and $E_{PC}^{S/M}$ are the dissipated energy by the PC, i.e. the update of $E_{out}^{Sb/Ma}$. f and g are functions that compute *in* and *out* energies as in (3.13) and (3.14) (take (5.23) as implementation example for the P-Fmsr case). The PCs are then implemented as in (4.20).

Passivity is proved using the same reasoning as in Sec. 4.2 with the difference that only the flow from the current source to the network is considered. Taking this into account and (4.6) and (4.7) passivity on the time domain is guaranteed since:

$$\begin{aligned} E_{in}^{Sa}(n) - E_{out}^{Ma}(n) + E_{PC}^{M}(n) \geq 0, \\ E_{in}^{Mb}(n) - E_{out}^{Sb}(n) + E_{PC}^{S}(n) \geq 0. \end{aligned} \tag{5.17}$$

The passivity controllers are then given by:

TDPN A

$$E_{PC}^{M}(n) = T_s \sum_{k=1}^{n-1} f_m^2(n)\beta_m(n), \tag{5.18}$$

$$v_{md}(n) = \hat{v}_{md}(n) - f_m(n)\beta_m(n). \tag{5.19}$$

where the dissipation factor, β_m, is given by:

$$\beta_m(n) = \begin{cases} 0 & \text{if } W_m(n) > 0 \\ \dfrac{-W_m(n)}{T_s f_m^2(n)} & \text{else} \end{cases}$$

TDPN B

$$E_{PC}^{S}(n) = T_s \sum_{k=1}^{n-1} f_s^2(n)\beta_s(n), \tag{5.20}$$

The Passivity Controller is defined as:

$$v_{sd}(n) = \hat{v}_{sd}(n) - f_s(n)\beta_s(n). \tag{5.21}$$

where the dissipation factor, β_s, is given by:

$$\beta_s(n) = \begin{cases} 0 & \text{if } W_s(n) > 0 \\ \dfrac{-W_s(n)}{T_s f_s^2(n)} & \text{else} \end{cases}$$

The system integrating the controllers can be seen in Fig. 5.3.1.

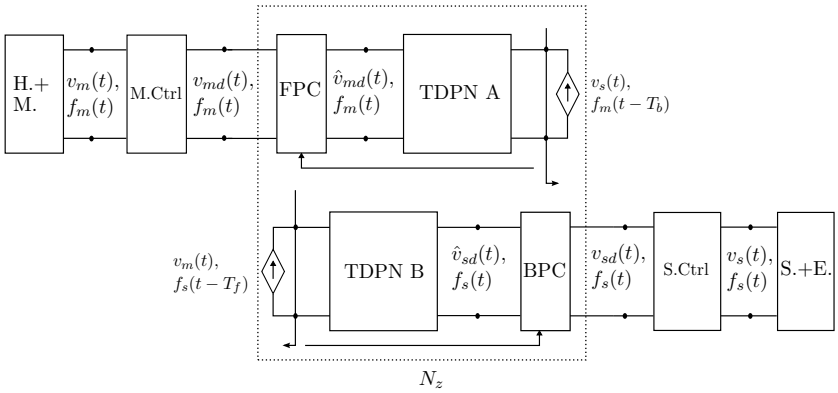

Figure 5.3.1: P-P with FPC and BPC, which keep the communication channel passive

Tab. 5.1 summarizes the four steps design for the Position-Position architecture.

Simulations

Master and slave robots are simulated (Matlab Simulink) as mass-damper systems with mass $M_r = 1\,Kg$ and viscous friction of $B_r = 0.3\,Ns/m$. The HO is simulated in a closed-loop system that generates the force to the master robot in order to follow a sinusoidal reference position with frequency of $0.25\,Hz$ and amplitude of $0.25\,m$. The control part of the system (Master PD, Slave PD, FPC and BPC) runs at a sampling rate of $T = 1\,ms$. The gain parameters of both PD controllers have been tuned using the Nyquist stability criterion such that the system is able to absorb a worst case round trip delay of $20ms$. Performance is first shown for the non-delayed system. Fig. 5.3.2 shows master and slave position and forces. Fig. 5.3.3(a) shows sent and received energies of N_b, that is the energy in the channel traveling from master to slave, which are obviously identical since no delay is present in the channel. Fig. 5.3.3(b) shows the same plots for N_a.

To see how those energies evolve when delay is inserted into the channel, a simulation has been performed inserting a delay slightly higher than the maximum allowed by the stability region for which the system has been designed. Fig. 5.3.4 shows the unstable behaviour. Fig. 5.3.5(a)/(b) show the activity of the channel, i.e. more energy is received than sent and the observed energies by the PO's are negative. Thus both networks, N_a and N_b, are active and the cause for unstable behavior. Fig. 5.3.6 and Fig. 5.3.9 show the response of the system with both, FPC and BPC activated, and a round trip delay of $T_{rt} = 300\,ms$ for free environment and hard wall contact cases

respectively. The energetic evolution of N_b and N_a can be seen in Fig. 5.3.7(a)/(b) and Fig. 5.3.10(a)/(b). In both situations, free environment and contact situation, it can be seen how N_a becomes active and how the BPC corrects the energy such that in never becomes higher than the sent energy. Fig. 5.3.8 shows a zoomed area of Fig. 5.3.7(a). These plots reveal very well the concept exposed in this work, since a) they depict the main problem, i.e. the channel as a source of activity, and b) show the approach, i.e. the active network plus the passivity controller create a passive network. The 3rd plot in Fig. 5.3.7 and Fig. 5.3.10 show the operation of the PCs, i.e. the observed energies never cross the activity boundary.

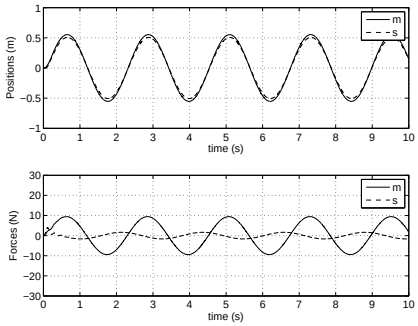

Figure 5.3.2: Master and slave positions and forces for the non-delayed case.

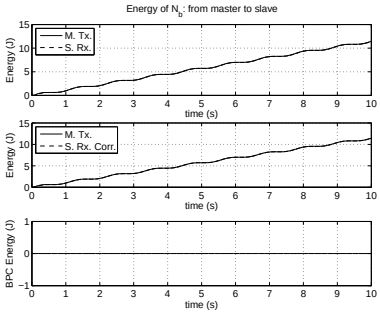

(a) Energies at N_b: Sent and received energies, sent and corrected received energies, and observed energy by the slave PO.(PC off)

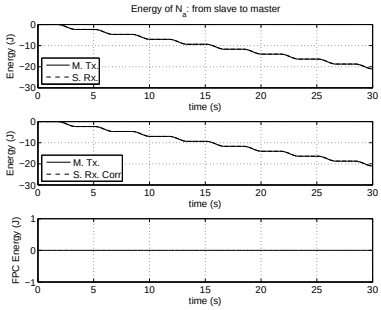

(b) Energies at N_a: Sent and received energies, sent and corrected received energies, and observed energy by the PO.(PC off)

Figure 5.3.3: Observed energies in N_z for the non-delayed case.

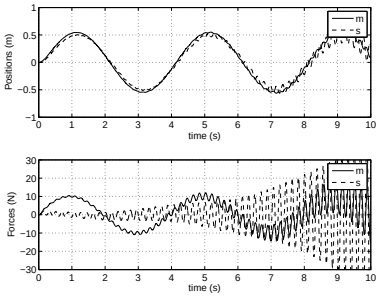

Figure 5.3.4: Master and slave positions and forces with 30ms delay. Unstable behavior.

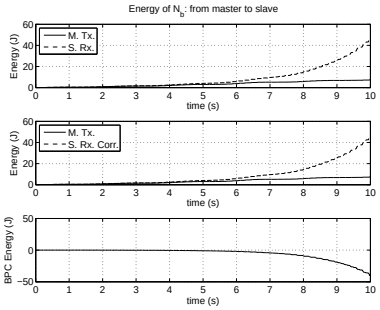

(a) Energies at N_b (from master to slave): Sent and received energies, sent and corrected received energies by PC, and observed energy by slave PO. Unstable behavior.

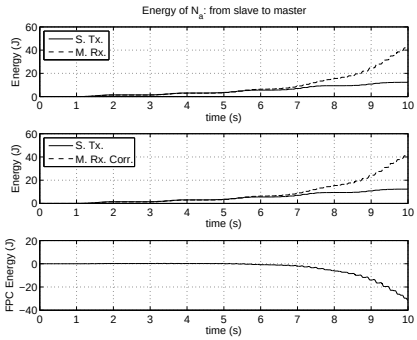

(b) Energies at N_a (from slave to master): Sent and received energies, sent and corrected received energies by PC, and observed energy by master PO. Unstable behavior.

Figure 5.3.5: Observed energies in N_z

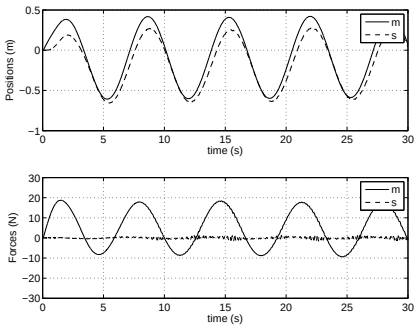

Figure 5.3.6: Master and slave positions and forces with 300 ms round trip delay. Free Environment.

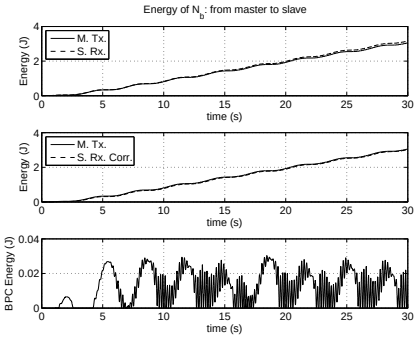

(a) Energies at N_b (from master to slave): Sent and received energies, sent and corrected received energies by PC, and observed energy by slave PO.

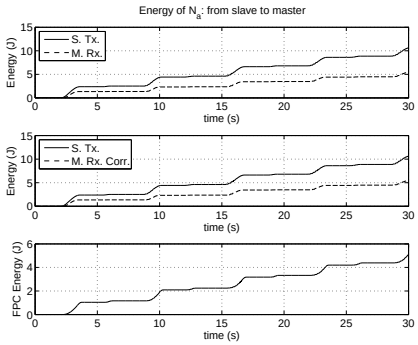

(b) Energies at N_a (from slave to master): Sent and received energies, sent and corrected received energies by PC, and observed energy by master PO.

Figure 5.3.7: Observed energies in N_a. 300ms round trip delay. Free Environment.

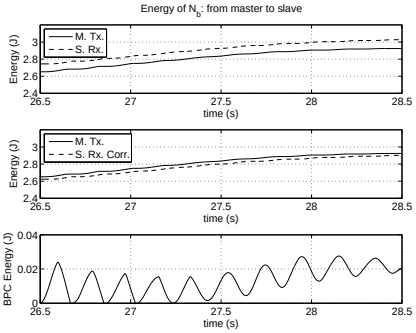

Figure 5.3.8: Zoomed view of energies at N_b (from master to slave): Sent and received energies, sent and corrected received energies, and observed energy by the slave PC. Free Environment.

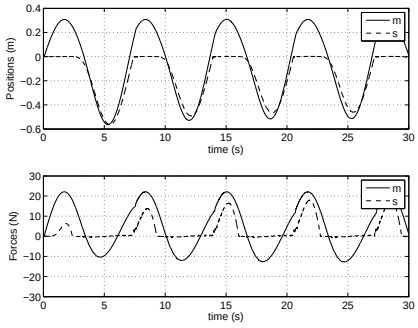

Figure 5.3.9:]

Master and slave positions and forces with 300 ms round trip delay. Wall Contact

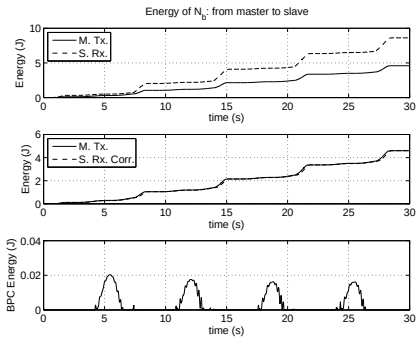

(a) Energies at N_b (from master to slave): Sent and received energies, sent and corrected received energies by PC, and observed energy by slave PO.

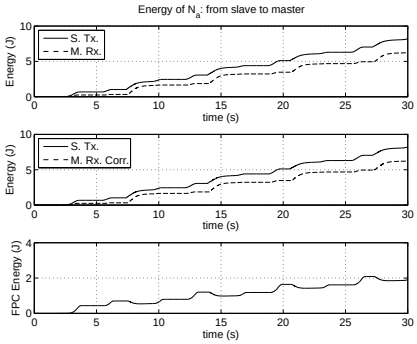

(b) Energies at N_a (from slave to master): Sent and received energies, sent and corrected received energies by PC, and observed energy by master PO.

Figure 5.3.10: Observed energies in N_z. 300 ms round trip delay. Wall Contact

Experiments

The setup uses the same control scheme employed for the simulations. Master and slave systems are both DLR - Light Weight Robots (LWR III), with 7 DoF and masses of around 20 Kg. For the testing purposes only the fourth joint of both robots have been coupled. Both robots are real time driven by VxWorks at a sampling rate of 1 kHz.

The PD controllers have been tuned such that the system can allow delays up to $T_{rt} = 5\,ms$ (when both passivity controllers deactivated). The following experiments are exposed: a) $T_{rt} = 100\,ms$ in free environment: Fig. 5.3.11, and Fig. 5.3.12; b) $T_{rt} = 100\,ms$ in hard wall contact: Fig. 5.3.13, and Fig. 5.3.14; c) $T_{rt} = 240\,ms$ in hard wall contact: Fig. 5.3.15 and Fig. 5.3.16; d) $T_{rt} = 500\,ms$ in hard wall contact: Fig. 5.3.17 and Fig. 5.3.18.

Note the different energy responses before and after the PCs in Fig. 5.3.12, 5.3.14, 5.3.16 and 5.3.18. The firsts (the left plots) show N_a and / or N_b active behavior; the seconds (the right plots) show passive networks, i.e. N_a plus FPC; and N_b plus BPC. Since the user actively moves the master, the energy flows mainly from left to right. The channel mostly generates energy toward the slave side as well, i.e. N_b has a more active tendency and therefore the BPC is triggered frequently.

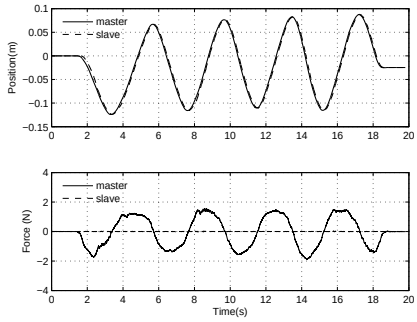

Figure 5.3.11: Experimental data. 100 ms round trip delay. Free Environment.

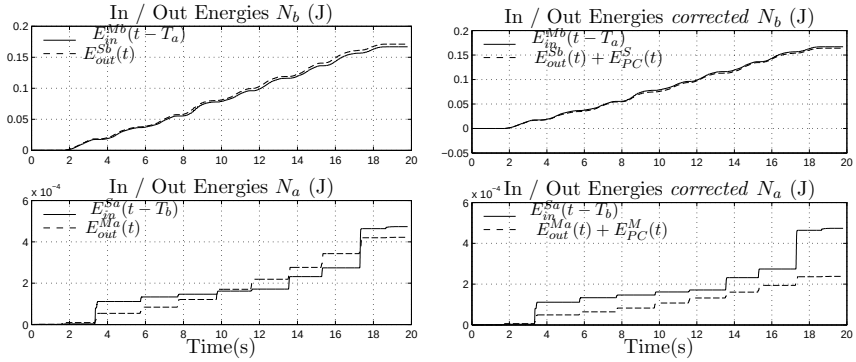

(a) Energies before PC (b) Energies after PC

Figure 5.3.12: Energy signals. 100 ms round trip delay. Free Environment.

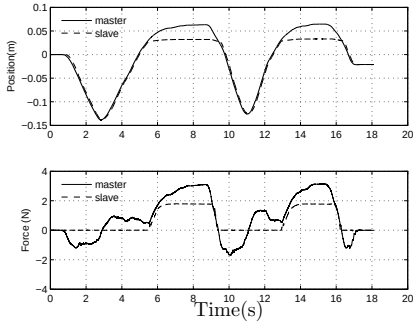

Figure 5.3.13: Experimental data. 100 ms round trip delay. Contact.

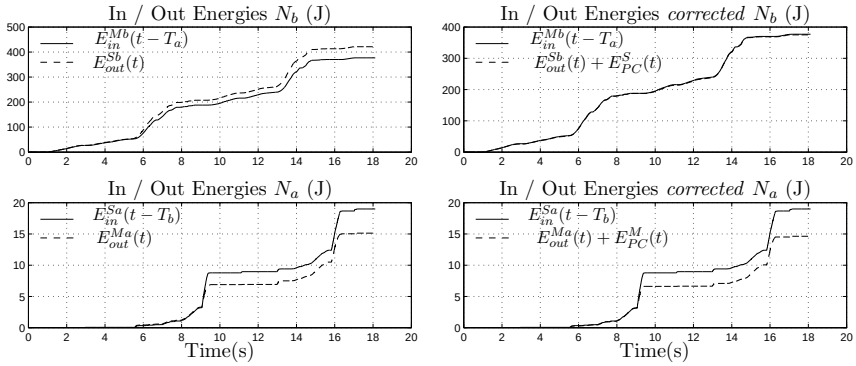

(a) Energies before PC (b) Energies after PC

Figure 5.3.14: Energy signals. 100 ms round trip delay. Contact.

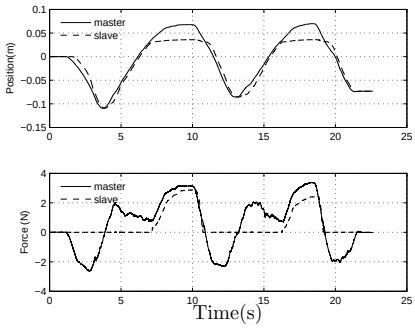

Figure 5.3.15: Experimental data. 240 ms round trip delay. Contact

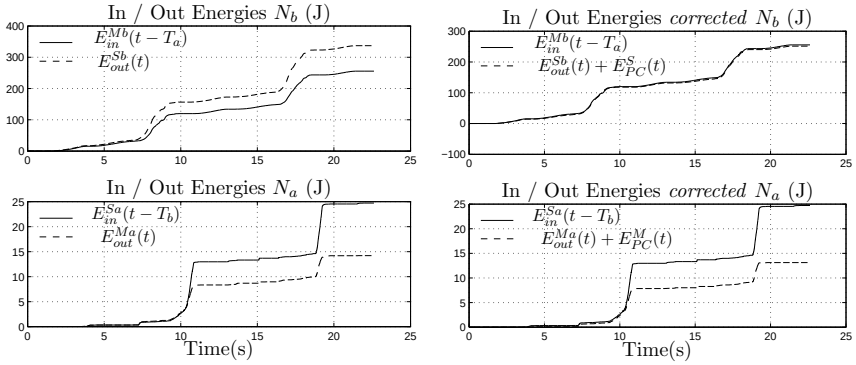

(a) Energies before PC (b) Energies after PC

Figure 5.3.16: Experimental data. 240 ms round trip delay. Contact

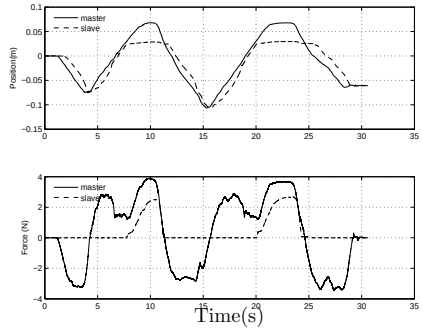

Figure 5.3.17: Experimental data. 500 ms round trip delay. Contact

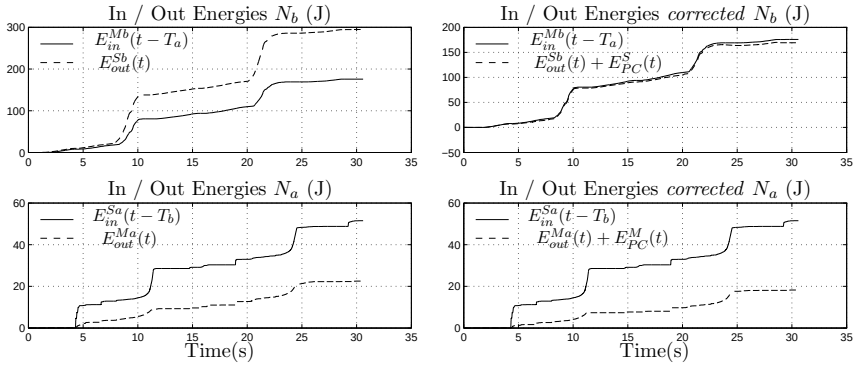

(a) Energies before PC (b) Energies after PC

Figure 5.3.18: Experimental data. 500 ms round trip delay. Contact

5.4 The Position-Force measured Architecture with Time Delay

The TDPN description for the Position-Force measured architecture was presented in Sec. 3.9. We follow the same procedure as for the Position-Position. Table 5.2 shows the diagrams involved in this architecture.

Recall the port variables defined found in Sec. 3.9:

$$\text{TDPN A}: \begin{cases} \langle \quad f_e(t-T)\ ,\ v_m(t) \quad\quad \rangle & \text{at the master} \\ \langle \quad\quad f_e(t)\ ,\ v_m(t-T) \ \rangle & \text{at the slave} \end{cases}$$

$$\text{TDPN B}: \begin{cases} \langle \quad\quad f_s(t-T)\ ,\ v_m(t) \ \rangle & \text{at the master} \\ \langle \ f_s(t)\ ,\ v_m(t-T) \quad\quad \rangle & \text{at the slave} \end{cases}$$

Note that the passivity of the communication channel is not (directly) dependent on the slave velocity signal v_s and the lower TDPN, B, is independent from the sensed force f_e.

TDPN A

The Passivity Observer is given by:

$$W_m(n) \quad = \quad E_{in}^{Sa}(n-D) - E_{out}^{Ma}(n) + E_{PC}^{M}(n), \tag{5.22}$$

$$E_{in}^{Sa}(n) \quad = \quad E_{in}^{Sa}(n-1) + T_s P_{in}^{Sa}(n) \tag{5.23}$$

$$E_{out}^{Ma}(n) \quad = \quad E_{out}^{Ma}(n-1) + T_s P_{out}^{Ma}(n) \tag{5.24}$$

$$P_{in}^{Sa}(n) = \begin{cases} f_e(n)(-v_m(n-D)) & \text{if } f_e(n)(-v_m(n-D)) > 0 \\ 0 & \text{else} \end{cases}$$
$$P_{out}^{Ma}(n) = \begin{cases} -f_e(n-D)v_m(n) & \text{if } f_e(n-D)v_m(n) < 0 \\ 0 & \text{else} \end{cases}$$

Note the negative sign of $v_m(n-D)$ in P_{in}^{Sa} due to the velocity direction defined as outgoing from the TDPN A. The negative sign of P^{Ma} is needed since all the powers and energies are positive defined (see Sec. 3.5).

$$E_{PC}^{M}(n) = T_s \sum_{k=1}^{n-1} v_m^2(k)\alpha(n), \tag{5.25}$$

The Passivity Controller is defined as:

$$f_m(n) = \hat{f}_m(n) + v_m(n)\alpha(n). \tag{5.26}$$

where $\hat{f}_m(n) = f_e(n-D)$ and the dissipation factor, α[4], is given by:

$$\alpha(n) = \begin{cases} 0 & \text{if } W_m(n) > 0 \\ \dfrac{-W_m(n)}{T_s v_m^2(n)} & \text{else} \end{cases}$$

TDPN B

The Passivity Observer is given by:

$$W_s(n) = E_{in}^{Mb}(n-D) - E_{out}^{Sb}(n) + E_{PC}^{S}(n), \tag{5.27}$$

$$E_{in}^{Mb}(n) = E_{in}^{Mb}(n-1) + T_s P_{in}^{Mb}(n) \tag{5.28}$$
$$E_{out}^{Sb}(n) = E_{out}^{Sb}(n-1) + T_s P_{out}^{Sb}(n) \tag{5.29}$$

$$P_{in}^{Mb}(n) = \begin{cases} f_s(n-D)v_m(n) & \text{if } f_s(n-D)v_m(n) > 0 \\ 0 & \text{else} \end{cases}$$
$$P_{out}^{Sb}(n) = \begin{cases} -f_s(n)(-v_m(n-D)) & \text{if } f_s(n)(-v_m(n-D)) < 0 \\ 0 & \text{else} \end{cases}$$

Note the negative sign of $v_m(n-D)$ in P_{out}^{Sb} due to the velocity direction defined as outgoing from the TDPN B. As for the TDPN A, P^{Sb} is positive defined (see Sec. 3.5).

$$E_{PC}^{S}(n) = T_s \sum_{k=1}^{n-1} f_s^2(n)\beta(n), \tag{5.30}$$

[4] a numerical *death zone* on v_m shall avoid potential divisions by zero

The Passivity Controller is defined as:

$$v_{sd}(n) = \hat{v}_{sd}(n) - f_s(n)\beta(n) = v_m(n-D) - f_s(n)\beta(n). \tag{5.31}$$

where the dissipation factor, β [5], is given by:

$$\beta(n) = \begin{cases} 0 & \text{if } W_s(n) > 0 \\ \dfrac{-W_s(n)}{T_s f_s^2(n)} & \text{else} \end{cases}$$

Experimental example

Some experiments where performed using the setup described in Sec. B.2 with a pair of PHANToMs 1.5 and a force-torque sensor mounted at the tip of the slave. The PD controller was parametrized for maximum performance assuming a nearly ideal case, i.e. high stiffness (P) and null damping (D). The sampling rate was set at 1000 Hz. Overall, the bare system configuration (without any PO / PC) presented very narrow stability regions, allowing a maximum round-trip delay of $T_{rt} = 3ms$. Fig. 5.4.1(a) shows position and force responses for a round trip delay of 100ms, $T_f = 50ms$ and $T_b = 50ms$. Fig. 5.4.1(b) shows *in* and *out* energies for each TDPN. As it can be seen, in both TPDN, the output values are higher than the input ones, showing evident active behavior. This proves empirically the activity of the TDPN networks. Fig. 5.4.1(c) shows the energy responses after the Passivity Controllers. As can be seen the dissipative term of the PC brings the make the output values drop to the input values, keeping thus the system passive.

[5] a numerical *death zone* on f_s shall avoid potential divisions by zero

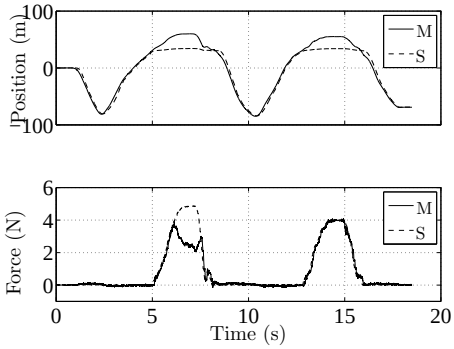

(a) Experimental data. 240 ms round trip delay. Contact

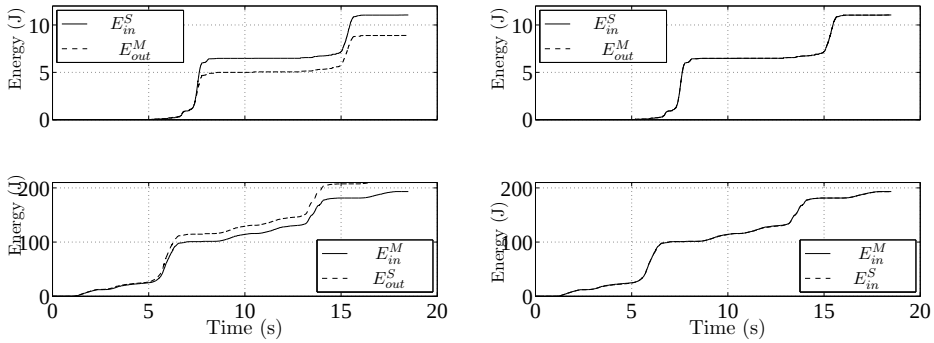

(b) Energies before PC

(c) Energies after PC

Figure 5.4.1: Experimental data. 100 ms round trip delay. Contact

5.5 Four Channels Architectures

Recalling the TDPN description of a four channels architecture presented in Sec. 3.10, the following port variables were found for each TDPN (Table 5.2 shows the diagrams involved in this architecture)

$$\text{TDPN A}: \begin{cases} \langle \; f_e(t-T) \; , \; v_m(t) \; \rangle & \text{at the master} \\ \langle \; f_e(t) \; , \; v_m(t-T) \rangle & \text{at the slave} \end{cases}$$

$$\text{TDPN B}: \begin{cases} \langle \; f_{m2}(t) \; , \; v_s(t-T) \; \rangle & \text{at the master} \\ \langle \; f_{m2}(t-T) \; , \; v_s(t) \; \rangle & \text{at the slave} \end{cases}$$

$$\text{TDPN C}: \begin{cases} \langle \; f_h(t) \; , \; v_s(t-T) \; \rangle & \text{at the master} \\ \langle \; f_h(t-T) \; , \; v_s(t) \; \rangle & \text{at the slave} \end{cases}$$

$$\text{TDPN D}: \begin{cases} \langle \; f_{s2}(t-T) \; , \; v_m(t) \; \rangle & \text{at the master} \\ \langle \; f_{s2}(t) \; , \; v_m(t-T) \rangle & \text{at the slave} \end{cases}$$

In order to simplify the analysis, the force feed-forward gains have been made unitary, i.e. $G_m = G_s = 1$. The four design steps of the four channels are illustrated in Table 5.3 and 5.4. For each TDPN a Passivity Observer and a Passivity Controller is introduced:

TDPN A

The Passivity Observer is given by:

$$W_{Ma}(n) = E_{in}^{Sa}(n-D) - E_{out}^{Ma}(n) + E_{PC}^{Ma}(n), \tag{5.32}$$

$$E_{in}^{Sa}(n) = E_{in}^{Sa}(n-1) + T_s P_{in}^{Sa}(n) \tag{5.33}$$
$$E_{out}^{Ma}(n) = E_{out}^{Ma}(n-1) + T_s P_{out}^{Ma}(n) \tag{5.34}$$

$$P_{in}^{Sa}(n) = \begin{cases} f_e(n)(-v_m(n-D)) & \text{if } f_e(n)(-v_m(n-D)) > 0 \\ 0 & \text{else} \end{cases}$$
$$P_{out}^{Ma}(n) = \begin{cases} -f_e(n-D)v_m(n) & \text{if } f_e(n-D)v_m(n) < 0 \\ 0 & \text{else} \end{cases}$$

And the energy signals are as:

$$E_{PC}^{Ma}(n) = T_s \sum_{k=1}^{n-1} v_m^2(k)\alpha_a(k), \tag{5.35}$$

The Passivity Controller is defined as:

$$f_{m1}(n) = f_e(n-D) + v_m(n)\alpha_a(n), \tag{5.36}$$

where the dissipation factor, α_a, is given by:

$$\alpha_a(n) = \begin{cases} 0 & \text{if } W_{Ma}(n) > 0 \\ \dfrac{-W_{Ma}(n)}{T_s v_m^2(n)} & \text{else} \end{cases}$$

TDPN B

The Passivity Observer is given by:

$$W_{Mb}(n) = E_{in}^{Sb}(n-D) - E_{out}^{Mb}(n) + E_{PC}^{Mb}(n), \tag{5.37}$$

$$E_{in}^{Sb}(n) = E_{in}^{Sb}(n-1) + T_s P_{in}^{Sb}(n) \tag{5.38}$$
$$E_{out}^{Mb}(n) = E_{out}^{Mb}(n-1) + T_s P_{out}^{Mb}(n) \tag{5.39}$$

$$P_{in}^{Sb}(n) = \begin{cases} f_{m2}(n-D)(-v_s(n)) & \text{if } f_{m2}(n-D)(-v_s(n)) > 0 \\ 0 & \text{else} \end{cases}$$
$$P_{out}^{Mb}(n) = \begin{cases} -f_{m2}(n)v_s(n-D) & \text{if } f_{m2}(n)v_s(n-D) < 0 \\ 0 & \text{else} \end{cases}$$

$$E_{PC}^{Sb}(n) = T_s \sum_{k=1}^{n-1} f_{m2}^2(k)\beta_b(k). \tag{5.40}$$

The Passivity Controller is defined as:

$$v_{md}(n) = v_s(n-D) - f_{m2}(n)\beta_b(n) \tag{5.41}$$

where the dissipation factor, β_b, is given by:

$$\beta_b(n) = \begin{cases} 0 & \text{if } W_{Sb}(n) > 0 \\ \dfrac{-W_{Sb}(n)}{T_s f_{m2}^2(n)} & \text{else} \end{cases}$$

TDPN C

The Passivity Observer is given by:

$$W_{Sc}(n) = E_{in}^{Mc}(n-D) - E_{out}^{Sc}(n) + E_{PC}^{Sc}(n), \tag{5.42}$$

$$E_{in}^{Mc}(n) = E_{in}^{Mc}(n-1) + T_s P_{in}^{Mc}(n) \tag{5.43}$$

$$E_{out}^{Sc}(n) = E_{out}^{Sc}(n-1) + T_s P_{out}^{Sc}(n) \tag{5.44}$$

$$P_{in}^{Mc}(n) = \begin{cases} f_h(n)v_s(n-D) & \text{if } f_h(n)v_s(n-D) > 0 \\ 0 & \text{else} \end{cases}$$

$$P_{out}^{Sc}(n) = \begin{cases} -f_h(n-D)(-v_s(n)) & \text{if } f_h(n-D)(-v_s(n)) < 0 \\ 0 & \text{else} \end{cases}$$

Note the negative sign of $v_s(n)$ in P_{out}^{Sc} due to the velocity direction defined as outgoing from the TDPN C and the positive defined power signals. For the sake of clarity, both negative signs are kept, that is, the one that makes the power value positive and the one due to the velocity direction of v_s w.r.t the TDPN C.

$$E_{PC}^{Sc}(n) = T_s \sum_{k=1}^{n-1} f_s^2(k)\alpha_c(k), \tag{5.45}$$

The Passivity Controller is defined as:

$$f_{s1}(n) = f_h(n-D) + v_s(n)\alpha_c(n). \tag{5.46}$$

where the dissipation factor, α_a, is given by:

$$\alpha_c(n) = \begin{cases} 0 & \text{if } W_{Sc}(n) > 0 \\ \dfrac{-W_{Sc}(n)}{T_s v_s^2(n)} & \text{else} \end{cases}$$

TDPN D

The Passivity Observer is given by:

$$W_{Sd}(n) = E_{in}^{Md}(n - T_b) - E_{out}^{Sd}(n) + E_{PC}^{Sd}(n), \tag{5.47}$$

$$E_{in}^{Md}(n) = E_{in}^{Md}(n-1) + T_s P_{in}^{Md}(n) \tag{5.48}$$
$$E_{out}^{Sd}(n) = E_{out}^{Sd}(n-1) + T_s P_{out}^{Sd}(n) \tag{5.49}$$

$$P_{in}^{Md}(n) = \begin{cases} f_{s2}(n-D)v_m(n) & \text{if } f_{s2}(n-D)v_m(n) > 0 \\ 0 & \text{else} \end{cases}$$
$$P_{out}^{Sd}(n) = \begin{cases} -f_{s2}(n)(-v_m(n-D)) & \text{if } f_{s2}(n)(-v_m(n-D)) < 0 \\ 0 & \text{else} \end{cases}$$

$$E_{PC}^{Sd}(n) = T_s \sum_{k=1}^{n-1} f_{s2}^2(k)\beta_d(k). \tag{5.50}$$

The Passivity Controller is defined as:

$$v_{sd}(n) = v_m(n-D) - f_{s2}(n)\beta_d(n) \tag{5.51}$$

where the dissipation factor, β_d, is given by:

$$\beta_d(n) = \begin{cases} 0 & \text{if } W_{Sd}(n) > 0 \\ \dfrac{-W_{Sd}(n)}{T_s f_{s2}^2(n)} & \text{else} \end{cases}$$

The scheme showing the final system is shown in Fig. 5.5.1.

Experiments

The system has been tested in an experimental 1-Dof master-slave setup Sec. B.1. Table 5.5 summarizes the experiments.

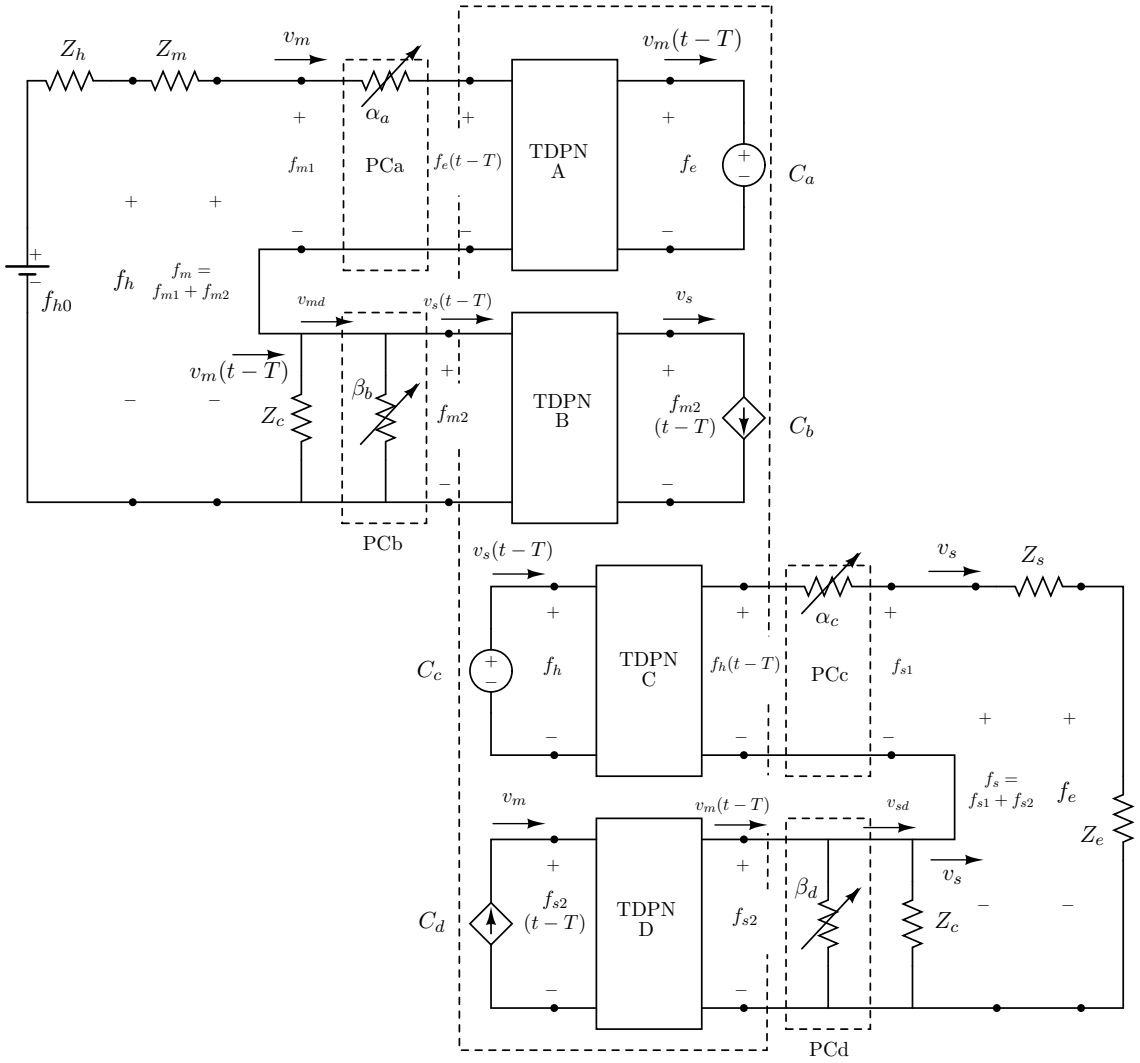

Figure 5.5.1: Four channel architecture with the Passivity Controllers

RT Delay	Ctrl. Architecture	Task	Figure	Remark
2 ms	4 Ch. TDPN/PC off	Free env	Fig. 5.5.2, 5.5.3	Stable system, however note the active TDPNs, specially TDPN C. A more *tight* control parameter setting could make the system unstable
2 ms	4 Ch. TDPN/PC off	Contact	Fig. 5.5.4, 5.5.5	Stable system, however note the active TDPNs, specially TDPN C. A more *tight* control parameter setting could make the system unstable.
30 ms	4 Ch. TDPN/PC off	free env./ contact	Fig. 5.5.6	Unstable system.
30 ms	4 Ch. TDPN/PC on	free env./ contact	Fig. 5.5.7	Stable system. The energy plots show how the output energies of each TDPN are bounded to the input energies from the other TDPN sides. TDPN C and B are the most active (note the different scales in the y axis of the energy plots).
100 ms	4 Ch. TDPN/PC on	free env./ contact	Fig. 5.5.8	Stable system. TDPN B is the most active network.
200 ms	4 Ch. TDPN/PC on	free env./ contact	Fig. 5.5.9	Stable system. TDPN B is the most active network.
300 ms	4 Ch. TDPN/PC on	free env./ contact	Fig. 5.5.10	Stable system. TDPN A and D are the most active networks.
500 ms	4 Ch. TDPN/PC on	free env./ contact	Fig. 5.5.11	Stable system. TDPN A and D are the most active networks.
900 ms	4 Ch. TDPN/PC on	free env./ contact	Fig. 5.5.12	Stable system. TDPN A is the most active network.

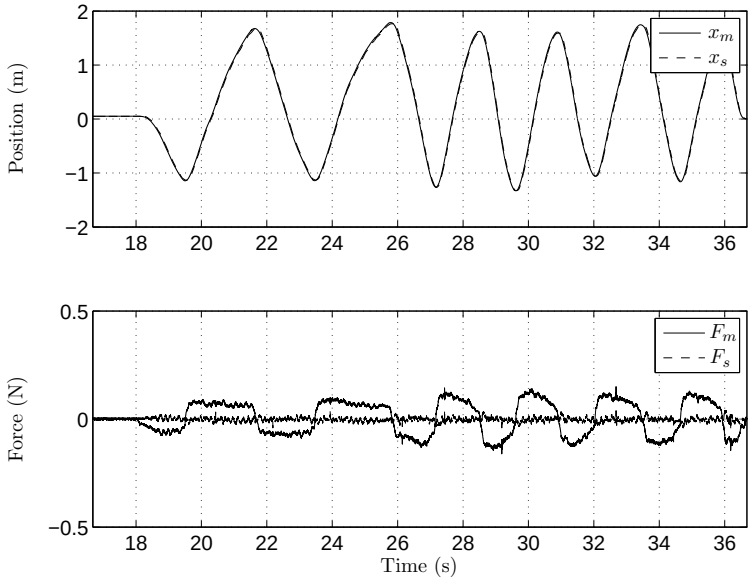

(a) Position and force responses

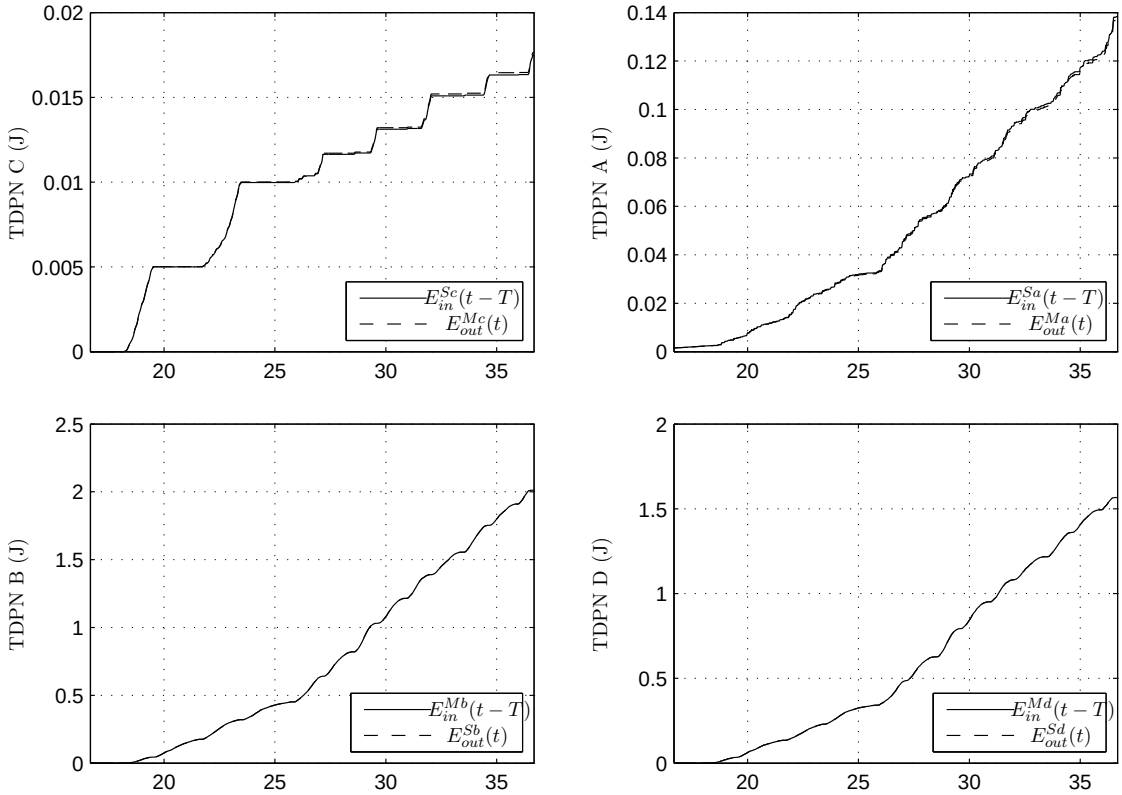

(b) TDPN A, B, C, D energy responses

Figure 5.5.2: Experimental data. 2 ms round trip delay. Free environment

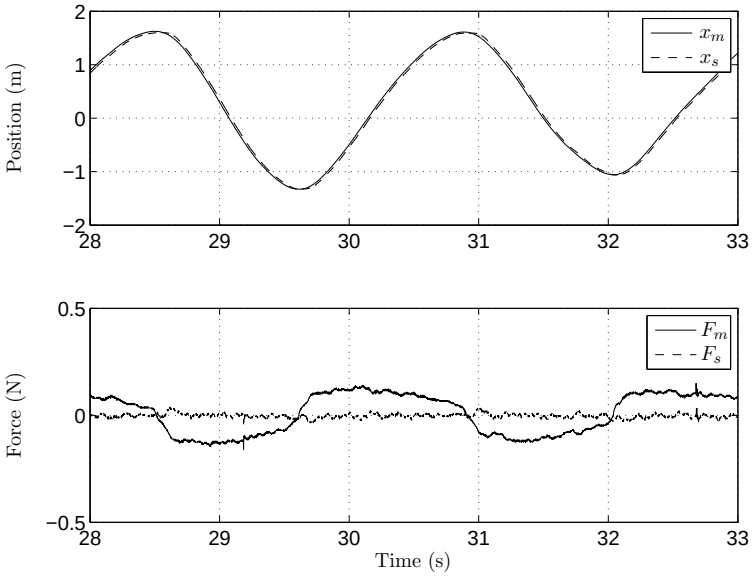

(a) Position and force responses

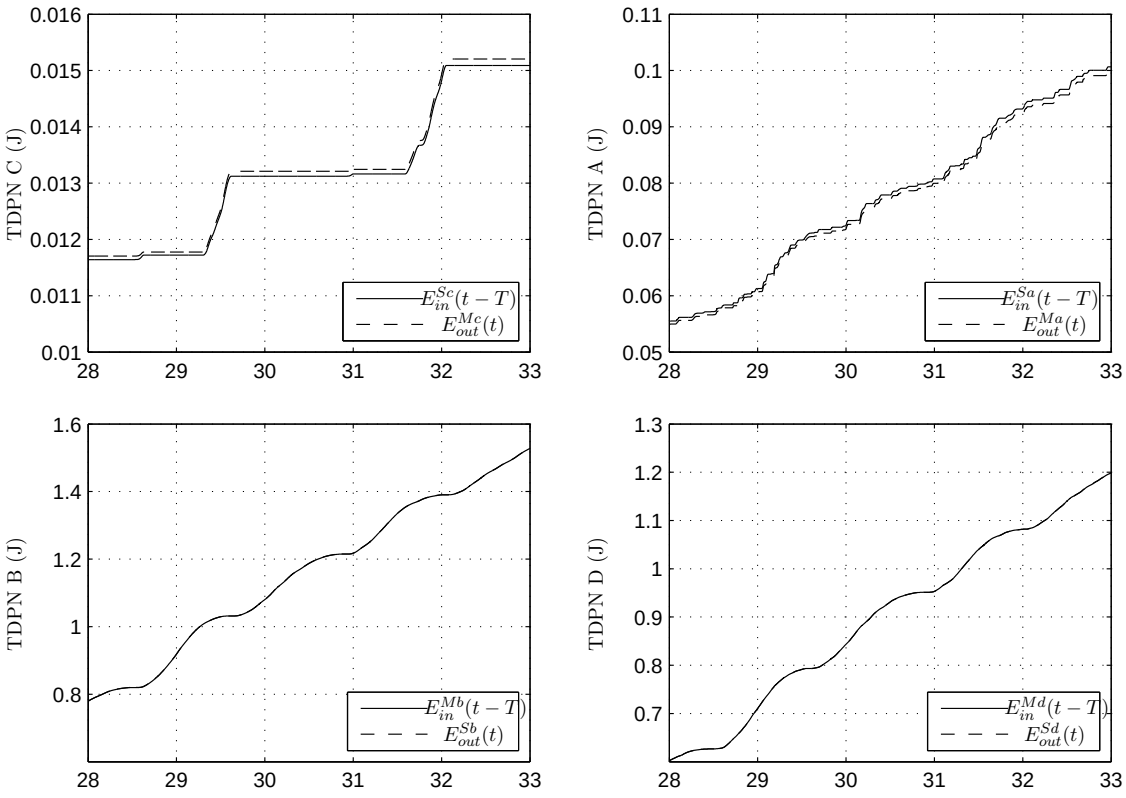

(b) TDPN A, B, C, D energy responses

Figure 5.5.3: Experimental data. Zoomed view. 2 ms round trip delay. Free environment

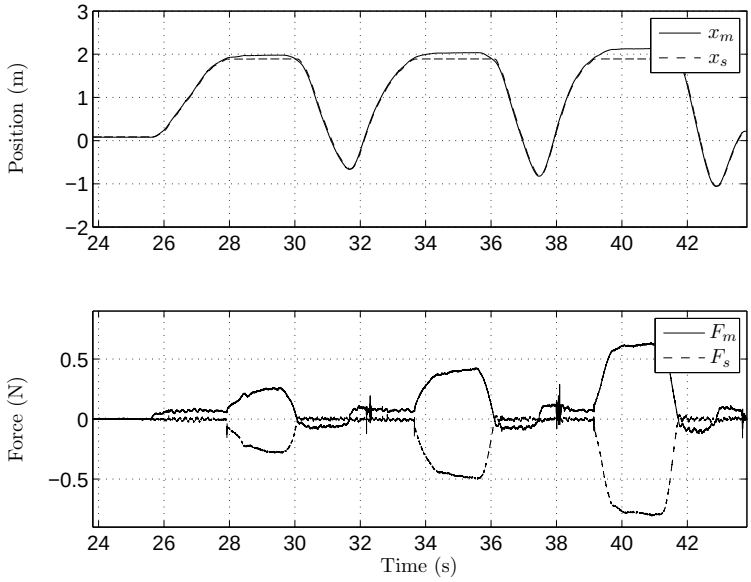

(a) Position and force responses

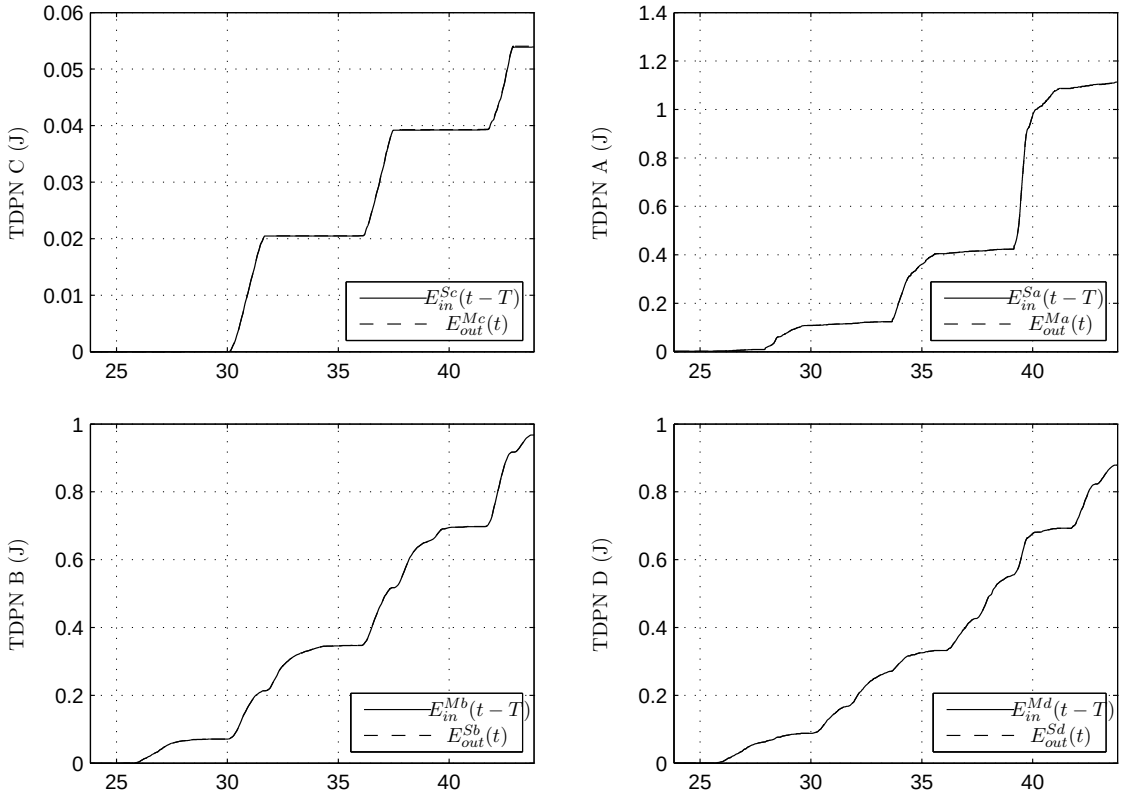

(b) TDPN A, B, C, D energy responses

Figure 5.5.4: Experimental data. 2 ms round trip delay. Free environment

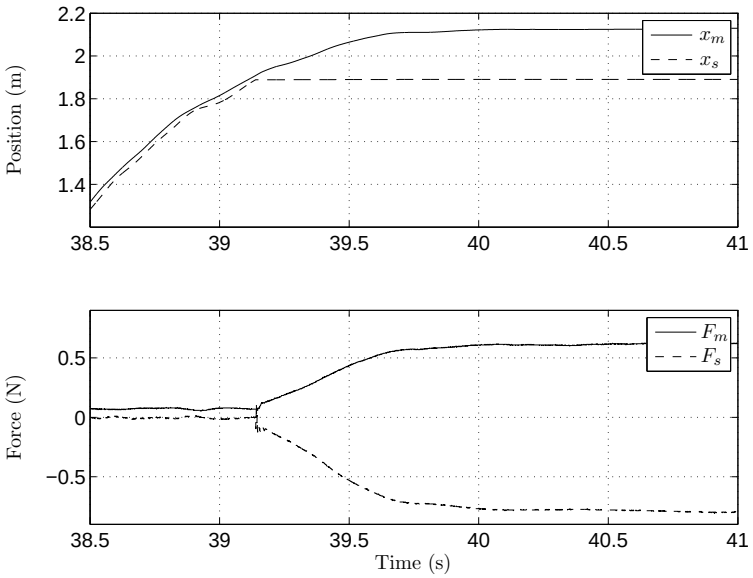

(a) Position and force responses

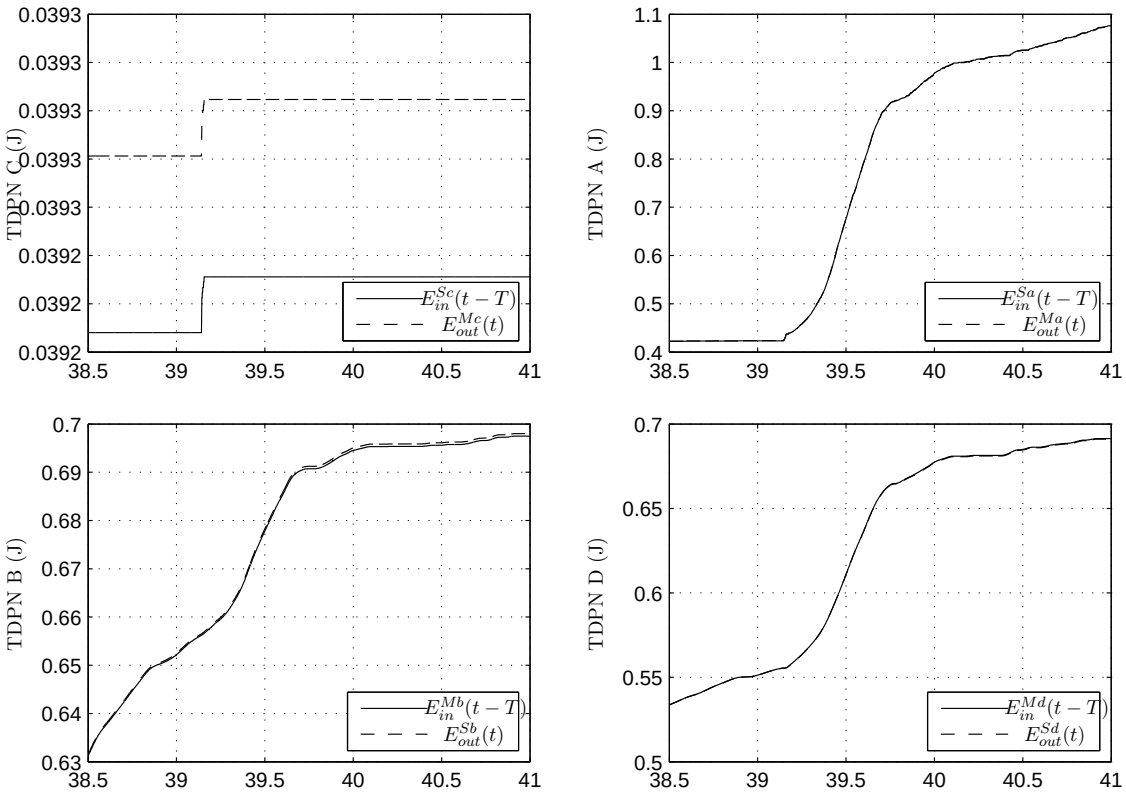

(b) TDPN A, B, C, D energy responses

Figure 5.5.5: Experimental data. Zoomed view. 2 ms round trip delay. Free environment

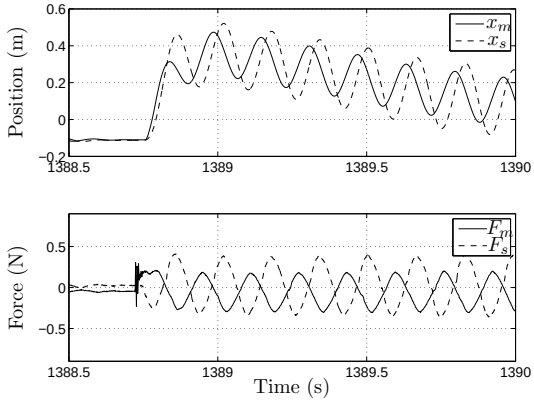

(a) Position and force responses

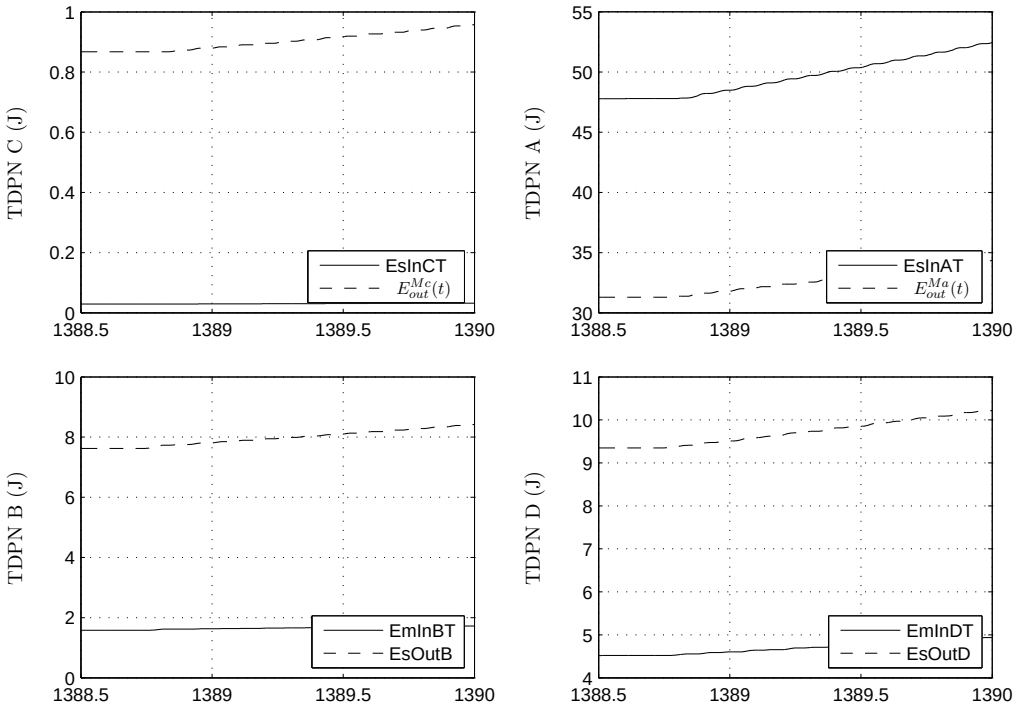

(b) TDPN A, B, C, D energy responses

Figure 5.5.6: Experimental data. 30 ms round trip delay. Passivity Controllers not activated.

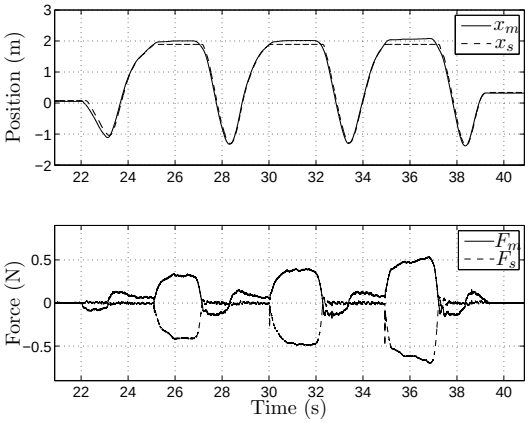

(a) Position and force responses

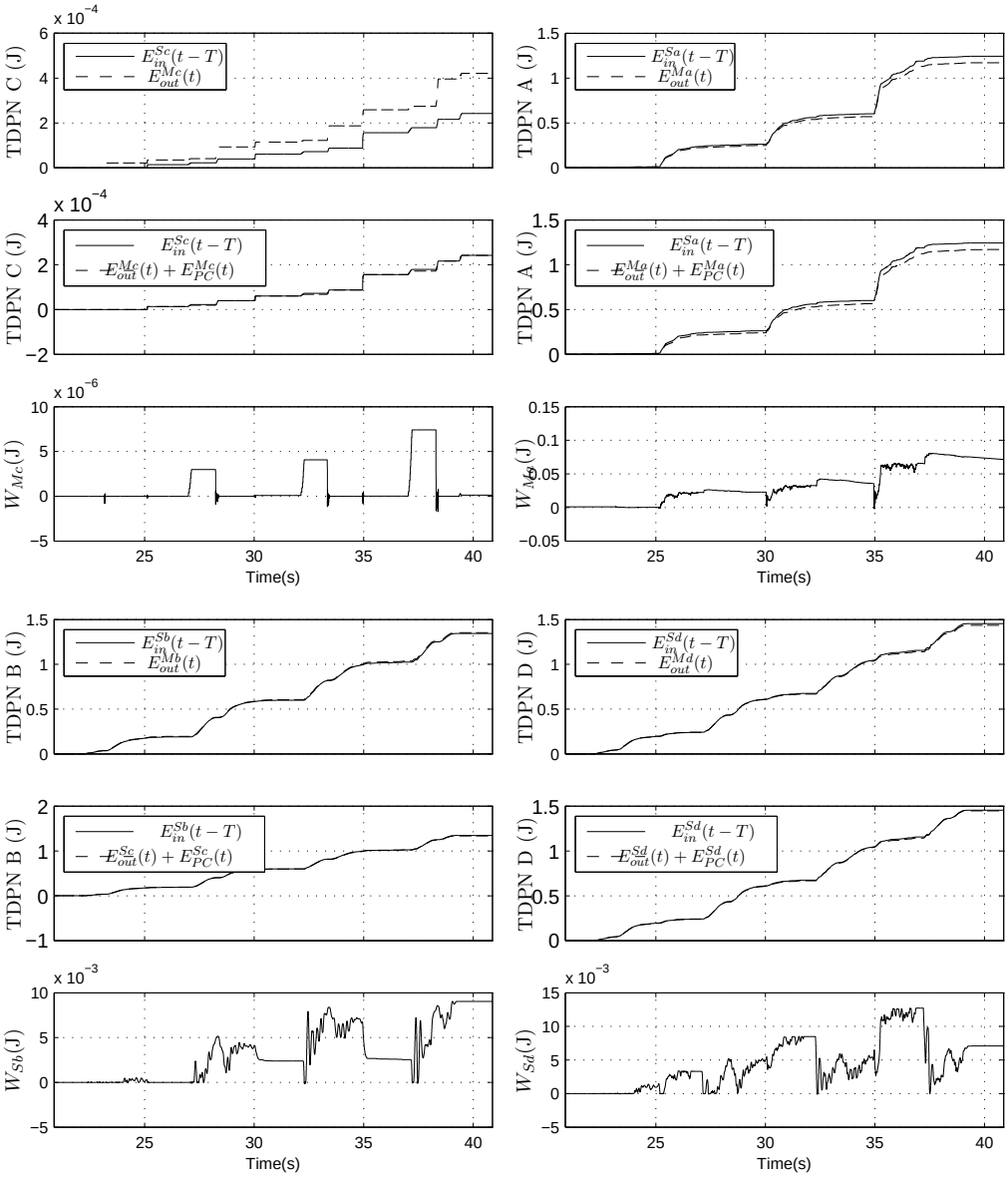

(b) TDPN A, B, C, D energy responses

Figure 5.5.7: Experimental data. 30 ms round trip delay. Passivity Controllers activated.

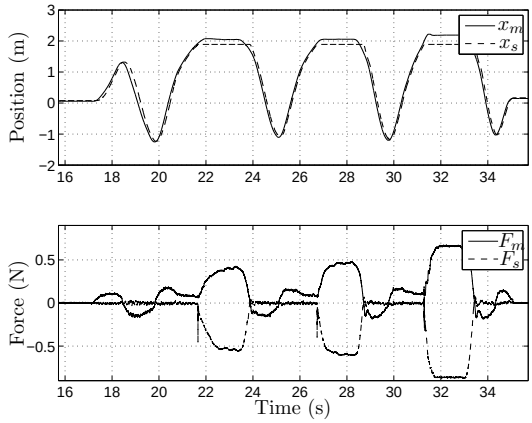

(a) Position and force responses

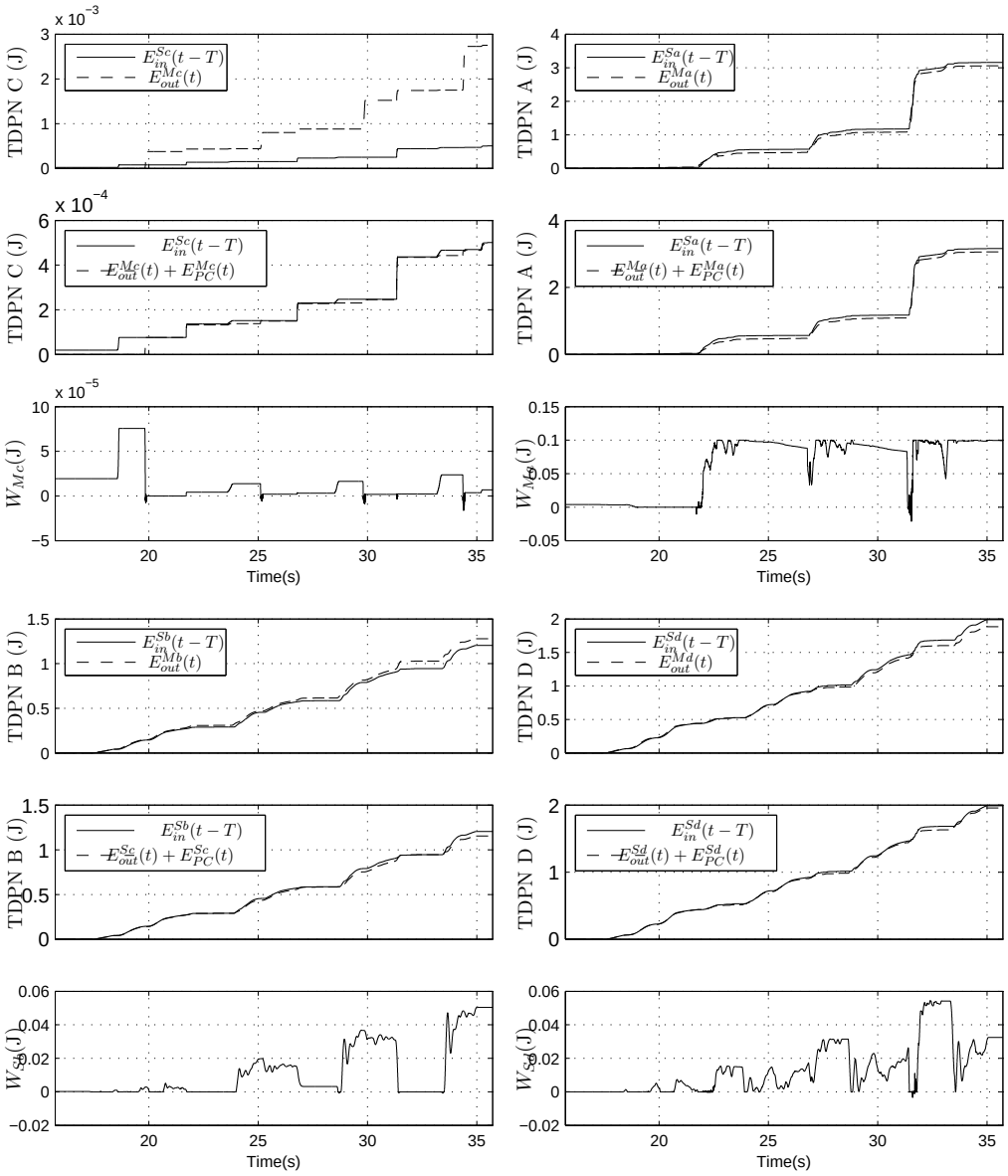

(b) TDPN A, B, C, D energy responses

Figure 5.5.8: Experimental data. 100 ms round trip delay

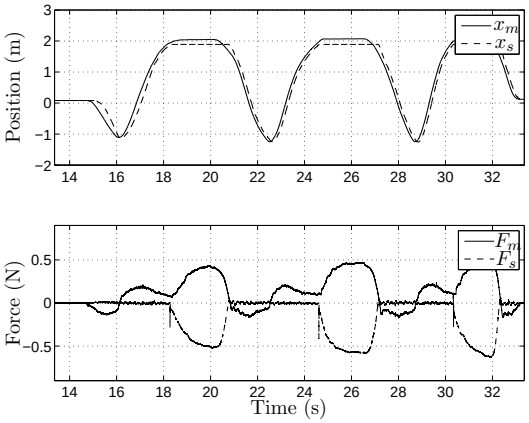

(a) Position and force responses

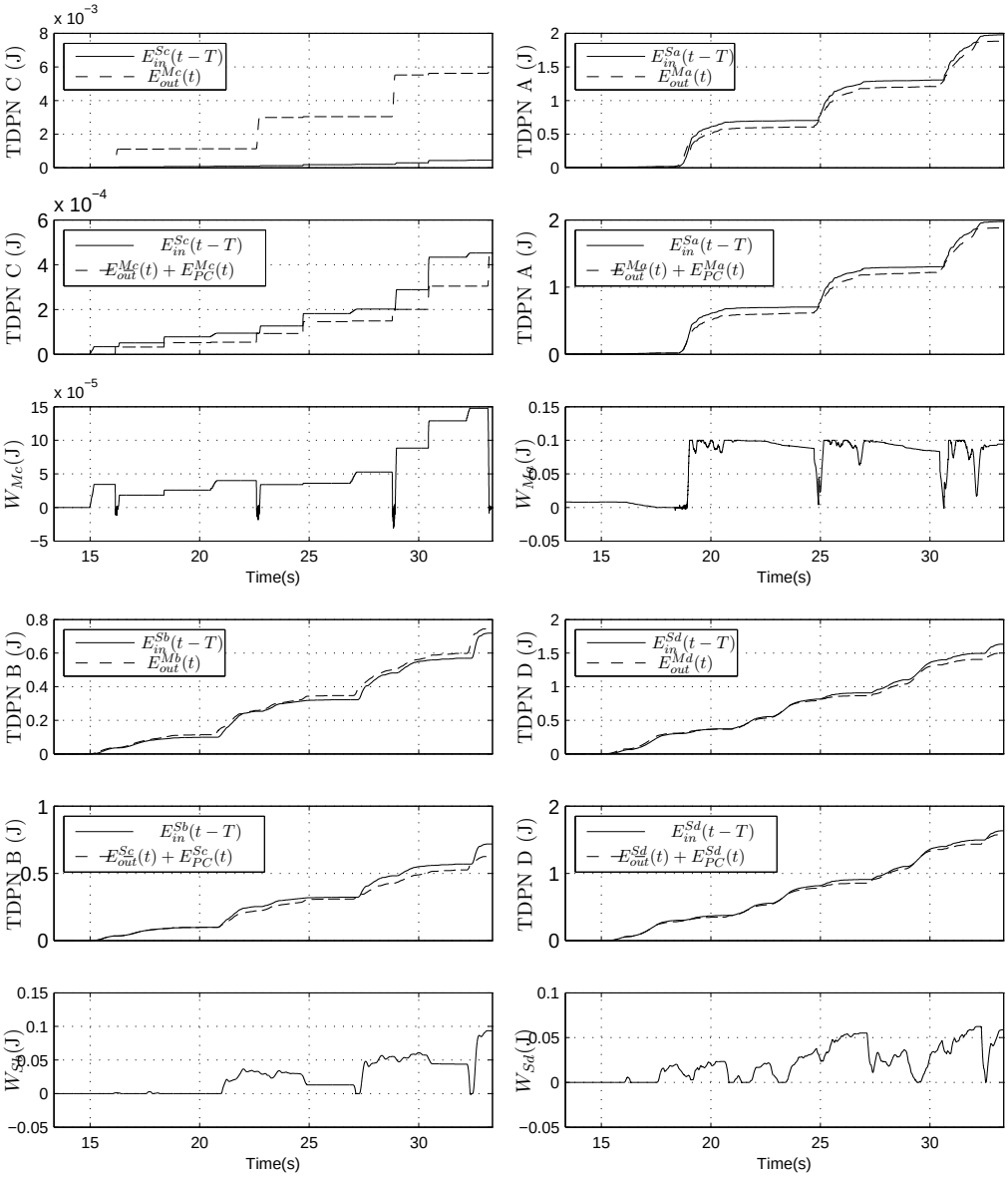

(b) TDPN A, B, C, D energy responses

Figure 5.5.9: Experimental data. 200 ms round trip delay

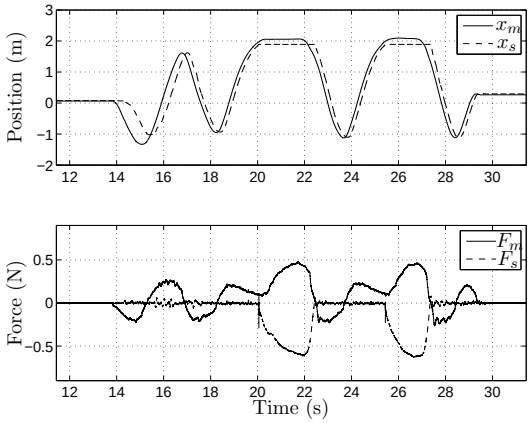

(a) Position and force responses

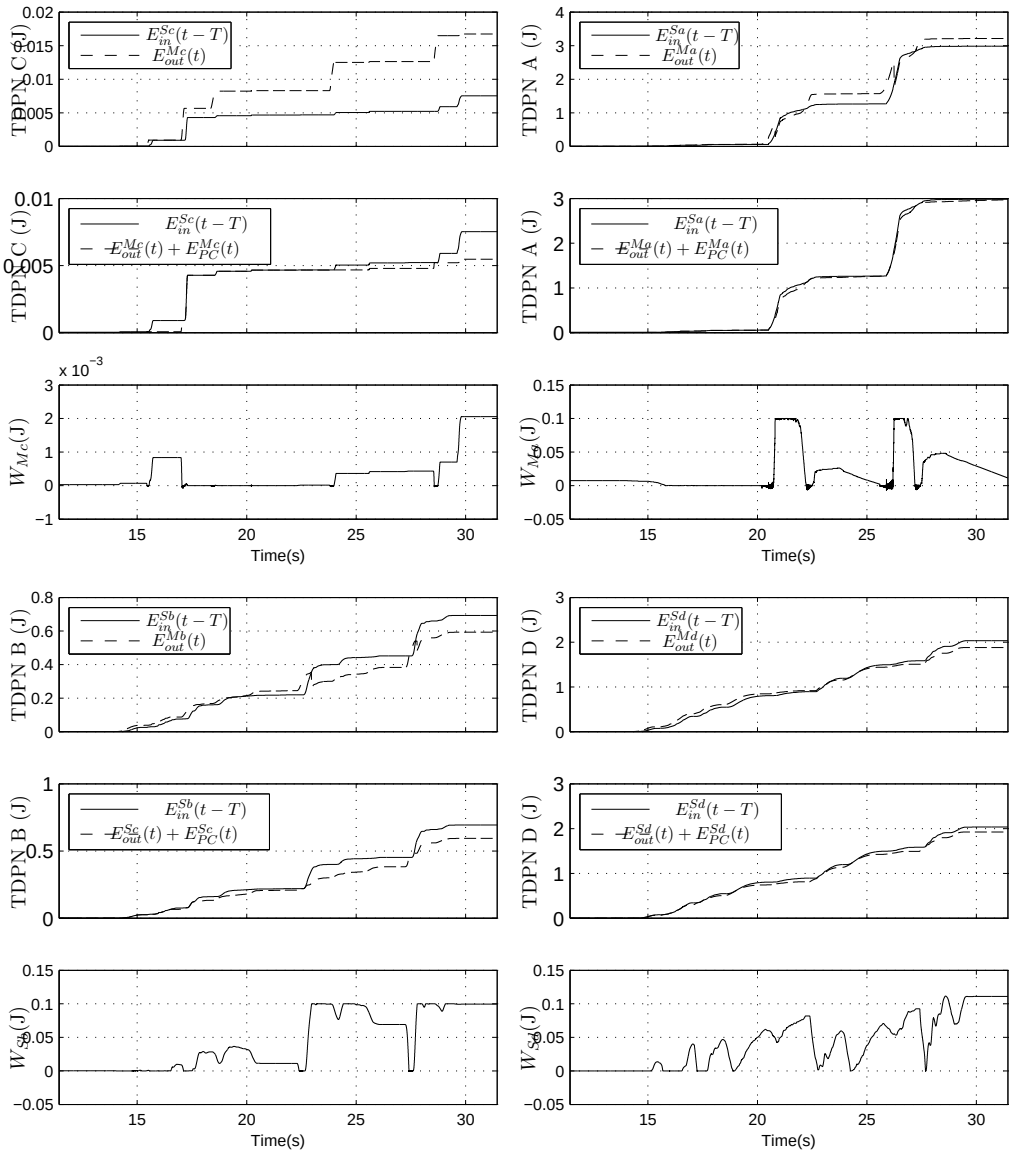

(b) TDPN A, B, C, D energy responses

Figure 5.5.10: Experimental data. 300 ms round trip delay

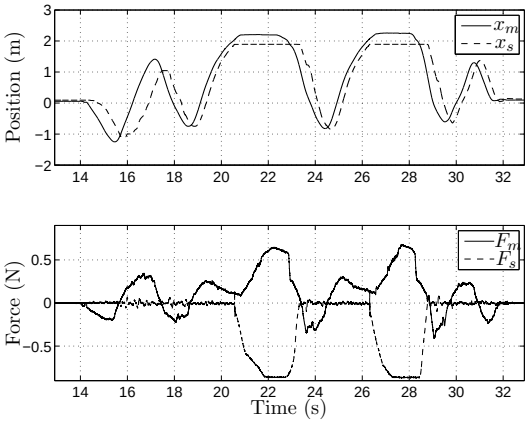

(a) Position and force responses

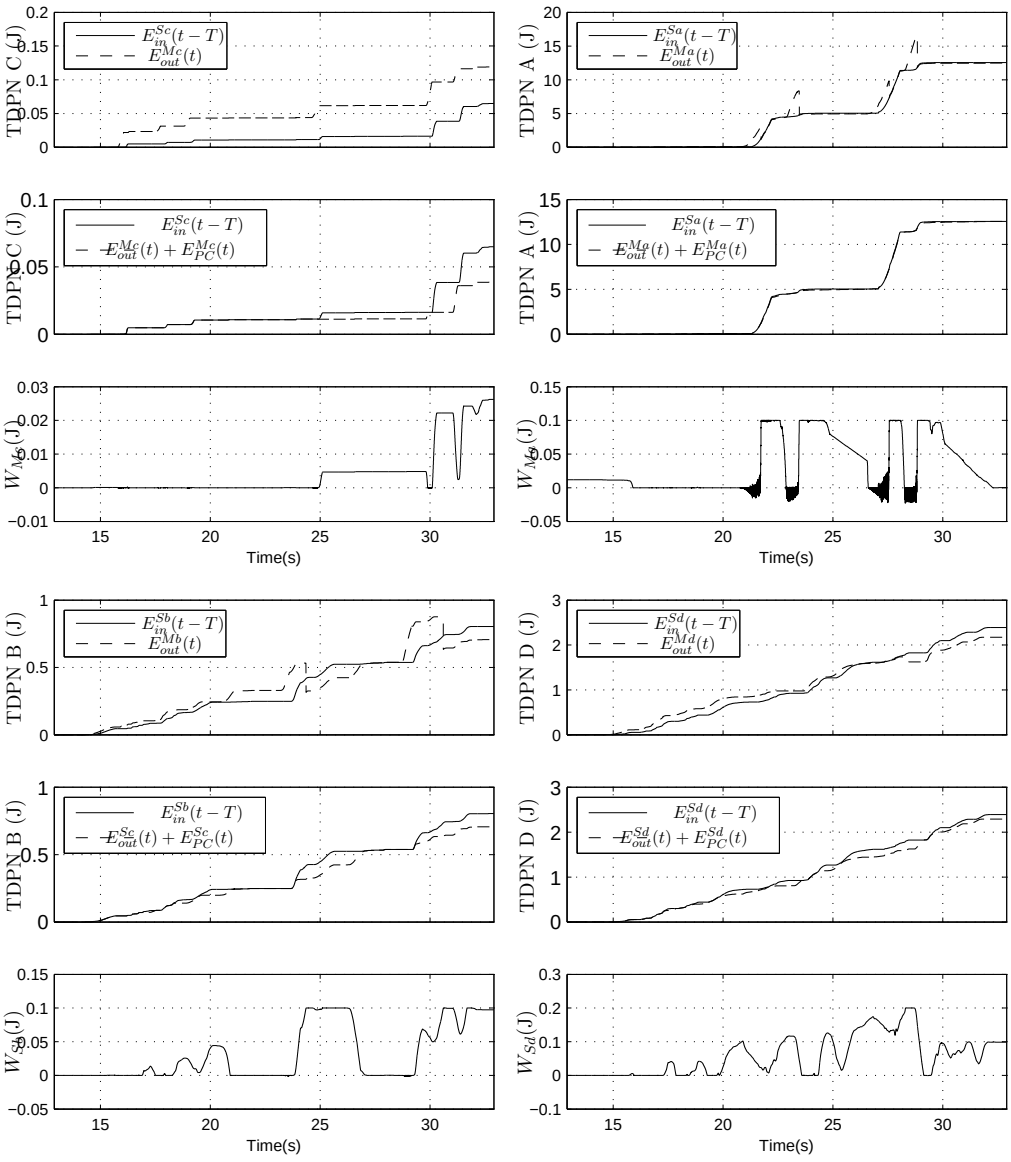

(b) TDPN A, B, C, D energy responses

Figure 5.5.11: Experimental data. 500 ms round trip delay

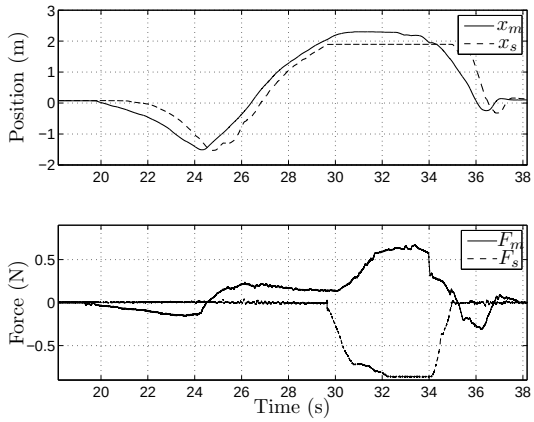

(a) Position and force responses

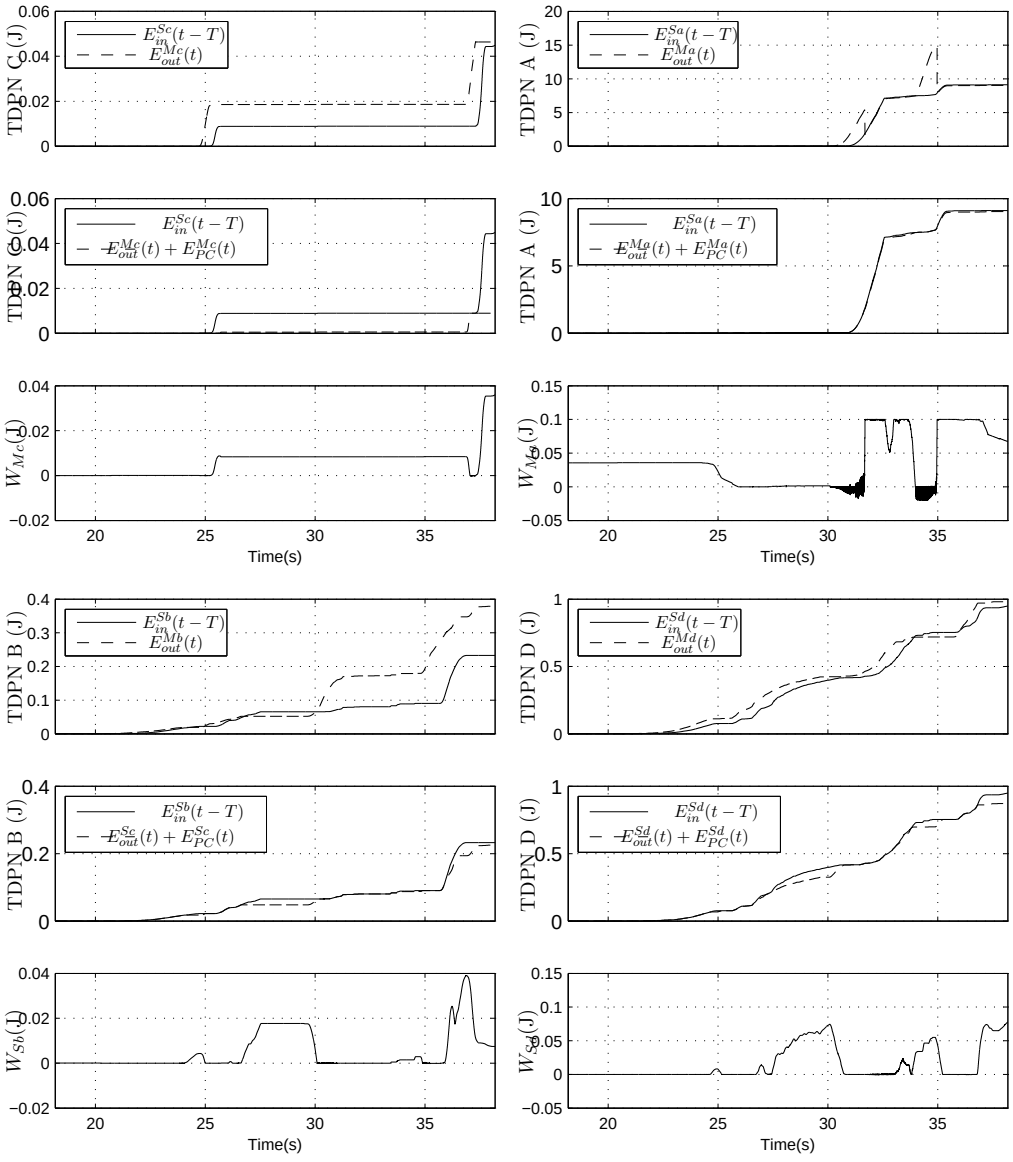

(b) TDPN A, B, C, D energy responses

Figure 5.5.12: Experimental data. 900 ms round trip delay

5.6 Schemes summary

Table 5.1: Design of the P-P architecture.

1. Flow Diagram	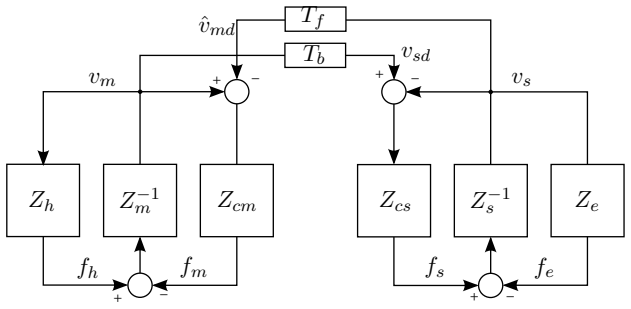
2. Electrical Scheme	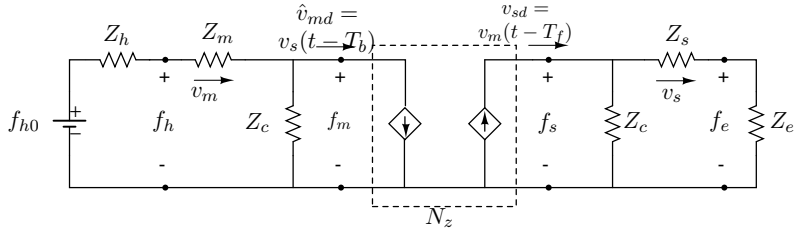
3. Augmented Electrical	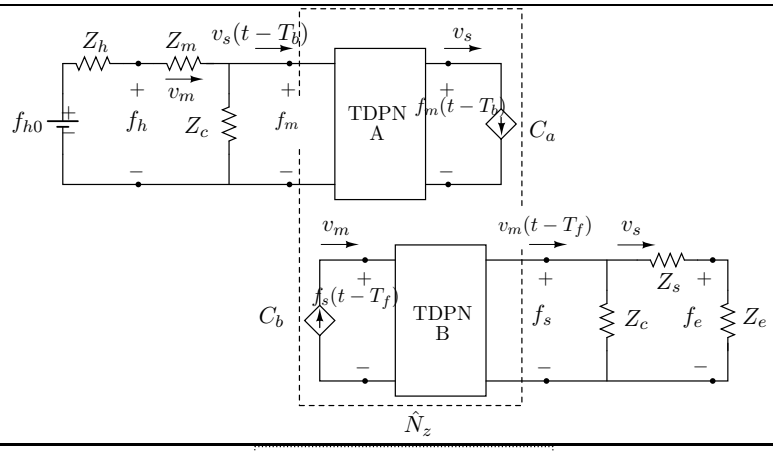
4. Passive Scheme	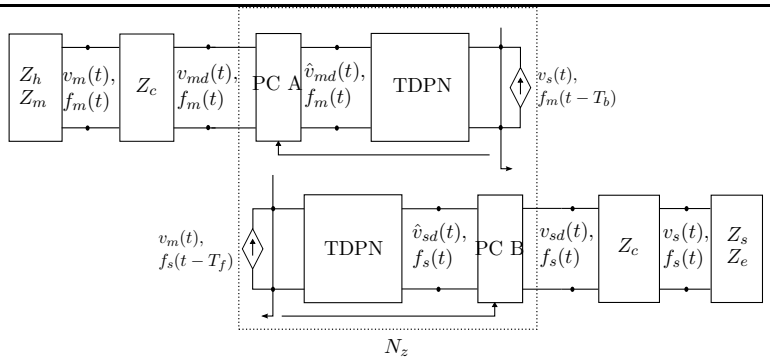

Table 5.2: Design of the P-F measured architecture.

1. Flow Diagram	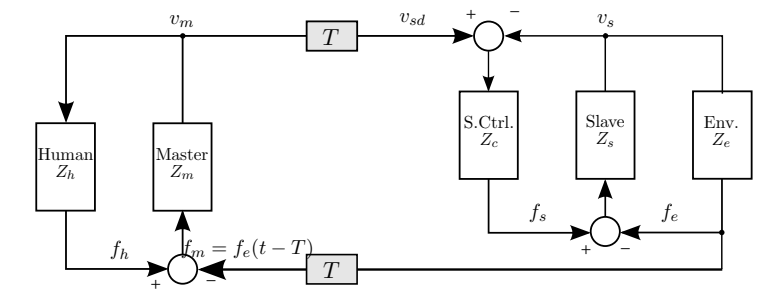
2. Electrical Scheme	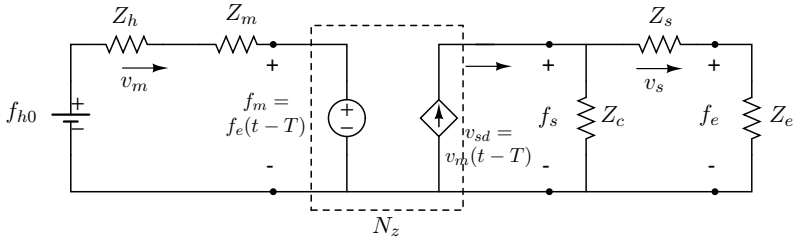
3. Augmented Electrical	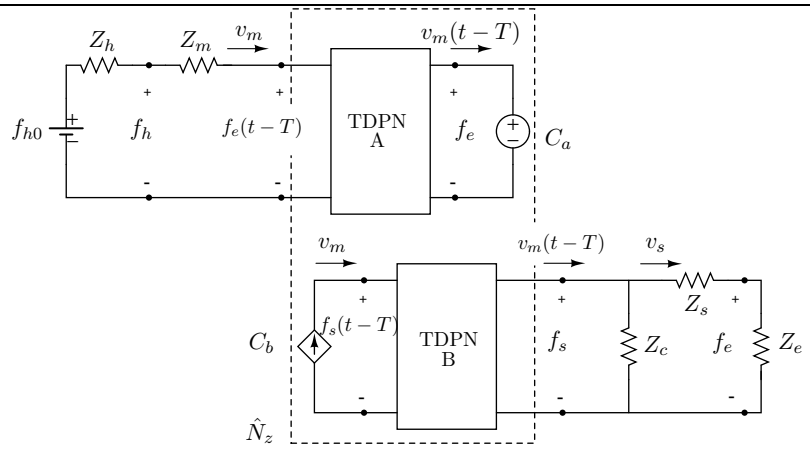
4. Passive Scheme	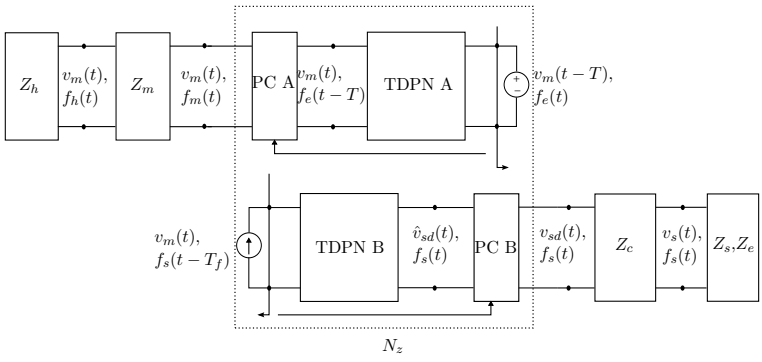

Table 5.3: Design of the four channels architecture (i)

1. Flow Diagram	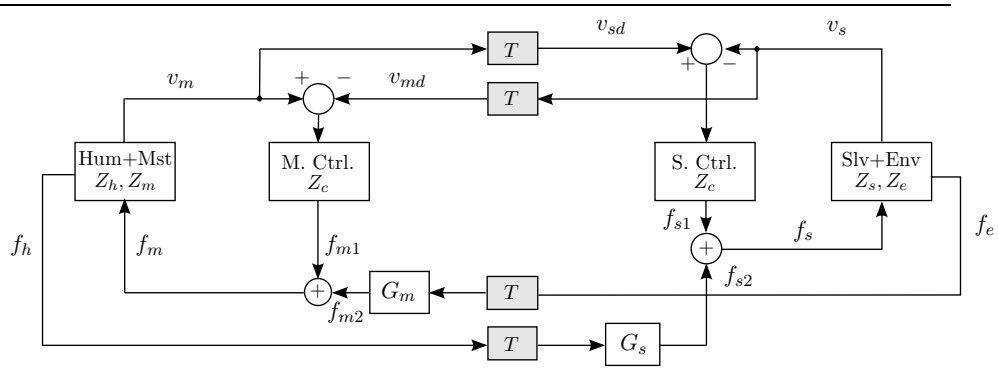
2. Electrical Scheme	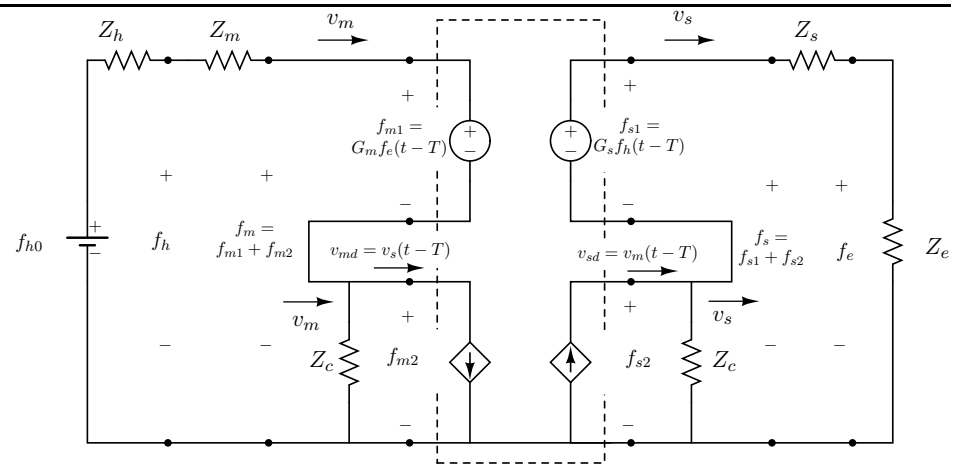

Table 5.4: Design of the four channels architecture (ii)

3. Augmented Electrical	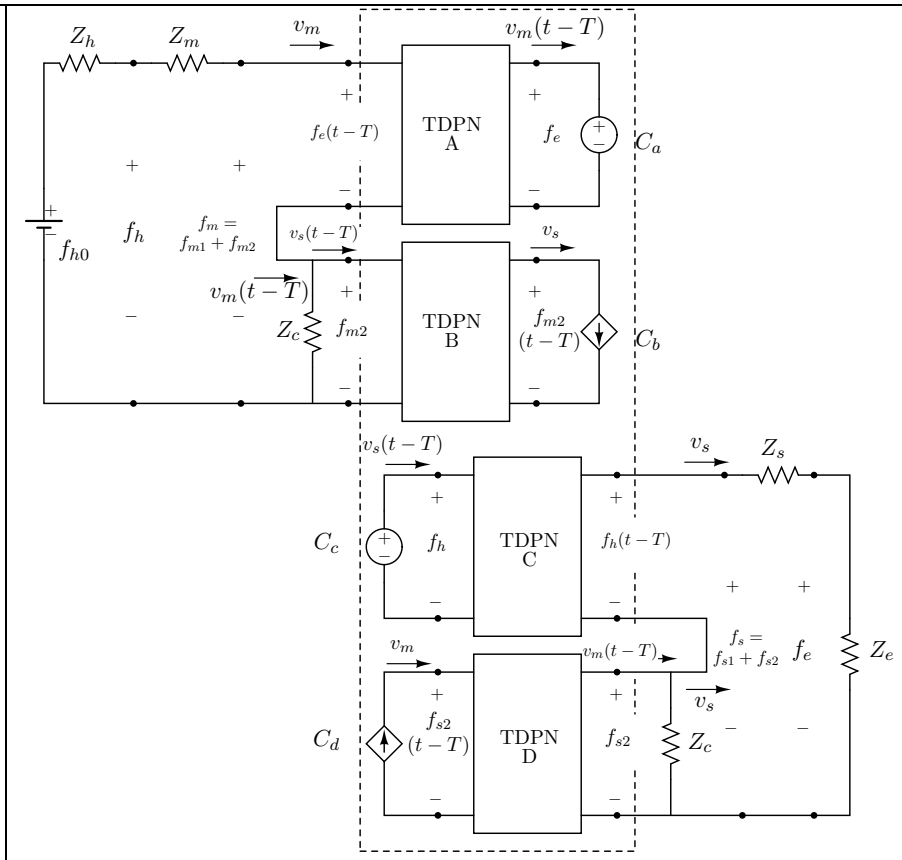
4. Passive Scheme	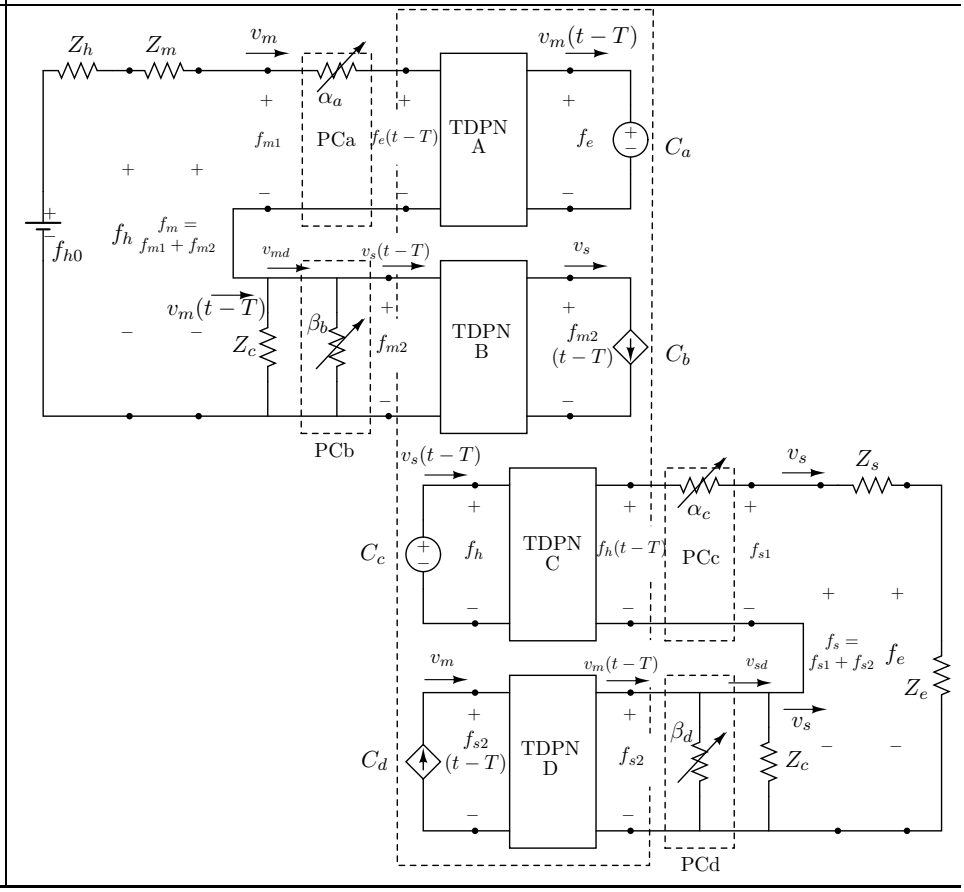

5.7 Final Remarks

In this chapter the utilization of TDPNs are justified. They a provide a powerful tool for designing passive teleoperation systems with independence of the signals conveyed through the communication channel, of the channel characteristics and independency of the dynamics of the master and the slave.

The four channels architecture offers many design possibilities to achieve performance related goals. In this thesis we have seen the TDPNs involved in it. By adjusting the controller gains, including those of the master and slave PD controllers, those of the force feed-forward and those of master and slave local force feedback [6], the behavior of the TDPNs can be modulated. The behavior of a TDPN is described by the amount of energy that carries. Performance related goals based on the amount of energy carried by each TDPN can be drawn. This remains for future work.

[6] Local force feedback controllers are not covered in this thesis

Chapter 6

Teleoperation through Internet and Space Links

An experiment has been conducted to show the performance of the presented methods in a real distributed master and slave setup using a combined Internet and space communication link. The space link is based on the geostationary communications satellite ASTRA, which has been used as a data package mirror server. Furthermore, this chapter presents the mathematical formulation to adapt the presented control methods to the multi DoF cases.

6.1 Teleoperation and On-Orbit Servicing

The interest in space robotics for on-orbit servicing (OOS), assembly of large structures and debris mitigation has increased substantially over the past few decades making the OOS and Active Debris Removal (ADR) missions an integral part of most agencies' space programs. Within this context the German Aerospace Agency (DLR) is developing the on-orbit servicing technology demonstration mission, DEOS (*Deutsches On-Orbit Servicing*) [1], to be launched in 2018, following the footsteps of former on-orbit robotic missions such as the Japanese ETS-VII [55] and the American Orbital Express (OE) [2] missions.

The DEOS space segment consists of two Low Earth Orbit (LEO) satellites, named Servicer and Client (see Fig. 6.1.1). The servicer is endowed with a 7 DoF robotic arm aimed at performing grasping, stabilization and docking maneuvers upon a passive client. Once the Client is docked on the Servicer, the robotic arm will be able to execute

servicing tasks, such as re-fueling or peg-in-hole like assembly tasks. DEOS will operate in two operational modes: Telepresence and Semi-autonomy.

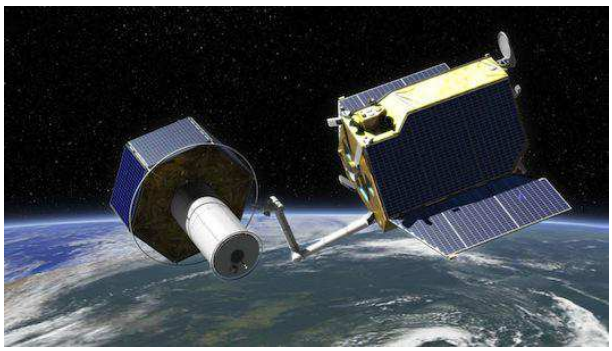

Figure 6.1.1: DEOS servicer and client satellites. (Source: [1])

OOS in LEO is a special problem since direct contact between a ground station and the servicing spacecraft can only be given in small time intervals, that is, when the spacecraft flies over ground station. Successful accomplishment of OOS tasks is highly dependent on whether and how long a communication link between the controlling ground station and the servicer spacecraft can be established. Typical time contact windows between LEO spacecrafts and a single ground stations are in the order of a few minutes.

A promising approach to increase the communication window between the ground station and the servicing spacecraft is the use of relay geostationary (GEO) satellites. The on-ground data is sent to a GEO communications satellite which relays the data packages to the spacecraft. The spacecraft in turn, send the processed data packages back to the GEO satellite, where the stream is relayed back to the ground station. This approach can increase the mean acquisition time of the spacecraft in LEO up to more than one hour per orbit revolution [67]. However, the use of geostationary data relay satellites increases the round trip time of the signal, that is, the time between operator action and spacecraft feedback.

To show the effects of a relay communication infrastructure two Space communication links are compared: The ROKVISS experiment [84], [13], and the ARTEMIS experiment [104]. In the ROKVISS experiment, a point-to-point Space link was used to couple a two DoF robot mounted on the outer part of the ISS and a force-feedback Joystick on ground. The mean round trip delay was 18 ms, including computer processing times. On the other hand, the ARTEMIS geostationary satellite was used to relay data from the ground station of the Institute of Astronautics (LRT) at Technische Universitat Munchen in Garching, Germany, to an antenna from the European Space Agency (ESA) located in Redu, Belgium. The antenna in Redu was meant to simulate the communication system of a spacecraft located in a LEO orbit. This antenna acted as a mirror server, bouncing back the data stream from the GEO satellite back to the GEO orbit, and from the ARTEMIS back to the Garching. This configuration resulted in an average

measured round trip delay of 622 ms, but it offered a much wider contact window. See the communication infrastructure used in the ARTEMIS experiment in Fig. 6.1.2.

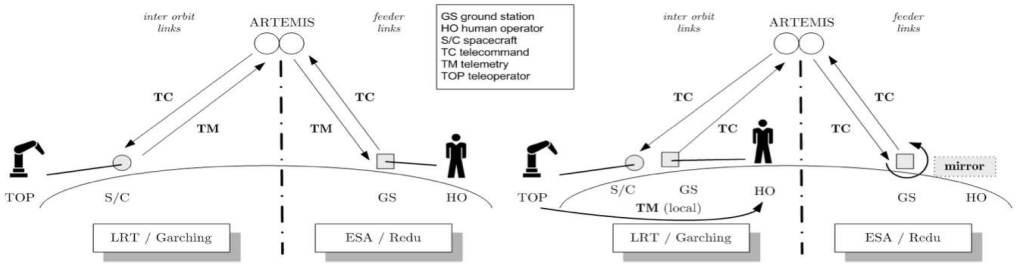

Figure 6.1.2: Relay communication infrastructure used in the ARTEMIS experiment (Source: [67])

Table 6.1 compares the results of both experiments. A similar relay communication infrastructure is planned for the DEOS mission, see Fig. 6.1.3.

	Round Trip Delay	**Contact time**
ROKVISS	18 ms	6 to 10 min
ARTEMIS	622 ms	Up to 1 hour

Table 6.1: Delay and contact times of two Space teleoperation experiments

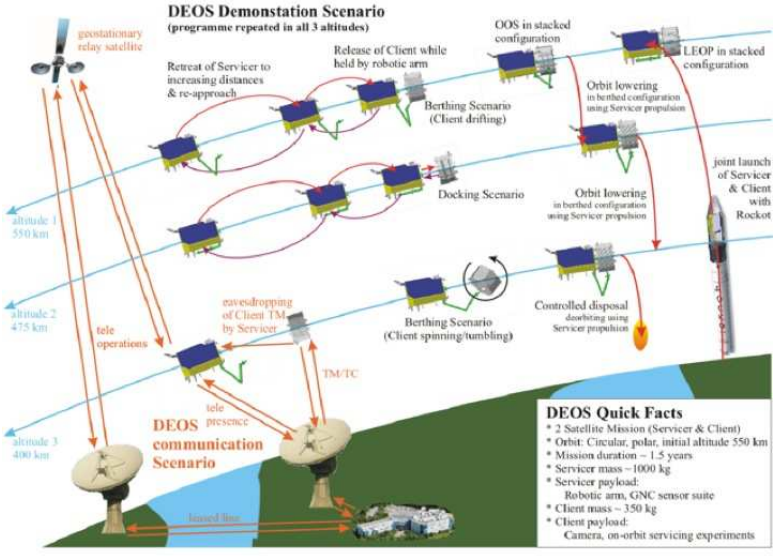

Figure 6.1.3: Relay communication structure for the DEOS mission

6.2 Teleoperation through the ASTRA Satellite

The goal of the experiment presented here is to prove that the utilization of geostationary satellites for OOS is reconcilable with a telepresent control of the servicer spacecraft. A communication test environment was set up on ground, which involved the Institute of Astronautics (LRT) ground station in Garching (Germany), the Institute of Mechatronics and Robotics at the German Aerospace Center (DLR) in Oberpfaffenhofen (Germany) and the ASTRA geostationary communications satellite. Both, master and slave systems were located in a laboratory located in the DLR but were coupled through the ASTRA satellite. The main goal of this experiment was to show the feasibility of teleoperation using relay-like communication infrastructures for robotic OOS. Extensive insights on the LRT communication infrastructure can be found in [42] and [43].

As will be seen, the tests showed similar performance to the experiments shown in Sec. 5.5, where constant delays were used. The properties of the Internet link and the Space link were measured and will be illustrated in the next sections.

An Integrated Modem and Baseband Unit (IMBU), as the core element of the communication, had been custom made by Satellite Services BV for the specific requirements to the test environment and configured by LRT. Fig. 6.2.1 show the communication setup of the test environment. Transmitting and receiving telepresence data at LRT was realized by utilizing specialized up- and downconverter in the S-band frequency range. Fig. 6.2.2 shows the computer network setup. As can be seen, the data generated at the master is sent to the LRT gateway. From the LRT, the data packages are sent to the satellite and bounced back to LRT. Then the received packages from the satellite are forwarded back to the DLR.

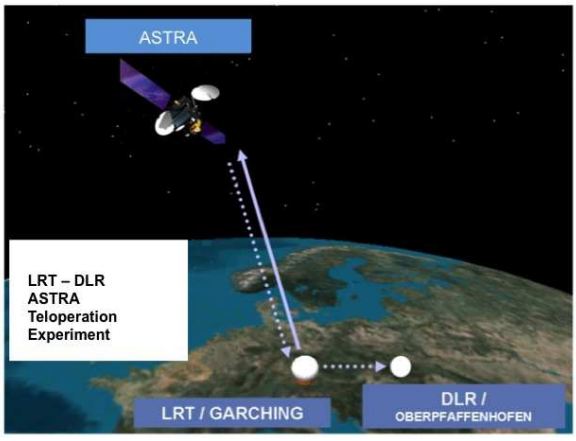

Figure 6.2.1: Communication setup

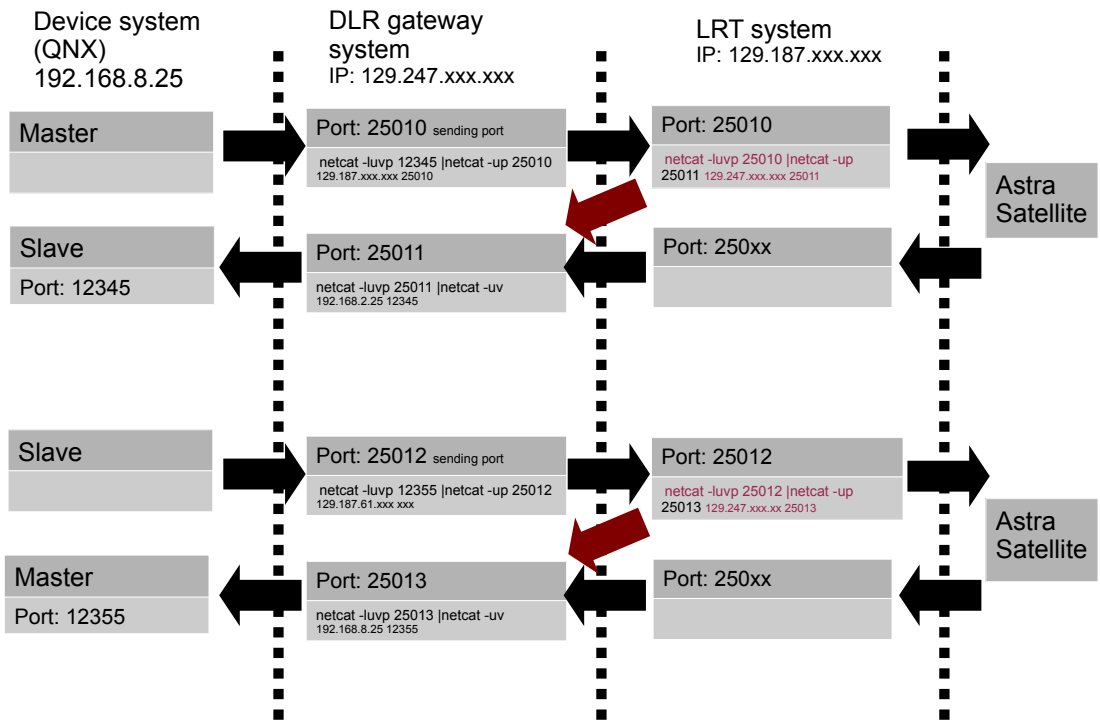

Figure 6.2.2: Computer network.

Internet link characteristics

Fig. 6.2.3 shows time delay and package loss plots of an Internet-UDP communication test. A data package mirror server located in LRT in Garching, Germany, was used to bounce a data stream sent from the DLR in Oberpfaffenhofen, Germany. As expected, delay is variable and package loss occurs. Table 6.2 shows measured values regarding the delay, jitter and package loss.

Mean round trip delay	40 ms
Average package loss	5 ms
Average jitter	2 %
Communication Protocol	UDP

Table 6.2: Internet link characteristics

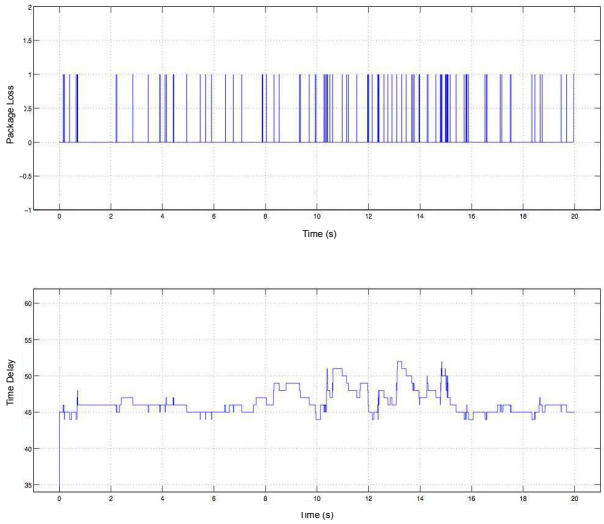

Figure 6.2.3: Delay and package loss due to the Internet udp link

Space link characteristics

The Space link was added to the previous Internet link. The route followed by the packages was:

- From the DLR to the LRT via *normal* Internet
- From the LRT to the ASTRA satellite
- From the ASTRA satellite to the LRT
- From the LRT to the DLR

Fig. 6.2.4 and Fig. 6.2.5 show the measured data plots of the communication link. Time delay, package loss and delay histograms are shown. A summary of the main characteristics of this link is given in Table 6.3. Note that the characteristics of both communication mediums, Internet and Space link are present in the measurements.

Experimental setup

The described communication link represents half of the constellation of a relay communication infrastructure. In a real relay configuration, the packets bounced by at the geostationary satellite would be sent to the slave robot, located in a spacecraft in a LEO orbit. In order to approximate a relay infrastructure, delay has been intentionally added to the combined Internet - Space Link. The round trip delay results gotten from the ARTEMIS experiment[1] [67] with a mean value of 620 ms have been used to set the amount of extra delay. Fig. 6.2.5 shows the incurred time delay and package loss during the experiment.

[1]The author of this thesis designed the bilateral control structure for the ARTEMIS experiment

Transmitted packets	72603 ms
Packet size	512 Bytes
Transmission frequency	1000Hz
Standard Deviation of transmission interval	0.002 ms
Mean round trip delay	270.56 ms
Round trip standard deviation	3.178 ms
Number of lost packets	2576
Package loss ratio	3.545 %
Communication Protocol	UDP

Table 6.3: Main Characteristics of the combined Internet and Space link

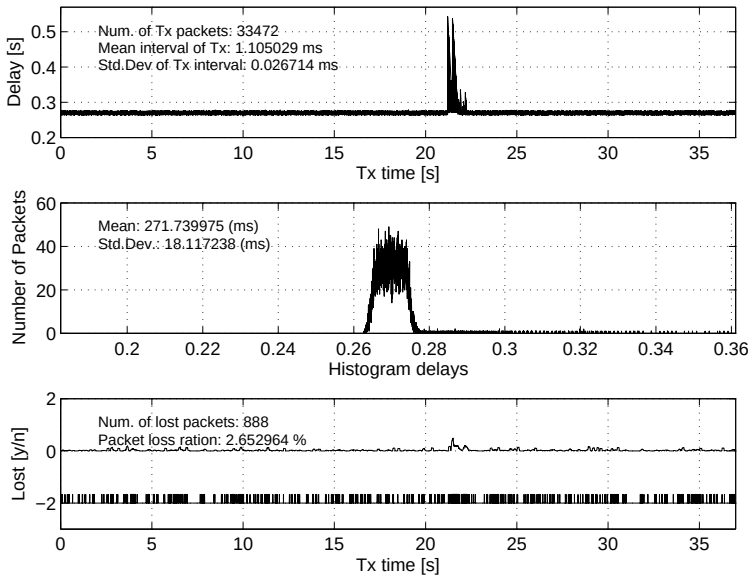

Figure 6.2.4: Delay and package loss of the combined Internet - Space with 300 Bytes packets

The four channels architecture described in Sec. 5.5 has been used. The system has been tested in the 1-DoF experimental master-slave setup described in Sec. B.1. Fig. 6.2.6. With the Passivity Controllers deactivated, the control parameters were tuned such that a maximum round trip delay value of 20ms was allowed without going unstable. Time delays above 20 ms quickly made the system unstable, even in the free environment case.

The results in Fig. 6.2.6 show stable operation and good performance. In fact, it should be noted that the use of Internet and Space links did not result in noticeable performance degradation. Only in those time intervals with very high package loss ratio or jitter, performance degradations were felt in the form of short small vibrations during

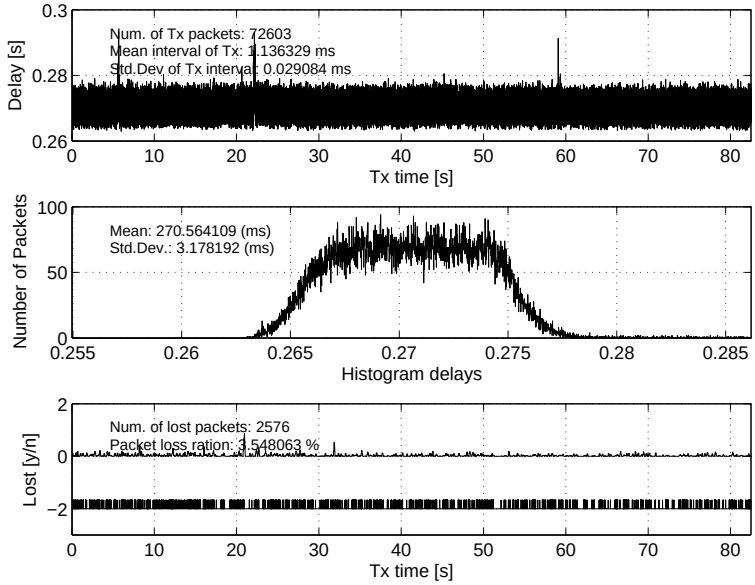

Figure 6.2.5: Delay and package loss of the combined Internet - Space with 512 Bytes packets

wall contact and short position drift intervals in the free environment operation. These effects however did not interfere with nor interrupted the operation. Indeed, when package loss occurs, the value of the previous data packet is held. This in results in energy generation, which in turn is dissipated by the Passivity Controller. Small amounts of energy dissipation, which is the normal case in communications with constant time delays and in the experiments presented here with the Space link, are not felt by the operator. The same hold for high jitter levels.

As can be derived from the energy plots, all the TPDNs become active being TDPN D the most active and TDPN C the less active. Compared to the results shown in Sec. 5.5, where constant time delays of similar orders were used, the results obtained from the combined Internet/Space link show a more energy generating communication channel; clearly, due to the package loss and jitter factors.

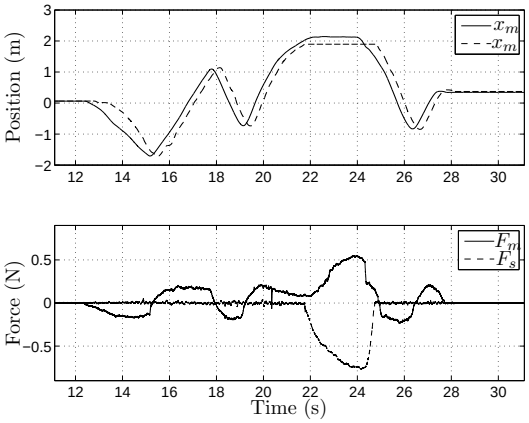

(a) Position and force responses

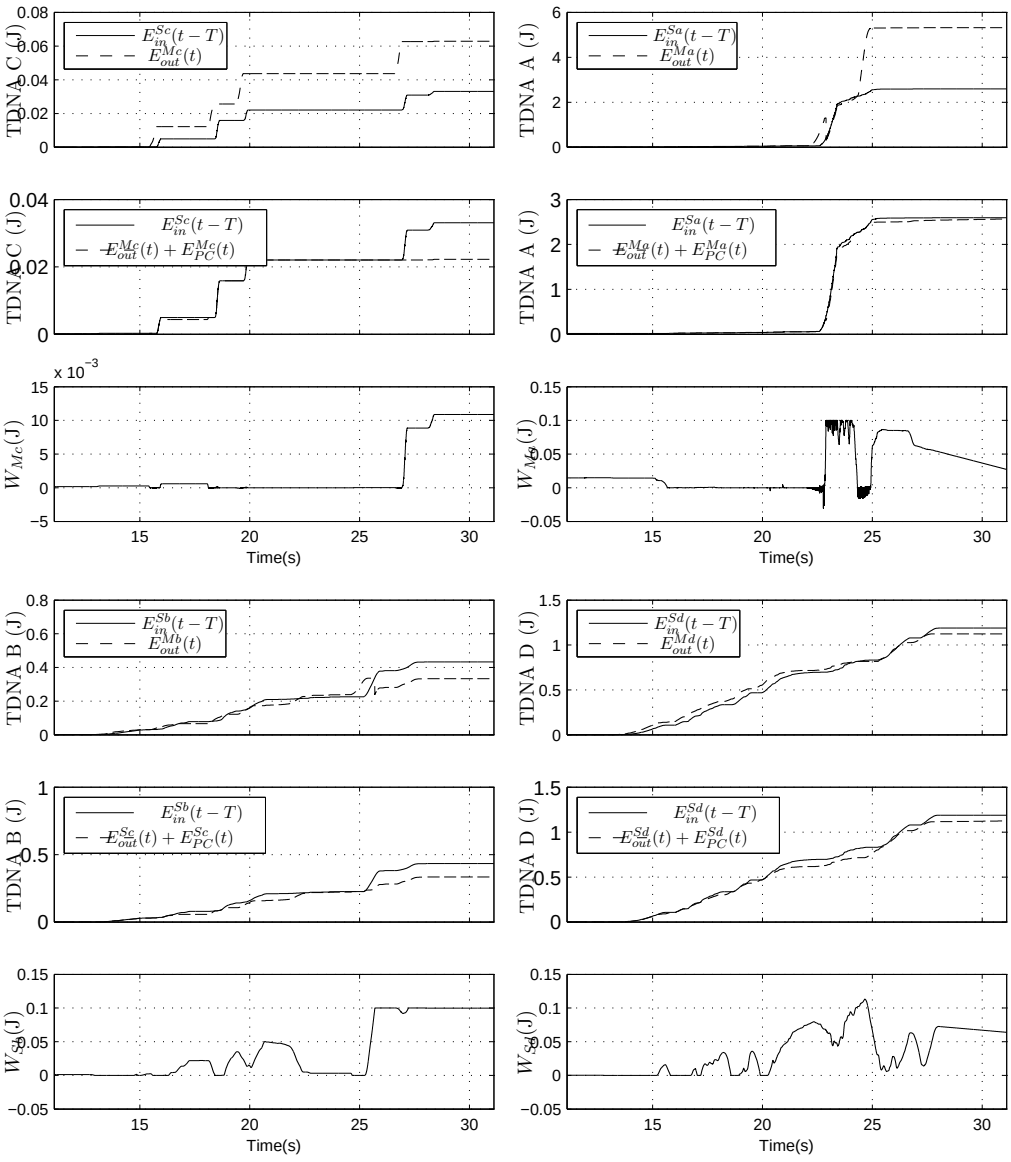

(b) TDPN A, B, C, D energy responses

Figure 6.2.6: Experimental data. Astra Satellite link

Chapter 7

Conclusion

Energy is a property of all physical objects, fundamental to their mutual interactions in which the energy can be transferred among the objects and can change form but cannot be created or destroyed. The methods that have been presented in this thesis are based on controlling the energy that is transferred between a human operator and an object located in a remote environment. We exploit the above physics principle to derive a new control rule. Control in terms of energy allows a more general treatment of the controlled system than the conventional control based on specific variables of the system. The rationale starts from the fact that the mechanical energy injected by the operator into the system must be conveyed to the remote environment and Vice Versa. The communication elements are found to be undermining factors that impair reliable transfer of energy between both ends of a teloperation system. The energy control treatment allows to capture such factors and compensate them. In particular, time delay is found to be a source of virtual energy. Since this energy is *added* to the system, the system can become unstable. The proposed methods in this thesis are based on the simple fact that this energy must be transformed into dissipation. Then the system becomes closer to the desired one, where only the energy injected from one end of the system is received into the other one. The results are two-fold, that is, system stability is guaranteed while performance is maximized in terms of energy transfer faithfulness.

The Time Delay Power Networks (TDPN) provide a model by which the transfer of mechanical energy through communication channels is well represented. The energy flows of a teleoperation system can be thus visualized and isolated. Once these networks are identified, the Time Domain Passivity Control approach for TDPNs has been proposed as a control mechanism to ensure system passivity. The passivity treatment in the time domain is versatile since it allows to cope with numerous un-shapeable and unforeseen factors as are communication time delays or data packet losses found in Internet based communications or Space links. Furthermore, the TDPNs allow description of arbitrary teleoperation architectures. In this thesis, we have seen examples of Position-Force computed, Position-Force measured, Position-Position and the four channels architectures.

The fact that the analysis takes place in the electrical domain suggests that TDPNs could be employed in other fields, ranging from digital control electronic circuits to any

other systems that can be represented using electrical analogs or networks. This remains for future work.

Appendix A

Useful Maths

Hermitian Matrix

If the conjugate transpose of a matrix $\boldsymbol{A}$ is equal to itself, $\boldsymbol{A}$ is said to be Hermitian. Define $\boldsymbol{A}^H = \boldsymbol{A}^{-T}$. If $\boldsymbol{A}^H = \boldsymbol{A}$ the $\boldsymbol{A}$ is Hermitian.

Partial Fraction Expansion

Given the function

$$H(s) = \frac{num(s)}{den(s)} = \frac{num(s)}{(s-p_1)(s-p_2)\cdots(s-p_n)}, \tag{A.1}$$

where the poles, p_i are simple and the degree of the numerator is less than that of the denominator. In this case, such a function can be expanded as:

$$H(s) = \frac{K_1}{(s-p_1)} + \frac{K_2}{(s-p_2)} + \cdots + \frac{K_n}{(s-p_n)}. \tag{A.2}$$

This expression is known as *partial fraction expansion of* $H(s)$ [31], where K_i are the *residues* and can be evaluated as:

$$K_i = H(s)(s-p_i)|_{s=p_i}. \tag{A.3}$$

Padé Series

In order to simplify the analysis of the delayed system the time delay element can be approximated using nth order Padé series. The first order serie is given by

$$D_t(s) \approx \frac{1-Ts}{1+Ts}, \tag{A.4}$$

where T is the time delay.

Appendix B

Experimental Setups

The methods presented in this work are sustained by a set of experiments. In this section the three experimental setups used for test and verification are described.

B.1 1 DoF DLR Master - Slave Teleoperation Testbed

The system is composed of two independent Motor-Gear-Units developed by SENSODRIVE GmbH [3], each of them equipped with a torque sensor. Both master and slave devices are based on a brushless motor with a nominal torque of 0.7 Nm and a peak torque of 2 Nm. The system runs on a real time OS (QNX) at a frequency of 1 KHz and each device is equiped with a 10 bit torque sensor which has a dynamic range of approximately 1.7 Nm. An s-function based Simulink interface has been developed for rapid development through Real-Time Workshop. The main feature are summarized in Table B.1. See Fig. B.1.1.

Table B.1: 1 DoF master - slave tested characterstics

Operational frequency	1 kHz
Bus interface	CAN or ethercat
Min. delay between master and slave	1 ms
Nominal torque	0.7 Nm
Pick Torque	2 Nm
Weight	500 gr.
Dimensions	120 x 220 x 220 mm
Motor characteristics	Brushless DC

B.2 3 DoF Teleoperation based on Phantoms

Fig. B.2.1 shows the experimental setup based on a pair of Sensable PHANToMs 1.5 controlled from the same computer at a sampling rate of 1Khz. Both Phantoms were equipped with the Nano17 ATI force-torque sensor.

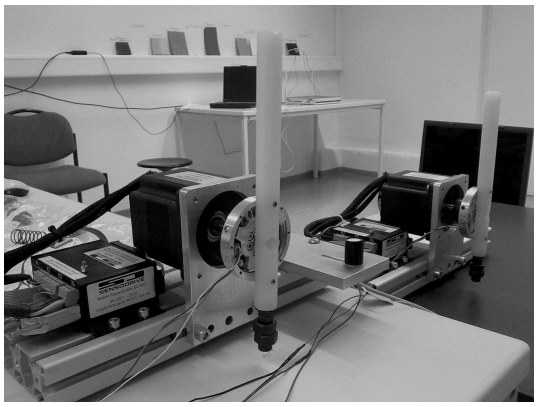

(a) Master and slave devices in an experimental setup.

(b) Design of the case.

Figure B.1.1: SENSODRIVE 1 DoF Master - Slave System.

Figure B.2.1: Experimental setup with a pair of Phantoms 1.5.

B.3 The DLR Light Weight Robot

The DLR Light-Weight-Robot (LWR), [50], [10], has an outstanding ratio of payload to total mass. Though it weights only 14kg, it is able to handle payloads of 14kg over the whole dynamic range. Very light gears, powerful motors and weight optimized brakes have been integrated into the robot. Similar to the human arm, the robot has seven degrees of freedom which results in advanced flexibility in comparison to standard industrial robots. The electronics, including the power converters, is integrated into the robot arm. No bulky external rack, known from standard systems, is needed. The integrated sensors are most progressive - each of the Light Weight Robots joints has a motor position sensor and a sensor for joint position and joint torque. Thus the robot can be operated position, velocity and torque controlled. This results in a highly dynamical system with active vibration damping. Tab. B.2 summarizes the main specifications of the LWR-III.

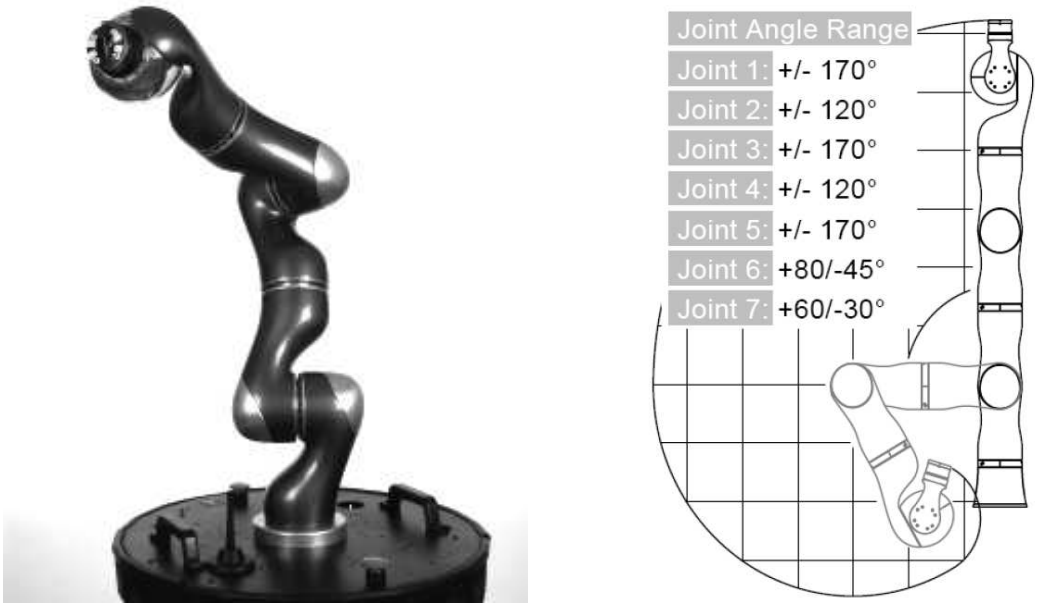

(a) (b)

Figure B.3.1: The LWR III.

B.4 LWR-III based Telepresence

A testbed for verifying and testing the methods on a 6-DoF platform was developed by the Institute of Mechatronics and Robotics at the German Aerospace Center [Deutsches Zentrum für Luft- und Raumfahrt (DLR)] located in Oberpfaffenhofen, Germany. It comprises two DLR lightweight robots (LWRs) as a bilateral force-coupled, masterslave system. One of the 7-DoF LWR-III robotic arm is used as the haptic interface. The

Table B.2: DLR LWR-III Specifications

Total Weight	14 Kg.
Max. Payload	≈14 Kg.
Max. Join Speed	120 deg.
Nr. of Axes	7 (R-P-R-P-R-P-P)
Maximum Reach	936 mm.
Motors	DLR - Robodrive
Gear	Harmonic Drive
Sensors (at each joint)	2 Position, 1 Torque
Brakes	Electromagnetic Safety Brake
Power Supply	48 V DC
Control Modes	Position, Torque, Impedance.
Current controller frequency	40 kHz
Joint controller frequency	3 kHz
Cartesian controller frequency	1 kHz
Electronics	Integrated electronics; internal cabling
Internal communication bus	SERCOS (optical)

(a) Single arm forward configuration with a joystick handle attached at the end-effector.

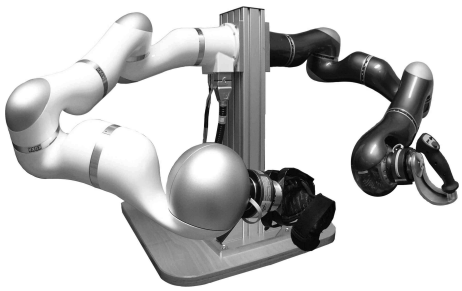

(b) The DLR Bimanual Haptic Device, with two LWR-III in a reversed configuration.

Figure B.4.1: Use of the LWR-III as haptic devices (i)

other one is used as slave robot.

The Light-Weight-Robot as Haptic Device

The DLR Light-Weight-Robot arm (LWR) is an adequate manipulator for being used as haptic device due two important characteristics: Its light weight and its size and workspace. The LWR-III weights around 15 Kg. In the gravity compensation mode the joint torques necessary to hold the robot's weight are commanded. In this mode, a human is able to freely move the robot with its hands exerting relatively small amount of forces. The mass and inertia felt by the user is that of the robot arm. The apparent mass and inertia can be down-scaled by using a force-torque sensor at the TCP of the robot. Indeed, through a feedforward compensation, the measured forces and torques at the TCP are mapped into the robot joint space and the resulting torques are commanded in addition to the gravity torques. Thus haptic experience is improved in both, free space operation and the hard contact situations. Moreover, the workspace of the robot can be set such that it allows nearly one-to-one mapping w.r.t the human-arm workspace. This can be achieved by using the so-called *reversed configuration*. In this configuration the base of the LWR-III is fixed in the vicinity of the back of the human shoulder and the end-effector tool, a coupling mechanism, is fixed at the palm of the hand. Thus robot mechanical structure is suspended in a parallel-like configuration for any configuration of the human arm and throughout the human arm workspace. See Fig. B.4.1 and Fig. B.4.2. These two characteristics allow LWR-III to be used as haptic device with a human scaled workscape.

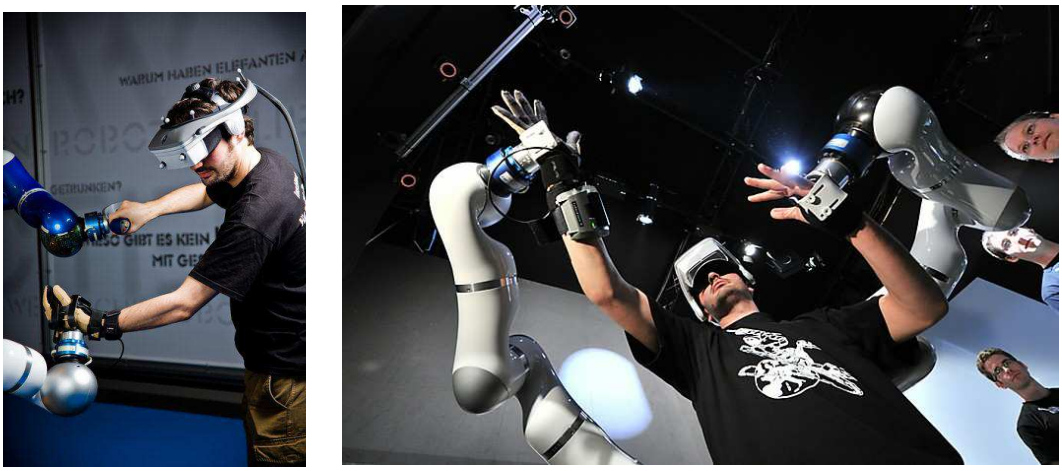

(a) Forward configuration of the LWR -based haptic device

(b) Reverse configuration of the LWR -based haptic device

Figure B.4.2: Use of the LWR-III as haptic devices (ii)

SpaceJustin based Telepresence

DLRs anthropomorphic Justin [80] and Space Justin are based on high-fidelity joint-torque-controlled light weight-technology and adjustable whole body compliance in Cartesian space. Justin is composed of a three-joint torso with, two seven-axis arms, a mobile platform, two five fingers DLR hands and a head equipped with sensors. Space Justin is composed of a one-joint torso with, two seven-axis arms and two five fingers DLR hands. With Space Justin, a three channels architecture (Position-Position / Force measured) based on the TDPN passivity approach has been verified using the DLR bimanual haptic device. Successful test with delays up to 700 msec have been conducted. In [58] and overview of the experiment is given. See Fig. B.4.3.

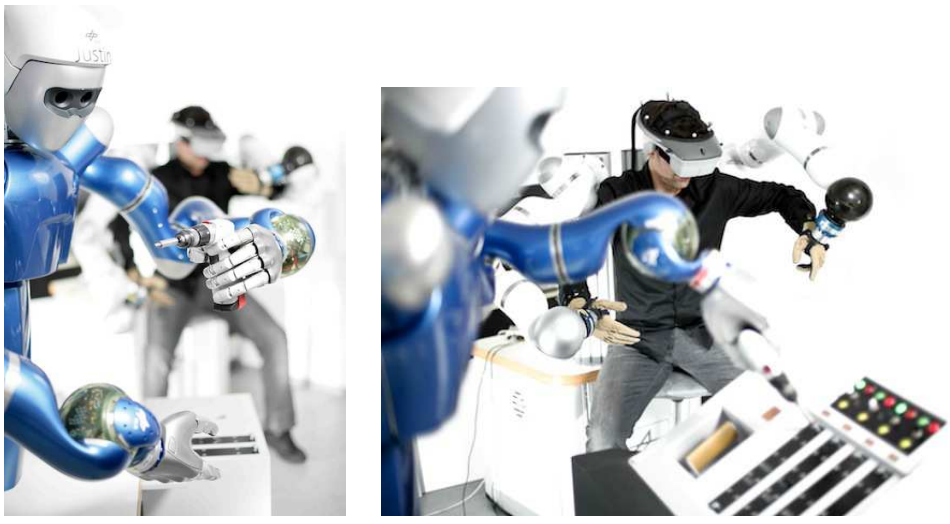

(a)

(b)

Figure B.4.3: Telepresence with Space Justin and the DLR Bimanual Haptic Device

Appendix C

TDPN Application to Wave Variables using measured Forces

The wave variables theory for teleoperation is based on modeling the communication channel as a transmission line. By applying the current-velocity analogy it is possible to map the mechanical variables of force and velocity traversing a communication channel into transmission line signals, that is, wave variables. The transmission line model is a delay-based model where passivity becomes a property rather than control goal. Thus, a system with delay modeled as a transmission line benefits from this property. This allows the communication channel to be rendered as a passive element interconnectable to other networks.

One essential characteristic of the transmission line model is that the signals at traversing the line are power conjugate variables, that is, they are a dual pair [1]. The wave variables are given by a linear, non-singular[2] algebraic combination of the dual signals traversing the line; in the electrical domain, current and voltage; in the translational mechanical domain, velocity and force; in the rotational mechanical domain, angular velocity and torque.

A review of wave variables is given in this work in Sec. 2.6. Application of TDPNs to Wave Variables was first presented by Artigas in [14].

On the use of measured forces

The Position-Force measured architecture has been reviewed in Sec. 3.9. See Fig. 2.7.13. Typical wave variable schemes do not allow the use of measured forces in the environment for encoding the wave variable traveling from the slave to the master. The corresponding wave variables for the scheme in Fig. 2.7.13 would be in that case given by:

$$\boldsymbol{\mu}_m(t) = \frac{b\boldsymbol{v}_m(t) + \boldsymbol{F}_m(t)}{\sqrt{2b}}, \qquad \boldsymbol{\nu}_m(t) = \frac{b\boldsymbol{v}_m(t) - \boldsymbol{F}_m(t)}{\sqrt{2b}}, \tag{C.1}$$

[1] Duality is a mathematical concepts which allows to associate a scalar two a pair of dual variables, see Def. 2 and Def. 3

[2] that the inverse transformation exists

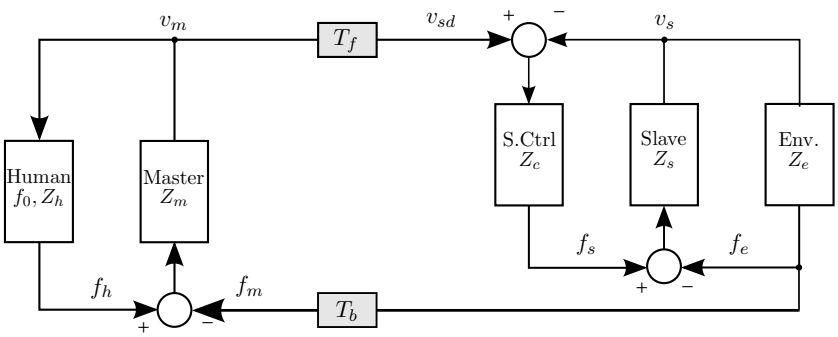

Figure C.0.1: Block diagram of the Position-Force measured teleoperation architecture.

$$\boldsymbol{\mu}_s(t) = \frac{b\boldsymbol{v}_{sd}(t) + \boldsymbol{F}_e(t)}{\sqrt{2b}}, \qquad \boldsymbol{\nu}_s(t) = \frac{b\boldsymbol{v}_{sd}(t) - \boldsymbol{F}_e(t)}{\sqrt{2b}}, \tag{C.2}$$

where μ is the outgoing wave signal from master to slave, ν the returning wave. That implies that the energy which actually flows through the communication channel is given by the integrated dual product of v_m and f_e. By examining the power entering the channel:

$$P_{ch} = \boldsymbol{v}_m^T \boldsymbol{F}_m - \boldsymbol{v}_{sd}^T \boldsymbol{F}_e. \tag{C.3}$$

And using the wave transformations:

$$P_{ch} = \frac{1}{2}\boldsymbol{\mu_m}^T\boldsymbol{\mu_m} - \frac{1}{2}\boldsymbol{\nu_m}^T\boldsymbol{\nu_m} - \frac{1}{2}\boldsymbol{\mu_s}^T\boldsymbol{\mu_s} + \frac{1}{2}\boldsymbol{\nu_s}^T\boldsymbol{\nu_s}. \tag{C.4}$$

We have that the energy flow is given by:

$$E_{ch} = \int_o^t P_{ch}\, d\tau. \tag{C.5}$$

E_{ch} becomes null [3] in the free environment since the sensor signal is $f_e \approx 0$, and gains some value as soon the slave robot interacts with the environment, that is, as soon the sensor measures some interaction forces. Paradoxically energy is clearly being transmitted in the free environment too since the slave, with its mass, moves according to the motions commanded by the master. Ignoring possible scaling factors, in a teleoperation system the main energy source is the operator arm. This energy is mechanically transferred to the master device, electrically transmitted through the communication channel and transformed into kinetic energy on the slave device. Therefore, although energy is clearly being transmitted from the human to the slave, the above wave variable formulation in (C.1) and (C.2) fails to represent that.

The Position-Force measured architecture assumes a tool with zero mass, that is, the environment is directly perceived by the operator through the master device ignoring the mass of the slave. The slave device has only the role of a sensor. In a sense, this

[3] ignoring the acceleration term

architecture can be interpreted as having the master device *in* the environment and thus the interaction is assumed to be between master device and environment. Therefore, the signals which connect master and slave sides, that is, the current position of the master and the measured force from the environment, do not represent a transfer of energy from master to slave and vice-versa due to the lack of carrier or tool. Instead, these variables represent the impedance of the environment displayed at the master device and the communication channel has the role of transferring this impedance rather than an energy.

To verify these arguments, we first look at the Fig. C.0.2, which shows the electrical representation of a Position-Force (computed) architecture. The 2-port N_{tool} containing the slave controller and the slave itself allows the energy coming from the master to be transferred to the environment. If the measured force signal is used instead, the assumption of the master directly interacting with the environment can be represented as in Fig. C.0.3. As it can be seen, the architecture assumes that there is no slave device interacting with the environment, that is, there is no physical tool that allows the energy transfer from master to slave and vice versa. Finally Fig. C.0.4 shows the electrical representation of the Position-Force measured. As can be seen, the energy delivered to the master is given by the dual pair $\langle v_m(t), F_m \rangle$ being $F_m = F_e(t - T)$, while the energy transferred to the environment is given by $\langle v_e(t), F_e(t) \rangle$.

Disregarding time delays and assuming a continuous system, the only solution to make the Position-Force measured energy consistent would be to ensure:

$$\int_0^t \boldsymbol{v}_m(t)^T \boldsymbol{F}_e(t) = \int_0^t \boldsymbol{v}_s(t)^T \boldsymbol{F}_e(t), \tag{C.6}$$

which leads to the condition:

$$\boldsymbol{v}_m(t) = \boldsymbol{v}_s(t), \tag{C.7}$$

or, equivalently:

$$Z_s(t) = 0. \tag{C.8}$$

Network Unfoldment

In order to apply the wave variables transformation in a Position-Force measured architecture, an energy carrier is needed which allows the passivity formulation on top of it. The energy carrier provides the energetic formulation which the architecture lacks itself. The energy carrier is one or more additional channels that allow to explicitly transfer the energy that flows between master and slave in both directions. The energy carrier does not impose any change in the functional structure of the architecture but rather just keeps track of the actual energy exchanged and can be used to apply passivity based methods.

Looking at the electrical representation of the position force measured, Fig. C.0.4, it can be observed that the master device interacts with the environment through the port

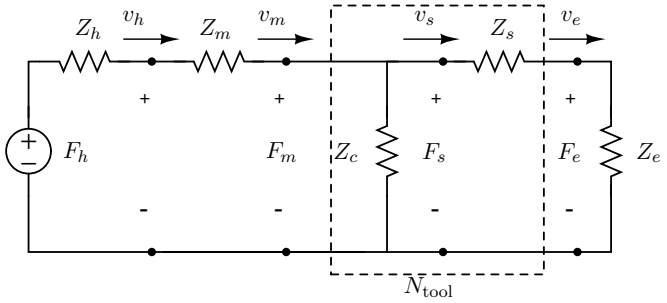

Figure C.0.2: Position-Force (computed) architecture: Energy is transferred from master to slave through the *tool*.

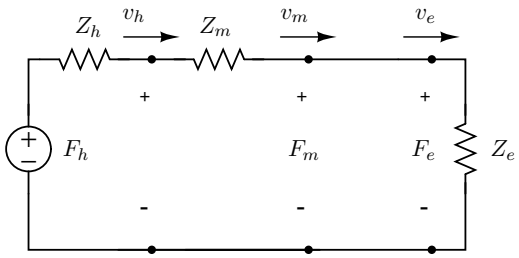

Figure C.0.3: Assumption in the Position-Force measured architecture: Interaction occurs directly between the master and the environment. The slave robot and controller are ignored.

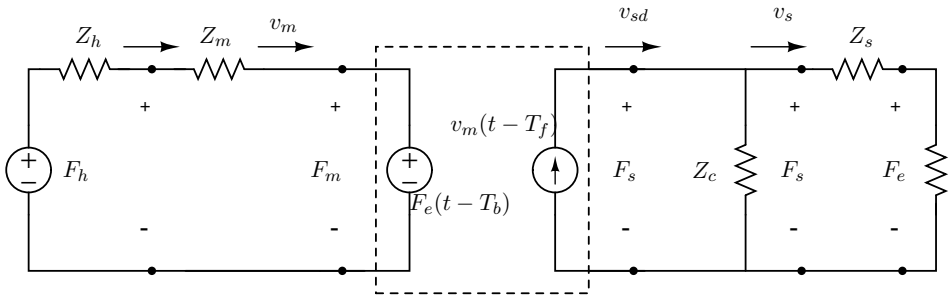

Figure C.0.4: The Position-Force measured architecture electrical scheme.

defined by the pair $\langle v_m(t), F_m(t)\rangle$, being $F_m(t) = F_e(t-T)$. On the other side, the slave device interacts with the master through the port defined by the pair $\langle v_{sd}(t), F_e(t)\rangle$, being $v_{sd}(t) = v_m(t-T)$. Energy is thus transferred through these two one-port networks. These one-port networks are particular because one signal of the conjugate pair is a delayed version of a signal which is located somewhere else in the circuit, that is, they contain delayed dependent force or velocity sources.

The representation shown in Fig. 3.9.1 is proposed, which characterized by:

- Moving the delayed dependent force source ($F_e(t-T_b)$) to its *non-delayed* location, that is, to the slave with $F_e(t)$. This source will be called C_a.

- Moving the delayed dependent velocity source ($v_m(t - T_f)$) to its *non-delayed* location, that is, to the master with $v_m(t)$. This source will be called C_b
- Adding a 2-port network for conveying the energy from the *non-delayed* dependent force source to the master.
- Adding a 2-port network for conveying the energy from the *non-delayed* dependent velocity source to the slave.

The two added 2-port networks are Time Delay Power Networks and contain the characteristics of the communication channel, i.e., delay, which can be constant or variable, and package loss. This augmented representation presents two main benefits: Energy consistency and isolation of the energy due to the time delay. Thus the two scalars corresponding to the energy flows from right to left (R2L) and left to right (L2R) are:

$$\begin{aligned} E^{R2L}(t) &= \int_0^t \boldsymbol{v}_m(t)\boldsymbol{F}_e(t - T_b) - \boldsymbol{v}_m(t - T_b)\boldsymbol{F}_e(t)d\tau, \\ E^{L2R}(t) &= \int_0^t \boldsymbol{v}_m(t)\boldsymbol{F}_s(t - T_f) - \boldsymbol{v}_m(t - T_f)\boldsymbol{F}_s(t)d\tau. \end{aligned} \tag{C.9}$$

Application case: Wave Variables based schemes with measured Forces

The remaining step is to transform the TDPN's, defined in the electrical domain, into transmission lines in order to apply wave variables: For the first, TDPN(a), we take the signals available at both ports to encode the wave variables. The corresponding wave transformer at the master side, referred to as $\mathrm{WT}_{\mathrm{am}}$ in Fig. C.0.5, outputs $\boldsymbol{F}_m$ and wave variable $\boldsymbol{\mu}_{\mathrm{a,m}}$ as:

$$\begin{aligned} \boldsymbol{F}(t) &= \sqrt{\frac{b}{2}}(\boldsymbol{\mu}_{\mathrm{a,m}}(t) - \boldsymbol{\nu(t)}_{\mathrm{a,m}}), \\ \boldsymbol{\mu}_{\mathrm{a,m}}(t) &= \frac{b\boldsymbol{v}_m(t) + \boldsymbol{F}_m(t)}{\sqrt{2b}}. \end{aligned} \tag{C.10}$$

Where $\boldsymbol{\nu}_{\mathrm{a,m}}$ is the wave variable at the master side coming from the slave.

The corresponding wave transformer at the slave side, referred to as $\mathrm{WT}_{\mathrm{as}}$ in Fig. C.0.5, outputs the wave variable $\boldsymbol{\nu}_{\mathrm{a,s}}$ and the velocity $\boldsymbol{v}_x$ as:

$$\begin{aligned} \boldsymbol{v}_x &= \sqrt{\frac{1}{2b}}(\boldsymbol{\mu}_{\mathrm{a,s}}(t) + \boldsymbol{\nu}_{\mathrm{a,s}}(t)), \\ \boldsymbol{\nu}_{\mathrm{a,s}}(t) &= \frac{b\boldsymbol{v}_x(t) - \boldsymbol{F}_e(t)}{\sqrt{2b}}. \end{aligned} \tag{C.11}$$

Where $\boldsymbol{\nu(t)}_{\mathrm{a,s}}$ is the wave variable at the slave side coming from the master.

$\boldsymbol{v}_x$ is the resulting velocity imposed by the causality of the wave transformer. This is in fact the theoretical velocity signal flowing through the dependent force source.

However, this source originates from the electrical model. As a such it is an ideal source analog to an ideal voltage source. An ideal voltage source keeps its voltage value independently of the current, i.e. velocity, across its terminals. In other words, $\boldsymbol{v}_x$ has no effect upon the source C_a nor in the overall system. This velocity is therefore only needed to compute $\boldsymbol{\nu}_{\mathrm{a,s}}$.

In a similar way, for the second Time Delay Power Network, TDPN(b), we take the signals available at both ports to encode the wave variables. The corresponding wave transformer at the master side, referred to as $\mathrm{WT}_{\mathrm{bm}}$ in Fig. C.0.5, outputs the force signal $\boldsymbol{F}_x$ and the wave variable $\boldsymbol{\mu}_{\mathrm{b,m}}$ as:

$$\begin{aligned} \boldsymbol{F}_x(t) &= \sqrt{\frac{b}{2}}(\boldsymbol{\mu}_{\mathrm{b,m}}(t) - \boldsymbol{\nu}_{\mathrm{b,m}}(t)), \\ \boldsymbol{\mu}_{\mathrm{b,m}}(t) &= \frac{b\boldsymbol{v}_m(t) + \boldsymbol{F}_{mb}(t)}{\sqrt{2b}}. \end{aligned} \tag{C.12}$$

Where $\boldsymbol{\nu}_{\mathrm{b,m}}(t)$ is the wave variable coming from the slave side.

The analogous case to $\boldsymbol{v}_x$ occurs here with $\boldsymbol{F}_x$, that is, the value of the velocity source C_b remains unaltered by $\boldsymbol{F}_x$.

The corresponding wave transformer at the slave side, referred to as $\mathrm{WT}_{\mathrm{bs}}$ in Fig. C.0.5, outputs the wave variable $\boldsymbol{\nu}_{\mathrm{b,s}}$ and the desired slave velocity $\boldsymbol{v}_{sd}$ as:

$$\begin{aligned} \boldsymbol{v}_{sd} &= \sqrt{\frac{1}{2b}}(\boldsymbol{\mu}_{\mathrm{b,s}}(t) + \boldsymbol{\nu}_{\mathrm{b,s}}(t)), \\ \boldsymbol{\nu}_{\mathrm{b,s}}(t) &= \frac{b\boldsymbol{v}_{sd}(t) - \boldsymbol{F}_s(t)}{\sqrt{2b}}. \end{aligned} \tag{C.13}$$

Where $\boldsymbol{\nu}_{\mathrm{b,s}}(t)$ is the wave variable coming from the master side and $\boldsymbol{F}_s(t)$ is the force signal computed by the controller at the slave side.

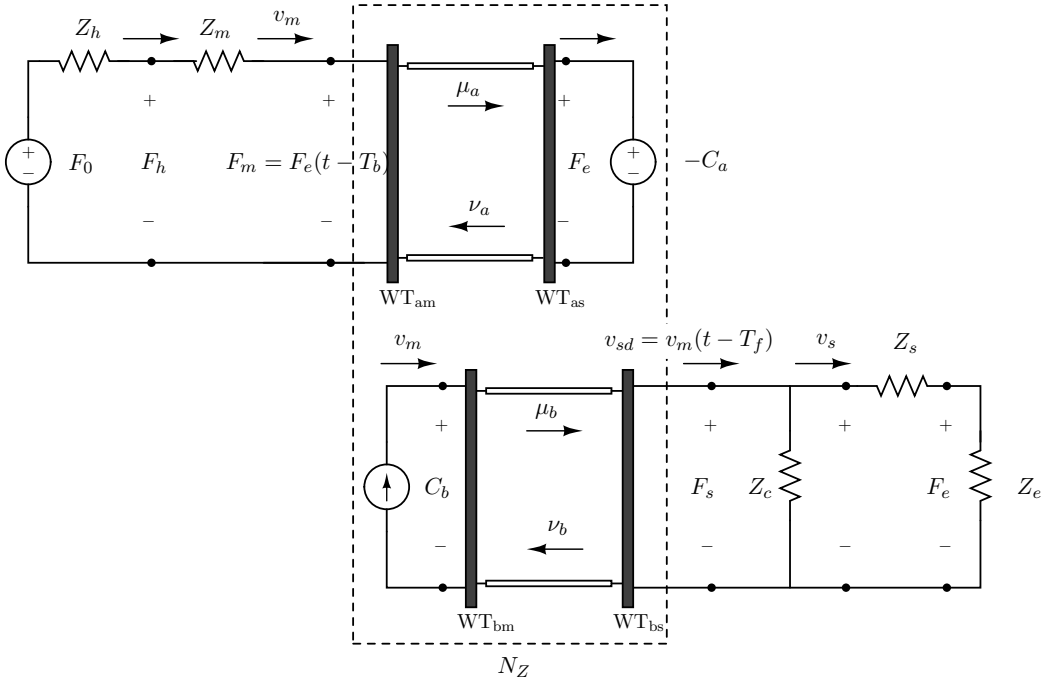

Figure C.0.5: Augmented representation of the Position-Force measured architecture with the wave transformers.

Appendix D

Differential Kinematics Representation

The differential kinematics representation is a central aspect in the designing multi DoF teleoperation system. The assumption in this work is that channel bandwidth is expensive and thus redundant descriptions such as the 3×3 rotation matrix for describing the orientation will be avoided. A minimal representation is therefore preferred. A minimal representation of a position and orientation of a body in space is composed by six orthogonal vectors. The problem of determining this minimal representation admits different solutions. A kinematic spatial representation must be chosen such that allows generalized and flexible formulation of position and orientation while keeping passivity. The transformed quantities will have to be derivable and integrable in order to manage velocity and desired position computations. This can be seen in (4.16), where the slave PI controller has an integrator, or in the impedance (4.43), where the desired command is taken as a position.

In this work two minimal representation are explored: The Euler angles and the angular velocity.

D.1 Euler angles representation

The minimal representation of the orientation using the three Euler angles is considered. The time derivative of the Euler angles presents a less intuitive representation of the body rotational velocity, since its axes may be non-orthogonal vectors describing the angular velocity defined with respect to the axes of a frame which varies as the orientation of the end-effector varies.

Being R_{XYZ} the frame orientation matrix of a body, the XYZ minimal representation is described as the set of elementary rotations with respect to the axes of the current frame as (later on the chose of XYZ will be justified):

$$R_{XYZ} = R_Z(\varphi)R_Y(\vartheta)R_X(\psi) \tag{D.1}$$

with the set of angles:

$$\boldsymbol{\phi} = \begin{bmatrix} \varphi \\ \vartheta \\ \psi \end{bmatrix}$$

The actual velocity using Euler angles is given by

$$\dot{\boldsymbol{\epsilon}}(t) = \begin{bmatrix} \dot{\boldsymbol{p}} \\ \dot{\boldsymbol{\phi}} \end{bmatrix}. \tag{D.2}$$

and the analytical Jacobian relates joint space to euler angles space as:

$$\dot{\boldsymbol{\epsilon}}(t) = \begin{bmatrix} \boldsymbol{J}_p(\boldsymbol{q}) \\ \boldsymbol{J}_\phi(\boldsymbol{q}) \end{bmatrix} \dot{\boldsymbol{q}} = \boldsymbol{J}_A(\boldsymbol{q})\dot{\boldsymbol{q}}. \tag{D.3}$$

This relationship can be found by computing the contribution of each rotational velocity produced by the Euler angles to the components of angular velocity [96]. In the case of the Roll-Pitch-Yall angles, the transformation is given by

$$\begin{bmatrix} cos(\psi(t))cos(\vartheta(t)) & -sin(\psi(t)) & 0 \\ sin(\psi(t))cos(\vartheta(t)) & cos(\psi(t)) & 1 \\ -sin(\vartheta(t)) & 0 & 1 \end{bmatrix} (\boldsymbol{\phi})\dot{\boldsymbol{\phi}} = \boldsymbol{w} = \boldsymbol{T}_A(\boldsymbol{\phi})\dot{\boldsymbol{\phi}}. \tag{D.4}$$

where ϕ are the Euler angles, w the angular velocity and T_A the transformation matrix from Euler angles to angular velocity. Furthermore, the *analytical Jacobian* J_A is related to the geomtrical Jacobian as:

$$\boldsymbol{J} = \boldsymbol{T}_A\boldsymbol{J}_A. \tag{D.5}$$

$\boldsymbol{J}_A$ differs from the Jacobian $\boldsymbol{J}$ in that it relates the contributions of each joint velocity to rotational velocity expressed by a set of Euler coordination angles as

$$\boldsymbol{v} = \begin{bmatrix} \dot{\boldsymbol{p}} \\ \dot{\boldsymbol{\phi}} \end{bmatrix} = \boldsymbol{J}_A(\boldsymbol{q})\dot{\boldsymbol{q}}, \tag{D.6}$$

and differs from angular velocity as described by (D.4).

Therefore, the velocity in the Euler angles representation can be computed as:

$$\dot{\boldsymbol{\phi}}_m = \boldsymbol{T}_A^T\boldsymbol{J}_m\dot{\boldsymbol{q}}_m. \tag{D.7}$$

Further, the differentiation of the Euler angles can be integrated as:

$$\int_0^t \dot{\boldsymbol{\phi}}(\boldsymbol{\tau})d\boldsymbol{\tau} = \int_0^t \frac{\partial\phi}{\partial q}\dot{\boldsymbol{q}}(\boldsymbol{\tau})d\boldsymbol{\tau} = \boldsymbol{\phi}(t), \tag{D.8}$$

The velocity signal, which e.g. has been modified to dissipate some energy, must be integrated in order to be commanded in the form of a desired position. Note integrability may not obvious using other representations as for instance the angular velocity.

The Euler angles allow therefore a complete description of the kinematics of a teleoperation system. It is however widely know that Euler angles are not exempt from singularities.

D.2 Representation Singularities

Indeed, the use of Euler angles introduce so-called representation or mathematical singularities which occur in the inversion of the transformation from angular velocity to rotational velocity in Euler coordinates, i.e. in (D.7). Since representation singularities are not due to physical limitations of the robot kinematics but rather due to the mathematical representation it is possible to find solutions at the controller level.

The set of Euler angles used in this approach is Roll - Pitch - Yaw. The transformation in (D.7) is rank-deficient with its determinant being $cos(\phi)$, which implies that the transformation cannot be inverted at $\phi = \frac{\pi}{2}$ and $\phi = \frac{3\pi}{2}$.

The strategy here presented is based on a transformation of the difference between current and desired frames in the Euler representation. The error in the angular velocity between desired and current frames is then transformed in the Euler coordinates.

If the stiffness of the spatial impedance is high enough it can be assumed that the difference will be always close to zero (i.e. close to identity I_{3x3}) and that therefore an orientation displacement of $\phi = \frac{\pi}{2}, \frac{3\pi}{2}$ will never occur. The rationale behind that argument is that in order to reach the singularities, very high torques would be needed (from the user mainly) in order to produce an orientation error higher than $\frac{\pi}{2}$ which would first overcome the robot dynamic limitations. Further, this justifies the choice of the Roll - Pitch - Yaw set of angles against other configuration such as Z-Y-Z, whose transformation matrix becomes rank-deficient at $\phi = 0$.

Note that $T_A(\phi_{md})$ losses one DoF at the singular locations. While this will not affect stability of the system, it can indeed produce a limitation in the working space depending on the redundancy of the robot.

D.3 Angular Velocity

In contrast to the analytical Jacobian, the geometrical Jacobian has clear physical meaning but it loses functionality when it is necessary to refer to differential quantities which need to be integrated. Using the angular velocity representation to encode the end-effector's pose can be problematic if the quantities are to be integrated in order to compute the corresponding position. The angular velocity

$$\boldsymbol{v} = \begin{bmatrix} \dot{\boldsymbol{p}} \\ \boldsymbol{\omega} \end{bmatrix} = \boldsymbol{J}(\boldsymbol{q})\dot{\boldsymbol{q}},$$

expresses the actual velocity with respect to the base frame. Its integral however

$$\int_0^t \boldsymbol{v}(\boldsymbol{\tau})d\boldsymbol{\tau} \neq \boldsymbol{x}(t). \tag{D.9}$$

Passivity of geometric Jacobian is first checked. The end-effector velocities relative to the base frame are related to the contribution of the joint velocities through:

$$\begin{aligned} \boldsymbol{v}_m &= \boldsymbol{J}_m(\boldsymbol{q}_m)\dot{\boldsymbol{q}}_m \\ \boldsymbol{v}_s &= \boldsymbol{J}_s(\boldsymbol{q}_s)\dot{\boldsymbol{q}}_s. \end{aligned} \tag{D.10}$$

where $\boldsymbol{J}_m$ and $\boldsymbol{J}_s$ are master and slave Jacobians expressed in base frame.

$$\boldsymbol{v}_m(t) = \begin{bmatrix} \dot{\boldsymbol{p}}_m(t) \\ \boldsymbol{\omega}_m(t) \end{bmatrix}, \quad \boldsymbol{v}_s(t) = \begin{bmatrix} \dot{\boldsymbol{p}}_s(t) \\ \boldsymbol{\omega}_s(t) \end{bmatrix}, \tag{D.11}$$

where $\dot{\boldsymbol{p}}_m$, $\boldsymbol{\omega}_m$ and $\dot{\boldsymbol{p}}_s$, $\boldsymbol{\omega}_s$ are master and slave translational and angular velocities. The forces at the end-effector are related to the joint space as

$$\begin{aligned} \boldsymbol{\tau}_m &= \boldsymbol{J}_m^T(\boldsymbol{q}_m)\boldsymbol{F}_m \\ \boldsymbol{\tau}_s &= \boldsymbol{J}_s^T(\boldsymbol{q}_s)\boldsymbol{F}_s, \end{aligned} \tag{D.12}$$

where $\boldsymbol{\tau}_m$, $\boldsymbol{\tau}_s$ are master and slave torques at the joints and $\boldsymbol{F}_m = [\boldsymbol{f}_m; \mu_m]$ and $\boldsymbol{F}_s = [\boldsymbol{f}_s; \mu_s]$ are master and slave end-effector wrenches where force, f, and moment, u, contributions are seperated.

The transformations in (D.10) and D.12 are lossless since ([73]):

$$\dot{\boldsymbol{q}}^T\tau = \dot{\boldsymbol{q}}^T\boldsymbol{J}^T\boldsymbol{F} = \boldsymbol{v}^T\boldsymbol{F} \tag{D.13}$$

v and F form a conjugate flow-effort pair whose product is power and can therefore be used for formulating network energy flows. Further, since the angular velocity is a minimal representation of motion, it is a good candidate for being used in those teleoperation schemes where bandwidth is expensive.

However, for this approach to be feasible, the inverted transformation must also hold, that is, the integral of the angular velocity in order to compute e.g. desired position values. Unfortunately, the integral of the angular velocity does not present a clear physical meaning and can output wrong end-effector orientations.

If $\boldsymbol{v}(t) = [\frac{\dot{\boldsymbol{p}}(t)}{\boldsymbol{\phi}(t)}]$ is the velocity of an object moving in space with a translational velocity $\dot{\boldsymbol{p}}(t)$ and an angular velocity $\boldsymbol{\omega}(t)$ computed as:

$$\boldsymbol{v}(t) = \begin{bmatrix} \dot{\boldsymbol{p}}(t) \\ \boldsymbol{\omega}(t) \end{bmatrix} = \boldsymbol{J}(t)\dot{\boldsymbol{q}}(t), \tag{D.14}$$

its integral may not correspond to the displacement $\boldsymbol{x}(t) = \left[\begin{smallmatrix} \boldsymbol{p}(t) \\ \boldsymbol{\phi}(t) \end{smallmatrix}\right]$:

$$\int_0^t \boldsymbol{v}(\tau)d\boldsymbol{\tau} \neq \boldsymbol{x}(t), \tag{D.15}$$

To overcome the issue of the integral of the angular velocity the definition of the derivative of the rotation matrix can be used in order to compute numerically the rotation matrix corresponding to a given angular velocity.

Given a time-varying rotation matrix $R = R(t)$ the following identity can be proved in regard to the orthogonality of R:

$$\dot{\boldsymbol{R}}(t)\boldsymbol{R}(t)^T + \boldsymbol{R}(t)\dot{\boldsymbol{R}}(t)^T = O, \tag{D.16}$$

where

$$\boldsymbol{S}(t) = \dot{\boldsymbol{R}}(t)\boldsymbol{R}^T(t) \tag{D.17}$$

is a (3x3) *skew-symmetric* matrix. It can be proved [96] that S contains the three components of the angular velocity $w(t) = [w_x; w_y; w_z]$ and is given by

$$\boldsymbol{S} = \begin{bmatrix} 0 & -w_x & w_y \\ w_z & 0 & -w_x \\ -w_y & w_x & 0 \end{bmatrix}. \tag{D.18}$$

Using (D.17) it is possible to compute the elements of R as a function of the components of w and the discrete derivative of R, ΔR. The elements of ΔR are orthonormalized[1] increments in time of the elements of R, i.e.:

$$\Delta R[K] = [\Delta r_{ij}[k]]_{i,j=1..3} = \left[\frac{r_{ij}[k] - r_{ij}[k-1]}{T_S}\right]_{i,j=1..3}, \tag{D.19}$$

where T_s is the sampling time. And therefore the current rotation elements of R:

$$[r_{ij}[k]]_{i,j=1..3} = f([r_{i,j}[k-1]]_{i,j=1..3}, w) \tag{D.20}$$

Once R is computed the corresonding desired frame H_{sd} for the slave can be constructed adjoining the rotation matrix with the translational elements.

D.4 Position-Force using Euler Angles and Angular velocity representations

We show two implementations of the Position-Force architecture for multi DoFmaster - slave systems using both, Euler angles and angular velocity representations.

The following coordinate system are distinguished.

- $\{T_m\}$: Master tool frame.
- $\{T_S\}$: Slave tool frame
- $\{B_m\}$: Master base frame
- $\{B_s\}$: Slave base frame
- $\{U\}$: World frame

Fig. D.4.1 shows a diagram with master and slave robots and their corresponding coordinate systems.

In these examples the positions and orientation of master and slave end-effectors are coupled to each other [2].

[1] They must be made orthogonal, this is not visible in the equation.

[2] Fig. D.4.1 shows the same joint configuration on both robots for simplification matters, but note that those are usually different.

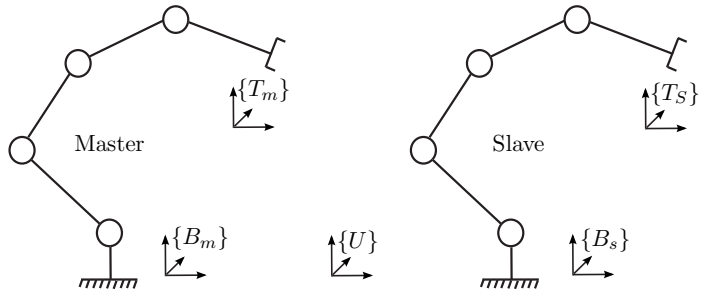

Figure D.4.1: Coordinate frames of a manipulator.

Euler Angles

The forward kinematics of the Master device are given by

$$\boldsymbol{H}_m(\boldsymbol{q}_m) = \begin{bmatrix} \boldsymbol{R}_m(\boldsymbol{q}_m) & \boldsymbol{p}_m(\boldsymbol{q}_m) \\ 0 & 1 \end{bmatrix}. \tag{D.21}$$

The forward kinematics of the Slave robot are as:

$$\boldsymbol{H}_s(\boldsymbol{q}_s) = \begin{bmatrix} \boldsymbol{R}_s(\boldsymbol{q}_s) & \boldsymbol{p}_s(\boldsymbol{q}_s) \\ 0 & 1 \end{bmatrix} \tag{D.22}$$

The equations of motion of the system can be expressed in the operational space using the Euler representation. Besides being an intuitive representation, the Euler angles allow direct differentiation and integration.
The world frame is chosen such that $\{U\} = \{B_s\}$ in order to simplify the transformations. Thus, the master the derivative of the euler angles vector with the orientation of the world frame is obtained as:

$$\dot{\epsilon}_m^U = \begin{bmatrix} p_m^U \\ \varepsilon_m^U \end{bmatrix} = \begin{bmatrix} R_b & 0 \\ 0 & R_b \end{bmatrix} \begin{bmatrix} R_m(q_m) & 0 \\ 0 & R_m(q_m) \end{bmatrix} J_A(q_m)\dot{q}_m = T_m(q_m)\dot{q}_m. \tag{D.23}$$

Being R_b the transformation between master and slave base frames, $\{B_m\}$ and $\{B_s\}$.
The desired values to the PD controller with tool frame orientation can be computed through the transformation from $\{U\}$ to $\{T_S\}$:

$$T_{Tool}^U(q_s) = \begin{bmatrix} R_s(q_s)^T & 0 \\ 0 & R_s(q_s)^T \end{bmatrix} \tag{D.24}$$

Angular Velocity

The command from the master at the slave, $\dot{\psi}_{sd}$ is integrated through by using (D.20). The output is thus a desired frame which can be fed into the impedance controller, which includes a spatial spring and damper. The output of the impedance controller is a generalized cartesian force vector, which represents the force commanded at the end-effector of the robot. Fig. D.4.2 shows a Position-Force computed scheme for multi DoF systems based on the angular velocity.

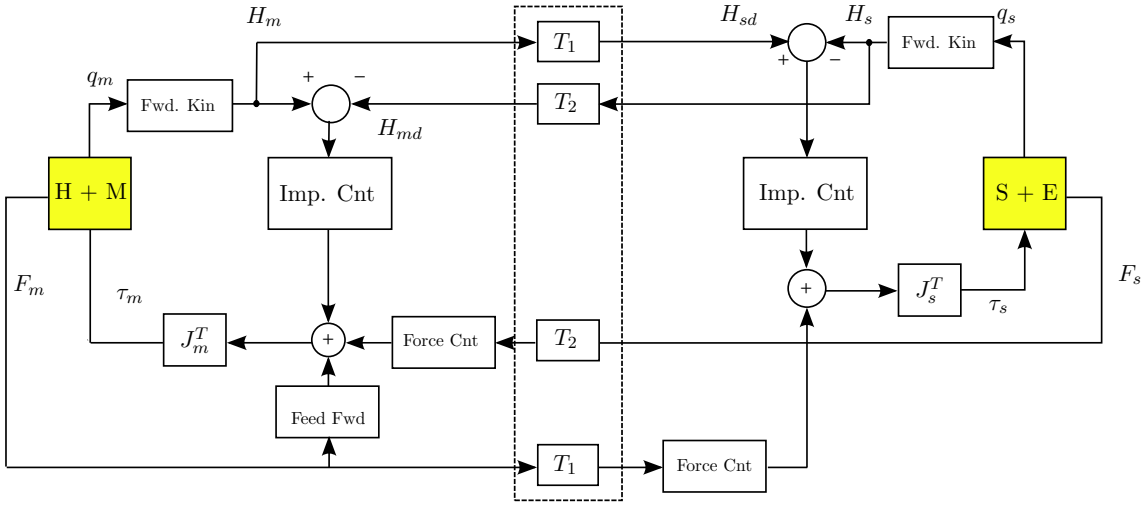

Figure D.4.2: Position-Force Scheme for multi DoF systems based on angular velocity.

Nomenclature

α	Dissipation coefficient for an impedance based Passivity Controller
β	Dissipation coefficient for an admittance based Passivity Controller
$\mu_m(t)$	Master outgoing wave (direction towards left (master))
$\mu_s(t)$	Slave outgoing wave (direction toward right (slave))
b	Characteristic impedance
$C_{a,b}$	Independent velocity or force sources
E^M	Energy flow at the left side of a TDPN (or master side)
E^M_{in}	Energy flowing into a TDPN from its left port (usually the master side)
E^M_{osb}	Observed Energy at the left side of a TDPN
E^M_{out}	Energy of a TDPN flowing out from its left port (usually the master side)
E^N	Energy of a network N
E^S	Energy flow at the right side of a TDPN (or slave side)
E^S_{in}	Energy flowing into a TDPN from its right port (usually the slave side)
E^S_{osb}	Observed Energy at the right side of a TDPN
E^S_{out}	Energy of a TDPN flowing out from its right port (usually the slave side)
$E^{Ca,b}$	1-port energy of an independent velocity or force source
E^{L2R}	Energy flow from left to right of a TDPN
E^{R2L}	Energy flow from right to left of a TDPN
E^{TDPN}	Energy of a TDPN
E_+	Positive component of an energy flow
E_-	Negative component of an energy flow
$E_{\hat{N}z}$	Energy of a communication channel revealed by the extraction of its TDPNs

E_{Nx}	Total energy of the TDPN N_x, where x can a, b, c and d, depending on the architecture under study
f_e	Environment force
f_m	Master force
f_s	Slave force
P	Power of system
P^M	Power at the left side of a TDPN (or master side)
P^S	Power at the right side of a TDPN (or slave side)
P_+	Positive component of a power signal
P_-	Negative component of a power signal
T_b	Backward time delay
T_f	Forward time delay
T_s	System sample time
v_m	Master velocity
v_s	Slave velocity
W_x	Passivity Observer, where x can represent any side of a TDPN
Z_c	Impedance of a controller
Z_e	Impedance of the environment
Z_h	Impedance of the human operator
Z_m	Impedance of the master device
Z_s	Impedance of the slave robot
Z_{cm}	Impedance of a controller located on the master side
Z_{cs}	Impedance of a controller located on the slave side
Z_{pd}	Impedance of a PD controller
4Ch	4 Channels architecture
ADR	Active Debris Removable
DoF	Degrees of freedom
GEO	Geostationary Earth Orbit
LEO	Low Earth Orbit

LTI Linear Time Invariant

LWR Light-Weight-Robot

OOS On-Orbit Servicing

P-Fc Position-Force computed architecture

P-Fmsr Position-Force measured architecture

P-P Position-Position architecture

PC Passivity Controller

PO Passivity Observer

TCP Tool Center Point

List of Figures

List of Tables

Bibliography

[1] DEOS - Deutsches On-Orbit Servicing Infolink. *www.dlr.de/rd/en/desktopdefault.aspx/tabid-2266/3398_read-36724* .

[2] Orbital Express Space Operation Architecture. *https://www.darpa.mil/tto/programs/oe.htm* .

[3] SENSODRIVE GmbH. *www.sensodrive.de/EN/* .

[4] Sonderforschugsbereicht SFB-453: Telepresence and Teleaction - German Collaborative Center 1999-2007). *www.ldv.ei.tum.de/en/research/projekte/sfb-453-telepraesenz* .

[5] J. J. Abbott and A. M. Okamura. Analysis of virtual fixture contact stability for telemanipulation. In *IEEE/RSJ Intl. Conf. Intelligent Robots and Systems, 2003, In*, pages 2699–2706. press, 2003.

[6] R. J. Adams. *Stable Haptic Interaction with Virtual Environments*. PhD thesis, University of Washington, 1999.

[7] R. J. Adams and B. Hannaford. Stable haptic interaction with virtual environments. *IEEE Transactions on Robotics and Automation*, 15:465–474, 1999.

[8] R. J. Adams and B. Hannaford. Control law design for haptic interfaces to virtual reality. *IEEE Transactions on Control Systems Technology*, 10:3–13, 2002.

[9] A. Albu-Schäffer, W. Bertleff, D. Rebele, B. Schäfer, K. Landzettel, and G. Hirzinger. Rokviss - robotics component verification on iss current experimental results on parameter identification. In *Robotics and Automation, 2006. ICRA 2006. Proceedings 2006 IEEE International Conference on*, pages 3879–3885, May 2006.

[10] A. Albu-Schäffer and G. Hirzinger. Parameter identification and passivity based joint control for a 7dof torque controlled light weight robot. In *ICRA*, pages 1087–1093, 2001.

[11] R. J. Anderson and M. W. Spong. Bilateral Control of Teleoperators with Time Delay. *IEEE Transactions on Automatic Control*, 34(5):494–501, May 1989.

[12] R. Aracil, J.M. Azorín, M. Ferre, and C. Pena. Bilateral control by state convergence based on transparency for systems with time delay. *Robotics and Autonomous Systems*, 61(2):86 – 94, 2013.

[13] J. Artigas. Development and implementation of bilateral control for the ROKVISS experiment using the Wave Variables Theory. Master's thesis, Universitat Ramon Llull (Barcelona, Spain) and DLR - Inst. Robotics and Mechatronics (Munich, Germany), June 2003.

[14] J. Artigas. Network unfoldment and application to wave variables using measured forces. In *Intelligent Robots and Systems (IROS), 2012 IEEE/RSJ International Conference on*, pages 5208–5213, Oct 2012.

[15] J. Artigas, C. Preusche, G. Hirzinger, G. Borghesan, and C. Melchiorri. Bilateral energy transfer in delayed teleoperation on the time domain. In *Robotics and Automation, 2008. ICRA 2008. IEEE International Conference on*, pages 671–676, May 2008.

[16] J. Artigas, C. Preusche, G. Hirzinger, G. Borghesan, and C. Melchiorri. Bilateral energy transfer for high fidelity haptic telemanipulation. In *EuroHaptics conference, 2009 and Symposium on Haptic Interfaces for Virtual Environment and Teleoperator Systems. World Haptics 2009. Third Joint*, pages 488–493, March 2009.

[17] J. Artigas, D. Reintsema, C. Preusche, and G. Hirzinger. DIMSART: A Real Time - Device Independent Modular Software Architecture for Robotic and Telerobotic Applications. In *ICINCO International Conference on Informatics in Control, Automation and Robotics*, volume 2, pages 102–109, Setúbal, Portugal, 2004. INSTICC.

[18] J. Artigas, J.H. Ryu, and C. Preusche. Position drift compensation in time domain passivity based teleoperation. In *IEEE International Conference on Robotics and Intelligent Systems*, Taipei, Taiwan, April 2010.

[19] J. Artigas, J.H. Ryu, and C. Preusche. Time domain passivity control for position-position teleoperation architectures. *Presence: Teleoperators and Virtual Environments*, 19(5):482–497, 2010.

[20] J. Artigas, J.H. Ryu, C. Preusche, and G. Hirzinger. Network representation and passivity of delayed teleoperation systems. In *IROS*, pages 177–183. IEEE, 2011.

[21] J. Artigas, J. Vilanova, C. Preusche, and G. Hirzinger. Time Domain Passivity - based Telepresence with Time Delay. In *IEEE International Conference on Intelligent Robots And Systems (IROS)*, 2006.

[22] J. M. Azorín, R. Aracil, N. M. García, and C. Pérez. Bilateral control of teleoperation systems through state convergence. In M. Ferre, M. Buss, R. Aracil, C. Melchiorri, and C. Balaguer, editors, *Advances in Telerobotics*, volume 31 of *Springer Tracts in Advanced Robotics*, pages 271–288. Springer Berlin Heidelberg, 2007.

[23] J. M. Azorín, O. Reinoso, R. Aracil, and M. Ferre. Control of teleoperators with communication time delay through state convergence. *J. Robot. Syst.*, 21(4):167–182, April 2004.

[24] J.M. Azorin, O. Reinoso, R. Aracil, and M. Ferre. Generalized control method by state convergence for teleoperation systems with time delay. *Automatica*, 40(9):1575 – 1582, 2004.

[25] L. Basañez and R. Suárez. Teleoperation. In Shimon Y. Nof, editor, *Springer Handbook of Automation*, pages 449–468. Springer Berlin Heidelberg, 2009.

[26] G. Borghesan, A. Macchelli, and C. Melchiorri. Simulation issues in haptics. In *Robotics and Automation, 2007 IEEE International Conference on*, pages 111–116, April 2007.

[27] G. Borghesan, A. Macchelli, and C. Melchiorri. Interconnection and simulation issues in haptics. *Haptics, IEEE Transactions on*, 3(4):266–279, Oct 2010.

[28] O. Brune. Synthesis of a finite two-terminal network whose drivingpoint impedance is a prescribed function of frequency. *J. Math. Phys.*, 10:191–236, 1931.

[29] A. Casals. Human - robot cooperation techniques in surgery. In J. Filipe, J. Andrade-Cetto, and J.-L. Ferrier, editors, *ICINCO (1)*, pages 7–11. INSTICC Press, 2010.

[30] J. E. Colgate and G. Schenkel. Passivity of a Class of Sampled-Data Systems: Application to Haptic Interfaces. In *Proc. American Control Conference*, pages 3236–40, Baltimore, USA, 1994.

[31] G. Daryanani. *Principles of Active Network Synthesis and Design*. Joh Wiley and Sons, Inc., 1976.

[32] C. A. Desoer and M. Vidyasagar. *Feedback systems: input-output properties*. Academic Press, New York, 1975.

[33] F. A. Firestone. A new analogy between mechanical and electrical systems. *The Journal of the Acoustical Society of America*, 4:5, 1932.

[34] M. Franken, S. Stramigioli, S. Misra, C. Secchi, and A. Macchelli. Bilateral telemanipulation with time delays: A two-layer approach combining passivity and transparency. *Robotics, IEEE Transactions on*, 27(4):741–756, Aug 2011.

[35] M. Franken, S. Stramigioli, R. Reilink, C. Secchi, and A. Macchelli. Bridging the gap between passivity and transparency. In *Proceedings of Robotics: Science and Systems*, Seattle, USA, June 2009.

[36] L. Geiger, M. Popp, B. Färber, J. Artigas, and P. Kremer. The influence of telemanipulation-systems on fine motor performance. In Ray Jarvis and Cosmin Dini, editors, *ACHI*, pages 44–49. IEEE Computer Society, 2010.

[37] L. Geiger, M. Popp, B. Färber, J. Artigas, and P. Kremer. Is a telepresence-system an effective alternative to manned missions? In *Proceedings of the 5th ACM/IEEE International Conference on Human-robot Interaction*, HRI '10, pages 145–146, Piscataway, NJ, USA, 2010. IEEE Press.

[38] U. Hagn, R. Konietschke, A. Tobergte, M. Nickl, S. Jörg, B. Kübler, G. Passig, M. Gröger, F. Fröhlich, U. Seibold, L. Le-Tien, A. Albu-Schäffer, A. Nothhelfer, F. Hacker, M. Grebenstein, and G. Hirzinger. Dlr mirosurge: a versatile system for research in endoscopic telesurgery. *International Journal of Computer Assisted Radiology and Surgery*, 5(2):183–193, 2010.

[39] B. Hannaford. A Design Framework for Teleoperators with Kinesthetic Feedback. *IEEE Transactions on Robotics and Automation*, 5(4):426–434, August 1989.

[40] B. Hannaford and J.H. Ryu. Time domain passivity control of haptic interfaces. In *Proc. IEEE ICRA '01*, pages 1863–1869, 2001.

[41] B. Hannaford, J.H. Ryu, D.S. Kwon, Y. S. Kim, and J.B. Song. Testing Time Domain Passivity Control of Haptic Enabled Systems. Technical report, UWEE Tech Repot Series, 2002.

[42] J. Harder and U. Walter. Communication architecture evaluation for real-time tele-operated spacecraft. In *Aerospace Conference, 2012 IEEE*, pages 1–9, March 2012.

[43] Jan Harder, Markus Wilde, and Andreas Fleischner. Technology development for real-time teleoperated spacecraft mission operations. In *Aerospace Conference, 2013 IEEE*, pages 1–10, March 2013.

[44] K. Hashtrudi-Zaad and S. E. Salcudean. Analysis of Control Architectures for Teleoperation Systems with Impedance/Admittance Master and Slave Manipulators. *The international Journal of Robotics Research*, 20(6):419–445, June 2001.

[45] K. Hashtrudi-Zaad and S.E. Salcudean. On the Use of Local Force Feedback for Transparent Teleoperation. In *Proceedings of the 1999 IEEE International Conference on Robotics and Automation*, Detroit, Michigan, USA, May 1999.

[46] A. Hernansanz, D. Zerbato, L. Gasperotti, M. Scandola, P. Fiorini, and A. Casals. Improving the development of surgical skills with virtual fixtures in simulation. In P. Abolmaesumi, L. Joskowicz, N. Navab, and P. Jannin, editors, *Information Processing in Computer-Assisted Interventions*, volume 7330 of *Lecture Notes in Computer Science*, pages 157–166. Springer Berlin Heidelberg, 2012.

[47] S. Hirche and M. Buss. Packet loss effects in passive telepresence systems. In *Proceedings of the 43rd IEEE Conference on Decision and Control*, pages 4010–4015, Nassau, Bahamas, 2004.

[48] S. Hirche and M. Buss. Telepresence control in packet switched communication networks. In *Proceedings of the IEEE International Conference on Control Applications*, pages 236–241, Taipei, Taiwan, 2004.

[49] G. Hirzinger. Rotex the first space robot technology experiment. In T. Yoshikawa and F. Miyazaki, editors, *Experimental Robotics III*, volume 200 of *Lecture Notes in Control and Information Sciences*, pages 579–598. Springer Berlin Heidelberg, 1994.

[50] G. Hirzinger, A. Albu-Schäffer, M. Hähnle, I. Schaefer, and N. Sporer. On a new generation of torque controlled light-weight robots. In *ICRA*, pages 3356–3363, 2001.

[51] G. Hirzinger, B. Brunner, J. Dietrich, and J. Heindl. ROTEX - The First Remotely Controlled Robot in Space. In *Proceedings of the IEEE International Conference on Robotics and Automation*, volume 3, San Diego, CA, USA, 1994.

[52] G. Hirzinger, G. Grunwald, B. Brunner, and J. Heindl. A sensor-based telerobotic system for the space robot experiment rotex. In Raja Chatila and G. Hirzinger, editors, *Experimental Robotics II*, volume 190 of *Lecture Notes in Control and Information Sciences*, pages 222–238. Springer Berlin Heidelberg, 1993.

[53] G. Hirzinger, K. Landzettel, and J. Heindl. Rotex: space telerobotic flight experiment. In *Proceedings of SPIE International Symposium on Optical Tools for Manufacturing and Advanced Automation*, Boston, USA, 1993.

[54] T. Hulin, K. Hertkorn, P. Kremer, S. Schätzle, J. Artigas, M. Sagardia, F. Zacharias, and C. Preusche. The dlr bimanual haptic device with optimized workspace. In *Robotics and Automation (ICRA), 2011 IEEE International Conference on*, pages 3441–3442, May 2011.

[55] T. Imaida, Y. Yokokohji, T. Doi, M. Oda, and T. Yoshikawa. Ground-space bilateral teleoperation of ETS-VII robot arm by direct bilateral coupling under 7-s time delay condition. *Robotics and Automation, IEEE Transactions on*, 20(3):499–511, June 2004.

[56] J.P. Kim and J. Ryu. Energy bounding algorithm based on passivity theorem for stable haptic interaction control. In *Haptic Interfaces for Virtual Environment and Teleoperator Systems, 2004. HAPTICS '04. Proceedings. 12th International Symposium on*, pages 351–357, March 2004.

[57] R. Konietschke, U. Hagn, M. Nickl, S. Jörg, A. Tobergte, G. Passig, U. Seibold, L. Le-Tien, B. Kübler, M. Gröger, F. Fröhlich, C. Rink, A. Albu-Schäffer, M. Grebenstein, T. Ortmaier, and G. Hirzinger. The dlr mirosurge - a robotic system for surgery. In *Proc. IEEE International Conference on Robotics and Automation ICRA*, Kobe, JP, 2009.

[58] P. Kremer, T. Wimböck, J. Artigas, S. Schätzle, K. Johl, F. Schmidt, C. Preusche, and G. Hirzinger. Multimodal telepresent control of dlr's rollin' justin. In *Robotics and Automation, 2009. ICRA '09. IEEE International Conference on*, pages 1601–1602, May 2009.

[59] B. Kulakowski, J. F. Gardner, and J. L. Shearer. *Dynamic Modeling and Control of Engineering Systems*. Cambridge University Press, New York, NY, USA, 2007.

[60] D. A. Lawrence. Stability and Transparency in Bilateral Teleoperation. *IEEE Transactions on Robotics and Automation*, 9(5), IEEE Transactions on Robotics and Automation 1993.

[61] D. A. Lawrence. Stability and transparency in bilateral teleoperation. *IEEE Transactions on Robotics and Automation*, 9(5):624–637, 1993.

[62] D. Lee and M. W. Spong. Passive bilateral teleoperation with constant time delay. *IEEE Transactions on Robotics*, 2006.

[63] D. Lee and M. W. Spong. Passive bilateral teleoperation with constant time-delay. *IEEE Transactions on Robotics and Automation*, 22(2):269–281, April 2006.

[64] C. S. Lindquist. *Active Network Design with Signal Filtering Applications*. Steward and Sons, 1977.

[65] Y.C. Liu and N. Chopra. Control of robotic manipulators under input/output communication delays: Theory and experiments. *Robotics, IEEE Transactions on*, 28(3):742–751, June 2012.

[66] F.B. Llewellyn. Some fundamental properties of transmission systems. *Proceedings of the IRE*, 40(3):271 –283, march 1952.

[67] R. Lundin and E. Stoll. Coverage time variation in a near-earth data relay satellite system. *57th International Astronautical Congress, International Astronautical Congress (IAF)*, Oct 2006.

[68] A. Marban, A. Casals, J. Fernandez, and J. Amat. Haptic feedback in surgical robotics: Still a challenge. In M. A. Armada, A. Sanfeliu, and M. Ferre, editors, *ROBOT2013: First Iberian Robotics Conference*, volume 252 of *Advances in Intelligent Systems and Computing*, pages 245–253. Springer International Publishing, 2014.

[69] J. E. Marshall. *Control of time-delay systems*. The Institution of Electrical Engineers, 1979.

[70] L. Marton and J. Artigas. Energetic approach for actuator fault accommodation: Application to bilateral teleoperation. In *Control and Fault-Tolerant Systems (SysTol), 2013 Conference on*, pages 720–726, Oct 2013.

[71] L. Marton, J. Artigas, P. Haller, and T. Vajda. Passive bilateral teleoperation with bounded control signals. In *Industrial Informatics (INDIN), 2013 11th IEEE International Conference on*, pages 337–342, July 2013.

[72] S. Kumar Mitra. *Analysis and Synthesis of Linear Active Networks*. Joh Wiley and Sons, Inc., 1969.

[73] G. Niemeyer. *Using Wave Variables in Time Delayed force Reflecting Teleoperation*. PhD thesis, Massachussetts Institute of Technology, September 1996.

[74] G. Niemeyer. *Using Wave Variables in Time Delayed force Reflecting Teleoperation*. PhD thesis, Massachussetts Institute of Technology, September 1996.

[75] G. Niemeyer and J.-J. E. Slotine. Towards Force-Reflecting Teleoperation Over the Internet. In *Proceedings of the 1998 IEEE International Conference on Robotics and Automation*, pages 1909–1915, Leuven, Belgium, May 1998.

[76] H. F. Olson. *Dynamic Analogies*. D. Van Nostrand Company, Inc., 1943.

[77] T. Ortmaier and G. Hirzinger. Cartesian control issues for minimally invasive robot surgery. In *Intelligent Robots and Systems, 2000. (IROS 2000). Proceedings. 2000 IEEE/RSJ International Conference on*, volume 1, pages 565–571 vol.1, 2000.

[78] T. Ortmaier, D. Reintsema, U. Seibold, U. Hagn, and G. Hirzinger. The DLR Minimally Invasive Robotics Surgery Scenario. In *Proc. of the Workshop on Advances in Interactive Multimodal Telepresence Systems*, 2003.

[79] C. Ott, J. Artigas, C. Preusche, and G. Hirzinger. Subspace-oriented Energy Distribution for the Time Domain Passivity Approach. In *IEEE International Conference on Intelligent Robots And Systems (IROS)*, San Francisco, CA, USA, 2011.

[80] C. Ott, O. Eiberger, W. Friedl, B. Bäuml, U. Hillenbrand, C. Borst, A. Albu-Schäffer, B. Brunner, H. Hirschmüller, S. Kielhöfer, R. Konietschke, M. Suppa, T. Wimböck, F. Zacharias, and G. Hirzinger. A humanoid two-arm system for dexterous manipulation. In *IEEE-RAS International Conference on Humanoid Robots*, pages 276–283, 2006.

[81] C. Ott and Y. Nakamura. Employing wave variables for coordinated control of robots with distributed control architecture. In *Robotics and Automation, 2008. ICRA 2008. IEEE International Conference on*, pages 575–582, May 2008.

[82] L.F. Penin, R. Aracil, M. Ferre, E. Pinto, M. Hernando, and A. Barrientos. Telerobotic system for live power lines maintenance: Robtet. In *Robotics and Automation, 1998. Proceedings. 1998 IEEE International Conference on*, volume 3, pages 2110–2115 vol.3, May 1998.

[83] C. Preusche, G. Hirzinger, J.H. Ryu, and B. Hannaford. Time Domain Passivity Control for 6 Degrees of Freedom Haptic Displays. In *Proceedings of the 2003 IEEE/RSJ*, pages 2944–2949, October 2003.

[84] C. Preusche, D. Reintsema, K. Landzettel, and G. Hirzinger. ROKVISS–Towards telepresence control in advanced space missions. In *Humanoids 2003 – The Third IEEE International Conference on Humanoid Robots and Systems*, Munich, Germany, October 2003.

[85] H. V. Quang, J.-H. Ryu, and Y. Kwon. A feasibility study of rate-mode mobile robot bilateral teleoperation with time domain passivity approach. In Sukhan Lee, Hyungsuck Cho, Kwang-Joon Yoon, and Jangmyung Lee, editors, *Intelligent Autonomous Systems 12*, volume 194 of *Advances in Intelligent Systems and Computing*, pages 207–215. Springer Berlin Heidelberg, 2013.

[86] H. V. Quang and J.H. Ryu. Stable multilateral teleoperation with time domain passivity approach. In *Intelligent Robots and Systems (IROS), 2013 IEEE/RSJ International Conference on*, pages 5890–5895, Nov 2013.

[87] M. Radi, J. Artigas, C. Preusche, and H. Roth. Transparency measurement of telepresence systems. In *EuroHaptics*, Madrid, Spain, 2008.

[88] G. Raisbeck. A definition of passive linear networks in terms of time and enregy. *Journal fo Applied Physics*, 25:1510 –1514, 1954.

[89] G.J. Raju, G.C. Verghese, and T.B. Sheridan. Design issues in 2-port network models of bilateral remote manipulation. In *IEEE International Conference on Robotics and Automation*, volume 3, pages 1316 – 1321, Scottsdale, AZ , USA, 1989.

[90] A. Rodríguez, L. Basañez, J.E. Colgate, and E.L. Faulring. Haptic display of dynamic systems subject to holonomic constraints. In *Intelligent Robots and Systems, 2008. IROS 2008. IEEE/RSJ International Conference on*, pages 3002–3007, Sept 2008.

[91] J.H. Ryu, J. Artigas, and C. Preusche. A passive bilateral control scheme for a teleoperator with time-varying communication delay. *Elsevier Journal of Mechatronics*, 20:812–823, October 2010.

[92] J.H. Ryu and J.H. Kim. Stable and High Performance Teleoperation with Time Domain Passivity Control: Reference Energy Following Scheme. In *Int. Conf. on Advanced Robotics 2005*, Seattle, USA, 2005.

[93] J.H. Ryu, D.S. Kwon, and B. Hannaford. Stable Teleoperation with Time Domain Passivity Control. In *IEEE Intl. Conference on Robotics and Automation, ICRA*, pages 3260–65, Washington, DC, USA, May 2002.

[94] J.H. Ryu, D.S. Kwon, and B. Hannaford. Control of a Flexible Manipulator With Noncollocated Feedback: Time-Domain Passivity Approach. *IEEE Transactions on Robotics*, 20(4), August 2004.

[95] J.H. Ryu, D.S. Kwon, and B. Hannaford. Stability Guaranteed Control: Time Domain Passivity Approach. *IEEE Trans. on control Systems Technology*, 12:2115–21, 2004.

[96] L. Sciavicco and B. Siciliano. *Modeling and Control of Robot Manipulators*. McGraw-Hill Companies, 1996.

[97] C. Secchi, S. Stramigioli, and C. Fantuzzi. Digital Passive Geometric Telemanipulation. In *International Conference on Robotics and Automation (ICRA)*, 2003.

[98] C. Secchi, S. Stramigioli, and C. Fantuzzi. Position drift compensation in port-hamiltonian based telemanipulation. In *Intelligent Robots and Systems, 2006 IEEE/RSJ International Conference on*, pages 4211–4216, Oct 2006.

[99] C. Secchi, S. Stramigioli, and C. Fantuzzi. *Control of interactive robotic interfaces A port-Hamiltonian approach*, volume 29 of *Springer Tracks in advanced robotics*. Springer Verlag, New York, 2007.

[100] C. Seo, J.P. Kim, J. Kim, and J. Ryu. Energy-bounding algorithm for stable haptic interaction and bilateral teleoperation. *World Haptics Conference*, 0:617–618, 2009.

[101] C. Seo, J.P. Kim, J.H. Yoon, and J. Ryu. Stable bilateral teleoperation using the energy-bounding algorithm: Basic idea and feasibility tests. In *Advanced Intelligent Mechatronics, 2008. AIM 2008. IEEE/ASME International Conference on*, pages 335–340, July 2008.

[102] T. B. Sheridan. Space Teleoperation Through Time Delay: Review and Prognosis. *IEEE Transactions on Robotics and Automation*, 9(5):592–606, October 1993.

[103] M. De Stefano, W. Rackl, and J. Artigas. Passivity of virtual free-floating dynamics. In *Intelligent Robots and Systems (IROS), 2014 IEEE/RSJ International Conference on*, pages 5890–5895, Sep 2014.

[104] E. Stoll, J. Artigas, J. Letschnik, C. Preusche, U. Walter, and G. Hirzinger. Ground verification of the feasibility of telepresent on-orbit servicing. *Journal of Field Robotics*, 2008.

[105] E. Stoll, J. Letschnik, U. Walter, J. Artigas, P. Kremer, C. Preusche, and G. Hirzinger. On-orbit servicing. *Robotics Automation Magazine, IEEE*, 16(4):29–33, December 2009.

[106] E. Stoll, J. Letschnik, M. Wilde, A. Saenz-Otero, R. Varatharajoo, and J. Artigas. The future role of relay satellites for orbital telerobotics. *Advances in Space Research*, 50(7):864 – 880, 2012.

[107] S. Stramigioli. Intrinsically passive control. In *Modeling and IPC control of interactive mechanical systems A coordinate-free approach*, volume 266 of *Lecture Notes in Control and Information Sciences*, pages 125–145. Springer London, 2001.

[108] N. A Tanner and G. Niemeyer. Practical Limitations of Wave Variable Controllers in Teleoperation. In *IEEE Conf. on Robotics, Automation and Mechtronics*, pages 25–30, December 2004.

[109] N. A Tanner and G. Niemeyer. Improving Perception in Time Delayed Teleoperation. *Int. Journal of Robotics Research*, 2005.

[110] A. Tobergte, R. Konietschke, and G. Hirzinger. Planning and control of a teleoperation system for research in minimally invasive robotic surgery. In *Robotics and Automation, 2009. ICRA '09. IEEE International Conference on*, pages 4225–4232, May 2009.

[111] M. E. Van Valkenburg, editor. *Intorduction To Modern Network Synthesis*. John Wiley and Sons, Inc., 1965.

[112] B. Willaert, B. Corteville, D. Reynaerts, H. Van Brussel, and E. B. Vander Poorten. Bounded environment passivity of the classical position-force teleoperation controller. In *IROS'09*, pages 4622–4628, 2009.

[113] M. Artigas y R. Aracil y M. Ferre y C. García. Sistema de control bilateral adaptativo por convergencia de estados en teleoperación. *RIAII*, 7(3), 2010.

[114] T. Yoshikawa Y. Yokokohji and Takashi Imaida. Bilateral teleoperation under time-varying communication delay. In *International Conference on Intelligent Robots and Systems*, 1999.

[115] Y. Yokokohji, Teruhiro Tsujioka, and T. Yoshikawa. Bilateral control with time-varying delay including communication blackout. In *Proceedings of the 10th Symposium on Haptic Interfaces for Virtual Environment and Teleoperator Systems*, HAPTICS '02, pages 285–, Washington, DC, USA, 2002. IEEE Computer Society.

[116] Y. Yokokohji and T. Yoshikawa. Bilateral Control of Master-Slave Manipulators for Ideal kinesthetic Coupling – Formulation and Experiment. *IEEE Transactions on Robotics and Automation*, 10(5):605–620, October 1994.

[117] W.K. Yoon, T. Goshozono, H. Kawabe, M. Kinami, Y. Tsumaki, M. Uchiyama, M. Oda, and T. Doi. Model-based teleoperation of a space robot on ets-vii using a haptic interface. In *Robotics and Automation, 2001. Proceedings 2001 ICRA. IEEE International Conference on*, volume 1, pages 407–412 vol.1, 2001.

[118] K. Yoshida. ETS-VII Flight Experiments For Space Robot Dynamics and Control. In Daniela Rus and Sanjiv Singh, editors, *Experimental Robotics VII*, volume 271 of *Lecture Notes in Control and Information Sciences*, pages 209–218. Springer Berlin Heidelberg, 2001.